Frank Flechtner
Nico Sneeuw
Wolf-Dieter Schuh *Editors*

Observation of the System Earth from Space – CHAMP, GRACE, GOCE and Future Missions

GEOTECHNOLOGIEN Science Report No. 20

GEOTECHNOLOGIEN

Springer

Advanced Technologies in Earth Sciences

Series Editors

Ute Münch
Ludwig Stroink
Volker Mosbrugger
Gerold Wefer

Frank Flechtner · Nico Sneeuw
Wolf-Dieter Schuh
Editors

Observation of the System Earth from Space - CHAMP, GRACE, GOCE and Future Missions

GEOTECHNOLOGIEN Science
Report No. 20

 Springer

Editors
Frank Flechtner
Department for Geodesy and Remote
   Sensing
GFZ German Research Centre
   for Geosciences
Wessling
Germany

Nico Sneeuw
Institute of Geodesy
University of Stuttgart
Stuttgart
Germany

Wolf-Dieter Schuh
Institute of Geodesy and Geoinformation
University of Bonn
Bonn
Germany

Foreword

Advanced Technologies in Earth Sciences is based in the German Geoscientific Research and Development Programme "GEOTECHNOLOGIEN" funded by the Federal Ministry of Education and Research (BMBF) and the German Research Foundation (DFG).

This programme comprises a nationwide network of transdisciplinary research projects and incorporates numerous universities, non-university research institutions and companies. The books in this series deal with research results from different innovative geoscientific research areas, interlinking a broad spectrum of disciplines with a view to documenting System Earth as a whole, including its various sub-systems and cycles. The research topics are predefined to meet scientific, socio-political and economic demands for the future.

<div align="right">

Ute Münch
Ludwig Stroink
Volker Mosbrugger
Gerold Wefer

</div>

Preface

Observing the Earth from space has undergone rapid developments in recent years and has a prominent position in geo-related scientific research today. Research satellites are indispensable tools for studying processes on the Earth's surface and within the System Earth. The view from space allows the observation of the entire planet uniformly in near-real-time. At the same time the resulting time series of measurements allow the detection and monitoring of changes in this very complex system.

Satellites like Challenging Mini-satellite Payload (CHAMP), Gravity Recovery and Climate Experiment (GRACE) and Gravity Field and steady state Ocean Circulation Explorer (GOCE) measure the gravity and magnetic fields of the Earth with unprecedented accuracy and resolution (in time and space) and provide the metrological basis for oceanography, climatology, glaciology, global change and geophysics in general. These missions have been—and continue to be—instrumental to establish a new segment of the Earth system science.

Based on these data it is possible to explore and monitor changes related to the Earth's surface, the boundary layer between atmosphere and solid Earth, oceans and ice shields. This boundary layer is our habitat and therefore in the focus of our interests. The Earth's surface is exposed to anthropogenic changes, to changes driven by Sun, Moon and planets, and to processes in the Earth system. The state parameters and their changes are best monitored from space. The theme "Observation of the System Earth from Space" offers comprehensive insights into a broad range of research topics relevant to geodesy, oceanography, atmosphere science (from meteorology to climatology), hydrology and glaciology, and to society as a whole.

The volume *Observation of the System Earth from Space-CHAMP, GRACE, GOCE and Future Missions* documents the third phase of the topic *Observation of the system Earth from space*. As opposed to the first two phases the range of topics was narrowed down to the projects *LOTSE-CHAMP/GRACE* (led by Frank Flechtner), *REAL GOCE* (led by Wolf-Dieter Schuh) and Future Gravity Field Satellite Missions (led by Nico Sneeuw). This structure is also mirrored by the table of contents in the volume.

Three seminars, the status seminars at the University of Bonn in October 2010 and at the University of Stuttgart in October 2011 and the final presentations at the GFZ, German Research Centre for Geosciences in Potsdam in May 2012 were

organized to keep track of the progress and to draw the conclusion of the work of the third funding phase, respectively. The advisory board thoroughly reviewed the progress at the status seminars in Bonn and in Stuttgart and made its recommendations for the completion of the work in two reports, which were made available to the involved scientists.

It is rather unusual—and as viewed from the outside—extraordinary that a *topic* of GEOTECHNOLOGIEN is funded over three phases and so for more than 10 years. The third phase could only be approved based on the very strong recommendation submitted by the international advisory committee consisting at that time of Alain Geiger, ETH, Zürich, Robert Weber, Technical University of Vienna, Suzanna Zerbini, University of Bologna, Kathrin A. Whaler, University of Edinburgh, and Gerhard Beutler from University of Bern (chair), on the occasion of the status seminar of phase 2 in Munich in November 2007. The recommendation in 2007 was based on the insights that

- the three space missions CHAMP, GRACE and GOCE would have a tremendous impact on the advance of Earth system science,
- the funding through GEOTECHNOLOGIEN was of paramount importance to create a strong, internationally competitive science community in Germany,
- a termination of funding in 2008 would have a devastating impact on Germany's standing in this important field of science. It was, in particular clear, that a termination would endanger the German participation in the GRACE follow on mission (GRACE-FO).

The advisory committee is convinced that the *Coordination Committee GEOTECHNOLOGIEN* made the right decision at its 22nd meeting on March 17, 2008, in Potsdam to approve the third phase of *Observation of the System Earth from Space* with the focus on the three space missions CHAMP, GRACE and GOCE. The reduced breadth of the project in the third phase allowed it to reduce the size advisory committee—Alain Geiger, Robert Weber and Gerhard Beutler (chair) accompanying the third phase.

Meanwhile, history has proven that the decision taken in 2008 was absolutely right:

- The GOCE satellite was successfully launched on March 17, 2009. The scientific exploitation of this mission proved to be a full success, not least thanks to the strong support of the third phase of the GEOTECHNOLOGIEN programme.
- After very long and at times tiresome negotiations, the German participation in the GRACE-FO mission, slated for launch in 2017, could be secured. Part of the work documented in the section *future gravity field missions* is related to GRACE-FO. It would have been close to impossible to achieve this participation without the strong support and standing of the united scientists documented by this volume.

The report we have in our hands now not only documents the outstanding work performed by German scientists in this last phase using the data of CHAMP, GRACE and GOCE, it also marks the end of the topic *Observation of the Earth from Space* within the GEOTECHNOLOGIEN programme.

A new chapter of Earth monitoring from space is about to begin with the launch of the US/German mission GRACE-FO. Let us hope that this new era—which must eventually be followed by a permanent monitoring of the Earth's gravity and magnetic fields—will be accompanied in Germany by a science programme to match that related to the exploitation of CHAMP, GRACE and GOCE. It will take dedication on the part of science and wisdom on the political side to invoke such a development in Germany.

<div align="right">

Ute Münch
Head of the GEOTECHNOLOGIEN coordination office

Gerhard Beutler
Chair, advisory committee of the R&D Programme
GEOTECHNOLOGIEN
Professor emeritus and former Director of the
Astronomical Institute of University of Bern (AIUB)

</div>

Acknowledgments

Contents

Part II REAL GOCE

Part III   Future Missions

Part I
LOTSE-CHAMP/GRACE

Chapter 1
LOTSE-CHAMP/GRACE: An Interdisciplinary Research Project for Earth Observation from Space

Frank Flechtner

Abstract The research project LOTSE-CHAMP/GRACE (Long time series of consistently reprocessed high-accuracy CHAMP/GRACE data products) has the overall goal to reprocess all CHAMP and GRACE gravity, magnetic and atmospheric mission data. The reprocessing will provide a 10 years long, consistent and high-quality time series of (a) static and time variable gravity field models describing the mass distribution and mass variation in the system Earth, (b) atmospheric parameters such as mean global temperatures or tropopause altitudes and (c) the state and change in the Earth's outer core and lithospheric magnetic field during the CHAMP (2000–2010) and/or GRACE (since 2002) mission life time. These consistent data sets are used by the national and international user community as a valuable and complementary source of information for global change analysis such as monitoring of the continental hydrological cycle, polar ice mass loss, sea level change or monitoring of global temperature variations, as well as for geological and tectonic studies.

1.1 Motivation

The LOTSE-CHAMP/GRACE project started in 2008 to initiate a consistent reprocessing of interdisciplinary satellite observation data from CHAMP (Challenging Mini-satellite Project) and GRACE (Gravity Recovery and Climate Experiment) and was driven by various reasons:

- CHAMP, launched in July 2000 during high solar activity with an initial altitude of 450 km, had reached in 2008 a quite low orbit of 340 km at minimum solar activity which already led to a very high quality of gravity and magnetic data.

F. Flechtner (✉)
German Research Centre for Geosciences – GFZ, Telegrafenberg, 14473 Potsdam, Germany
e-mail: flechtne@gfz-potsdam.de

- This orbit decay—less pronounced—and the low solar activity also existed for GRACE. Although we had gathered and improved our experience with the highly complex GRACE sensor system in parallel, there were still a lot of open questions related to instrument data processing (especially with respect to the K-band satellite-to-satellite tracking and accelerometer data) and background modeling (e.g. the de-aliasing of tidal and non-tidal atmospheric and oceanic mass variations).
- For CHAMP and GRACE long time series of up to 8 and 6 years, respectively, of gravity field data were already available. But for GRACE these time series still did not meet the pre-launch simulated baseline accuracy and therefore needed to be reprocessed with improved observation and background models and processing standards to get a reliable data set to be used for global change analysis and climate research e.g. in the German Special Priority program of the German Research Foundation SPP1257 "Mass Transport and Mass Distribution in the Earth System".
- CHAMP provided the only and world-wide unique long-term set of globally distributed GPS radio occultation (RO) data, which was started in 2001 and was extended by the GRACE RO measurements since 2006. These data were in use by numerous scientists and demonstrated, e.g., the potential to detect even small variations of the Earth's atmosphere. Therefore there was consensus of the international user community to generate an appropriate and high-quality atmospheric data set for detailed climatological investigations, based on the CHAMP and GRACE RO measurements.
- The number of CHAMP and GRACE data users was more or less growing exponentially till 2008. At GFZ's ISDC (Information System and Data Center) we had 400 registrations end of 2003, 670 mid of 2005 and in 2008 already more than 1800 registered users. In parallel the number of GRACE publications increased in a similar way. Both pointed to the fact that a growing interest in high-precision long time series of CHAMP and GRACE data and products exists.

Consequently, the high level goals of the joint and interdisciplinary research project are to:

- Find the reasons for the yet not achieved GRACE baseline gravity field accuracy.
- Reprocess all CHAMP and GRACE gravity, magnetic and radio occultation mission data to derive long, consistent and high-quality time series for the analysis of the continental hydrological cycle, polar ice mass and sea level change, atmospheric parameters (e.g. tropopause height, temperature, humidity) or the state and change in the Earth's outer core and lithospheric magnetic field. These consistent data sets can then be used as a valuable and complementary source of information for global change analysis, climate research and for geological and tectonic studies.
- Derive a high-accuracy static GRACE satellite-only gravity field and its seasonal variations to be combined with GOCE real data.
- Demonstrate the feasibility to derive reliable information on climatological variations of the Earth's atmosphere based on the GPS RO data sets from CHAMP and GRACE.

To reach these goals, a consortium of GFZ German Research Centre for Geosciences and three German universities in Bonn (Institute for Geodesy and Geoinformation, IGG), Munich (Institute for Astronomical and Physical Geodesy of the Technical University in Munich, IAPG-TUM) and Potsdam (Institute for Mathematics of the University Potsdam, IM-UP) has been build. The joint project was led by GFZ.

1.2 Organization of the Project

The joint project goals are divided into three major topics: gravity field determination (WP100), magnetic field determination (WP200) and analysis of atmospheric data (WP300) all based on exploitation of CHAMP and/or GRACE instrument data. The findings of WP100 have also strong relevance to the other two joint projects REAL-GOCE and NGGM (Next Generation Gravity Missions) described in this book. Also WP100, WP200 and WP300 cooperate—at least partly—with each other (see Fig. 1.1).

Gravity field determination (WP100) was performed by a consortium of three partners and had the following primary objectives:
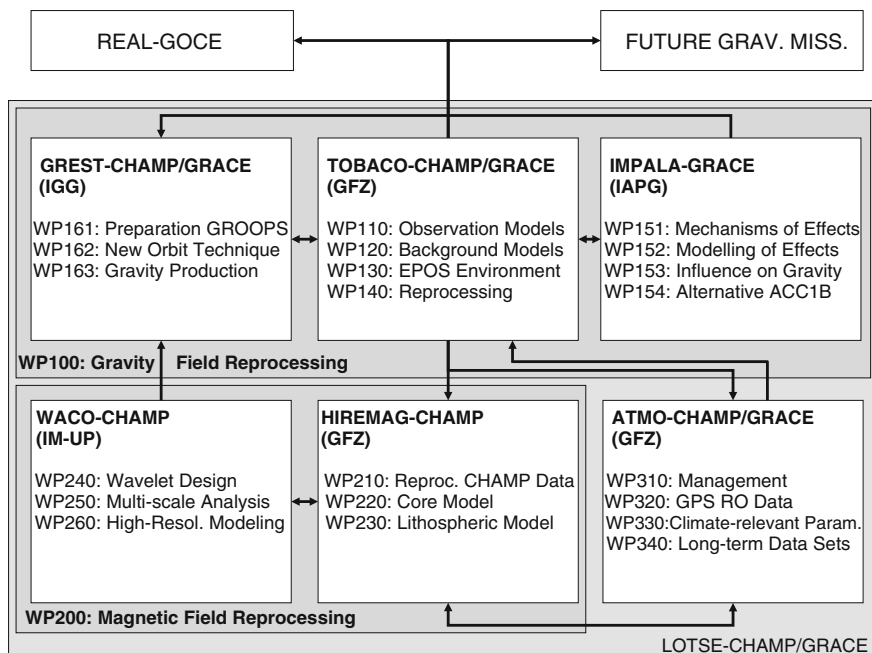
Fig. 1.1 LOTSE-CHAMP/GRACE individual projects and their main work packages and internal and external interfaces

TOBACO-CHAMP/GRACE (Towards baseline consistent CHAMP and GRACE gravity fields), led by GFZ, aimed at (for details see Dahle et al. in this book)

- refinement of the used observation models for GPS, K-band and accelerometer data,
- improvement of the applied background models to correct seasonal gravity variations as well as tidal and non-tidal mass variations,
- improvement of the processing standards and environment to decrease computing time for reprocessing or to update to latest IERS (International Earth Rotation and Reference Service) and ITRF (International Terrestrial Reference Frame) processing standards, and
- a consistent reprocessing of CHAMP and GRACE gravity mission data to derive improved static and time-variable gravity field models.

GREST-CHAMP/GRACE (Reprocessing of CHAMP and GRACE observations for the determination of improved static and temporal gravity field models with regional refinements), led by IGG, aimed at similar results as TOBACO-CHAMP/ GRACE but (for details see Shabanloi et al. in this book)

- the reprocessing shall be done based on alternative (with respect to spherical harmonic analysis performed by GFZ) recovery techniques with regional refinements, and
- CHAMP and GRACE orbit determination shall be performed based on an improved approach developed at IGG.

IMPALA-GRACE (Improved acceleration modeling and Level-1 processing alternative), led by IAPG-TUM, aimed at (for details see Peterseim and Schlicht in this book)

- Determination of source mechanisms causing the observed heater switching spikes, magnetic torquer spikes, and vibrations in GRACE accelerometer data,
- generation of time series of empirically modeled accelerations due to satellite-induced effects, and determination of the accuracy of modeling results, and analysis– in cooperation with GFZ- which modeling choices for satellite-induced effects lead to improvements in GRACE gravity field solutions.

Magnetic field determination (WP200) was performed by in a consortium of two partners and had the following primary objectives:

HIREMAG-CHAMP (High-resolution CHAMP magnetic field modeling), led by GFZ, aimed at

- utilizing the CHAMP magnetic fieldmeasurements to the best possible extend,
- constructing, based on the reprocessed dataset,magnetic field models with a temporal and spatialresolution beyond any previous representation to be used as a candidate model for the IGRF (International Geomagnetic Reference Field), and
- generation of geomagnetic field modelsfocusing on the lithospheric field.

WACO-CHAMP (Wavelet correlation analysis of CHAMP magnetic field models), led by IM-UP), aimed at

- analyzing GFZ's reprocessed geomagnetic field models with the help of the newly developed directional Poisson wavelets on the sphere.

ATMO-CHAMP/GRACE (Analysis of atmospheric data from CHAMP and GRACE and their application for climatological investigations), WP300 led by GFZ, aimed at (for details see Heise et al. in this book)

- improvement of the scientific GPS RO processing software as base for a reprocessing of the complete set of CHAMP and GRACE GPS RO data to generate a validated, consistent and high-quality long-term set of globally distributed vertical profiles of temperature, refractivity and water vapor, and
- derivation and interpretation of long-term variations of global atmospheric parameters with relevance for climate change, e.g. mean temperature and refractivity trends in the upper troposphere and lower stratosphere region, water vapor trends for the lower troposphere, tropopause parameters (altitude, temperature), atmospheric wave activity or ionospheric disturbances in the E-region.

1.3 Major Results

The high level goals of the joint project mentioned above have all been reached. Some prominent results which should be mentioned here (for details please refer to the following articles) are:

- A complete reprocessed release 05 (RL05) time series of monthly gravity field solutions up to degree and order 90 for the complete GRACE mission has been derived within TOBACO-CHAMP/GRACE. This time series is about a factor of 2 more precise than the precursor RL04 and much more closer to the pre-launch simulated baseline accuracy due to improved background modeling, processing standards and GPS orbit determination. Also a new GRACE high-accuracy static satellite-only gravity field and its seasonal variations which were combined with GOCE data (EIGEN-6S) has been derived.
- Within GREST-CHAMP/GRACE a new GRACE time series called ITG-GRACE2010 has been reprocessed which consists of daily and monthly time variable models as well of a new static model. The spatial resolution of the monthly models has also been increased using space localizing radial base functions. Corresponding ice mass trend for Greenland show good agreement with trends derived from ICESat data.
- The IMPALA-GRACE model clearly identified signal artifacts in the GRACE accelerometer data as well as possible reasons for their existence. A software was developed which significantly reduced the erroneous spikes and thus the measurement noise.
- Within ATMO-CHAMP/GRACE the complete set of CHAMP and GRACE GPS RO data has been reprocessed based on an improved analysis software version. Most significant improvements in comparison to other processing centers were

achieved especially to increase the accuracy of the derived profiles above 25 km. The resulting long-term data set of improved quality and consistency has been used for various atmospheric applications, such as global temperature and tropopause trends and also global characterization of gravity wave or sporadic E-layer occurrence. In addition to the climatological applications the GRACE RO data (and CHAMP until 2010) are/were continuously provided by GFZ to the world-leading numerical weather prediction centers (e.g. MetOffice, ECMWF, NCEP, DWD, JMA, MeteoFrance) with a maximum delay of 3 hours. This activity was also supported by the developments in ATMO-CHAMP/GRACE and the base for the current operational extension by TerraSAR-X data.

- The new magnetic field model derived within HIREMAG-CHAMP was produced in one run providing homogeneous quality which was important to derive reliable temporal variations.The noise floor of the magnetic field instrument data has been reduced by a factor of 10, a good prerequisite for high-resolution crustal field modeling.
- The number of registered users at GFZ's ISDC has increased from 1800 at the beginning of the project to 3265 at the end of the project in May 2012.

1.4 Outlook

The CHAMP satellite burned up in space on 19th of September 2010 after having provided high quality gravity and magnetic field as well as atmospheric data for more than 10 years. The time series of magnetic field data will be extended with the launch of the ESA SWARM mission in November 2012 and we expect from the three satellite constellation another gain in magnetic field modeling.

The GRACE instrument data are still performing perfectly after more than 10 years. Unfortunately, the batteries onboard each spacecraft need special attention due to the failure of two cells (out of 20). This results in switch-off of the accelerometers and (partly) also of the K-band ranging system roughly every 161 days. Nevertheless, the project is still optimistic that the time series of monthly gravity field models can be extended till 2014/2015. This would minimize the gap to a GRACE Follow-on mission which is currently developed in a joint NASA/GFZ partnership and which is due for launch in 2017.

Chapter 2
Improvement in GPS Orbit Determination at GFZ

Grzegorz Michalak, Daniel König, Karl-Hans Neumayer and Christoph Dahle

Abstract Precise orbits of the GPS satellites are required at GFZ for generation of Earth's gravity field models, precise determination of baselines between Low Earth Orbiters (LEOs) such as TerraSAR-X and TanDEM-X, for processing of various LEO radio occultation data as well as in research following the integrated approach where ground and space-borne GPS data are used together to estimate parameters needed for determination of a geodetic terrestrial reference frame. For this GFZ has implemented many GPS modelling improvements including GPS phase wind-up and attitude model, improved ambiguity fixing, absolute antenna phase centre offsets and variations, global constrains for the terrestrial reference system, frame transformation according to IERS Conventions 2010, higher order ionospheric corrections and improvements in the parameterization of the solar radiation pressure model. In this paper the influence of all these modelling improvements on the accuracy of the GPS orbits is presented. It is shown, that the application of the new models reduced the mean 3D difference of our orbits from 7.76 to 3.01 cm when compared to IGS final orbits.

Keywords GPS orbits · Modelling improvements

2.1 Reference Processing

To demonstrate the impact of the modelling improvements we started from the GPS orbits generated using modelling standards close to that used in the Release 04 (or RL04) of the GFZ GRACE gravity field modelling (Flechtner et al. 2010). These orbits were generated using EPOS-OC (Earth Parameter and Orbit System—Orbit

G. Michalak (✉) · D. König · K.H. Neumayer · Ch. Dahle
GFZ German Research Centre for Geosciences, Telegrafenberg, 14473 Potsdam, Germany
e-mail: michalak@gfz-potsdam.de

Computation module) software package (Zhu et al. 2004) and the applied background models include:

- Earth gravity potential model: EIGEN-6C (Shako et al. 2013),
- Lunar gravity field model: Ferrari (1977),
- Sun, Moon and planets ephemeris: JPL DE421,
- Earth Tide model: Wahr (1981),
- Nutation and precession models: IERS Conventions 2003 (McCarthy and Petit 2004),
- Earth Orientation Parameters (EOP): EOP04C05,
- Ocean Tide model: EOT11 (Savcenko and Bosch 2012),
- Ocean pole tide model: Desai (2002),
- Atmospheric Tide model: Biancale and Bode (2006),
- Relative station antenna phase centre offsets and variations: igs_01.pcv,
- Solar radiation pressure: GPS model ROCK 4 (Fliegel et al. 1992),
- Tropospheric delay estimated with the Vienna Mapping Function 1,
- Empirical periodic accelerations (1/rev), unconstrained cosine and sine in transversal and normal direction,
- Post-Newtonian relativistic corrections, Lense-Thirring and deSitter effect,
- Elevation cut-off angle: $20°$, no elevation dependent weighting,
- Arc length: 26 h (1d $\pm$ 1h),
- GPS data: undifferenced ionosphere-free L3 code and phase combinations
- A-priori standard deviation for GPS code $=$ 250 cm, phase $=$ 2.5 cm,
- Ambiguity fixing: double difference integer wide-lane/narrow-lane ambiguity fixing, constraining combinations of 4 undifferenced L3 ambiguities (Blewitt 1989; Ge et al. 2005) and
- Station coordinates: a-priori coordinates from IGS08 solution with 10-cm constraints.

Parameters which are estimated are the following:

- Satellite initial state vectors,
- Ground station coordinates,
- Global scaling factor and Y-bias of the solar radiation pressure model for each satellite,
- 10 tropospheric scaling factors for each station (every 2.6 h),
- Empirical periodic accelerations, unconstrained cosine and sine in transversal and normal direction, once per revolution,
- Floating L3 ambiguities and
- Satellite and ground station clock offsets.

One month of GPS data collected by a network of ~80 globally uniformly distributed ground stations (June 2008) was selected as a test period, and orbits for all GPS satellites were generated using the modelling standards given above. The orbits were compared next with the International GNSS Service (IGS) final orbits. The daily 3D RMS values, both before and after applying of the ambiguity fixing, are shown in
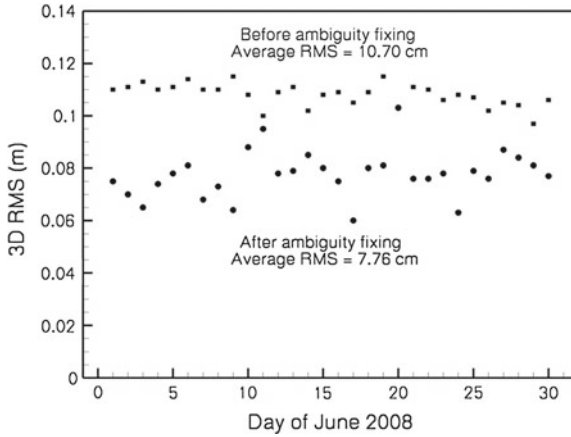
Fig. 2.1 Comparison of the initial RL04 orbits with IGS final orbits. The daily 3D RMS values before applying ambiguity fixing are plotted as *squares*; those after applying ambiguity fixing are plotted as *circles*

Fig. 2.1. The mean values are 10.70–7.76 cm, before and after applying of the ambiguity fixing, respectively. These modelling standards and orbits (denoted hereafter as RL04) are used as a reference for subsequent tests.

2.2 Improvements of the Processing

The modelling standards given in the previous sections for RL04 orbits were next sequentially changed by updating/adding new models. The resulting orbits were again compared with the IGS final orbits. From this comparison the daily RMS values of the 3D position differences ("3D RMS") were obtained, both without and with ambiguity fixing. A table summarizing the results of the modeling improvements will be given in the Sect. 2.2.7.

2.2.1 Phase Wind-Up and the GPS Attitude Model

The corrections due to GPS phase wind-up (Wu et al. 1993) and the GPS attitude model (Bar-Sever 1996; Kouba 2009) were implemented into EPOS-OC and were applied for the RL04 orbits. Additional details of the implementation can be found also in (Michalak and König 2010). The mean 3D RMS value for solution without ambiguity fixing reduced by 0.14 cm from 10.7 cm (Fig. 2.1) to 10.56 cm. For the ambiguity-fixed solution it dropped significantly by 2.03 cm from 7.76 cm (Fig. 2.1) to 5.73 cm.

2.2.2 Improved Ambiguity Fixing

For the original RL04 orbits and orbits from the Sect. 2.1 the ambiguity fixing was done by means of an old external procedure. Since many deficiencies of this procedure were found, a new one was written and applied. The new procedure is essentially based on an approach described in Blewitt (1989) and Ge et al. (2005) but is made more flexible. The ambiguity fixing is performed using the well-known double differenced wide-lane/narrow-lane approach and applying constraints to the combinations of four L3 floating undifferenced ambiguities. The fixing decision for the double differenced ambiguities is based on the fixing probability, in contrast to the old procedure which mainly used simply the difference to the nearest integer. After application of the new ambiguity fixing to orbits from Sect. 2.1 the mean 3D RMS value improved by another 1.5 cm to just 4.24 cm. In all following tests only the new ambiguity fixing procedure was applied.

2.2.3 Absolute Antenna Phase Centre Offset/Variation

The EPOS-OC software was updated to enable application of absolute antenna phase centre offsets and variations for GPS measurements. The relative antenna phase centres were replaced by the absolute ones used by the IGS analysis centres (IGS08.atx file). The 3D RMS for the solution without ambiguity fixing was significantly reduced by 2.65 cm (from 10.56 to 7.91 cm), for ambiguity-fixed solution by 0.4 cm (from 4.24 to 3.84 cm).

2.2.4 No-Net Translation/Rotation/Scale Conditions

In the previous orbits 10-cm constraints are imposed on all a-priori station coordinates (RL04 standards). This constraining scheme originates from operational GPS orbit determination to prevent bad measurements taken at a ground station with reliable station coordinates to destroy the whole solution. By applying individual constraints on the coordinates of each station, however, makes the whole solution overly constrained, as there are maximally seven datum defects possible (three translations, one global scale, three rotations) that should be removed. To make the solution as free as possible on the one hand, and to tighten the solution to the underlying terrestrial reference frame, only No-Net Translation/Scale/Rotation conditions with an a priori sigma of 0.1 mm are imposed over the whole ground station network. This allows each single station moving free but keeping the ground network fixed as a whole. The application of these conditions, in addition to all previous changes improved the ambiguity-free solution by 0.09 cm (from 7.91 to 7.82 cm), the ambiguity-fixed solution improved by 0.17 cm (from 3.84 to 3.67 cm).

2.2.5 *Change of the Observations Weight, Frame Transformations and Applications of Higher Order Ionospheric Corrections*

In the next step the a priori standard deviations for code and phase observations were changed, respectively, from 250 to 2.5 cm (RL04 standards) to 100–1 cm as adopted in the new release 05 (RL05) orbits (Dahle et al. 2012). In addition the frame transformations according to IERS Conventions 2010 (Petit and Luzum 2010) as well as higher order ionospheric corrections (Bassiri and Hajj 1993) were implemented and used. For the ambiguity float solution the daily 3D RMS improved by 0.33 cm (from 7.82 to 7.49 cm); the ambiguity-fixed orbits improved by 0.2 cm (from 3.67 to 3.47 cm). The modelling standards at this point are the same as used for generating the latest RL05 GRACE gravity field models (see Dahle et al. this book).

2.2.6 *Solar Radiation Pressure Model Reparameterization*

It was also found, that the GPS orbit accuracy is significantly sensitive to modelling the solar radiation pressure. In the current version of EPOS-OC only the ROCK-4 model is implemented with the possibility of estimating global scaling factors as well as biases and periodic accelerations in all 3 directions X, Y, and Z of the satellite body fixed system. Up to this point only the global scaling factor and the Y-bias has been estimated. After a series of tests it was found that improvement of the RL05 orbits can be achieved, if the estimation of a bias in Z (radial) direction is added. The average 3D RMS of the ambiguity-free orbits decreased noticeable from 7.49 to 6.89 cm; the ambiguity-fixed solution reduces the RMS from 3.47 to 3.01 cm, i.e. by 0.46 cm. The daily RMS values for these orbits are given in Fig. 2.2.
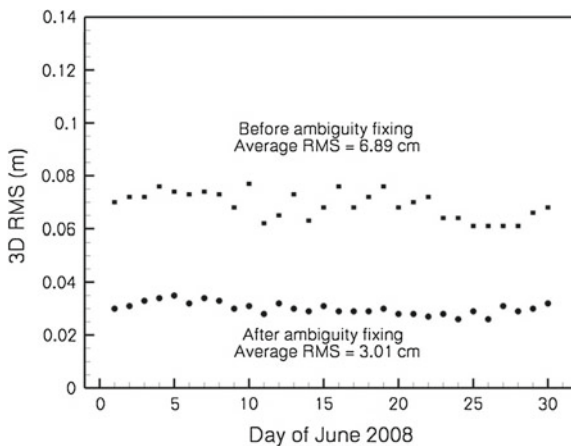
Fig. 2.2 Comparison of the GPS orbits after application of all modelling improvements to IGS final orbits. The daily 3D RMS values before applying ambiguity fixing are plotted as *squares*, those after applying ambiguity fixing are plotted as *circles*

Table 2.1 Cumulative effects of modelling improvements

Modelling characteristics	Without ambiguity fixing	With ambiguity fixing	
	3D RMS before/after Helmert transf. (cm)	3D RMS before/after Helmert transf. (cm)	Code /Phase RMS (cm)
Reference orbits (modelling standards similar to RL04)	10.70/10.47	**7.76** /7.14	60.66/0.689
+ Wind-up + GPS attitude model	10.56/10.27	**5.73** /5.34	60.50/0.666
+ New ambiguity fixing	10.56/10.27	**4.24**/3.96	60.48/0.643
+ Absolute phase center offsets/variations	7.91/7.61	**3.84**/3.62	57.80/0.559
+ No-Net translation/Rotation/Scale conditions	7.82/7.63	**3.67**/3.57	57.81/0.559
+ Weights/frame of RL05, higher-order ionospheric corrections	7.49/7.30	**3.47**/3.38	50.20/0.372
+ Reparameterization of GPS solar radiation pressure model	6.89/6.69	**3.01**/2.91	50.11/0.369

2.2.7 Summary of the Modelling Improvements

The cumulative effect of the modelling improvements applied sequentially as described in previous sections is summarized in Table 2.1.

In this table the 3D RMS values come from the comparison to the IGS final orbits for the solution without and with ambiguity fixing, before and after applying a Helmert transformation. The resulting post-fit code and phase RMS values are also presented there. From analysis of the 3D RMS values for ambiguity-fixed solutions before Helmert transformation (highlighted using bold-type) it can be seen, that the largest impacts come from the application of phase wind-up and the GPS attitude model, the new procedure for ambiguity fixing, absolute phase centre offsets/variations, reparameterization of the solar radiation pressure model, and No-Net Translation /Rotation/Scale conditions.

2.3 Influence of Single Modelling Components on RL05 Orbits

In the previous section the cumulative impact of the modelling components or groups of components on the GPS orbits was presented. In this section more detailed analysis of the influence of a single modelling component on the RL05 orbits is done. For this purpose the RL05 modelling standards (as in Sect. 2.2.5) were taken as a reference and series of test runs were carried out with changing/deactivating only

Table 2.2 Sensitivity of the RL05 orbit accuracy to different modeling components

Changes in modelling	Without ambiguity fixing	With ambiguity fixing		
	3D RMS before/after Helmert tr. (cm)	3D RMS before/after Helmert tr. (cm)	Difference to RL05 orbits (cm)	Code /Phase RMS (cm)
Ref. RL05	7.49/7.30	**3.47**/3.38	–	50.20/0.372
1	7.85/7.60	**6.35**/5.86	+2.88	50.10/0.372
2	10.90/10.68	**4.15**/4.01	+0.68	53.00/0.416
3	7.49/7.20	**4.13**/4.00	+0.66	50.21/0.374
4	6.89/6.69	**3.01**/2.91	−0.46	50.11/0.369
5	7.83/7.34	**3.73**/3.42	+0.26	50.18/0.372
6	7.80/7.62	**3.64**/3.54	+0.17	57.81/0.559
7	7.50/7.31	**3.49**/3.40	+0.02	50.19/0.372
8	7.74/7.46	**3.47**/3.36	0.00	50.24/0.372
9	7.50/7.29	**3.47**/3.39	0.00	50.20/0.372
10	7.49/7.30	**3.47**/3.38	0.00	50.20/0.372
11	7.48/7.29	**3.47**/3.38	0.00	50.19/0.372

The modelling changes applied to the Ref. RL05 orbits are following: (1) No phase wind-up.
(2) Relative instead of absolute antenna phase centres. (3) Old procedure for ambiguity fixing
(3 days failed). (4) Reparameterization of the solar radiation pressure model. (5) Disabling of
No-Net Translation/Rotation/Scale conditions. (6) A-priori Std. Dev. 250/2.5 cm for Code /Phase
(RL04). (7) Frame transformations of RL04 instead of RL05. (8) No GPS attitude model. (9) No
higher order ionospheric corrections. (10) Gravity potential max. degree 12×12 changed to 24×24.
(11) No de-aliasing models

one modelling component. Resulting orbits were compared with IGS final orbits and
the average 3D RMS values were computed. The results are summarized in Table 2.2
where we provide the information on modelling changes, 3D RMS values for the
cases without and with ambiguity fixing applied (both before and after applying
the Helmert transformation), the difference to the reference RL05 RMS values and
the post fit code/phase RMS values. The RMS differences to the RL05 orbits were
computed using values for the cases with ambiguity fixing and before the Helmert
transformation (bold-type in Table 2.2). The results presented in Table 2.2 are sorted
with decreasing absolute value of the difference, e.g. the modelling components
having largest impact are given in the top of the table. Analysis of the results allows
drawing the following conclusions:

- The largest impact on the accuracy of the GPS orbits has the application of phase
  wind-up corrections, while the influence of the GPS attitude model turned out
  to be negligible. Also large impact has the application of absolute phase centre
  offsets/variations to the GPS sender and receiver antennas, the improved procedure
  of ambiguity fixing, the reparameterization of the ROCK-4 solar radiation pressure
  model and the application of No-Net Translation/Scale/Rotation constraints.
- Noticeable total impact of the three following components: changing the a-priori
  weights of code and phase observations, frame transformations according to the

IERS Conventions 2010 and applying higher-order ionospheric corrections (see Table 2.1) comes mainly from the first of these components. The RL04 weights resulted in 50 % increase in the phase RMS value (from 0.372 to 0.559 cm) but did not translate into comparable large degradation of the orbit accuracy (only 0.17 cm, i.e. about 5 %). The impact of the application of higher-order ionospheric corrections turned out to be negligible. The maximum orbit difference was found to be on the level of 1.5 mm what is in contrast to 1.6 cm reported in Fritsche et al. (2005) using the Bernese software. This issue requires further investigation.

- No impact was found when increasing the degree and order of the background gravity potential expansion or taking into account the short term atmospheric and oceanic mass variations (GRACE de-aliasing products, Flechtner 2007). This is due to large distance of the GPS satellites from the Earth surface.

2.4 Summary

During the last years GFZ has achieved remarkable improvement in the quality of its GPS orbits used for a variety of applications (e.g. Earth gravity field modelling, processing of LEO radio occultation data, precise LEO baseline determination, integrated approach for estimating terrestrial reference system parameters) by implementing a number of new models and standards. It was found that the modelling improvements (see Table 2.1) reduced the average 3D RMS of the differences to IGS final orbits by 60 %, from 7.76 to 3.01 cm. The largest impact has the application of phase wind-up corrections (improvement by 2 cm), the new procedure for ambiguity fixing (1.5 cm), the absolute antenna phase centre offsets/variations (0.4 cm), the No-Net Translation/Scale/Rotation conditions (0.2 cm), the change of observation weighting (0.2 cm), and improved modelling of the solar radiation pressure (0.5 cm). No influence was found when increasing the resolution of the gravity field, using GRACE de-aliasing models, the GPS attitude model and higher-order ionospheric corrections. The lack of the influence of the last component needs future investigations.

References

Bar-Sever YE (1996) A new model for GPS yaw-attitude. JoG 70:714–723

Bassiri S, Hajj G (1993) Higher-order ionospheric effects on the global positioning system observables and means of modeling them. Manuscr Geod 18:280–289

Biancale R, Bode A (2006) Mean annual and seasonal atmospheric tide models based on 3-hourly and 6-hourly ECMWF surface pressure data. Scientific Technical Report. STR 06/01, GeoForschungsZentrum, 33

Blewitt G (1989) Carrier phase ambiguity resolution for the global positioning system applied to geodetic baselines up to 2000 km. J Geophys Res 94/B8:10187–10203

Dahle Ch, Flechtner F, Gruber C, König D, König R, Michalak G, Neumayer KH (2012) GFZ GRACE level-2 processing standards document for level-2 product release 0005, (Scientific Technical Report - Data, 12/02), Revised Edition, January 2013), Potsdam, 21 p. doi:10.2312/GFZ.b103-1202-25

Desai S (2002) Observing the pole tide with satellite altimetry. J Geophys Res 107(C11):3186. doi:10.1029/2001JC001224

Ferrari AJ (1977) Lunar gravity: a harmonic analysis. J Geophys Res 82(20):3065–3084. doi:10.1029/JB082i020p03065

Flechtner F (2007) AOD1B product description document for product releases 01 to 04 (Rev. 3.1). GRACE project document 327–750. http://isdc.gfz-potsdam.de/

Flechtner F, Dahle Ch, Neumayer KH, König R, Förste Ch (2010) The release 04 CHAMP and GRACE EIGEN gravity model. In: Flechtner et al (ed) System earth via geodetic-geophysical space techniques, Adv. technologies in earth sciences, Springer, Berlin. doi:10.1007/978-3-642-10228-8_4

Fliegel HF, Gallini TE, Swift ER (1992) Global positioning system radiation force model for geodetic applications. Geophys Res Let 97(B1):559–568

Fritsche M, Dietrich R, Knoefel C, Ruelke A, Vey S, Rothacher M, Steigenberger P (2005) Impact of higher-order ionospheric terms on GPS estimates. Geophys Res Lett 32(L23311). doi:10.1029/2005GL024342

Ge M, Gendt G, Dick G, Zhang FP (2005) Improving carrier-phase ambiguity resolution in global GPS network solutions. JoG 79(1–3):103–110. doi:10.1007/s00190-005-0447-0

Kouba J (2009) A simplified yaw-attitude model for eclipsing GPS satellites. GPS Solut 13:1–12

McCarthy DD, Petit G (eds.) (2004) IERS Conventions (2003). IERS Technical Note 32, Frankfurt am Main: Verlag des Bundesamts für Kartographie und Geodäsie. ISBN 3-89888-884-3, http://www.iers.org/TN32. Accessed 20 March 2012

Michalak G, König R (2010) Improvements for the CHAMP and GRACE observation model. In: Flechtner F, Gruber T, Güntner A, Mandea M, Rothacher M, Schöne T, Wickert J (eds) System earth via geodetic-geophysical space techniques. Springer, pp 29–39. doi:10.1007/978-3-642-10228-8_3

Petit G, Luzum B (eds) (2010) IERS Conventions 2010. IERS Technical Note 36; Frankfurt am Main: Verlag des Bundesamts für Kartographie und Geodäsie. ISBN 3-89888-989-6. http://www.iers.org/TN36. Accessed 20 March 2012

Savcenko R, Bosch W (2012): EOT11a - empirical ocean tide model from multi-mission satellite altimetry. Report No. 89, Deutsches Geodätisches Forschungsinstitut, München

Shako R, Förste Ch, Abrikosov O, Bruinsma S, Marty JC, Lemoine JM, Flechtner F, Neumayer KH, Dahle Ch (2013) EIGEN-6C: A high-resolution global gravity combination model including GOCE data. In: Flechtner F et al. (eds.) Observation of the system earth from space - CHAMP, GRACE, GOCE and future missions, advanced technologies in earth sciences, Springer, Berlin

Wahr J (1981) Body tides on an elliptical, rotating, elastic and oceanless earth. Geoph J Inter 64(3). doi:10.1111/j.1365-246X.1981.tb02690.x

Wu JT, Wu SC, Hajj GA, Bertiger WI, Lichten SM (1993) Effect of antenna orientation on GPS carrier phase. Manusc Geod 18:91–98

Zhu S, Reigber Ch, König R (2004) Integrated adjustment of CHAMP. GRACE and GPS Data JoG 78(1–2):103–108

Chapter 3
Using Accelerometer Data as Observations

Karl-Hans Neumayer

Abstract By established convention, non-gravitational accelerations measured on-board satellites are not treated as genuine observations in the "observed minus computed" sense, like other data types. Instead, they appear as an additional perturbation on the right hand side of satellite dynamics and accelerometer calibration factors (scaling, biases) play the role of dynamical parameters. The more logical method would be to treat them conceptually in the same manner as other kinds of measurements, like SLR (satellite laser ranging), GPS or inter-satellite ranging. This alternative method has been investigated and compared to the conventional method. Benefits and disadvantages are discussed and the performance of the conventional and the new method is assessed in the context of gravity field recovery, for a simulated scenario and using real-world CHAMP and GRACE mission data.

3.1 Introduction

In the context of gravity field recovery, modern satellites such as CHAMP (Reigber et al. 2002), GRACE (Tapley et al. 2004) and GOCE (Rummel et al. 2002) carry on-board accelerometers. In combination with star tracker data it is thus possible to provide measured surface accelerations in the inertial frame for orbit integration and to separate non-conservative from conservative forces.

Parameter adjustment from measurement data runs along the well-established "observed minus computed" routine. From the actual observation data, a modeled observation is subtracted that depends on parameters. The "true" values of those parameters are not known; therefore the difference (residuals) is nonzero. A linearization process yields the design equations, which are transformed into normal equations in

---

K. H. Neumayer (✉)
GFZ German Research Centre for Geosciences, Department 1, Geodesy and Remote Sensing, Münchner Str. 20, 82234 Oberpfaffenhofen, Germany
e-mail: neumayer@gfz-potsdam.de

order to obtain corrections in the parameters. This is the classical approach for various geodetic measurement types such as satellite laser ranging (SLR), GPS, altimetry or inter-satellite ranging.

Somewhat surprisingly, the prevailing method to process satellite on-board accelerations is significantly different. After a pre-processing step of the "raw" data that amounts to closure of data gaps, outlier removal or re-sampling, the acceleration vector is inserted "as is" into the right hand side of the differential equation of satellite motion. It replaces the "classically" used sum of modeled surface accelerations: air drag, solar radiation pressure and albedo. The adjustable parameters the acceleration vector depends on, namely biases and scaling factors, take the role of dynamical parameters of satellite motion. An observation equation for the observation type "surface acceleration" does not exist in this approach. In the following, we will call this the "conventional method".

The more intuitive procedure would be the above-mentioned "observed minus computed" adjustment technique. The "observed" part comprises the measured on-board accelerations. The "computed" part is the sum of modeled values for air drag, solar radiation pressure and albedo. In the accelerometer observation equation, two types of solve-for parameters appear. First, the accelerometer calibration factors (scaling, biases). Second, scaling factors separately for air drag, radiation pressure and albedo. On the right-hand side of the satellite differential equations, the surface accelerations are *not* the measured values, but rather the sum of the models for air drag, solar radiation pressure and albedo. Despite the fact that this approach is more logical than the established conventional method, it was apparently never seriously investigated. We will do this here, and show its benefits and impacts in the context of gravity field recovery.

The conventional method of real accelerometer data processing has of course clear advantages. Satellite dynamics are much simpler, as the only dynamical parameters the surface accelerations depend on are the accelerometer biases and scale factors. Also, e.g. modeled air drag is only as good as the models for the underlying air densities, and there are effects that cannot be properly represented by models at all. An example would be rapid density variations around the poles, where ionized particles collide with molecules of the upper atmosphere (polar light crown).

However, there are many points that are more appropriately addressed by the alternative method proposed here. The most important are the following:

- Handling of measurement noise: In the conventional approach, we suppose that there is no noise at all. If this is not true, the formal accuracies of the solved parameters obtained from the overall adjustment are too optimistic.
- Handling of data gaps: As the accelerometer data vector is inserted "as is" into the right hand side of the equation of motion of the satellite, a stream of gapless data must exist on the integration time grid. If the accelerometer has severe data gaps the consequence is a cumbersome cutting of the integrated orbital arcs.
- The measured surface accelerations must be 3D vectors in the conventional approach, as they appear directly on the right hand side of the satellite dynamics. In the alternative setting, we have no original accelerometer data in the satellite

dynamics, but only model forces, thus it plays no role if we observe e.g. the along-track channel alone. A good example for that is CHAMP. Here the radial channel of the accelerometer is essentially flawed. It would be desirable in that case to have the liberty to entirely omit the radial channel, and to use only along-track and cross-track values.

In the following, we show how the alternative method performs in the context of gravity field recovery when compared with the conventional method. In order to see what we can gain in ideal conditions, we first discuss a simulated GRACE-like scenario (two tandem satellites, GPS and K-band Satellite-to-Satellite (SST) tracking) first. We will then look at real-world examples for CHAMP and GRACE.

3.2 Test of the Alternative Method in a Simulated Environment

A first assessment of the new approach was obtained with the simulation of a GRACE-like configuration: two coplanar satellites with on-board GPS receivers, accelerometers and star trackers connected by a microwave inter-satellite link. The time horizon of the simulation was 28 days and was realized in the following way:

- The orbit elements at the begin of the integration were chosen such that the initial orbit heights were about 350 km, the along-track separation 200 km and the inclination of the orbit plane 89°.
- Both satellites were integrated with a step size of 5 s over the whole 28 days. The simulated surface accelerations were the sum of the three model components
  - DTM air drag model by Barlier (Berger et al. 1998),
  - Solar radiation pressure model with a shadow transition function, and
  - The Knocke albedo model (Knocke 1989).
- Furthermore, simulated star tracker data were derived from nominal attitude (yaw steering) in the form of "attitude quaternions".
- Orbital, surface acceleration and attitude quaternion data sets were then divided into 28 batches of one day length, and the one-day LEO (low earth orbiter) orbits were combined with real-world GPS SP3 files to generate artificial GPS code and phase as well as K-band range rate measurements. All data were endowed with appropriate measurement noise of 30 and 3 mm rms for GPS code and phase, respectively, and 0.05 μm/s rms for the K-band link.
- Simulated (from modeled values) accelerometer data were provided alternatively with noise-free as well as with 10^{-9} m/s^2 noise on all three channels (radial, along-track, cross-track).

In the recovery step, the one-day batches of simulated data were fed to LEO screening orbits of one day length each. First, with the parameters of the initial gravity field fixed, the LEO orbits were adjusted to fit the measurements as close as possible. Second, arc-wise normal equations, now with gravity field expansion

coefficients free, were produced and added, and the resulting normal equation was inverted. For the derived adjusted gravity field degree variances (per degree) of the geoid differences versus the "true" gravity field of the simulation were computed and plotted in order to assess the quality of the solution.

To test the new method versus the established method, several recovery scenarios were realized.

1. The conventional recovery strategy, with noise-free simulated accelerometer data. Accelerometer biases and scaling factors were estimated for all three spatial directions. Both scaling factors and biases were linear functions with one solve-for parameter at the beginning and one at the end of the arc.
2. The conventional recovery strategy, however with noise added to all three spatial channels of the accelerometer data.
3. Recovery with accelerometer measurements according to the new method. On the right hand side of the satellite dynamics, the surface forces are provided by models, and the model parameters are adjusted (indirectly) from the GPS and the K-band measurements and (directly) from the accelerometer data. In addition to the calibration factors for the accelerometers, one scaling factor each for the air drag, the solar radiation pressure and the albedo models for both satellites were adjusted.
4. Recovery according to the new method, however not for all three spatial channels, but only using the along-track channel of the on-board accelerometers.

The results of recovery scenarios 1 and 2 are depicted in Fig. 3.1. It is quite obvious that the conventional recovery method cannot cope appropriately with noise on the accelerometer data. The error degree variance curve for the noisy-data case is more than an order of magnitude above the curve for noise-free data.
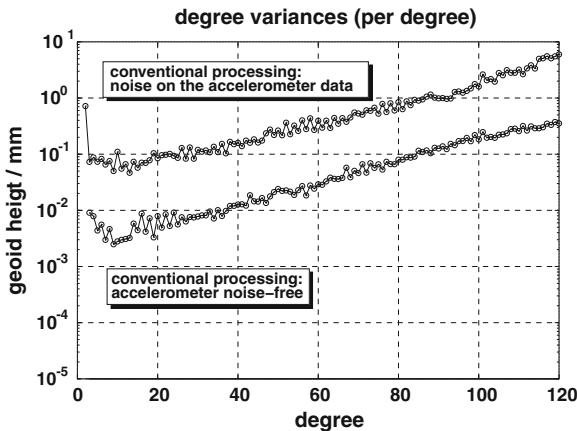
Fig. 3.1 Degree variances of the differences between the recovered and the true gravity field in the simulated GRACE scenario. In both cases, the adjustment procedure is the same. The *upper curve* results if white noise of 10^{-9} m/s^2 rms is added to the accelerometer data
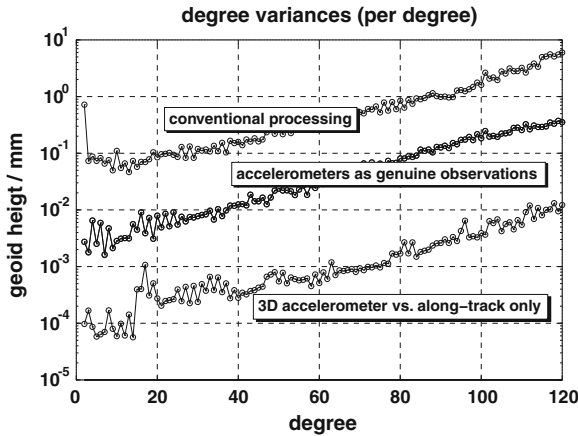
Fig. 3.2 Degree variances of the difference between true and recovered gravity field (*upper two curves*) and of the difference between the scenarios where the whole 3D surface acceleration vector and only the along-track channel has been processed (*lowermost curve*). Note that the *middle curve* actually is made of two curves superimposed so closely that they cannot be separated visually (see text)

The uppermost curve in Fig. 3.2 is the same as the upper curve in Fig. 3.1 showing the conventional recovery with noisy accelerometer data. The middle curve in Fig. 3.2 results from the alternative method. By treating accelerometer measurements as genuine observations, the noise on the accelerometer data is taken into account in the correct manner, and the curve of error degree variances is lowered almost to the level of the case where the recovery has been performed with the conventional method with noise-free accelerometer data. Actually, in the middle we have two curves, namely for the case where all three spatial components of the accelerometer data vector are observed as well as the case where only the along-track channel is processed. Both curves are so close that they appear as one, however they actually differ. The lowermost curve is the degree variance plot of their difference. We may therefore conclude that most of the information about the surface forces is contained in the along-track channel alone.

A notable disadvantage of the alternative processing method is a considerable increase in processing time. As accelerometer data feature as genuine observations, they appear in the budget of data that have to be processed, and their number can be considerable. Whereas we have, for both satellites, some 40000 GPS measurements with 30 s data step size, and 17280 K-band 5-second range rate data per day, we can expect, at a integration step size of 5 s, for 3 spatial measurement channels and two satellites, (86400/5) times 3 times 2 = 103680 additional (accelerometer) measurements per arc in addition to the original 57000 GPS and K-band observations. The situation is somewhat ameliorated when only the along-track channel is processed. The additional data amount here to some 35000 per day. Still, this is almost as much

as the number of GPS data alone, so even in this case we can expect the processing time to be two times as long as for the conventional technique.

3.3 Test of the Alternative Method with Real-World CHAMP Data

One month (August 2008, containing 29 usable days) of CHAMP GPS and accelerometer data were processed according to the standards of the GRACE release 05 products (Dahle et al. 2012) along the lines of the conventional and the alternative method. There were altogether 583103 GPS code/phase observations (30 s step size) and 751680 accelerometer measurements (3 axes with 10 s step size). For the alternative method, only the along-track accelerometer channel was observed, resulting in 250560 measurements of the type "surface acceleration" in addition to the GPS data. For the alternative method, the rms value of the adjusted surface acceleration model data to the observed data was around $5.5 \cdot 10^{-9}$ m/s^2, which conforms well to the nominally reported $3 \cdot 10^{-9}$ m/s^2 accuracy of the CHAMP accelerometer (Grunwaldt and Meehan 2003).

The adjustable parameters for the conventional method were chosen as follows:

- Two accelerometer scaling factors per day in every spatial direction.
- Accelerometer radial biases: 40 min step size (approximately one half-revolution).
- Accelerometer cross/along-track biases: 93 min step size (one per orbit)
- Thruster misalignment parameters.
- Empirical accelerations in the radial direction: once-per-rev cosine and sine terms.

The many parameters for the radial channel are necessary as the accelerometer data of that channel are known to be inherently flawed for CHAMP (Perosanz et al. 2003; Loyer et al. 2003).

For the alternative processing method, the surface acceleration was assumed to be the sum of the three model components:

- Jacchia-Bowman air drag model 2008 (Bowman and Tobiska 2008)
- A solar radiation pressure model with a shadow transition function
- The Knocke albedo model (Knocke 1989)

From all three model accelerations, only the air drag and the solar radiation parts were endowed with adjustable scaling factors:

- The air drag scaling factor is a time-dependant polygon with 3 min step size.
- The solar radiation pressure is scaled by one global parameter.

Figure 3.3 shows the degree variances of the differences of the gravity field solutions of the conventional and the alternative method versus the static gravity field ITG-Grace 2010 (Mayer-Gürr et al. 2010).

The alternative method is obviously capable to reproduce the results of the conventional method using only one third of the accelerometer data (along-track), albeit
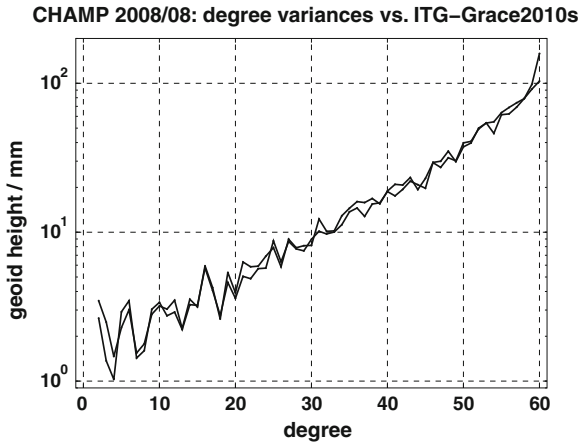
Fig. 3.3 Degree variances of the differences between adjusted CHAMP gravity fields and the ITG-Grace2010s static gravity field. The two close and nearly coinciding curves correspond to the conventional and the alternative recovery method

at the expense of increased processing time and an increase of arc-specific parameters: for the air drag model scaling factors were estimated all three minutes, resulting in 480 additional parameters per day.

3.4 GRACE Scenario with Real Data

The results of the same month (August 2008, with 31 usable days) are presented here analyzing GRACE data according to the standards of the GRACE release 5 products (Dahle et al. 2012). The gravity field adjustment is based on 1019610 GPS code/phase measurements and 492631 K-band range-rate inter-satellite observations, as well as 2977776 measurements of the on-board accelerometers (2 satellites, 3 spatial axes, 5 s sampling). The calibration of the accelerometers was handled such that the scaling factors were fixed to one, and biases were estimated with a step size of one hour. The measured surface accelerations were modeled as a sum of air drag, solar radiation pressure, Earth albedo and revolution-periodical empirical accelerations in all three spatial directions. The models for air drag and albedo are almost the same as in the CHAMP case. We estimated scaling factors for solar radiation pressure and air drag; the former globally, the latter as a polygon with 6 h stepping size. Furthermore, we estimated cosine/sine amplitudes for the empirical accelerations, with frequencies of 1/rev and 6/rev. The amplitudes of the former were assumed to be polygons with 45 min stepping size, the latter to be polygons with 15 min step size.

Again the new method is capable to produce an adjusted gravity field with a quality that is at least as high as the one achieved with the conventional method, as can be

GRACE 2008/08: degree variances vs. ITG–Grace2010s
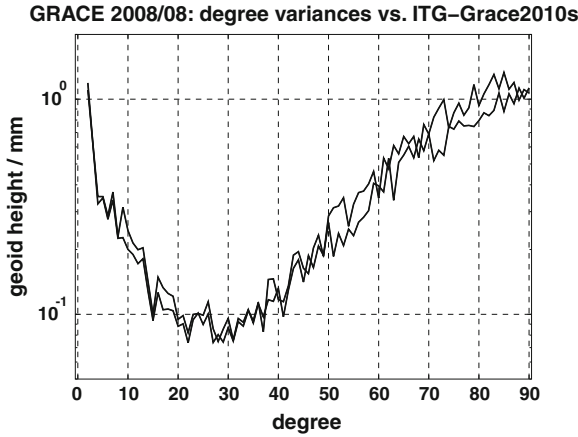
Fig. 3.4 Degree variances of the difference compared to the static model ITG-Gace2010, for the conventional and the alternative recovery method. Both curves have not been separately labeled, as they almost coincide

seen in Fig. 3.4. From the way how the measured surface accelerations are modeled it can be inferred that for every arc of one day length we have 1548 auxiliary solve-for parameters. Thus the inflation of the parameters vector inherent to the alternative method stays within reasonable limits.

3.5 Conclusions

The established method for the processing of satellite on-board accelerometer measurements has been compared with a novel approach that fits logically more into the framework of the general treatment of measurement data. The method has been assessed in the context of gravity field recovery. Results have been presented for a simulated GRACE-like scenario as well as for a month of real-world GRACE and CHAMP data. It has been established that the method copes correctly with noisy accelerometer measurements, which is not the case for the conventional method. In the real-world case it can at least produce adjusted gravity fields of the same quality level as the established approach. It has been demonstrated that for the alternative method, it is not necessary to process the entire three-dimensional surface acceleration vector; instead using the along-track channel alone is sufficient. Disadvantages are a certain increase of arc-specific parameters and a growth of processing time, but both are in a range that can be handled. The results all in all are somewhat sobering, as it was not possible to surpass the performance of the conventional approach, however, there is some promise that this can be achieved by further investigation of alternative parameterization of the surface acceleration models and by dedicated

techniques for de-correlation of the gravity field parameters on the one hand and the arc-wise dynamical parameters on the other.

References

Berger C, Biancale R, Ill M, Barlier F (1998) Improvement of the empirical thermospheric model DTM: DTM-94- comparative review on various temporal variations and prospects in space geodesy applications. J Geodesy 72(3):161–178

Bowman B, Tobiska WK (2008) A new empirical thermospheric density model JB2008 using new solar and geomagnetic indices, AIAA/AAS astrodynamics specialists conference, 18–21 August 2008, Honolulu

Dahle Ch, Flechtner F, Gruber C, König D, König R, Michalak G, Neumayer KH (2012) GFZ GRACE Level-2 processing standards document for level-2 product release 0005, (Scientific Technical Report - Data, 12/02, Revised Edition, January 2013), Potsdam, 21 p. doi:10.2312/GFZ.b103-1202-25

Grunwaldt L, Meehan TK (2003) CHAMP orbit and gravity instrument status. In: Reigber C, Lühr H, Schwintzer P, Wickert J (eds) Earth observation with CHAMP—results from three years in Orbit, Springer

Knocke PC (1989) Earth radiation pressure effects on satellites, dissertation presented to the faculty of the graduate school of the University of Texas at Austin, in partial fulfillment of the requirements for the degree of doctor of philosophy, The University of Texas at Austin

Loyer S, Bruninsma S, Tamagnan D, Lemoine JM, Perosanz F, Biancale R (2003) STAR accelerometer contribution to dynamic orbit and gravity field model adjustment. In: Reigber C, Lühr H, Schwintzer P, Wickert J(eds) Earth observation with CHAMP—results from three years in Orbit, Springer

Mayer-Gürr T, Kurtenbach E, Eicker A (2010) ITG-2010, http://www.igg.uni-bonn.de/apmg/index.php?id=itg-grace2010, last visited 2012/08/20

Perosanz F, Biancale R, Loyer S, Lemoine JM, Perret A, Touboul P, Foulon B, Pradels G, Grunwald L, Fayard T, Vales N, Sarrailh M (2003) On board evaluation of the STAR accelerometer. In: Reigber C, Lühr H, Schwintzer P, Wickert J (eds) Earth observation with CHAMP—results from three years in Orbit, Springer

Reigber Ch, Luehr H, Schwintzer P (2002) CHAMP mission status. Adv Space Res 30(2):129–134

Rummel R, Balmino G, Johannessen J, Visser P, Woodworth P (2002) Dedicated gravity field missions—principles and aims. J Geodyn 33:3–20. doi:10.1016/S0264-3707(01)00050-3

Tapley BD, Bettadpur S, Watkins M, Reigber C (2004) The gravity recovery and climate experiment: Mission overview and early results. Geophys Rea Lett 31:9607-+. doi:10.1029/2004GL019920

Chapter 4
GFZ RL05: An Improved Time-Series of Monthly GRACE Gravity Field Solutions

Christoph Dahle, Frank Flechtner, Christian Gruber, Daniel König, Rolf König, Grzegorz Michalak and Karl-Hans Neumayer

Abstract After publishing its release 04 (RL04) time-series of monthly GRACE gravity field solutions starting end of 2006, GFZ has reprocessed this time-series based on numerous changes covering reprocessed instrument data, observation and background models as well as updated processing environment and standards. The resulting GFZ RL05 time-series features significant improvements of about a factor of two compared to its precursor. By analyzing 72 monthly solutions for the time span 2005 till 2010, a remarkable noise reduction and a noticeably higher spatial resolution become obvious. The error level has significantly decreased and is now only about a factor of six above the pre-launch simulated baseline accuracy. GFZ RL05 solutions are publically available at ISDC and PO.DAAC archives.

4.1 Introduction

As part of the GRACE Science Data System (SDS) the German Research Centre for Geosciences (GFZ) has been processing its release 04 (RL04) time-series of GRACE gravity field solutions since end of the year 2006 (Flechtner et al. 2010). This time-series has been widely used by scientists worldwide to investigate various time-varying mass variation signals in the system Earth such as the continental hydrological cycle, ice mass change in Antarctica and Greenland, surface and deep ocean currents or secular effects induced by Glacial Isostatic Adjustment (GIA). As a matter of fact, the error level of the RL04 time-series is still about a factor of 15 above the pre-launch simulated baseline accuracy derived by Kim (2000). This is caused by errors and degradations due to inaccurate background models or instrument data processing. Most evidently, this becomes visible by spurious striping artefacts in the

C. Dahle (✉) · F. Flechtner · C. Gruber · D. König · R. König · G. Michalak · K. H. Neumayer
GFZ German Research Centre for Geosciences, Department 1, Geodesy and Remote Sensing,
Münchner Str. 20, 82234 Oberpfaffenhofen, Germany
e-mail: dahle@gfz-potsdam.de

monthly solutions, which have to be filtered by the users before further analysis. In the framework of the LOTSE-CHAMP/GRACE project (Flechtner 2013), numerous investigations regarding observation and background models as well as processing environment and standards have been performed which led to a complete reprocessing of the whole GRACE mission published as GFZ RL05 (Dahle et al. 2012). This paper gives a short overview of the changes and improvements going from RL04 to RL05.

4.2 Changes in Observation Models

In parallel to preparing a new Level-2 (gravity field solution) release, also the generation of a new Level-1B instrument data release (Kruizinga 2012) has been subject within the GRACE SDS. For the generation of the GFZ RL05 time-series the following observations based on this new Level-1B RL02 dataset are used:

- GPS high-low Satellite-to-Satellite (SST) observations (GPS1B)
- K-Band low-low SST range-rate (KBRR) observations (KBR1B)
- Accelerometer observations (ACC1B)
- Star camera observations (SCA1B)

All relevant changes in the handling and processing of these observations are described in the subchapters below.

4.2.1 GPS Data

GPS observations are an essential part in the generation of GRACE gravity field models as they significantly contribute to the determination of long wavelength structures. In the so-called 2-step approach based on the dynamic method (further details are given in e.g. Reigber et al. 2005) which is applied at GFZ the first step comprises the computation of precise GPS orbit and clock solutions which serve as reference frame in the second step, the adjustment of the GRACE satellite orbits, where the GRACE GPS-SST observations are adopted. Compared to the RL04 processing, several improvements in the GPS orbit and clock determination such as phase wind-up correction, GPS attitude model, absolute antenna phase center corrections and an improved integer ambiguity fixing method have been implemented; details can be found in Michalak et al. (2013). Furthermore, the reprocessed GPS constellation for RL05 provides a reference frame consistent with the IGS08 realization of the International Reference Frame 2008 (ITRF2008, http://itrf.ensg.ign.fr/ITRF_solutions/2008/). The GPS orbit quality improved significantly by nearly a factor of two when comparing against final International GNSS Service (IGS) products and became much more homogeneous featuring less outliers (Fig. 4.1).
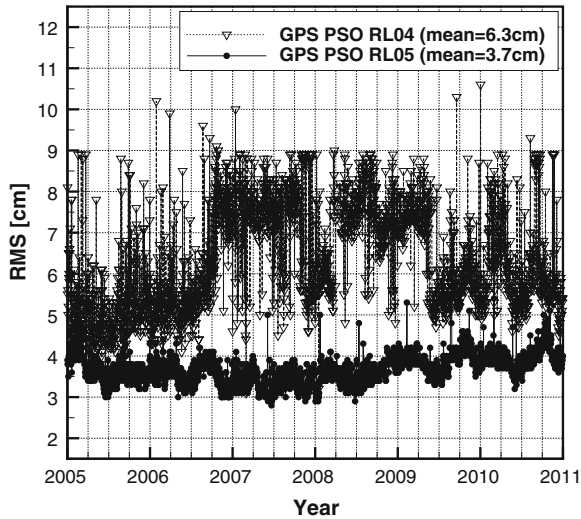
Fig. 4.1 3D Root Mean Square (RMS) of RL04 and RL05 GPS precise orbits with respect to IGS final orbits for the period 01/2005 till 12/2010

In addition to the already mentioned changes, the GRACE GPS-SST observations are now corrected by GFZ-derived antenna phase residual patterns for GRACE-A and –B instead of using the patterns provided by JPL shortly after launch of the GRACE mission.

4.2.2 K-Band Data

By analyzing the spatial distribution of K-Band range-rate (KBRR) observations which have been eliminated in the screening process of the RL04 solutions, it turned out that these eliminations are clearly geographically correlated (Fig. 4.2, left) which is due to un-modeled seasonal and long-term trend gravity field variations. As in the
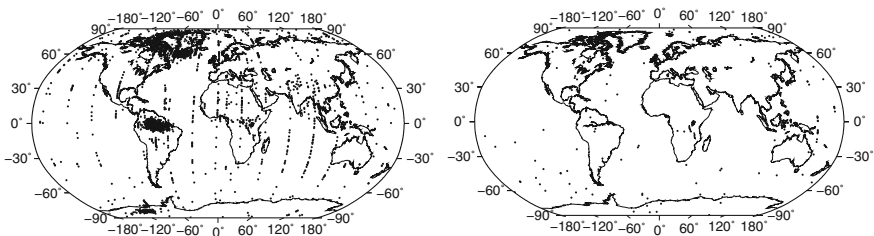
Fig. 4.2 Eliminated KBRR observations for the RL04 (*left*) and RL05 (*right*) 09/2008 solution

RL05 processing such variations are now included a priori in the background models (see Sect. 4.3.1), this effect is now overcome (Fig. 4.2, right). Also in this context, the 3σ elimination criterion for KBRR used so far has become too restrictive and has been widened from 3σ to 8σ.

4.2.3 Accelerometer Data

Following an established way in GFZ's orbit and gravity field determination software, also for GFZ RL05 the accelerometer data are not used as proper observations but directly fed into the right hand side of the differential equation of satellite motion as perturbing accelerations. However, an alternative way using these data as real observations has been developed and is described in Neumayer (2013). No matter which way is chosen, additional accelerometer calibration parameters (scaling factors, biases) have to be solved for. As the RL04-type of parameterization with scales and biases in all 3 directions (along-track, cross-track, radial) estimated only twice (begin and end) per arc is suspected to be insufficient for the generally used arc length of 24 h, the accelerometer parameterization has been reviewed. Analyzing the results of experiments with shorter arc lengths has led to the conclusion that a denser parameterization of accelerometer biases will improve the quality of the gravity field solutions. Based on these results and some further tests, the final choice for RL05 processing has been to estimate accelerometer biases in all three directions every 60 min and, due to this much more dense bias parameterization, to no longer estimate the scaling factors but keep them fixed at their initial value of 1.

4.3 Changes in Background Models

GRACE gravity field time-series are well-known to represent geophysically induced mass variations caused by hydrological, oceanic or cryospheric changes, GIA or large-scale earthquakes (Tapley et al. 2004). Other possible sources of gravity variations such as tides or short-term non-tidal atmospheric and oceanic mass variations are taken into account by the background modeling and thus are not supposed to be contained in the GRACE solutions. However, the latter are degraded by errors present in the applied background models. To overcome these kinds of deficiencies in the GFZ RL05 time-series effectively, the latest available background models are used. A complete overview of changed background models is given in (Dahle et al. 2012). Here we focus on new models for the time-variable gravity field, for ocean tides and for atmosphere and ocean de-aliasing.

4.3.1 Time-Variable Gravity Field Model

So far, in all releases of GFZ GRACE time-series previous to RL05, just the static (i.e. long-term mean) part of the Earth's gravity field has been used as background model, because time variations of gravity are the main subject to be solved for in monthly GRACE gravity field determination. However, as already mentioned in Sect. 4.2.2, this leads to unwanted eliminations of KBRR observations in regions of large gravity field variations. Besides that, the idea of getting closer to geophysical reality during the GRACE orbit integration and parameter estimation process and thus to obtain a better linearization in the adjustment model has triggered the decision to switch to a time-variable gravity field model. In particular, the EIGEN-6C model (Shako et al. 2013) is used which contains time-variable (trend, annual and semi-annual) coefficients till degree and order (d/o) 50. In order to provide solutions with the same information content as mentioned above, the time-variable part of EIGEN-6C is added back following the same philosophy as known from the GAA, GAB, GAC and GAD products (Flechtner 2007). Further details are given in Dahle et al. (2012).

4.3.2 Ocean Tide Model

Concerning ocean tides, the FES2004 model (Lyard et al. 2006) which has been used for GFZ RL04 has been replaced by the EOT11a model (Savcenko and Bosch 2012). Generally, the choice which ocean tide model is used as background model does not significantly affect the global quality of individual GRACE solutions, but regional deficiencies in the models can become visible in time-series analysis. This is shown in Fig. 4.3, where a 161-day (GRACE tidal alias period for S2) fit which has been simultaneously estimated with an annual fit from 6 years of monthly GRACE solutions is displayed. In the GFZ RL04 time-series several artifacts around Indonesia and in the East China Sea show up and indicate problems of the FES2004 model which vanish in the GFZ RL05 time-series. These findings match very well with the findings of Fig. 4.1 in Mayer-Gürr et al. (2012) showing S2 tide residuals of an EOT11a precursor with respect to FES2004.

4.3.3 De-Aliasing Model

To avoid aliasing of short-term non-tidal atmospheric and oceanic mass variations the Atmosphere and Ocean De-aliasing Level-1B product (AOD1B) is used as background model in GRACE processing. Input data for this model are meteorological ECWMF (European Centre for Medium-range Weather Forecast) data for the atmospheric part and output from the Ocean Model for Circulation and Tides (OMCT) for the ocean part (Flechtner 2007). The AOD1B RL04 product used for
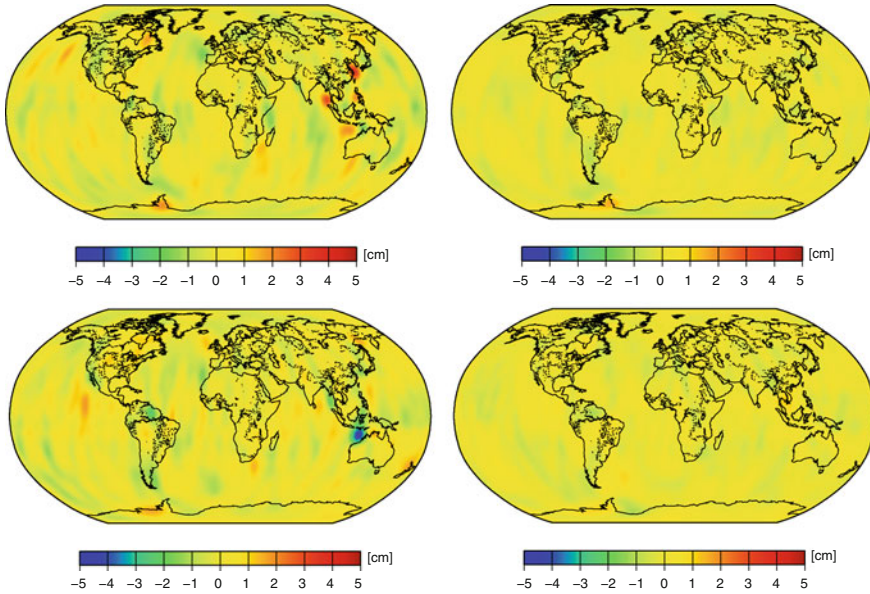
Fig. 4.3 Cosine (*top*) and sine (*bottom*) part of a 161d fit through 6 years (2005–2010) of GFZ RL04 (FES2004) (*left*) and GFZ RL05 (EOT11a) (*right*) solutions (all maps show equivalent water height (EWH), maximum d/o 60, 500 km Gaussian smoothing)

GFZ RL04 is based on an OMCT version as of January 2006, and weaknesses in this product have emerged during the years (e.g. Bonin and Chambers 2011). A recently updated OMCT version with increased spatial (1° regular grid instead of 1.875°, 20 vertical levels instead of 13) and temporal (20 min time step instead of 30 min) resolution plus improved parameterization allowed for the generation of a new AOD1B RL05 product (with the same atmospheric forcing as used in AOD1B RL04) which is now used for GFZ RL05 (Dobslaw et al. 2013). Comparing the influence of using either AOD1B RL04 or RL05 in GFZ RL05 processing, a positive impact of the latter one becomes visible in means of smaller KBRR residuals as well as by a lower noise level of the gravity field solutions.

4.4 Processing Environment and Standards

To allow for a reprocessing of the whole GRACE mission (over 10 years) within an acceptable computational effort, the whole processing environment has been optimized. The key modification has been the move of the normal equation computation from previously used SunOS machines to recently installed LINUX-based high-performance computers (24×3.5 GHz, 96 GB memory) using the OpenMP method for parallelization.

Beside hardware-related changes, also the EPOS (Earth Parameter and Orbit System) software (for some general features of the software system see Zhu et al. 2004) as the main program used for GRACE processing at GFZ has been adapted to be consistent with the latest IERS standards (IERS Conventions 2010, Petit and Luzum 2010). Amongst other items like e.g. the use of DE421 planetary ephemerides or the ITRF2008 reference frame which can be handled by changing input files and auxiliary data the implementation of the following standards have required recoding of the EPOS software:

- the celestial intermediate origin/celestial intermediate pole (CIO/CIP) based transformation between the Earth-fixed and the inertial reference frame of orbit integration,
- the determination of the tropospheric propagation delay for GPS via the Vienna Mapping Function, and
- the higher order ionospheric corrections for GPS measurements.

4.5 Results

At the time of writing, 72 monthly GFZ RL05 solutions covering the period 01/2005 till 12/2010 have already been reprocessed. Compared to GFZ RL04, the maximum resolution has been lowered from d/o 120 to 90. This is due to experiences from RL04 processing where for some months during the 7d-repeat orbit peaked in 12/2009 a maximum d/o of 120 has turned out to be impossible to solve for due to the sparse ground track patterns. Consequently, alternative solutions with maximum d/o 60 have been published. Such inconsistencies in the time-series are now avoided in RL05. It has to be noted that this does not cause any loss in spatial resolution as the high degrees in GRACE solutions are anyway dominated by noise and therefore smoothing has to be applied. In case of even more problematic repeat orbit periods (e.g. 4d-repeat peaked in 09/2004, 3d-repeat peaked in 05/2012), stabilized RL05 solutions up to d/o 90 will be provided.

Large improvements of GFZ RL05 with respect to GFZ RL04 can already be recognized by looking at KBRR and GPS-phase residuals over the six years (Fig. 4.4): the former decrease by $\sim 30\%$ (from 0.34 to 0.23 μm/s), the latter by $\sim 50\%$ (from 0.76 to 0.39 cm), both are now much less scattered. Whereas the structure of the KBRR residuals is correlated with the separation distance between the GRACE satellites, the RL05 GPS phase residuals reveal a clear systematic structure which is subject to be further investigated in the future.

Figure 4.5 shows the improvement from GFZ RL04 to RL05 in terms of accumulated degree variances of calibrated errors. It becomes obvious that the spatial resolution of the RL05 time-series is significantly higher; the level of mm-geoid accuracy is now reached at ~ 350 km resolution (RL04: ~ 525 km). Furthermore, the month-to-month variability of the RL05 errors is much smaller and in contrast to RL04 there are no more outstanding "bad" months visible. The average error level
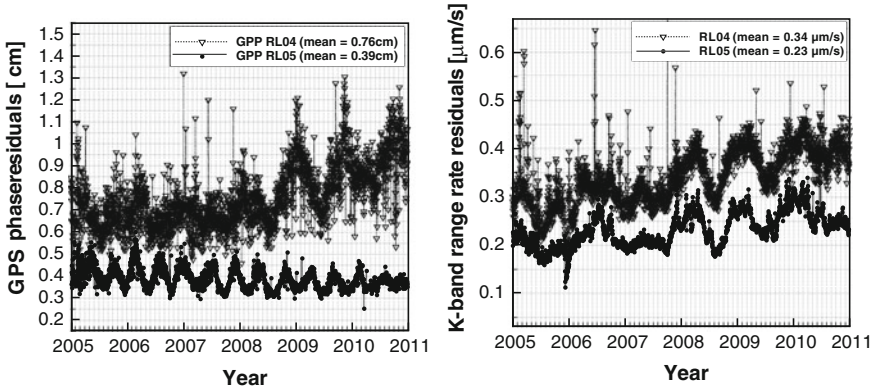
Fig. 4.4 GPS phase (*left*) and KBRR (*right*) RL04 and RL05 residuals for the years 2005–2010
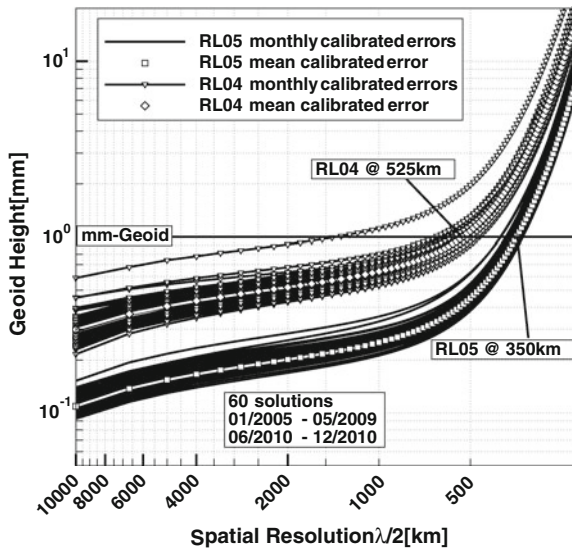
Fig. 4.5 Accumulated calibrated errors of 60 GFZ RL04 and RL05 solutions in terms of geoid height. The months from 06/2009 till 05/2010 are not included due to a 7d-repeat orbit period causing inconsistencies in the RL04 time-series

for RL05 has decreased by ∼50 % and is now only about a factor of 6 (or factor of 7.5 if the maximum d/o would still be 120) above GRACE baseline accuracy (Kim 2000).

In order to get a quality assessment in the spatial domain, weighted RMS (wRMS) values for EWH grids have been computed for both RL04 and RL05 using different versions of the DDK decorrelation filter (Kusche et al. 2009): DDK1 (∼530 km), DDK2 (∼340 km) and DDK3 (∼240 km) with the corresponding Gaussian radius
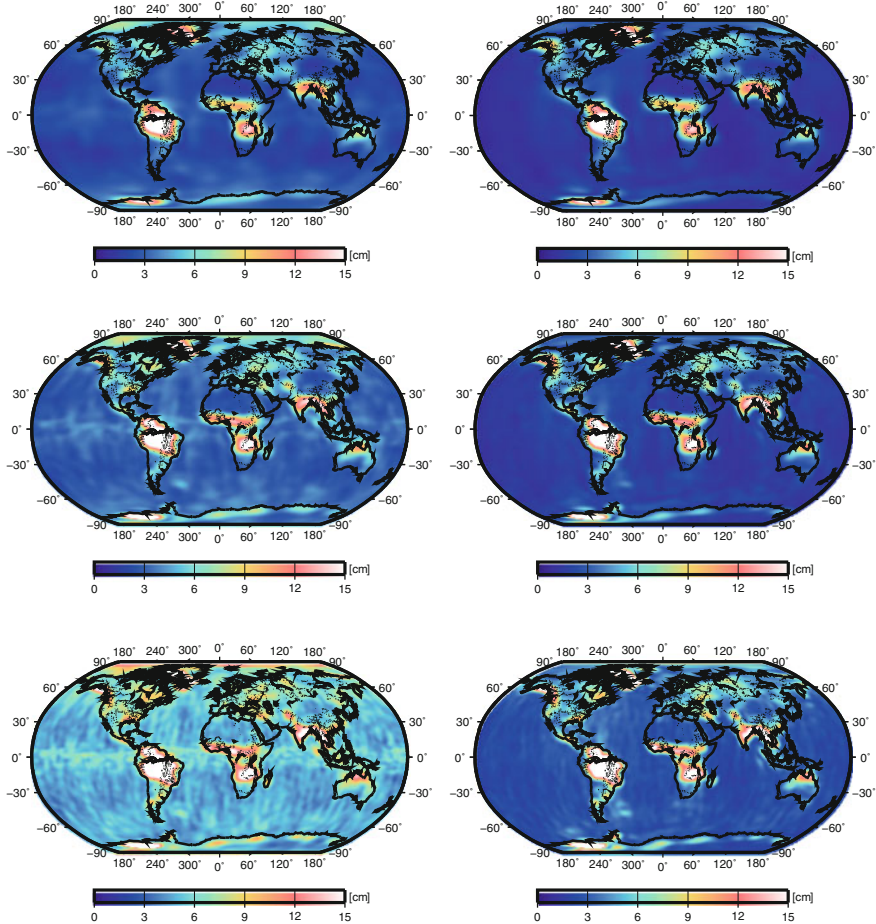
Fig. 4.6 wRMS variability in terms of EWH over 6 years (2005-2010) for GFZ RL04 (*left*) and RL05 (*right*), smoothed with DDK1 (*top*), DDK2 (*middle*) and DDK3 (*bottom*)

given in parentheses (Fig. 4.6). For all cases, the well-known regions of large mass variability (e.g. Amazon basin, Greenland, West Antarctica) are more or less identically visible, however over the oceans or in the Sahara, i.e. regions where much less or almost no variability can be expected, there is much less noise in the new GFZ RL05 time-series. This fact can be observed most impressively for the DDK3-smoothed grids. Looking at the statistics of the wRMS variability for the Sahara region given in Table 4.1 even in case of relatively strong smoothing like with DDK1 a major improvement has been achieved. Both the weighted mean and the wRMS of the wRMS grids for the Sahara have decreased for all versions of DDK filters. Following Table 4.1, the GFZ RL05 accuracy level in terms of EWH is ∼1 cm at a spatial scale of ∼530 km, ∼1.5 cm at ∼340 km or ∼2.5 cm at ∼240 km.

Table 4.1 Statistics of wRMS variability in terms of EWH [cm] for the Sahara region

| Release | Filter version | | | | | |
| | DDK1 | | DDK2 | | DDK3 | |
	wMean	wRMS	wMean	wRMS	wMean	wRMS
GFZ RL04	1.58	0.20	2.45	0.29	4.71	0.54
GFZ RL05	1.13	0.15	1.53	0.21	2.49	0.35

It should be noted that these values are valid for a region of almost no variability and therefore can be considered as an optimistic accuracy boundary. Another conclusion from Table 4.1 is that GFZ RL05 at a spatial scale of ∼340 km is as good as GFZ RL04 at ∼530 km confirming the previous findings from Fig 4.5.

4.6 Summary

An improved time-series of monthly GRACE gravity field solutions has been processed at GFZ. This GFZ RL05 time-series benefits from changes in observation and background models. At the same time, a modified processing environment enables an efficient reprocessing of the whole GRACE mission in acceptable time and consistent with IERS2010 standards. Compared to its precursor RL04, a remarkable improvement of about a factor of two has been achieved showing up already in the observation residuals but more importantly in the new gravity field model time-series in both spectral and spatial domain. A considerable reduction of noise, i.e. less striping artefacts, and a significant gain in spatial resolution are the key features of the new monthly GRACE solutions by GFZ. The GFZ RL05 time-series is available at GFZ's ISDC archive (http://isdc.gfz-potsdam.de/grace) or at JPL's PO.DAAC archive (ftp://podaac.jpl.nasa.gov/allData/grace/L2/GFZ/RL05/) along with their calibrated errors and monthly mean non-tidal mass variation products (GAA, GAB, GAC, GAD; Flechtner 2007).

References

Bonin J, Chambers D (2011) Evaluation of high-frequency oceanographic signal in GRACE data: implications for de-aliasing. Geophys Res Lett 38:L17608. doi:10.1029/2011GL048881
Dahle Ch, Flechtner F, Gruber C, König D, König R, Michalak G, Neumayer KH (2012) GFZ GRACE level-2 processing standards document for level-2 product release 0005, (Scientific Technical Report - Data, 12/02, Revised Edition, January 2013), Potsdam, 21 p. doi:10.2312/GFZ.b103-1202-25

Dobslaw H, Flechtner F, Bergmann-Wolf I, Dahle Ch, Dill R, Esselborn S, Sasgen I, Thomas M (2013) Simulating high-frequency atmosphere-ocean mass variability for de-aliasing of satellite gravity observations: AOD1B RL05. J Geophys Res-Oceans. doi:10.1002/jgrc.20271

Flechtner F (2007) AOD1B product description document for product releases 01 to 04 (Rev. 3.1). GRACE project document 327–750. http://isdc.gfz-potsdam.de/

Flechtner F, Dahle Ch, Neumayer KH, König R, Förste Ch (2010) The release 04 CHAMP and GRACE EIGEN gravity model. In: Flechtner et al. (eds) System earth via geodetic-geophysical space techniques, Adv. technologies in earth sciences, Springer, Berlin. doi:10.1007/978-3-642-10228-8_4

Flechtner F (2013) LOTSE-CHAMP/GRACE: An interdisciplinary research project for earth observation from space. In: Flechtner F et al (eds) Observation of the System Earth from Space - CHAMP, GRACE, GOCE and Future Missions, Advanced Technologies in Earth Sciences, Springer, Berlin

Kim J (2000) Simulation study of a low-low satellite-to-satellite tracking mission. PhD thesis, The University of Texas at Austin, Austin, USA

Kruizinga (2012) L1B V02 reprocessing status and results, Handouts from the GRACE science team meeting 2012, GFZ Potsdam, September 17–19, 2012. http://www.gfz-potsdam.de/en/research/organizational-units/departments-of-the-gfz/department-1/global-geomonitoring-and-gravity-field/topics/development-operation-and-analysis-of-gravity-field-satellite-missions/grace/proceedings-2012/

Kusche J, Schmidt R, Petrovic S, Rietbroek R (2009) Decorrelated GRACE time-variable gravity solutions by GFZ, and their validation using a hydrological model. J Geod 83:903–913. doi:10.1007/s00190-009-0308-3

Lyard F, Lefevre F, Letellier T, Francis O (2006) Modelling the global ocean tides: Modern insights from FES2004. J. Ocean Dyn. doi:10.1007/s10236-006-0086-x

Mayer-Gürr T, Savcenko R, Bosch W, Daras I, Flechtner F, Dahle Ch (2012) Ocean tides from satellite altimetry and GRACE. J Geodyn 59–60:28–38. doi:10.1016/j.jog.2011.10.009

Michalak G, König D, Neumayer KH, Dahle Ch (2013) Improvement in GPS orbit determination at GFZ. In: Flechtner F et al (eds), Observation of the System Earth from Space - CHAMP, GRACE, GOCE and Future Missions, Advanced Technologies in Earth Sciences, Springer, Berlin

Neumayer KH (2013) Using accelerometer data as observations. In: Flechtner F et al (eds) Observation of the System Earth from Space - CHAMP, GRACE, GOCE and Future Missions, Advanced Technologies in Earth Sciences, Springer, Berlin

Petit G, Luzum B (eds) (2010) IERS Conventions (2010) IERS Technical Note No. 36, Verlag des Bundesamts für Kartographie und Geodäsie, Frankfurt am Main, Germany, ISBN 3-89888-989-6, 2010

Reigber Ch, Schmidt R, Flechtner F, König R, Meyer U, Neumayer KH, Schwintzer P, Zhu S (2005) An earth gravity field model complete to degree and order 150 from GRACE: EIGEN-GRACE02S. J Geodyn 39(1):1–10. doi:10.1016/j.jog.2004.07.001

Savcenko R, Bosch W (2012) EOT11a—empirical ocean tide model from multi-mission satellite altimetry. Report No. 89, Deutsches Geodätisches Forschungsinstitut, München

Shako R, Förste Ch, Abrikosov O, Bruinsma S, Marty JC, Lemoine JM, Flechtner F, Neumayer KH, Dahle Ch (2013) EIGEN-6C: A high-resolution global gravity combination model including GOCE data. In: Flechtner F et al (eds) Observation of the System Earth from Space - CHAMP, GRACE, GOCE and Future Missions, Advanced Technologies in Earth Sciences, Springer, Berlin

Tapley BD, Bettadpur S, Ries JC, Thompson PF, Watkins MM (2004) GRACE measurements of mass variability in the earth system. Science 305:503–506. doi:10.1126/science.1099192

Zhu S, Reigber Ch, König R (2004) Integrated adjustment of CHAMP, GRACE, and GPS data. J Geod 78:103–108. doi:10.1007/s00190-004-0379-0

Chapter 5
GRACE Gravity Modeling Using the Integrated Approach

Daniel König and Christoph Dahle

Abstract Monthly gravity field solutions up to d/o 60 are derived by applying the Integrated (one-step) Approach of space geodesy, i.e. by simultaneously processing of the GPS constellation and the twin GRACE satellites. The results are based on latest GRACE RL05 standards (without constraining L3-ambiguities), and consists of 24-h arcs covering the test month April 2008 where the monthly solution was obtained by accumulation of the daily normal equations. The alternative gravity model is compared with the corresponding two-step solution derived by standard two-step GFZ RL05 GRACE processing (including constrained L3-ambiguities). It is shown, that difference degree amplitudes with respect to the static satellite-only model ITG-GRACE2010s for both the Integrated Approach and the two-step solution only differ significantly beyond d/o 17 where the two-step approach still performs slightly better. A great advantage of the Integrated Approach is the largely reduced formal errors indicating higher stochastic significance.

Keywords GRACE · Integrated processing · Gravity field determination

5.1 Introduction

The integrated approach (Zhu et al. 2004) for deriving GRACE gravity field models follows the idea to process GPS ground data as well as the GRACE on-board data in a single step using an updated version of the GFZ Earth Parameter and Orbit System (EPOS) software. König et al. (2005) already gave a dim hint of a possible improvement of the gravity field coefficients (GFCs) of d/o two. The current integrated solution was derived for April 2008 with GFCs solved up to d/o 60 and

D. König (✉) · C. Dahle
GFZ German Research Centre for Geosciences, Department 1,
Geodesy and Remote Sensing,Münchner Str. 20,
82234 Oberpfaffenhofen, Germany
e-mail: dkonig@umbc.edu

compared with the latest RL05 "standard" two-step solution (Dahle et al. 2012 this book). Specifications of the processing as well as the results of the comparison are presented here.

5.2 Specifications

The specifications chosen for the processing are as follows:

- satellites: GPS constellation, GRACE
- observations: GPS-ground (L3), GRACE High-low GPS-SST (L3), GRACE low-low K-band range-rate (KBRR), measured accelerations (ACC) and attitude
- standards and models: GFZ RL05 (Dahle et al. 2012; except constraining of L3-ambiguities for GPS-ground)
- arc length: 24 h
- estimated parameters:

    - ground stations coordinates,
    - gravity field coefficients,
    - initial elements,
    - solar radiation pressure model (ROCK4) scale and y-bias for GPS satellites,
    - empirical forces (amplitudes of periodic model),
    - KBRR empirical coefficients and
    - ACC calibration coefficients.

- constraints: 0.1-mm NN (No Net) conditions (translation in three directions (TX,TY,TZ), scale DS and three rotations (RX,RY,RZ) on ground stations network.

5.3 Processing and Results

Orbit determination and parameter estimations in the integrated mode are carried out as specified above resulting in daily normal equations (NEQs). The daily NEQs are accumulated to monthly NEQs and solved resulting in monthly gravity field coefficients (GFCs) and ground stations coordinates. It has to be emphasized that for the integrated solution no integer-constraining of double-difference wide-lane L3-ambiguities according to Blewitt (1989) and Ge et al. (2005) is applied in contrast to the two-step solution where the L3-ambiguities of GPS-ground measurements are integer-constrained.

Beside the April 2008 solution presented here, also for the period covering the whole year 2008 an attempt was made to produce as well a solution with GPS-ground constrained L3-ambiguities. Such a solution would be fully comparable to current RL05 two-step solutions, and certainly more accurate. However, up to now it is not
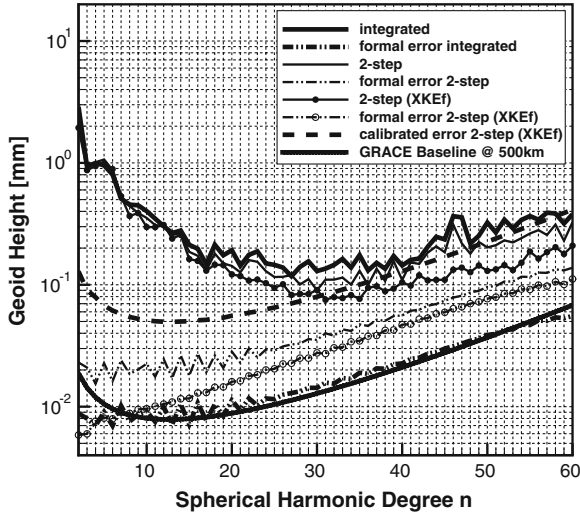
Fig. 5.1 Difference degree amplitudes per degree with respect to ITG-GRACE2010s
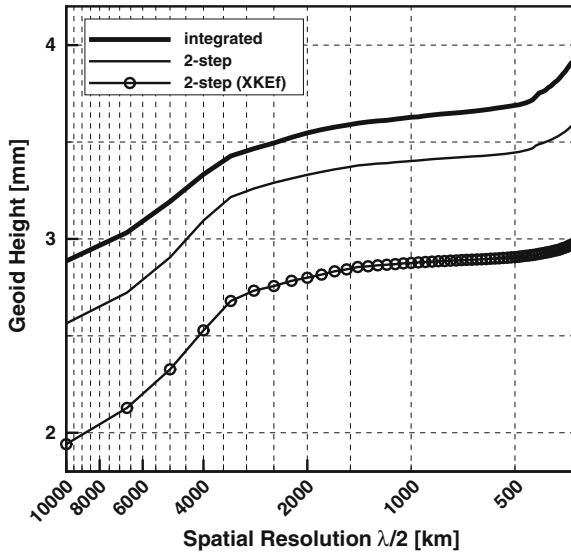
Fig. 5.2 Accumulated difference degree amplitudes with respect to ITG-GRACE2010s

possible within the GFZ EPOS processing chain to reduce and accumulate such NEQs. Difference degree amplitudes (Figs. 5.1 and 5.2) with respect to the static gravity field ITG-GRACE2010s (Mayer-Gürr et al. 2010) are shown for both the integrated and the two-step approach. Up to d/o 17 no significant differences can be seen, but beyond d/o 17 the two-step approach with unfixed parameters performs
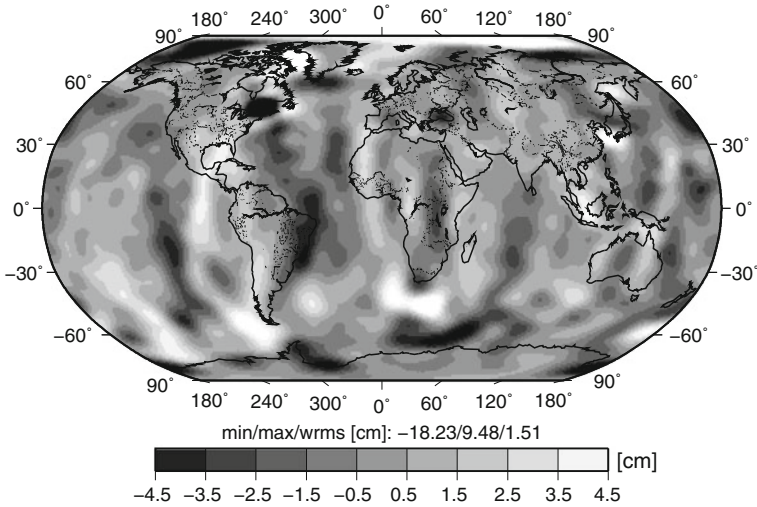
Fig. 5.3 Difference between the integrated and two-step approach for April 2008 and d/o ≤ 60; w/o C20

still slightly better. On the other hand the formal errors of the integrated approach are significantly smaller compared to the standard two-step approach.

The accumulated difference degree amplitudes (Fig. 5.2) show that the differences between both approaches are mainly caused by degree two, where the integrated approach seems to perform slightly worse. Figure 5.3 shows the spatial difference between both the integrated and two-step approach expressed in terms of equivalent water height. Note that the effect of C20 is excluded as the large differences in degree two would dominate the signal difference. The global wRMS of 1.51 cm is on the level of the accuracy of the standard two-step RL05 monthly gravity field solutions but the minimum and maximum values are quite pronounced indicating possible difficulties of the integrated approach in separating gravity field signal from other parameters. A similar effect can be seen in the two-step approach itself when only GFCs are solved, and all other parameters are fixed (case "XKEf" in Figs. 5.1 and 5.2).

5.4 Discussion

As a main achievement a processing scheme was successfully developed to generate gravity field solutions up to d/o 60 following the integrated approach. Nevertheless, the integrated approach still requires a high computational burden and several processing steps as it is based on cleaned observational data generated by preceding GPS/ground-only as well as GPS/SST-only processings according to a two-step

approach. At the current stage reached a gravity field solution up to d/o 60 of the integrated approach is quite close to the solution obtained by the two-step approach although no integer ambiguity fixing is applied. Visible differences in the difference degree amplitudes occur mainly beyond d/o 17. In order to fully exploit the potential of the integrated approach further research is necessary above all to produce solutions with integer-fixed ambiguities of the GPS measurements. Additionally, an adapted weighting scheme as well as an optimal parameterization is certainly helpful.

References

Blewitt G (1989) Carrier phase ambiguity resolution for the global positioning system applied to geodetic baselines up to 2000 km. J Geophys Res 94(B8):10187–10203

Dahle Ch, Flechtner F, Gruber Ch, König D, König R, Michalak G, Neumayer KH (2012) GFZ GRACE level-2 processing standards document for level-2 product release 0005 (ScientificTechnical Report - Data, 12/02, Revised Edition, January 2013), Potsdam, 21 p. doi:10.2312/GFZ. b103-1202-25

Ge M, Gendt G, Dick G, Zhang FP (2005) Improving carrier-phase ambiguity resolution in global GPS network solutions. J Geodesy 79(1–3):103–110. doi:10.1007/s00190-005-0447-0

König R, Reigber Ch, Zhu S (2005) Dynamic model orbits and Earth system parameters from combined GPS and LEO data. Adv Space Res 36: doi:10.1016/j.asr.2005.03.064,pp.431-437

Mayer-Gürr T, Kurtenbach E, Eicker A (2010) The ITG-GRACE2010s gravity field. http://www. igg.uni-bonn.de/apmg/index.php?id=itg-grace2010

Zhu S, Reigber Ch, König R (2004) Integrated adjustment of CHAMP, GRACE and GPS data. J Geodesy 78(1–2):103–108

Chapter 6
Comparison of Daily GRACE Solutions to GPS Station Height Movements

Annette Eicker, Enrico Kurtenbach, Jürgen Kusche and Akbar Shabanloui

Abstract In Kurtenbach (2011) and Kurtenbach et al. (2012) an approach has been introduced that allows to calculate daily gravity field solutions from GRACE data within the framework of a Kalman filter and smoother estimation. The method utilizes spatial and temporal correlations of the expected gravity field signal derived from geophysical models in addition to the daily observations, thus effectively constraining the spatial and temporal evolution of the GRACE solution. Here, we offer an extended validation of these daily solutions by comparing the derived mass variations to vertical displacements at various permanent GPS stations. The comparison confirms the conclusion that the daily solutions contain significant high-frequent temporal gravity field information, especially in higher latitudes.

6.1 Introduction: The GRACE Kalman Filter Approach

The standard analysis approach for GRACE data aims at the calculation of monthly (Watkins and Yuan 2007; Bettadpur 2007; Flechtner et al. 2010), 10-day (Bruinsma et al. 2010) or weekly (Flechtner et al. 2010) gravity field solutions. A temporal evolution of the mass variations, however, also occurs on much shorter time scales. It is therefore our goal to increase the temporal resolution of GRACE in order to determine these fast changes, which are for example present in atmospheric or barotropic

A. Eicker (✉) · E. Kurtenbach · J. Kusche · A. Shabanloui
University of Bonn, Institute of Geodesy and Geoinformation,
Nußallee 17, 53115 Bonn, Germany
e-mail: eicker@geod.uni-bonn.de

E. Kurtenbach
e-mail: kurtenbach@geod.uni-bonn.de

J. Kusche
e-mail: kusche@geod.uni-bonn.de

A. Shabanloui
e-mail: shabanloui@geod.uni-bonn.de

ocean variations. Since the data coverage provided by GRACE is not sufficient to allow for a recovery of gravity field snapshots on a day-to-day basis, the introduction of stochastic prior information from geophysical models as described in Kurtenbach et al. (2012) has to be used to stabilize the solutions.

The Kalman filter combines this prior information and the daily GRACE observations in a joint estimation process and delivers an updated state of the gravity field for each day. Stochastic information is introduced in terms of the process model which formulates a prediction of the current state resulting from the state of the previous time step. The process model is constructed from spatial and temporal covariance matrices derived from the output of the geophysical models. The daily solutions described by the present paper are part of the GRACE gravity field model ITG-Grace2010 (Mayer-Gürr et al. 2010) and can be downloaded at http://www.igg.uni-bonn.de/apmg/index.php?id=itg-grace2010. For details of the method, a comparison to other constraint approaches, and some first validation results, please refer to Kurtenbach (2011) and Kurtenbach et al. (2012). In the following, the results will be evaluated more thoroughly by comparison to a larger number of vertical GPS station movements.

6.2 Validation of Daily Solutions

In order to evaluate the temporal high frequency information content of the daily GRACE models, they have to be compared to independent data sets. Mass variations at the Earth's surface result in geometrical deformations of the Earth's crust which can be measured by GPS receivers. Therefore, the global network of permanent GPS stations provides a set of independent observations which can be used for comparing with GRACE gravity field models. Vertical station displacements of the reprocessed time series of the International GPS Service (IGS), see Steigenberger et al. (2006), were compared on a daily basis to the GRACE Kalman solutions after transforming them to vertical loading using the load Love numbers of Gegout (2005). For a detailed description of the method for comparing GRACE and GPS, including the treatment of the degree 1 coefficients, see Tesmer et al. (2011).

Figure 6.1 shows the time series for four exemplary GPS stations. The in-situ GPS observations are plotted in the black curve, the GRACE time series is given by the red curve. As a comparison vertical loading as computed from the de-aliasing product (AOD1B RL04, blue line) used in the GRACE L1B data analysis (Flechtner 2007) is displayed by the green line. The AOD1B RL04 product represents our knowledge of global temporally high-frequent mass variations before the calculation of daily GRACE solutions. The left part of each figure shows the time span 2003–2007, while the right part presents a zoom-in on the year 2004. The top three images Fig. 6.1a–c reveal a better agreement between the daily GRACE solutions and the independent GPS observations than between GPS and AOD1B RL04. This implies that, here, significant gravity field information has been recovered that is not present in the AOD1B RL04. The three stations are located in the mid to high latitude region where
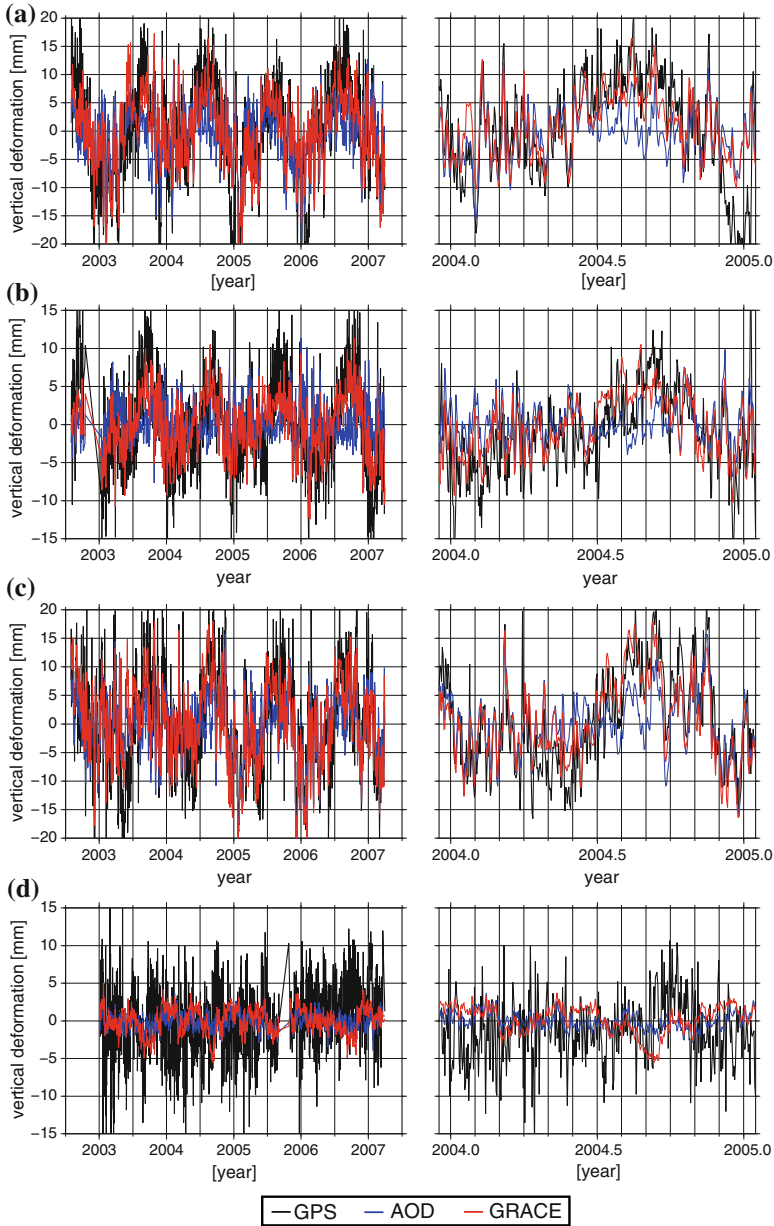
Fig. 6.1 Time series of observed vertical GPS station movements (*black*) compared to ITG-Grace daily solutions (*red*) and the AOD1B RL04 dealiasing product (*blue*). *Left* complete time series. *Right* zoom-in for one year. **a** ARTU—Arti (Russia)—$\lambda = 58.6°$, $\varphi = 56.4°$, **b** NANO—Nanoose Bay (Canada)—$\lambda = 235.9°$, $\varphi = 49.3°$, **c** NRIL—Norilsk (Russia)—$\lambda = 88.4°$, $\varphi = 69.4°$, **d** GLPS—Puerto Ayora (Galapagos Islands)—$\lambda = 269.7°$, $\varphi = -0.7°$
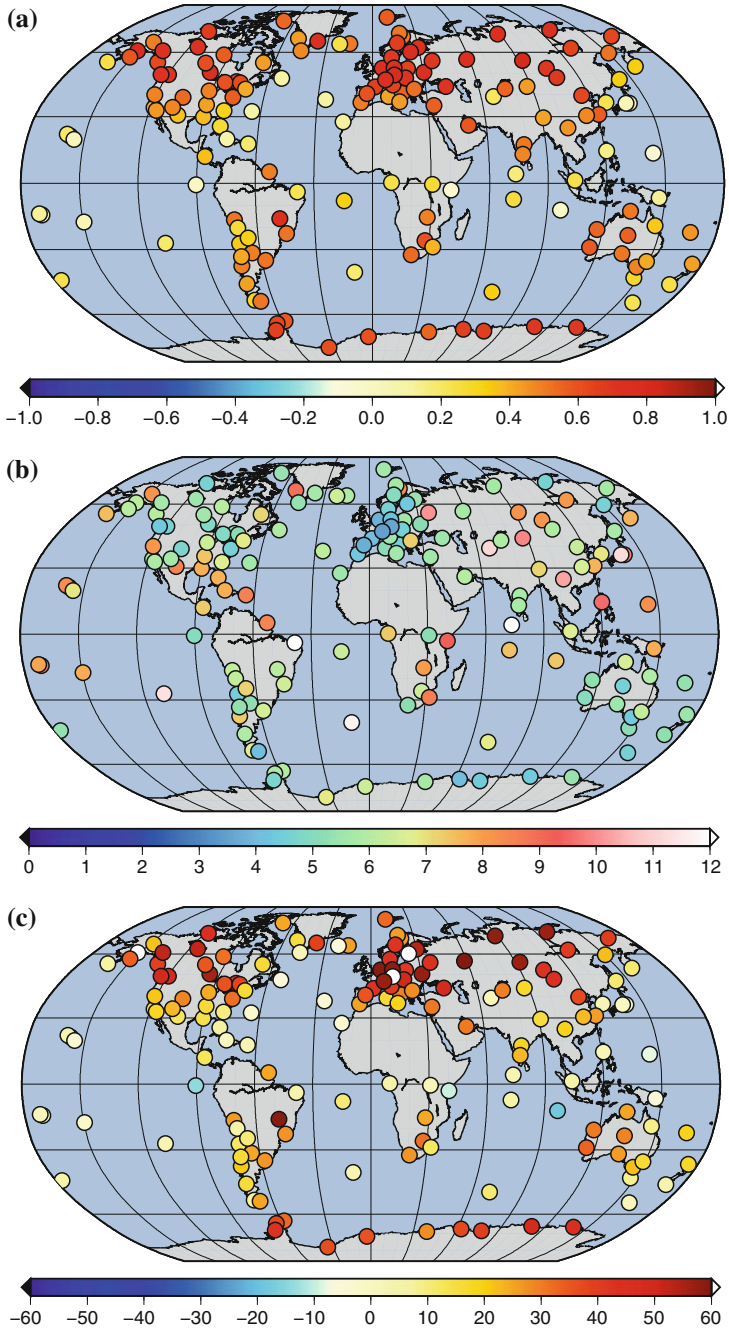
Fig. 6.2 Quality measures for the correspondence of daily GRACE solutions with global GPS station displacements. (**a**) correlation coefficient, (**b**) error RMS, (**c**) signal reduction

the GRACE data coverage is dense due to the orbit geometry and the high-frequent temporal signal is strong due to large atmospheric mass variations. Figure 6.1d displays the vertical motion of a station near the equator, where the data coverage is less dense and the mass signal exhibits a lower amplitude. The evaluation of the curves leads us to the conclusion that at this station no significant gain in information can be obtained from GRACE. The differences between GPS and GRACE, however, cannot only be addressed to errors in the gravity field determination, as it is known (see for example van Dam et al. 2007) that the quality of GPS time series is quite inhomogeneous; i.e. other signals (e.g. troposphere, station movements, antenna effects) may be affecting the comparison.

Figure 6.2 shows different accuracy measures for all the compared global GPS stations. Figure 6.2a illustrates the correlation coefficient between GRACE and GPS. As expected, a high correlation can be found in the higher latitudes, whereas the correlation along the equator is low. Obviously, the correlation is in particular low at stations located on islands in the Atlantic and Pacific ocean. This can be attributed to the fact that the ocean reacts to atmospheric mass changes by the inverse barometer effect and therefore mass variations at island stations are particularly small, as is also the case for the station GLPS in Fig. 6.1d. As second quality measure, Fig. 6.2 displays the error RMS between the GPS and GRACE time series for each station, i.e. representing the mean squared differences between the two time series. Again it can be observed that the errors are smaller in higher latitudes with values around 4–6 mm, whereas in the lower latitudes values up to 12 mm can be reached. As the correlation coefficient is only sensitive to phase shifts and the error RMS depends strongly on the magnitude of the signal, a third quality measure is introduced in Fig. 6.2c. The signal reduction represents the percentage of the signal of each at the stations that can be explained by the GRACE observations. It can be interpreted as the ratio between error RMS and signal RMS. Again the conclusion is confirmed that especially in the higher latitude regions a large part of the temporally high-frequent gravity field signal can be explained by the daily GRACE solutions.

6.3 Conclusions and Outlook

We note that the gravity field variations observed independently by GRACE and GPS show a good agreement for a large part of the global IGS stations. This allows the conclusion that the GRACE Kalman filter approach is able to recover temporally high-frequent gravity field variations. These variations can be considered as an improved de-aliasing product. The improvement can be attributed to two effects which cannot easily be separated: First of all the daily GRACE solutions represent, beside the atmospheric and oceanic variations contained in the AOD1B RL04 product, also high-frequent hydrological mass changes. Furthermore, they also account for model errors in the atmosphere and ocean models, as was independently proven by Bonin and Chambers (2011).

References

Bettadpur S (2007) UTCSR Level-2 processing standards document for level-2 product release 0004. CSR Publ. GR-03-03

Bonin JA, Chambers DP (2011) Evaluation of high-frequency oceanographic signal in GRACE data: implications for de-aliasing. Geophys Res Lett 38(L17608)

Bruinsma S, Lemoine J-M, Biancale R, Valés N (2010) CNES/GRGS 10-day gravity field models (release 2) and their evaluation. Adv Space Res 45(4):587–601. http://www.sciencedirect.com/science/article/B6V3S-4XHM1CC-1/% 2/8394fd9d92b0bb8c99df396bb61ad0d7

Flechtner F (2007) AOD1B product description document for product releases 01 to 04. Technical Report, Geoforschungszentrum, Potsdam. http://dx.doi.org/10.1016/j.asr.2009.10.012

Flechtner F, Dahle C, Neumayer K-H, Koenig R, Foerste C (2010) The release 04 CHAMP and GRACE EIGEN gravity field models. In: Flechtner F, Gruber T, Guentner A, Mandea M, Rothacher M, Wickert J (eds) Satellite geodesy and Earth system science G observation of the Earth from Space. Springer, Berlin

Gegout P (2005) Load love numbers. http://gemini.gsfc.nasa.gov/aplo/Load_Love2_CM.dat

Kurtenbach E (2011) Entwicklung eines Kalman-Filters zur Bestimmung kurzzeitiger Variationen des Erdschwerefeldes aus Daten der Satellitenmission GRACE. Ph.D. thesis, University of Bonn

Kurtenbach E, Eicker A, Mayer-Gürr T, Holschneider M, Hayn M, Fuhrmann M, Kusche J (2012) Improved daily GRACE gravity field solutions using a Kalman smoother. J Geodyn 59–60:39–48

Mayer-Gürr T, Kurtenbach E, Eicker A (2010) ITG-Grace2010 gravity field model. http://www.igg.uni-bonn.de/apmg/index.php?id=itg-grace2010

Steigenberger P, Rothacher M, Dietrich R, Fritsche M, Rulke A, Vey S (2006) Reprocessing of a global GPS network. J Geophys Res 111:B05402

Tesmer V, Steigenberger P, van Dam T, Mayer-Gürr T (2011) Vertical deformations from homogeneously processed GRACE and global GPS long-term series. J Geodesy 85:291–310

van Dam T, Wahr J, Lavallée D (2007) A comparison of annual vertical crustal displacements from GPS and Gravity recovery and climate experiment (GRACE) over Europe. J Geophys Res 112:B03404

Watkins M, Yuan D-N (2007) JPL level-2 processing standards document for level-2 product release 04. ftp://podaac.jpl.nasa.gov/pub/grace/doc/

Chapter 7
Identification and Reduction of Satellite-Induced Signals in GRACE Accelerometer Data

Nadja Peterseim, Anja Schlicht, Jakob Flury and Christoph Dahle

Abstract Although the GRACE satellite mission has achieved outstanding results in the ten years since it has been launched, signals within accelerometer data remain non-understood. We analyzed 10 Hz Level 1a Accelerometer data (ACC1A) and could link signals to switch events due to magnetic torquers and heaters, and also were able to find a systematic for so called "twangs". Those signals could be either empirically or physically modelled. With those signals time-series consisting of spikes only could be computed, with which a possible impact onto the gravity field could be determined. It showed that especially the radial component could have an impact. In order to investigate the impact onto the gravity field sufficiently we subtracted the modelled signals from ACC1A, downsampled that data to 1 Hz in order to obtain ACC1B data format and derived a gravity field with the use of our ACC1B dataset. The results appear to have a little, but visible effect of up to 2 cm equivalent water height onto the gravity field determined by GRACE.

N. Peterseim (✉)
Institut für astronomische und physikalische Geodäsie, Technische Universität München, Munich, Germany
e-mail: Nadja.Peterseim@bv.tu-muenchen.de

A. Schlicht
Forschungseinrichtung für Satellitengeodäsie, Technische Universität München, Munich, Germany

J. Flury
Institut für Erdmessung, QUEST, Leibniz Universität Hannover, Hannover, Germany

C. Dahle
Helmholtz-Zentrum Potsdam, Deutsches GeoForschungsZentrum (GFZ), Potsdam, Germany

7.1 Introduction

The GRACE satellite mission is in orbit since March 2002 and is since then collecting valuable information about the Earth gravity field. In the past ten year the results within the temporal as well as spatial gravity field are outstanding and remarkable.

GRACE determines the Earth gravity field by measuring the inter-satellite ranges, which is carried out by the onboard K-Band Ranging System (KBR). This system detects the range with micrometer accuracy (Kim and Lee 2009).

In order to retrieve the gravitational part only, the non-gravitational forces, such as atmospheric drag or solar radiation pressure, must be well known. For this purpose both GRACE satellites are equipped with a SuperSTAR accelerometer manufactured by ONERA in France. The accelerometer is located in the center of mass (CoM) of the satellite and has in the case of SuperSTAR an accuracy of 10^{-10} m/s$^2/\sqrt{Hz}$ (Rodrigues et al. 2003; Flury et al. 2008).

However, there are very few investigations and studies available concerning the quality of the accelerometer data. Furthermore, it is rather difficult to make an actual distinction between accelerometer sensor error and effects from the onboard environment onto the accelerometer. The determined gravity field could be an indicator of the quality of the accelerometer, but is rather unspecific and can only reveal the quality to a certain extend. Also, the predicted performance for the gravity field carried out by simulations prior to mission launch has not yet been achieved (Förste et al. 2008).

The 10 Hz Level 1a accelerometer data (ACC1A) of GRACE offers an opportunity to identify sensor errors and impacts by other onboard instruments. These signals often have a very high frequency and are therefore hard to be observed and analyzed in the 1 Hz Level 1b accelerometer data (ACC1B).

In our study, we focused on the ACC1A data of 2008 and investigated effects onto the accelerometer data due to the onboard heaters as well as magnetic torquers and also analyzed the phenomenon referred to as "twangs".

7.2 Magnetic Torquer Spikes

One of the signals investigated are due to changes in the electric current in the magnetic torquers which are used for maintenance of the attitude. The magnetic torquer system is part of the Attitude and Orbit Control System (AOCS) and is used for attitude maintenance of the spacecraft. It consists of a set of three rods consisting of a nickel-alloy core wrapped by a coil, forming an electro magnet. By applying an electric current to a magneto torquer rod a magnetic dipole is evoked, which will in combination with the Earth magnetic field enforce a torque upon the spacecraft. The needed torque for attitude maintenance is determined by the AOCS under detection of the Earth magnetic field as well as the divergence of the mandatory attitude derived by the onboard star sensor system. By combining the three magnetic dipoles evoked by the three torque rods and the Earth magnetic field the needed torque can be enforced.
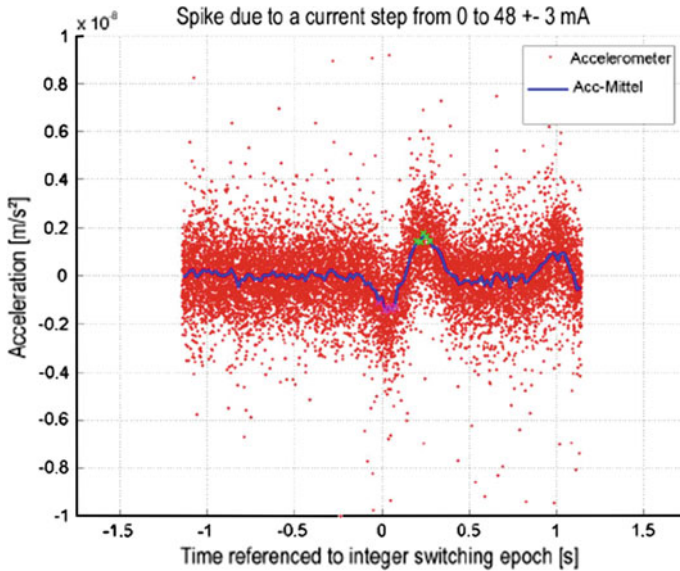
Fig. 7.1 Spike due to a current change in Magnetic Torquer in the along Track accelerometer component. *Red dots* plot the superimposed 10 Hz accelerometer data (ACC1A), the *blue solid line* the mean of the superimposed ACC1A data at the given time

The electric current used for the magneto torquers may range from 0 to 120 mA, whereas the current is able to flow both ways in order to provide the magnetic dipole with the direction needed. A signal in 10 Hz Level 1a accelerometer (ACC1A) data can be detected each time the magnitude of the electric current is changed in one of the torque rods. Accelerometer data for both GRACE satellites show the same behavior for the same current steps due to the same torque rods and hence we will describe this phenomenon as one. This signal usually consists of 2 peaks with a period of less than one second. The orientation of the peaks is strictly correlated to an increasing or decreasing electric current (cf. Fig. 7.1). When a stronger current is applied, a down-up pattern can be detected, whereas an up-down pattern is observable for a decreasing electric current. The amplitude of the signal is depending on the magnitude of the current step and can be as high as 20 nm/s^2 (Peterseim et al. 2012; Peterseim 2010). However, the behavior of the amplitude is not linear to the magnitude of the current change, but rather exponential (cf. Fig. 7.2).

Due to the availability of the MAG1B data product, where the current of the magentic torquer is being saved, it is easy to superimpose accelerometer data due to a certain magnitude of current change. In fact, for one single spike the 10 Hz would not resolve the spike clearly enough, but if a sufficient number of samples can be superimposed the spike is resolved quite clearly (cf. Fig. 7.1). This allows us to build mean models for a spike which we can use afterwards for a signal reduction due to Magneto Torquers. Upon that mean model, a time-series consisting of spikes due to
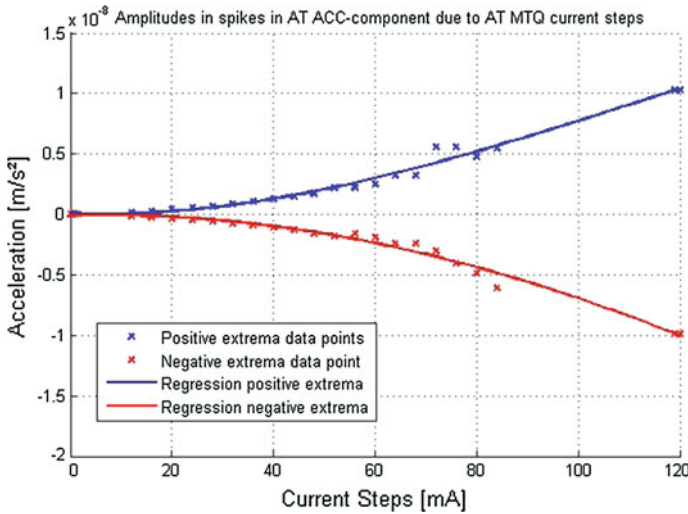
Fig. 7.2 Amplitudes of spikes in along track accelerometer data due to electric current changes in along track magnetic torquer rod with an initial current of 0 mA

current changes can be computed. For this, the period and the starting point of the spike are known and we alter the amplitude of the spike with respect to the magnitude of the current change.

Being able to model any given spike due to current changes in Magneto Torquers allows us to compute time-series consisting of these spikes only, which can furthermore be used to reduced torquer induces spikes in Level 1a accelerometer data. This is one step to improve the existing accelerometer data products as the current changes are not expected to enforce an actual acceleration upon the spacecraft.

7.3 Heater Spikes

Similar to the spikes induced by Magneto Torquers the onboard heaters evoke a spike in the 10 Hz accelerometer data as well. Heaters onboard of GRACE are used to maintain a certain temperature needed by a variety of payloads that may only function properly in a given temperature range. Therefore, each GRACE satellite is equipped with 64 heater circuits consisting of at least one or more heaters that control one or more spacecraft payloads.

A spike in accelerometer data occurs each time a heater is being activated or deactivated. Due to the larger amount of heater onboard of the satellites, this can lead up to 120,000 of such switch events per day (Flury et al. 2008).

Activation and Deactivation of the heaters are stored in the THHC data, which is indeed not an official Level 1B data product. By that data we were able to refer-
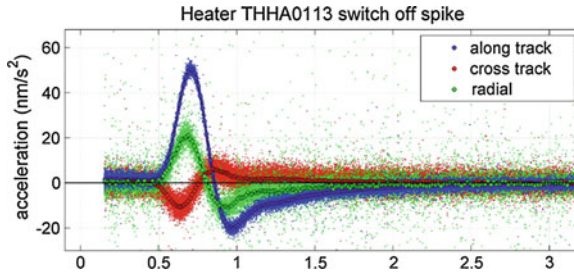
Fig. 7.3 Spike in ACC1A data due to deactivation of THHA0113 heater circuit. The small *colored dots* display the superimposed accelerometer data

ence and superimpose accelerometer data due to switch events of single heaters and determine the period and amplitudes of the spikes evoked by these events. We found, that the same heater would evoke always the same peak as in period and amplitude, except for a small variance in the amplitude which is due to the battery voltage at the time the given event took place.

Considering that battery voltage, which is like the heater data no official product but yet available, amplitudes and periods can be predicted very accurately.

With the same approach used for modeling the spikes due to current changes in the Magneto Torquer we were able to derive mean models for each switch event of the heater by building the mean spike of the superimposed accelerometer data (cf. Fig. 7.3).

Also here, time-series of spikes could be computed which can be used for reduction of heater induced spikes.

7.4 Twangs

The biggest spikes that can be found in GRACE accelerometer data are so called "twangs". The name originates in its shape, a major spike often followed by an oscillating decay. Twangs cannot be linked to any onboard instrument and the mechanisms causing a twang are up to date not clearly resolved. Twangs can be easiest identified in the radial component of the accelerometer data, where they can have an amplitude of up to $50\,\mu m/s^2$.

Twangs can easiest be spotted by eliminating all other described effects as well as avoiding any data that may have be impacted by the thruster activations. By means of cross-correlation of reconstructed signal to 100 Hz, twangs can be superimposed with respect to the highest correlation coefficient analogue to the approach used for magneto torquers and heater switch events. In order to determine the highest correlation coefficient more accurate than 10 Hz would actually allow it is feasible
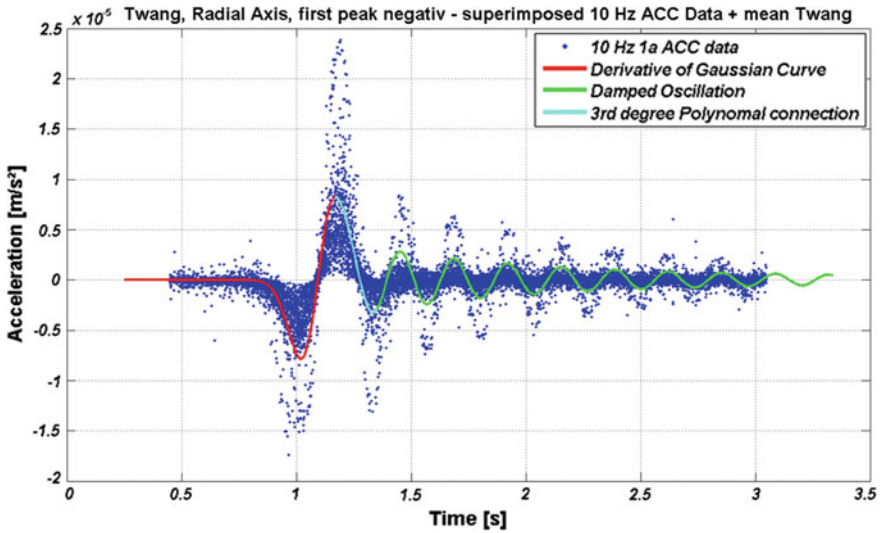
Fig. 7.4 'Negative' Twang, where first peak is negative. The *blue dots* display superimposed ACC1A data found by means of cross-correlation, the *colored solid line* constitutes the physical model, whereas *red* is the derivative of the Gaussian curve including an anisotropic scaling factor, *green* a double damped oscillation and *cyan* a third degree polynomial connecting these two

to resample the accelerometer data up to 100 Hz by means of a reconstruction filter, such as a Sinc, Lanczos or Gaussian filter. Figure 7.4 displays that superimposed twangs appear to have the same period and similar behavior, independent from the selected cross-correlation factor. This allows us basically to divide into to types of twangs, namely a positive and a negative oriented twang.

With this knowledge a physical model can be build, that consists of the derivative of the Gaussian bell for the first two peaks, whereas the amplitude as well as the anisotropy need to be considered with a factor, and a double damped oscillation for the oscillating decay, as one damping factor alone could not describe the oscillation in many cases (cf. Fig. 7.4).

This physical model can be fit to any twang in accelerometer data using the Least Square Adjustment method, considering keeping strongly correlated parameters apart from each other in order to avoid ambiguities. Using this approach, approximately 95 % of all twangs can be modeled sufficiently. By subtracting the adjusted model from the real accelerometer we expect to reduce the twang from data but keep the subjacent signal as untouched as possible (cf Fig. 7.5).

Also, the modeled twangs can be stored in time series consisting merely of the twangs, which will become feasible in investigating the possible influence of twangs onto the Earth gravity field determined by the GRACE mission.
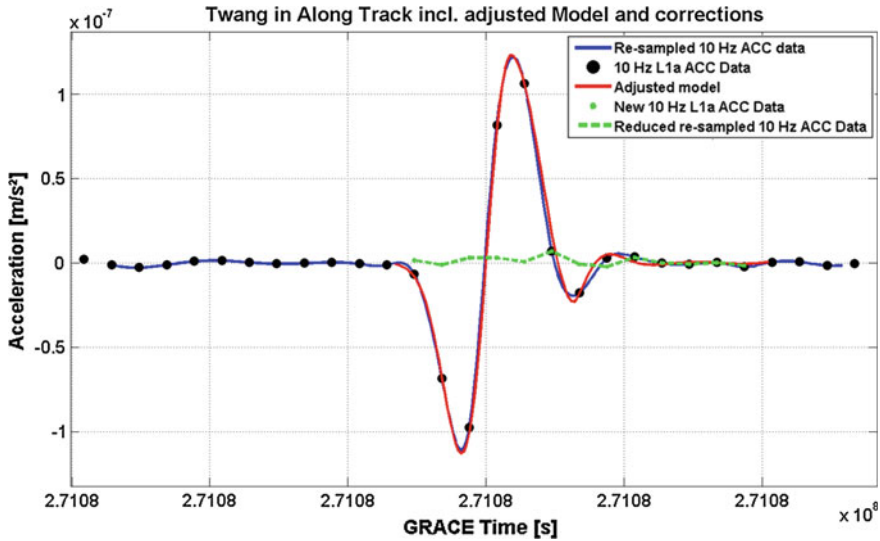
Fig. 7.5 Negative Twang in along track ACC1A data. The *black dots* display the actual ACC1A data, the *blue solid line* is a reconstruction filter upon these data points to supply with a 100 Hz signal, the *red line* is the adjusted physical model, and the *green line/dots* is the signal remaining after subtracting the model from actual ACC1A signal

7.5 Impact onto the Gravity Field

Considering a time series consisting of spikes due to the three effects mentioned previously we are able to derive Power Spectrum Densities (PSD) for each axis which we can compare to the error model curve for each specific axis. While high frequencies most likely will not impact the gravity field, low frequencies have a theoretical chance of influencing it. A first approach was carried out with a less sensitive reduction of twangs, where we simply reduced ACC1A to the mean acceleration values at the given point of a twang. It shows that for 10 Hz data especially the radial and the along track components of the accelerometer data could have an impact, but when low-pass filtered to 1 Hz (ACR1B data) only the radial component shows to have a real influence as nearly all amplitudes are greater than the error model curve for the radial accelerometer data (cf. Fig. 7.6).

A comparison of the gravity fields with the official ACC1B and new processed ACC1B has been carried out. We refer to the new ACC1B as to ACR1B in order to avoid misunderstandings. ACR1B data consists of low-passed filtered 1 Hz signal liberated ACC1A data. It shows that the actual impact of the described signals onto the Earth gravity field for the GFZ monthly solution for August 2008 is merely 2 cm equivalent water height (EWH) and can be mainly seen in striping effects (cf. Fig. 7.7). The processing of the gravity field with our ACR1B data has been carried out by GFZ analogue to their standard processing. Yet, it has to be mentioned
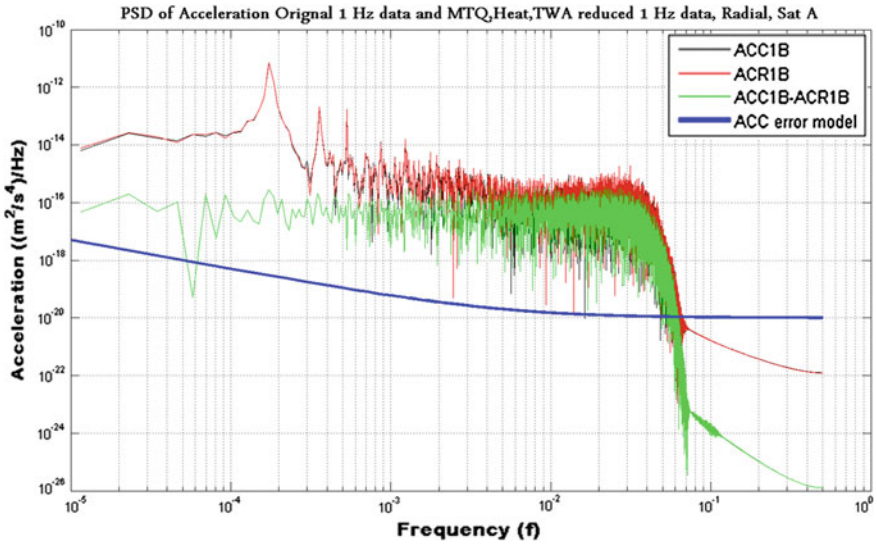
Fig. 7.6 PSD of time-series consisting only of spikes (*green*), ACC1B (*black*), ACR1B (*red*) and the error model curve (*blue*), all for radial component, 1 Hz
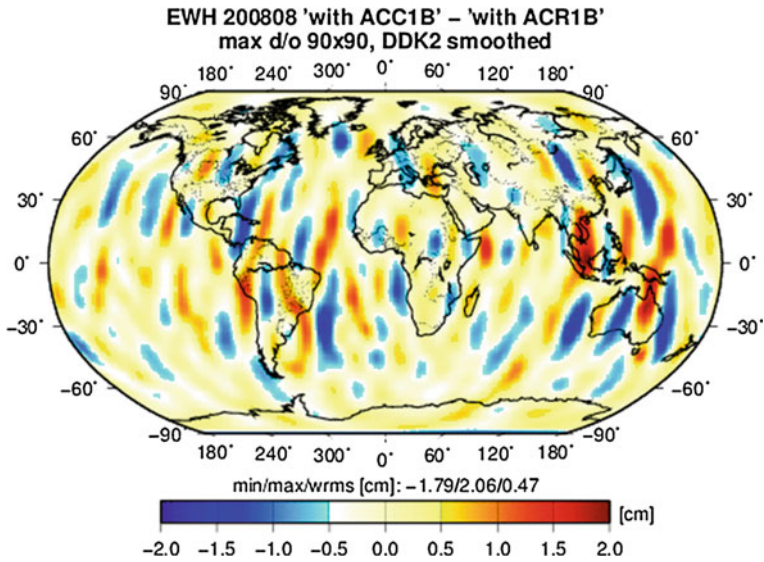
Fig. 7.7 Residuals between official ACC1B data product and ACR1B data, which are liberated from satellite-induced signals in ACC1A data. Data is displayed in equivalent water height

that GFZ automatically eliminates outliers within the ACC1B data, and hence the results seen in Fig. 7.7 might not show the actual influence by these signals to the full extend.

7.6 Conclusions and Outlook

We could investigate, model and reduce signals from ACC1A data influenced by magnetic torquer current changes, onboard heater activations and deactivations as well as so called "Twangs", whereas the actual source for the twangs remain unclear. The mechanism behind either of the signals is unknown up to date. The amplitude of the signals may range from smaller amplitudes for Magneto Torquer with a maximum amplitude of $20\,nm/s^2$ to great amplitudes found for twangs in the radial accelerometer component of up to $50\,\mu m/s^2$.

10 Hz accelerometer data liberated from these signals can be low-pass filtered into 1 Hz data, analogue to the actual ACC1A to ACC1B processing chain, in order to investigate the influence onto the Earth gravity field. For a single monthly solution we determined an impact of up to 2 cm in EWH. However, these results were achieved with a simple approach of twang-reduction, and the new model adjustments as described in this article where not applied yet. The introduced approach shall be used as a next step to obtain more accurate results. Also, it would be helpful to investigate the actual impact of signals, which would yield at a co-operation with GFZ in order to avoid their algorithm which automatically eliminates spike affected data.

Despite the little impact onto the Earth gravity field, investigations concerning these issues should be ongoing as many of the mechanism are not understood yet, and as gravity satellite missions are becoming more accurate and sensitive they might, in fact, become more vulnerable to such satellite-induced impacts.

References

Flury J, Bettadpur S, Tapley BD (2008) Precise accelerometry onboard the GRACE gravity field satellite mission. Adv Space Res 42:1414–1423. doi:10.1016/j.asr.2008.05.004

Förste C, Flechtner F, Schmidt R, Stubenvoll R, Rothacher M, Kusche J, Neumayer KH, Biancale R, Lemoine J-M, Barthelmes F, Bruinsma S, König R, Meyer U (2008) EIGEN-GL05C—A new global combines high-resolution GRACE-based gravity field model of the GFZ-GRGS cooperation, Geophysical Res. Abs. 10, EGU2008-A-03426, SRef-ID: 1607–7962/gra/EGU2008-A-03426

Kim J, Lee SW (2009) Flight performance analysis of GRACE K-Band ranging instrument with simulation data. Acta Astronaut 65:1571–1581

Peterseim N (2010) Acceleration disturbances onboard of GRACE satellites due to magnetic torquers. Thesis (Diplomarbeit), Leibniz Universität Hannover

Peterseim N, Flury J, Schlicht A (2012) Magnetic torquer induced disturbing signals within GRACE accelerometer data. Adv Space Res 49:1388–1394

Rodrigues M, Foulon B, Liorzou F, Touboul P (2003) Flight experience on CHAMP and GRACE with ultra-sensitive accelerometers and return for LISA. Class Quant Grav 20:S291–S300

Chapter 8
Reprocessing and Application of GPS Radio Occultation Data from CHAMP and GRACE

Stefan Heise, Jens Wickert, Christina Arras, Georg Beyerle, Antonia Faber, Grzegorz Michalak, Torsten Schmidt and Florian Zus

Abstract In recent years, the GPS radio occultation (RO) technique has become an established approach for global atmospheric remote sensing. For instance, GPS RO data are operationally used in numerical weather prediction since 2006. At the beginning of the GEOTECHNOLOGIEN research project ATMO-CHAMP/GRACE, the German CHAMP (CHAllenging Minisatellite Payload) satellite provided the first and only long-term GPS RO data set, comprising nearly eight years. Around 440,000 occultation measurements were performed between Feb. 2001 and Oct. 2008. This data set is complemented and continued by GPS RO measurements aboard the GRACE-A (Gravity Recovery And Climate Experiment) satellite. To generate a homogeneous and high quality long-term set of CHAMP/GRACE GPS-RO data for climatological applications and trend analyses, a consistent reprocessing was needed. Major results of the ATMO-CHAMP/GRACE project are: (a) significant improvement of the GPS RO analysis software at GFZ, including capability of open-loop processing (TerraSAR-X, TanDEM-X); (b) consistently reprocessed GPS RO data set from CHAMP and GRACE applying the improved analysis software; (c) based on the reprocessed long-term data set: temperature trends in the Upper Troposphere Lower Stratosphere region (UTLS), results on variability and trend behavior of tropopause parameters, results on gravity wave activity and occurrence of sporadic E-layers.

8.1 Introduction

The installation of the U.S.-American satellite navigation system GPS in the nineties established the basis for the innovative GPS radio occultation (RO) technique, allowing for atmospheric remote sensing on a global scale. GPS RO data are recorded

S. Heise (✉) · J. Wickert · C. Arras · G. Beyerle · A. Faber · G. Michalak · T. Schmidt · F. Zus
GFZ German Research Centre for Geosciences, Department 1, Geodesy and Remote Sensing,
Telegrafenberg, 14473 Potsdam, Germany
e-mail: heise@gfz-potsdam.de
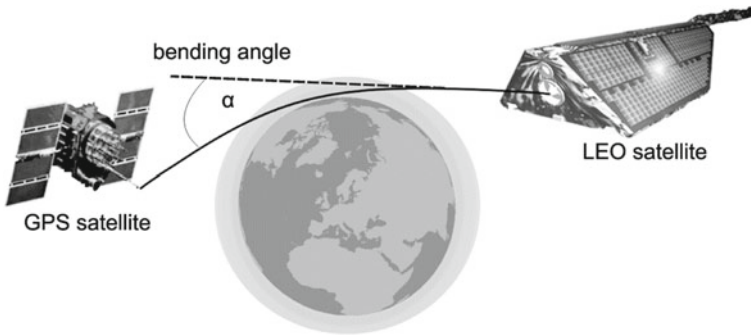
Fig. 8.1 GPS radio occultation principle

aboard Low Earth Orbiting satellites (LEOs, Fig. 8.1) and provide a number of favorable characteristics, as global coverage, high accuracy and vertical resolution, all-weather capability and long-term stability. The GPS RO technique (e.g., Kursinski et al. 1997) exploits atmospheric refraction and delay of GPS signals in both the neutral atmosphere and ionosphere. Observed phase path delays can be inverted to vertical profiles of bending angle, refractivity and meteorological quantities (temperature, humidity, e.g., Heise et al. 2008). Extensive validation studies with data generated by classical methods (e.g., radiosonde measurements), and several applications demonstrated the high potential of the new data for atmospheric remote sensing on a global scale (e.g., Anthes et al. 2008; Wickert et al. 2009). Nevertheless, it has also been shown that GPS RO analysis results differ between the different processing centers (Ho et al. 2009). These differences have to be analyzed carefully before application of GPS RO data in comprehensive climatological studies.

Up to now, the CHAMP satellite provides the longest available consistent time series of GPS RO measurements comprising nearly eight years (e.g., Wickert et al. 2009). Continued by GRACE and several following GPS RO missions (FORMOSAT-3/COSMIC, Metop, TerraSAR-X, TanDEM-X), this data set allows for first climatological investigations based on GPS radio occultation measurements. The reprocessing activities and climatological results presented in this study are funded within the research project "Analysis of atmospheric data from CHAMP/GRACE and application for climatological investigations" (ATMO-CHAMP/GRACE) of the GEOTECHNOLOGIEN program of the German Federal Ministry of Education and Research.

8.2 Improvement of GPS RO Data Analysis and Reprocessing

The improvement of the operational GPS RO processing software was of high priority during the entire project. In a first step, the GFZ RO analyses software has
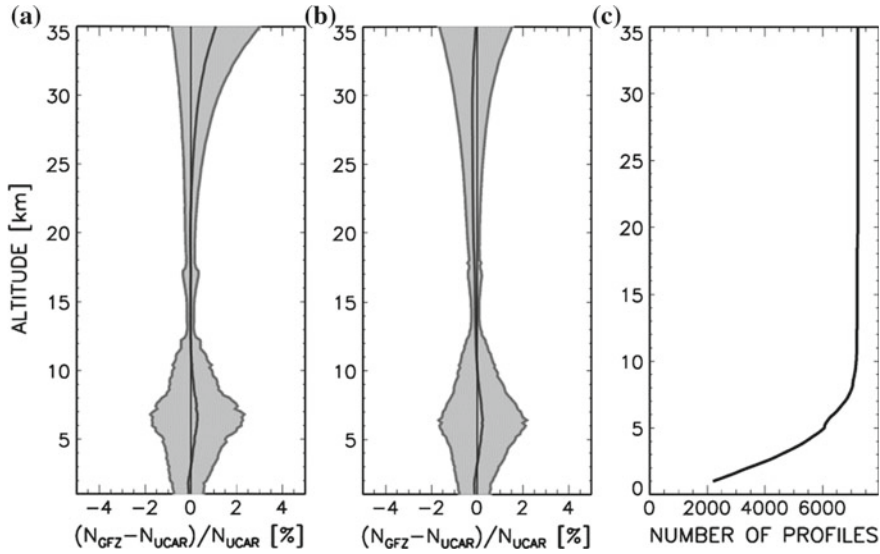
Fig. 8.2 Global CHAMP refractivity comparison (bias and standard deviation) between GFZ and UCAR for January/February 2006: **a** before reprocessing; **b** after reprocessing; **c** number of compared profiles

been adapted for application on Linux platforms regarding reduction of computation time needed for reprocessing of the large CHAMP/GRACE data set. Comprehensive intercomparisons with analysis results from other RO processing centres (e.g. UCAR, JPL) and with independent meteorological data (e.g., ECMWF analyses and radiosonde observations) were performed as a basis for the improvement of the GPS RO processing software.

In this context, GFZ participated in a comparison study of several CHAMP RO data processing centers (Ho et al. 2009). These comparisons revealed excellent agreement of GFZ atmospheric products with analysis results from other processing centers (e.g. UCAR) especially in the altitude range between 10 and 25 km. However, a positive refractivity bias was observed above 25 km (Fig. 8.2a). The detailed investigation and abolishment of this bias has been the major goal regarding improvement of the RO processing software in the course of the ATMO-CHAMP/GRACE project. To improve the GPS RO data analysis, the entire processing chain starting from raw data to the final atmospheric products has been investigated concerning possible error sources. The impact of software changes has been evaluated by consecutive comparisons with other processing centers and independent meteorological data. Finally it showed up that handling of the occultation and reference antenna phase center correction was the main reason for the refractivity bias above 25 km. This correction has been improved in GPS RO analysis software for all processed satellite missions (CHAMP, GRACE, TerraSAR-X, TanDEM-X). Another significant change was introduced to the statistical optimization of the bending angle (see Sokolovskiy
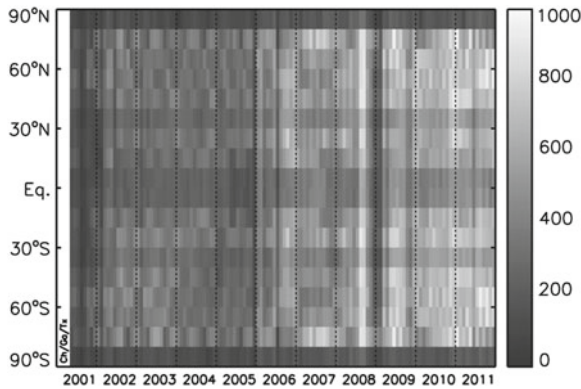
Fig. 8.3 Zonal distribution (monthly number of profiles within 10° zonal bands) of the GPS RO data base from CHAMP (89 months), GRACE (70 months) and TerraSAR-X (38 months), May 2001 up to December 2011

and Hunt 1996). In the optimization process the assumed observation error is divided by 4, which increases the weighting of the measured bending angles in opposite to the modeled bending angles (MSISE-90 climatology). This led to an improved agreement between CHAMP RO refractivity results and independent meteorological data from radiosondes and ECMWF analyses in altitudes above 30 km. Furthermore, the data exploitation has been improved by application of more robust assumptions for the automated quality control.

Finally, the improved GPS RO processing software version (006) has been applied for reprocessing of the whole CHAMP/GRACE data set comprising more than 680,000 globally distributed occultation events collected in more than ten years (Fig. 8.3). This reprocessed data set is provided to the scientific community via the GFZ Information System and Data Center (ISDC). The significantly improved agreement between the reprocessed GFZ CHAMP data set and other processing centers (e.g. UCAR, see Fig. 8.2b) is documented in comprehensive comparison studies by Ho et al. (2012) and Steiner et al. (2013).

In addition to the project goals, the RO analysis software has been upgraded for processing of open-loop RO data from TerraSAR-X and TanDEM-X. In result, atmospheric profiles from TerraSAR-X RO observations are routinely provided since October 2010 to numerical weather prediction centers (e.g., UK MetOffice, ECMWF, NCEP, DWD) in near real time.

8.3 Global Temperature and Tropopause Trends

The upper troposphere and lower stratosphere (UTLS) is one of the key regions of the atmosphere with significant importance for the stratosphere-troposphere exchange.
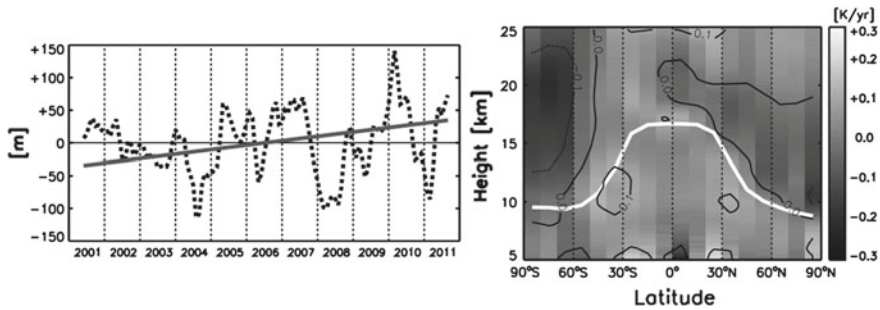
Fig. 8.4 *Left* Global tropopause height trend (*solid line*) based on CHAMP and GRACE (2001–2011); *Right* Global temperature trends in the upper troposphere and lower stratosphere based on CHAMP and GRACE (2001–2011), update from Schmidt et al. (2010b). The *solid white line* denotes the tropopause height

Thus, the UTLS is of certain interest in atmospheric and climate research. In particular the determination of UTLS temperature and tropopause height trends are crucial for the monitoring of climate change processes. GPS radio occultation data provide a unique source for global high-resolution temperature observations, and the first long-term RO data set starting with the CHAMP mission in 2001 meanwhile allows for first climatological applications.

To derive monthly mean global temperature fields, the RO profiles have been divided into 18 zonal bands (each 10° wide). The corresponding data distribution is shown in Fig. 8.3. De-seasonalized global monthly temperature anomalies from CHAMP/GRACE are the basis for linear trend analyses considering also Quasi Biennial Oszillation (QBO) effects and El Niño-Southern Oscillation (ENSO) signals. The trend analysis revealed an overall slightly warming of up to 0.1 K per year in the upper troposphere (from 5 km to the tropopause) with strongest signals in the subtropical region of both hemispheres. On the other hand, in the lower stratosphere at mid and high latitudes there is a predominant negative temperature trend (cooling) reaching up to −0.2 K per year in the Antarctic region (Fig. 8.4 right; Schmidt et al. 2010b). These results are consistent with the observed tropopause altitude trend (Fig. 8.4 left, solid line), which shows a mean global increase of 65 m within the decade from 2001 to 2011. Despite the briefness of the data set in terms of climatology, this result is in well agreement with climatological tropopause studies based on radiosonde data (Schmidt et al. 2010b) and reveals the trend of global warming.

The CHAMP/GRACE temperature and tropopause data sets have also been used in a comprehensive study of the tropopause inversion layer and its seasonal cycles in the northern hemisphere mid latitude region (Schmidt et al. 2010a).

8.4 Ionospheric Irregularities in the E-Region

Sporadic E layers (Es) are defined as thin sheets of enhanced electron density that form in the ionospheric E region, preferably in the midlatitudes of the summer hemi-

sphere between 80 and 120 km altitude. These high electron density gradients have significant impact on the propagation of radio signals. It has been shown that fluctuations in the signal to noise ratio of GPS RO observations are outstandingly suited for detection of sporadic E layers (Arras et al. 2010a).

Figure 8.5 gives an overview on the global distribution of sporadic E layers during the seasons of the year 2008. Highest Es rates are found in the mid-latitudes on the respective summer hemisphere. During winter and in polar regions Es rates are generally low. Moderate Es activity is observed during equinox seasons in lower latitudes. In equatorial regions, a slim line of nearly no observed Es events appears during all seasons. This line follows exactly the magnetic equator. Also the minimum in Es occurrence rates in the South Atlantic region that correlates well with the minimum in the Earth's magnetic field's intensity suggests a close connection of both parameters.

Currently, CHAMP provides the longest available consistent time series of GPS RO measurements comprising nearly eight years. Figure 8.6 shows the time series
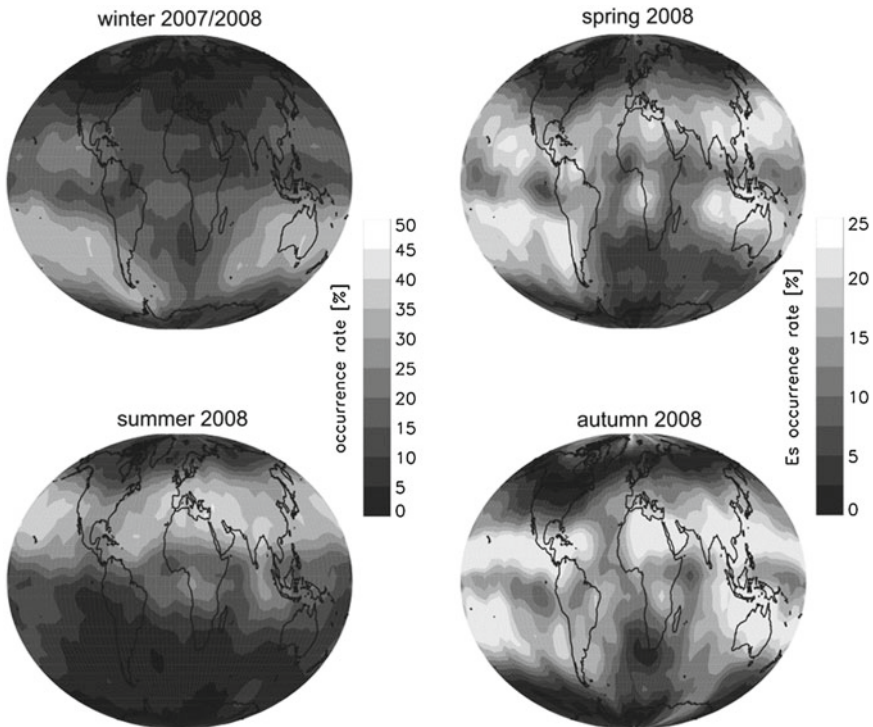
Fig. 8.5 Seasonal global distribution of sporadic E occurrence rates in 2008 derived from CHAMP, GRACE and COSMIC GPS RO data. Each plot contains measurements collected during three months; winter (December 2007, January and February 2008), spring (March, April, May 2008), summer (June, July, August 2008) and autumn (September, October, November 2008) in a 5° × 5° resolution, update from Arras et al. (2008)
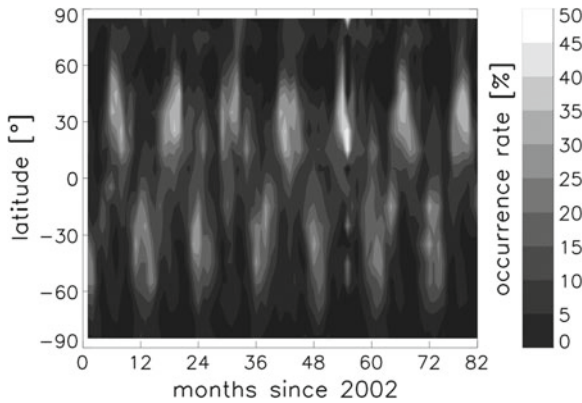
Fig. 8.6 Time series of monthly latitude dependent (10° resolution) sporadic E rates between 2002 and 2008 derived from CHAMP GPS radio occultation data, update from Arras et al. (2008)

of latitude dependent monthly Es rates measured by CHAMP between January 2002 and October 2008. The expected summer maximum alternating between the northern and southern hemisphere is clearly visible. The individual summer maxima are interrupted by very low Es rates in spring and autumn. Weak secondary maxima are found at low latitudes on the winter hemisphere. In general, the Es rates in the southern hemisphere are apparently reduced by 25 % compared to the northern hemisphere. The summer maxima vary in intensity, duration and dimension. But usually values around 40 % (30 %) in Es occurrence frequency are observed in the northern (southern) hemisphere. For more comprehensive results of Es investigations with GPS radio occultation data from CHAMP, GRACE and FORMOSAT-3/COSMIC see (Arras 2010b).

8.5 Summary and Outlook

In the course of the ATMO-CHAMP/GRACE project the GPS RO analysis software at GFZ has been improvement significantly. The new software version (006) was applied for consistent reprocessing of the GPS RO long-term data set from CHAMP and GRACE and is also capable for processing of open-loop data (e.g. TerraSAR-X, TanDEM-X). The reprocessed CHAMP/GRACE data set is successfully used for several atmospheric applications such as temperature trends in the upper troposphere lower stratosphere region, studies on variability and trend behavior of tropopause parameters, investigations on gravity wave activity and occurrence of sporadic E-layers.

The GPS RO data set from CHAMP and GRACE is used by the international user community and requested regularly at the user portal ISDC. GPS RO atmospheric profiles from GRACE and TerraSAR-X are continuously used in operational numeri-

cal weather prediction by the leading weather centers (e.g., UK MetOffice, ECMWF, NCEP, DWD). The reprocessed CHAMP/GRACE-A data set provides the basis for a global GPS RO climatological series whose importance for climate change monitoring will significantly increase in the future, especially regarding new global navigation satellite systems (e.g., Galileo, GLONASS, BEIDOU) and GPS RO satellite missions (e.g., MetOp-B, COSMIC-2, GRACE follow-on).

References

Anthes R, Bernhardt P, Chen Y, Cucurull L, Dymond K, Ector D, Healy S, Ho SP, Hunt D, Kuo YH, Liu H, Manning K, McCormick C, Meehan T, Randel W, Rocken C, Schreiner W, Sokolovskiy S, Syndergaard S, Thompson D, Trenberth K, Wee TK, Yen N, Zhang Z (2008) The COSMIC/FORMOSAT-3 mission: early results. Bull Am Met Soc (March):1–21

Arras C, Jacobi C, Wickert J, Heise S, Schmidt T (2010) Sporadic E signatures revealed from multi-satellite radio occultation measurements. Adv Radio Sci 8:225–230. doi:10.5194/ars-8-225-2010

Arras, C. (2010b) A global survey of Sporadic E Layers based on GPS radio occultations by CHAMP, GRACE and FORMOSAT-3/COSMIC, PhD thesis, University Leipzig

Arras C, Wikert J, Beyerle G, Heise S, Schmidt T, Jacobi C (2008) A global climatology of ionospheric irregularities derived from GPS radio occultation. Geophys Res Lett 35:L14809. doi:10.1029/2008GL034158

Heise S, Wickert J, Beyerle G, Schmidt T, Smit H, Cammas J-P, Rothacher M (2008) Comparison of water vapour and temperature results from GPS radio occultation aboard CHAMP with MOZAIC aircraft measurements. IEEE Trans Geosci Remote Sens 46(11):3406–3411. doi:10.1109/TGRS.2008.920268,2008

Ho S-P, Hunt D, Steiner AK, Mannucci AJ, Kirchengast G, Gleisner H, Heise S, Engeln AV, Marquardt C, Sokolovskiy S, Schreiner W, Scherllin-Pirscher B, Ao C, Wickert J, Syndergaard S, Lauritsen KB, Leroy S, Kursinski ER, Kuo Y-H, Foelsche U, Schmidt T, Gorbunov M (2012) Reproducibility of GPS radio occultation data for climate monitoring: profile-to-profile inter-comparison of CHAMP climate records 2002 to 2008 from six data centers. JGR 117(D18111):38. doi:10.1029/2012JD017665

Ho S-P, Kirchengast G, Leroy S, Wickert J, Mannucci AJ, Steiner A, Hunt D, Schreiner W, Sokolovskiy S, Ao C, Borsche M, Engeln AV, Foelsche U, Heise S, Iijima B, Kuo Y-H, Kursinski R, Pirscher B, Ringer M, Rocken C, Schmidt T (2009) Estimating the uncertainty of using GPS radio occultation data for climate monitoring: inter-comparison of CHAMP refractivity climate records 2002–2006 from different data centers. J Geophys Res 114:D23107. doi:10.1029/2009JD011969

Kursinski ER, Hajj GA, Hardy KR, Schofield JT, Linfield R (1997) Observing Earth's atmosphere with radio occultation measurements using the global positioning system. J Geophys Res 102:23429–23465

Schmidt T, Cammas J-P, Heise HGJSS, Wickert J, Haser A (2010a) Observational characteristics of the tropopause inversion layer derived from CHAMP/GRACE radio occultations and MOZAIC aircraft data. J Geophys Res 115:D24304. doi:10.1029/2010JD014284

Schmidt T, Wickert J, Haser A (2010) Variability of the upper troposphere and lower stratosphere observed with GPS radio occultation bending angles and temperatures. Adv Space Res doi:10.1016/j.asr.2010.01.021

Sokolovskiy S, Hunt D (1996) Statistical optimization approach for GPS/MET data inversion, paper presented at the URSI GPS/MET workshop. University of Arizona, Tucson

Steiner AK, Hunt D, Ho S-P, Kirchengast G, Mannucci AJ, Scherllin-Pirscher B, Gleisner HV, Engeln A, Schmidt T, Ao C, Leroy SS, Kursinski ER, Foelsche U, Gorbunov M, Kuo Y-H, Lauritsen KB, Marquardt C, Rocken C, Schreiner W, Sokolovskiy S, Syndergaard S, Heise S, Wickert J (2013) Quantification of structural uncertainty in climate data records from GPS radio cccultation. ACP 13:1469–1484. doi:10.5194/acp-13-1469-2013

Wickert J, Michalak G, Schmidt T, Beyerle G, Cheng CZ, Healy SB, Heise S, Huang CY, Jakowski N, Köhler W, Mayer C, Offiler D, Ozawa E, Pavelyev AG, Rothacher M, Tapley B, Arras C (2009) GPS radio occultation: results from CHAMP, GRACE and FORMOSAT-3/COSMIC, Terrestrial, Atmospheric and Oceanic Sciences (TAO). 20:35–50. doi:10.3319/TAO.2007.12.26.01

Part II
REAL GOCE

Chapter 9
Real Data Analysis GOCE (REAL GOCE): A Retrospective Overview

Wolf-Dieter Schuh and Boris Kargoll

9.1 Introduction

Many years of intensive research led to the realization of the Gravity Field and Steady-State Ocean Circulation Explorer (GOCE) satellite mission (cf. ESA 1999), which was launched on 17 March 2009. The primary goal of this mission is the determination of the static component of the Earth's gravity field with the unprecedented global accuracy and resolution of at least 1 mGal for gravity anomalies and 1–2 cm for the geoid at a global scale of at least 100 km. With the availability of this model other geoscientific core goals can be realized: the Earth system with all its interacting geophysical and oceanographic processes may be modeled with much higher reliability by means of a high-precision GOCE gravity field, while a high-precision geoid will finally enable geodesists to unify and connect the heterogeneous national height reference systems.

This outstanding leap in both accuracy and resolution of Earth gravity field determination has been made possible by the innovations in sensor and satellite technology. With the GOCE mission the measurement principle of satellite gravity gradiometry (SGG, cf. Rummel 1986) was applied for the first time in history. Another innovation in this mission was the first European satellite-borne GPS receiver, mounted on board the GOCE satellite to determine its orbital positions via satellite-to-satellite tracking (SST).

The electrostatic gravity gradiometer consists of mutually orthogonal arranged accelerometers, designed to measure, in differential mode, the second derivatives of the Earths gravity field potential and, in common mode, rotational accelerations and the non-conservative forces acting on the satellite. Based on these input signals a drag-free control regulates the thrusters to keep the satellite in free fall at a low altitude of approximately 260 km.

W.-D. Schuh (✉) · B. Kargoll
Institute of Geodesy and Geoinformation, University of Bonn,
Nussallee 17, 53115 Bonn, Germany
e-mail: schuh@uni-bonn.de

In the first six month after launch all of the system components have been switched on and calibrated successively. Then the first measurement period (1 November 2009–11 January 2010) was carried out and resulted in the recording of approximately 6.1 million observations, which were used to compute *Release01* gravity field models. Subsequently, the *Release02* models were determined from the approximately 19.5 million observations collected until 5 July 2010. Finally, the *Release03* models were derived from the ca. 31.1 million observations obtained until 13 April 2011. Meanwhile, a better understanding of the actual measurement characteristics implied some modifications in the angular rate reconstruction and the calibration approach, and required a reprocessing of the all data.

The GOCE data processing has been performed on several levels. Firstly, the processing of Level 0 to Level 1b data has been carried out by ESA's Payload Data Segment (PDS); its main output are the gravity gradients and the corresponding attitude and GPS orbit data with a sampling rate of 1 Hz. The Level 1b to Level 2 data processing is supported by ESA and performed by the High-level Processing Facility (HPF, cf. Rummel et al. 2004). The HPF, which is a consortium of eight universities and two research institutions, determines precise orbits and GOCE gravity field models and orbital gravity gradients.

The research produced by this consortium has been enabled by the long-standing co-sponsorship of the Federal Ministry of Education and Research (BMBF) through the Geotechnologien Programme (which was initially also co-funded by the German Research

Foundation (DFG)). Since its initiation in 2001 this support programme sponsored scientists specifically of up to ten German research institutions. In the course of their research activities (which included the development of tailored theoretical methods, algorithms and software, as well as technical, operational and collaborative skills), German research institutions were thus enabled to build up a sufficiently high level of know-how enabling them to carry out the intricate GOCE data-processing chain from GOCE measurements up to the final gravity field products independently and in its entirety.

The focus of the first collaborative Geotechnologien project "GOCE-Gravitationsfeldanalyse Deutschland I" (GOCE GRAND I, 2001–2004, cf. Part III in Flury et al. 2006) was on the implementation of standard procedures for the analysis, processing, calibration and validation of GOCE data, as well as on their combination with GRACE data. During GOCE GRAND II (2005–2008, cf. Part III in Flechtner et al. 2012), research was chiefly concerned with adaptations of the methods, algorithms and software modules to the final configuration of the GOCE satellite and its instruments. The goals of the subsequent third research project "REal data AnaLysis GOCE" (REAL GOCE, 2009–2012) were the complete implementation of the GOCE data processing chain and its application to the GOCE real data and contribute in particular to the fields of GOCE data analysis, gravity field modeling, validation, and combination with other geoscientific data and models (see Fig. 9.1). The REAL GOCE team consisted of seven university departments: the Departments of Theoretical Geodesy and of Astronomical, Mathematical and Physical Geodesy of the Institute of Geodesy and Geoinformation (IGG-TG and IGG-APMG) at
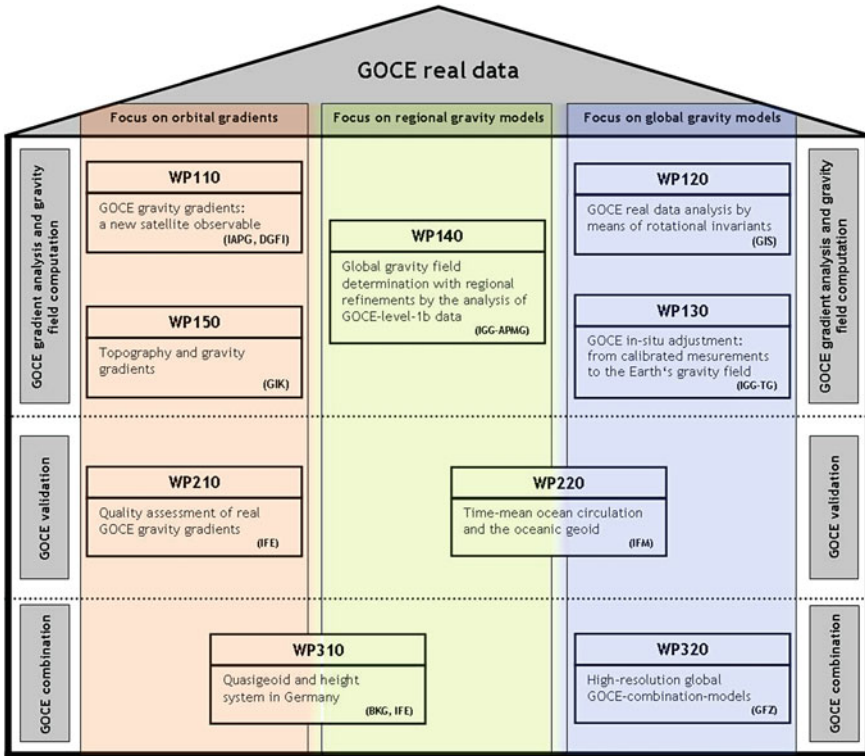
Fig. 9.1 REAL GOCE comprised nine work packages (WP) with different spatial (orbital, regional, global) and thematic focuses (GOCE gradient analysis and gravity field computation, GOCE validation, GOCE combination)

the University of Bonn, the Institute of Oceanography (IFM) at the University of Hamburg, the Institute of Geodesy (IFE) at the Leibniz University Hannover, the Geodetic Institute (GIK) at the Karlsruhe Institute of Technology, the Institute of Astronomical and Physical Geodesy (IAPG) at the Technical University Munich, and the Institute of Geodesy (GIS) at the University of Stuttgart; two research centers: the German Geodetic Research Institute (DGFI) and the GFZ German Research Centre for Geosciences at the Helmholtz Centre Potsdam; and one federal agency: the Federal Agency for Cartography and Geodesy (BKG). The individual contributions of these institutions to the achievement of the scientific goals of REAL GOCE are summarized in the following section (see also Fig. 9.1).

9.2 Contributions

Based on the general structure of REAL GOCE (as shown in Fig. 9.1), we will now introduce the reader into the specific contributions to REAL GOCE as described by the individual project partners in the subsequent, peer-reviewed papers.

Three contributions deal specifically with analyses of the orbital gravity gradients and their processing into gravity fields models. To begin with, Murböck et al. ("GOCE gravity gradients: reprocessed gradients and spherical harmonic analyses", WP110) demonstrate the improvements of GOCE-only as well as GOCE-GRACE-combined gravity field models obtained by using re-processed (Level 1b) GOCE data. Furthermore, they analyze the formal errors of GOCE-only models in terms of spherical harmonics (based on, respectively, the *time-wise*, *space-wise* and the *direct approach*) via validating comparisons with Quick-Look models (based on the *semi-analytic approach*). Bouman et al. ("GOCE gravity gradients: combination with GRACE and satellite altimetry", WP110) describe a strategy for avoiding the problem that relatively inaccurate gravity tensor components deteriorate the accuracy of the entire tensor when it is rotated from the *gradiometer reference system* into a geographical reference frame. They also investigate a regional method for comparing (thus validating) and combining GOCE gravity gradients with satellite altimetry data. The contribution of Grombein et al. ("Incorporating topographic-isostatic information into GOCE gravity gradient processing", WP150) propose a *remove-restore* approach based on the *Rock-Water-Ice topographic-isostatic gravity field model* as part of the processing GOCE gravity gradients in order to avoid potential numerical instabilities due to the presence of high- and mid-frequency topographic-isostatic signal content in the gradients. As the result of their studies concerning regional gravity field determination, Shabanloui et al. ("Global gravity field models from different GOCE orbit products", WP140) evaluate the solution of their *geometrical precise orbit determination* approach as an alternative to the ESA's official *precise science orbits* by comparing the GOCE gravity field models determined from the respective orbit products. Two articles address GOCE gradient analysis and global gravity field computation. In Krasbutter et al. ("Adjustment of digital filters for decorrelation of GOCE SGG data", WP130), we find an exposition of various *cascaded autoregressive moving-average* filtering strategies for taking the autocovariance patterns of the gravity gradients into account in the *in-situ* estimation of global gravity field models. As an alternative to this *in-situ* approach, Cai et al. (2012, "GOCE real data analysis by means of rotational invariants", WP120) describe a method for computing global gravity field models, which avoids the use of potentially inaccurate rotation measurements by adjusting certain (decorrelated) functionals of the gravity tensor. This contribution also addresses the problem of decorrelation-filtering of the various invariants.

Addressing GOCE validation (with a subsidiary focus on the combination of GOCE data with other sources) as the second thematic cornerstone of REAL GOCE, Brieden and Müller ("Cross-overs assess quality of GOCE gradients", WP210) present the results of their work on assessing the quality of gravity gradients by analyzing their differences at the locations of *satellite track cross-overs*. A different kind of GOCE validation method, which is based on gravity field models instead of gradients, is described in Siegismund et al. ("Consistency of GOCE geoid information with in-situ ocean and atmospheric data, tested by ocean state estimation", WP220); in this approach, a gravity field model based on GOCE data is used alongside *mean sea surface* and further ocean data to determine an *ocean general circulation model*,

whose consistency is then checked by mean of the *German part of Estimating the Circulation and Climate of the Ocean* model.

The third major topic of REAL GOCE, GOCE combination (with applications also to the validation of GOCE data), is covered by three contributions. Voigt and Denker ("Regional validation and combination of GOCE gravity field models and terrestrial data", WP310) present a *remove-compute-restore* approach to combining GOCE gravity field models with terrestrial gravity datasets, astrogeodetic vertical deflections, GPS/leveling data, and gravimetric quasigeoid models. In the second article dedicated to combination issues, Rülke et al. ("Height system unification based on GOCE gravity field models—benefits and challenges", WP310) present results from validating GOCE gravity field models by means of GNSS/leveling data. Then they discuss an approach to combining global and regional gravity field models based on *low-pass* filtering of the former and *high-pass* filtering of the latter. Finally, they address the problem of unifying the various height systems in Europe by using GOCE gravity field models in combination with GNSS/leveling data. Other sources of gravity field related data combinable with GOCE data include Gravity Recovery and Climate Experiment (GRACE), Laser Geodynamics Satellites (LAGEOS), and surface gravity data. Shako et al. ("EIGEN-6C—a high-resolution global gravity combination model including GOCE data", WP320) describe their procedure for computing such a GOCE combination gravity field model and evaluate its characteristics via comparison with the Earth Gravitational Model (EGM) 2008.

References

ESA (1999) Reports for mission selection: the four candidate Earth explorer core missions Gravity Field and Steady-State Ocean Circulation mission. ESA-SP12333(1), ESA Publication Division

Flechtner F, Gruber T, Güntner A, Mandea M, Rothacher M, Schöne T, Wickert J (eds) (2012) System earth via geodetic-geophysical space techniques. In: Advanced technologies in earth sciences, Springer, Berlin

Flury J, Rummel R, Reigber Ch, Rothacher M, Boedecker G, Schreiber U (eds) (2006) Observation of the system earth from space. Springer, Berlin

Rummel R (1986) Satellite gradiometry. In: Sünkel H (ed) Mathematical and numerical techniques in physical geodesy, lecture notes in earth sciences, vol 7. Springer, Berlin, pp 317–363

Rummel R, Gruber T, Koop R (2004) High level processing facility for GOCE: products and processing strategy. In: Lacoste H (ed) Proceedings of the 2nd international GOCE user workshop GOCE, the geoid and oceanography, ESA SP-569, ESA, ISBN (Print) 92-9092-880-8, ISSN 1609-042X

Chapter 10
GOCE Gravity Gradients: Reprocessed Gradients and Spherical Harmonic Analyses

Michael Murböck, Claudia Stummer, Roland Pail, Weiyong Yi, Thomas Gruber and Reiner Rummel

Abstract Detailed analyses of the original GOCE data have shown that specific improvements can be achieved by a Level 1b (L1b) processor update Stummer et al. (2011, 2012). In the first part of this work the four processor update steps are discussed, and the impact on GOCE gravity fields is shown. The largest improvements occur in the lower spherical harmonic (SH) degrees. But furthermore significant improvements of the sectorial SH coefficients up to high SH degrees can be achieved. Therefore also combined models based on GOCE and GRACE data benefit from the reprocessed L1b data Pail et al. (2012). The second part of this study gives an overview of the operational GOCE Quick-Look (QL) models, which have been computed as part of ESA's calibration/valida-tion activities. These QL gravity field solutions give consistent and realistic estimates of GOCE gravity fields, with short latency. It is shown that already the first GOCE QL models revealed important new gravity field information contained in GOCE data. One of the results of QL processing is a realistic estimate of the observation noise of all GOCE gradiometer components. Based on this stochastic information, the goal of the last part of this work is a formal error validation of three recent GOCE-only models. The time-wise approach pail (2011) leads to the most realistic formal errors.

10.1 Introduction

The overall goal of the REAL GOCE project is the integrated analysis of the GOCE data addressing all aspects of gravity field determination. In the frame of the REAL GOCE project, the present contribution deals with the internal calibration of the gradiometer, the analysis of the gradiometer data, and SH analysis.

M. Murböck (✉) · C. Stummer · R. Pail · W. Yi · T. Gruber · R. Rummel
Institut für Astronomische und Physikalische Geodäsie, Technische Universität München, 80290 München, Germany
e-mail: murboeck@bv.tum.de

Improved L1b strategies could be developed, which are by now implemented in ESA's L1b processor, and the reprocessing of the gravity gradient and attitude data of the whole GOCE mission period results in improved data to be provided to the user community.

This paper is structured as follows: In Sect. 10.2 the upgraded strategies of L1b processing and their impact on GOCE gravity field modelling is discussed. Section 10.3 deals with the processing of QL gravity field models applying a semi-analytic approach, and evaluates the gravity field models resulting from this fast gravity field processing. Section 10.4 describes an approach of spectral analysis in order to derive specific stochastic properties of GOCE gravity field models and to validate their formal error estimates. Finally, Sect. 10.5 provides an overall discussion and conclusions.

10.2 Upgrades of Level 1b Processing Methods

In the frame of this project upgrades of the ESA L1b processing algorithms have been developed and implemented (Stummer et al. 2011, 2012). Finally, ESA has decided to re-process the L1b data of the complete mission period, in order to provide upgraded gravity gradient and attitude products to the GOCE user community. The upgrades include:

1. an improved method for the angular rate reconstruction (ARR),
2. a new method for the determination of the gradiometer's inertial attitude,
3. the use of all simultaneously available star sensor data (STR) and
4. an improved calibration of the gradiometer measurements (ICM).

Figure 10.1 shows the power spectral density (PSD) of the satellite gravity gradient (SGG) tensor trace of the original data (blue curve) and after successive application of the above-mentioned upgrades. The largest improvements are achieved with the new method for the angular rate reconstruction, especially for low to medium frequencies and for multiples of the orbit frequency ($1.86 \cdot 10^{-4}$ Hz). The impact of the new method for the attitude determination is not shown here, as the SGG tensor trace is invariant on rotations.

Stummer et al. (2011, 2012) show in detail the upgraded L1b processing and first estimates of their impact on GOCE-only gravity fields. Here we show two gravity field models based on SGG data for the period November to December 2009, resolved up to SH degree and order (d/o) 224 based on full normal equations Pail et al. (2012). Since we used the original (old) and reprocessed (new) EGGNOM1b data as input, we refer to these models as "old" and "new" SGG-only model. Figure 10.2a–c shows gravity field differences at SH d/o 190 to the combined model EGM2008 (Pavlis et al. 2012), which is based on GRACE, satellite altimetry, and terrestrial data and serves as a good reference in this spectral range. The performance in the long wavelengths is clearly enhanced by the new processor data. The same conclusion can be drawn from the coefficient differences between these two SGG solutions, cf. Fig. 10.2d.
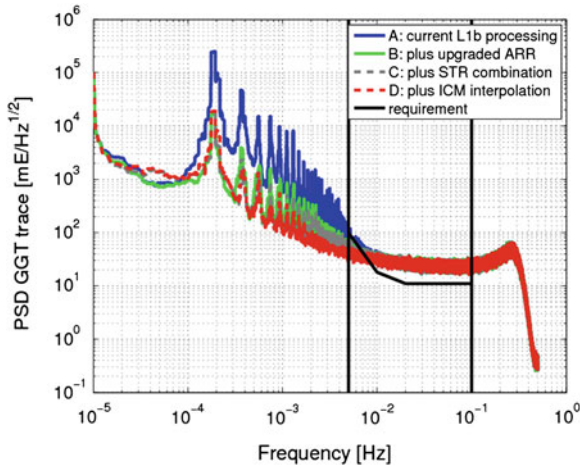
Fig. 10.1 SGG tensor trace PSDs with the original L1b processing (*blue*) and the updates in the GOCE L1b gradiometer processor: new angular rate reconstruction (*green*), star sensor data combination (*gray dashed*), and calibration parameter interpolation (*red dashed*)
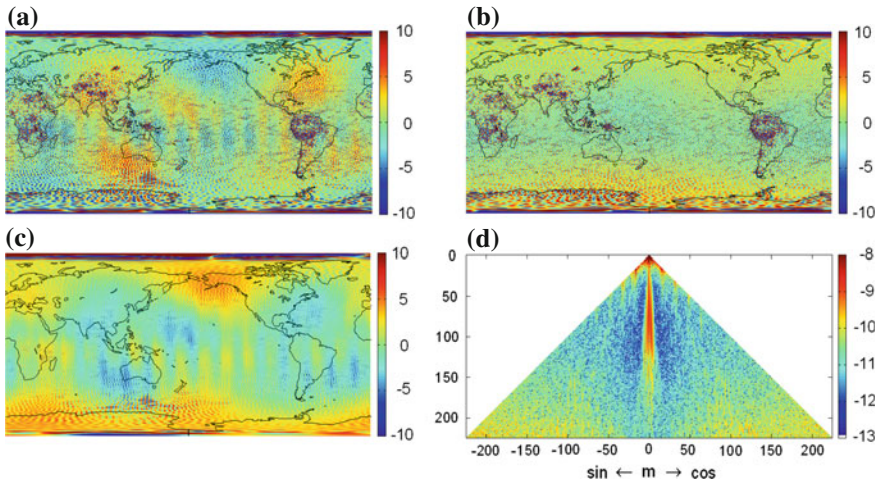
Fig. 10.2 Gravity anomaly differences in *m*Gal up to SH degree and order 190 between, (**a**) EGM2008 and the old SGG-only model, (**b**) EGM2008 and new SGG-only model, (**c**) old and new SGG-only models, (**d**) absolute differences of SH coefficients of the old and new SGG-only models

In addition to significant differences in the low degrees, also coefficients around SH order 16 and multiples of it, are evident. These improvements result from the reduction of the characteristic peaks at the revolution frequency and integer multiples of it, cf. Fig. 10.1.

In Pail et al. (2012) the impact of the L1b processor updates are analyzed individually for all SGG components. Additionally, the effect on combined gravity field models, by including either GOCE GPS-SST data or GRACE, is analyzed. It could be demonstrated that the cross-track SGG component V_{yy} shows the largest relative improvements. For the sectorial and near-sectorial SH coefficients significant improvements even up to SH degree 200 can be achieved. Even a combined GOCE+GRACE model can benefit from improved gravity gradient data by more than 10 % in terms of gravity field performance.

10.3 Semi-Analytic Gravity Field Analysis

In the frame of the operational GOCE data processing the semi-analytic gravity field analysis has been applied for a QL quality assessment of the GOCE data, and to provide a fast feedback to ESA's calibration/validation activities (Pail et al. 2007). During the nominal mission phase of GOCE more than 200 QL gravity field solutions have been produced with short latencies of a few days after the actual measurements have been taken. With this software, the first high-resolution GOCE gravity field model ever has been derived (Mayrhofer et al. 2010).

Figure 10.3a shows SH degree medians of QL gravity field solutions based on data periods between 20 and 60 days. As reference model either ITG-GRACE2010S (Mayer-Gürr et al. 2010) or EGM2008 (Pavlis et al. 2012) have been used. The differences to the GRACE-only model are much smaller than to the combined gravity field model EGM2008 in the degree range 80 to 160. When compared to EGM2008, the characteristic bump is an expression of systematic deviations in certain regions of low data quality of terrestrial gravity data included in this combined model. The variety of QL solutions shows great consistency among each other, as well as a good matching with the reference models, demonstrating the remarkable quality of these
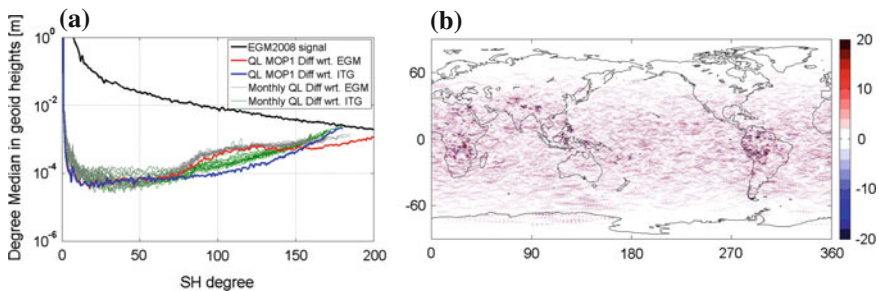
Fig. 10.3 a SH degree median of QL differences with respect to EGM2008 and ITG-Grace2010. The thick *red* and *blue lines* belong to the 2 monthly QL solution of Nov/Dec 09 (MOP1). The *thin lines* represent several QL solutions for selected data periods in 2010 and 2011. **b** Gravity anomaly differences of the combined QL solution for Nov./Dec. 2009 and EGM2008 up to d/o 200 in mGal

fast QL solutions. Figure 10.3b shows gravity anomaly differences to EGM2008 up to d/o 200. They demonstrate that the meanwhile well-known deviations in South America, Africa or the Himalayan region (cf. also Fig. 10.2a, b), representing new gravity field information obtained by GOCE, could be seen already half a year before the first post-processing solutions have been released.

10.4 Spectral Analysis of GOCE Gravity Models

Based on QL results, also the stochastic properties of the official ESA GOCE gravity field models are analyzed. The goal is the comparison of SH formal errors of current GOCE-only gravity field models (second releases of the ESA GOCE models applying the time-wise (TIM), space-wise (SPW) and direct (DIR) approach (pail 2011), based on effectively six months of GOCE data) with semi-analytic estimations. The semi-analytic error estimations of the SH coefficients are based on PSDs of the SGG-residuals of a QL solution, which are shown in Fig. 10.4a. Below the measurement bandwidth (MBW) ($f < 5$ mHz) the gradiometer noise increases, superimposed with sharp peaks at multiples of the orbit frequency. Applying the semi-analytic approach (Sneeuw 2000) this spectral noise information is propagated onto the SH spectrum resulting in SH formal errors of a GOCE gravity field model, including a simplified GPS-SST part (Fig. 10.4b). Since no regularization (REG) was applied, large errors occur around the zonal coefficients.

Figures 10.5 and 10.6 display the results of the comparison of the semi-analytic reference with the three models (TIM, SPW, DIR). Figure 10.5 shows relative differences of the coefficient errors (log. scaled). Figure 10.6 illustrates the geoid height degree median of the formal errors of the model (blue) and the semi-analytic
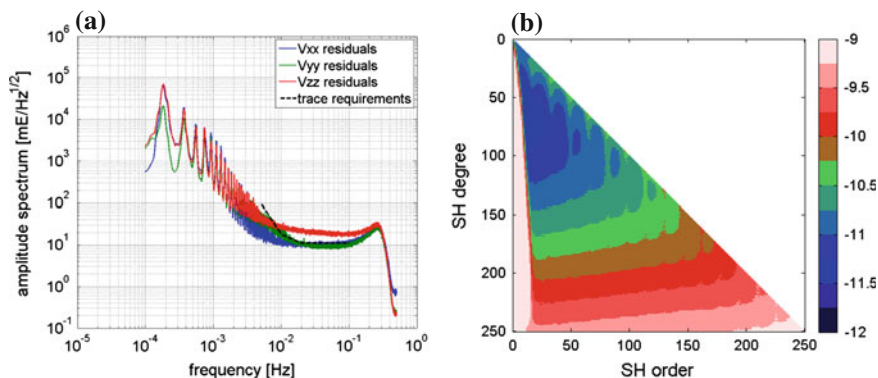
Fig. 10.4 **a** SGG residual PSDs of a GOCE QL solution and **b** their semi-analytic propagation onto the SH spectrum in a combined GOCE gravity field solution with a simplified GPS-SST component and without any regularization applied
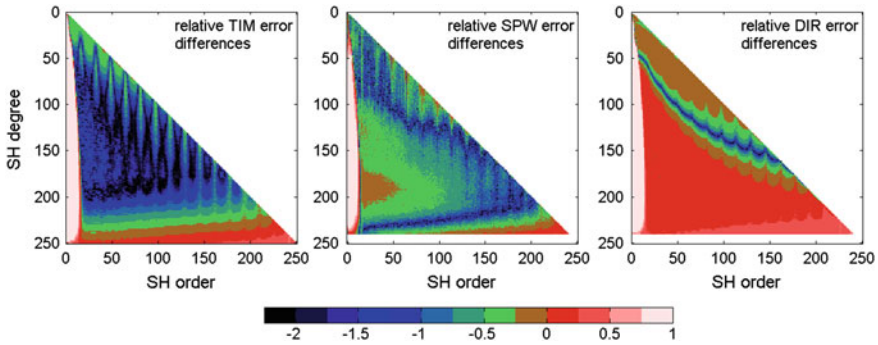
Fig. 10.5 Relative error differences ($\log_{10}\left(|\Delta\sigma|/\sigma_{\text{semi-analytic}}\right)$) of the three models to the reference values resulting from semi-analytic error propagation as shown in Fig. 10.4b
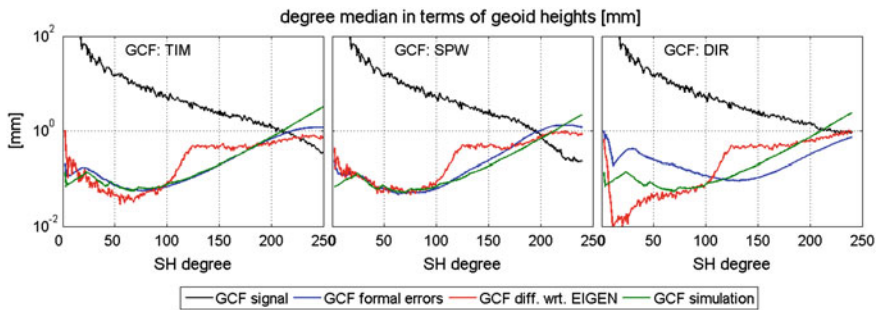
Fig. 10.6 SH degree median in terms of geoid heights of formal errors of the models (*blue*), semi-analytic reference (*green*); differences to EIGEN-51C (*red*) and the estimated signal (*black*)

reference (green), compared with the corresponding coefficient differences to a reference model (red), here EIGEN-51C (Bruinsma et al. 2010), and to the estimated signal (black).

Specific characteristics of the ESA GOCE models can be derived, and the consistency of their formal errors can be validated. In contrast to the semi-analytic reference, all three models contain some kind of REG, which leads to the large differences around the zonal coefficients. TIM agrees best with the reference compared to the other two models. In large areas of the SH spectrum the absolute differences between the two formal error sets are more than two magnitudes smaller than the formal errors themselves. SPW gives a homogeneous agreement as well. DIR shows the largest differences compared to the semi-analytic reference, mainly caused by a priori information from the GRACE-only ITG-GRACE2010S model (Mayer-Gürr et al. 2010) as well as an inconsistent stochastic modelling of SGG. These differences show up clearly in the degree median differences to EIGEN-51C in Fig. 10.6.

None of the three models includes the characteristic peaks (Fig. 10.4a) in their stochastic models. Therefore all three underestimate the formal errors around multiples of SH order 16. In summary, these comparisons show, that the stochastic model of

TIM and therefore also the formal SH coefficient errors are closest to the stochastic characteristics of a GOCE-only gravity field. The formal errors of TIM therefore can be considered as very good estimates of the true errors of the model.

10.5 Discussion and Conclusions

Software developments achieved in the framework of the REAL GOCE project lead to an update of ESA's L1b processor and the reprocessing of the GOCE SGG and attitude data. As the most significant improvements of the SGG performance is below the MBW, GOCE gravity fields benefit mainly in the low SH degrees. Particularly the improvement of the V_{yy} component up to 10 mHz results in improved estimates of the (near-)sectorial SH coefficients up to high degrees, so that even combined GOCE-GRACE gravity fields benefit from the reprocessed L1b data (Pail et al. 2012). Additionally, the characteristic large errors around multiples of the orbit frequency are reduced, leading to an improved signal-to-noise ratio of SH coefficients around order 16 and multiples of it.

Within the operational GOCE processing the QL gravity field solutions have been computed with very short latencies. The high quality of these solutions has been shown by comparing them with different reference models. It could be demonstrated, that already these first-ever computed GOCE gravity fields have clearly revealed the new gravity field information contained in the GOCE measurements.

Analysis of the spectra of SGG residuals of a GOCE QL solution reveals the main characteristics of the noise in the SGG observations. Based on a semi-analytic propagation of GOCE QL SGG residual PSDs to the SH spectrum, the formal errors of ESA GOCE-only models have been validated. The formal errors of the TIM model provides the most realistic error estimates.

In summary, in the frame of this contribution to REAL GOCE important knowledge and expertise about the specific characteristics of the new observation type of GOCE gradients could be gained.

References

Bruinsma SL, Marty JC, Balmino G, Biancale R, Förste C, Abrikosov O, Neumayer H (2010) GOCE gravity field recovery by means of the direct numerical method. In: Proceedings of the ESA living planet symposium, ESA Publication SP-686, ISBN 978-92-9221-250-6, ISSN 1609-042X

Mayer-Gürr T, Eicker A, Kurtenbach E, Ilk K-H (2010) ITG-GRACE: global static and temporal gravity field models from GRACE data. In: System earth via geodetic-geophysical space techniques, Springer, pp 159–168. doi:10.1007/978-3-642-10228-813

Mayrhofer R, Pail R, Fecher T (2010) Quicklook gravity field solutions as part of the GOCE quality assessment. In: Proceedings of the ESA living planet symposium, ESA Publication SP-686, ISSN 1609–042X

Pail R, Metzler B, Preimesberger T, Lackner B, Wermuth M (2007) GOCE quick-look gravity field analysis in the framework of HPF. In: Proceedings of the 3rd international GOCE user workshop, ESA SP-627, pp 325–332, ISBN 92-9092-938-3, ISSN 1609-042X, http://earth.esa.int/cgi-bin/confg6.pl?abstract=36

Pail R, Bruinsma S, Migliaccio F, Förste C, Goiginger H, Schuh W-D, Höck E, Reguzzoni M, Brockmann JM, Abrikosov O, Veicherts M, Fecher T, Mayrhofer R, Krasbutter I, Sansò F, Tscherning CC (2011) First GOCE gravity field models derived by three different approaches. J Geodesy 85(Nr. 11):pp 819–843. Special issue: GOCE—The gravity and steady-state ocean circulation explorer, Springer, ISSN 0949–7714. doi:10.1007/s00190-011-0467-x.

Pail R, Fecher T, Murböck M, Rexer M, Stetter M, Gruber T, Stummer C (2013) Impact of GOCE Level 1b data reprocessing on GOCE-only and combined gravity field models. Studia Geophysica et Geodaetica 57(2):155–173. ISSN (Print) 0039–3169, doi:10.1007/s11200-012-1149-8

Pavlis N.K., Holmes S.A., Kenyon S.C., Factor J.K. (2012) The development and evaluation of the Earth Gravitational Model 2008 (EGM2008). Journal of Geophysical Research, 117, B04406, 38, doi:10.1029/2011JB008916

Sneeuw N (2000) A semi-analytical approach to gravity field analysis from satellite observations. DGK, Reihe C, Heft 527, Verlag der Bayerischen Akademie der Wissenschaften, ISBN (Print) 3-7696-9566-6, ISSN 0065-5325

Stummer C, Fecher T, Pail R (2011) Alternative method for angular rate determination within the GOCE gradiometer processing. J Geodesy, Springer, ISSN 0949–7714: doi:10.1007/s00190-011-0461-3

Stummer C, Siemes C, Pail R, Frommknecht B, Floberghagen R (2012) Upgrade of the GOCE Level 1b gradiometer processor. Adv Space Res 49(Nr. 4):739–752, Elsevier, ISSN 0273–1177, doi:10.1016/j.asr.2011.11.027

Chapter 11
GOCE Gravity Gradients: Combination with GRACE and Satellite Altimetry

Johannes Bouman, Martin Fuchs, Verena Lieb, Wolfgang Bosch, Denise Dettmering and Michael Schmidt

Abstract GOCE gravity gradients are a new satellite observable, which are given in the instrument frame that is only indirectly connected to the Earth. A rotation to other frames requires to take the different accuracies of the gradients into account. We show that replacing the less accurate gradients with model information allows to rotate the tensor, but for the diagonal gradients V_{XX} and V_{YY} the model information can reach up to 50 % in the Local-North Oriented Frame, whereas it is only a few percent for V_{ZZ}. We also show that in the direct comparison of GOCE gravity gradients and satellite altimetry derived gradients one has to account for the difference between the along-track altimeter derivatives and the GOCE gradients in a Cartesian frame, as well as the dynamic ocean topography signal. A validation of GOCE using ERS-1 data shows that both data sets are consistent at levels where GOCE is sensitive. For high spatial resolutions below 40 km wavelength GOCE does not contribute, as expected.

11.1 Introduction

The goal of the GOCE mission is to determine the Earth's mean gravitational field with unprecedented accuracy up to a spatial resolution of about 100 km. The gravity gradients, derived from the on-board gradiometer, are the main data source to achieve that aim. The gradients are used in geophysical applications and to derive global gravity field models. It is therefore important to carefully assess these data by comparing them against independent information. On the other hand, the GOCE gradients are given in an instrument frame, which may be less straightforward to use and therefore the gradients are also rotated to the so-called Local North-Oriented Frame (LNOF) with the X-axis North, the Y-axis East and the Z-axis in radial

J. Bouman (✉) · M. Fuchs · V. Lieb · W. Bosch · D. Dettmering · M. Schmidt
Deutsches Geodätisches Forschungsinstitut (DGFI), 80537 München, Germany
e-mail: bouman@dgfi.badw.de

direction. Because the GOCE gradiometer provides four gradients with high accuracy and two with less accuracy, rotation mixes accurate and less accurate components.

In this paper we discuss the validation of the GOCE gravity gradients by comparing them directly with altimeter derived gravity gradients and by combining them with satellite altimeter data in a regional approach. The consistency of the GOCE and satellite altimeter gravity information is analysed at different resolution levels. We start, however, by discussing the rotation of the gravity gradient tensor as this is needed in the validation procedure. We discuss a method to circumvent the mixing of less accurate and accurate gradients and assess the quality of the rotated gradients.

11.2 Rotation of the Gravity Gradient Tensor

The GOCE gravity gradients are given in the Gradiometer Reference Frame (GRF), which is an instrumental frame approximately Earth pointing, but with continuous rotations around all three axes[1] (Bouman et al. 2011b). It may therefore be advantageous to rotate the gravity gradient tensor to a geographical reference frame such as the LNOF. A complicating factor thereby is that four of the GOCE gradients in the GRF have high accuracy in the Measurement Bandwidth (MB) between 0.5 mHz and 0.1 Hz (V_{XX}, V_{YY}, V_{ZZ} and V_{XZ}), whereas the other gradients (V_{XY} and V_{YZ}) are less accurately determined. A direct rotation of the gradient tensor from GRF to other local frames would project part of the larger V_{XY} and V_{YZ} errors onto the other gradients in the rotated frame (Müller 2003; Bouman 2007).

To circumvent this problem, one may substitute the less accurate GOCE gradients with more accurate model gradients and perform tensor rotation (Bouman 2007; Fuchs and Bouman 2011; Brieden and Müller 2012). One of the disadvantages of the point-wise method may be that model and measured components are mixed and the result is biased towards the model input. The signal below the MB for all gradients is replaced by model signal, e.g. from a GRACE-based gravity field model, which is more accurate at these wavelengths. The GOCE gradients are combined with model gradients by band-pass filtering the former and by low-pass filtering the latter with the complement of the band-pass filter. The gradients in the rotated local frame will be a combination of original GOCE gradients and model gradients. It is therefore useful to be able to assess how much gravity field information in the rotated gradients stems from GOCE and how much from the model.

Fuchs and Bouman (2011) present the relative model content in rotated frames by taking the ratio of the total model signal and GOCE gravity gradient signal inside the measurement bandwidth. Figure 11.1 shows the model contribution after rotation to the LNOF for the diagonal gravity gradients V_{XX}, V_{YY} and V_{ZZ}. Because the rotation from GRF to LNOF is mainly around the Z-axis, V_{ZZ} contains relatively little model information. For the other two gradients the rotations increase towards the poles and the model contribution reaches up to 50 %.

---

[1] We here follow the discussion in (Fuchs and Bouman 2011).
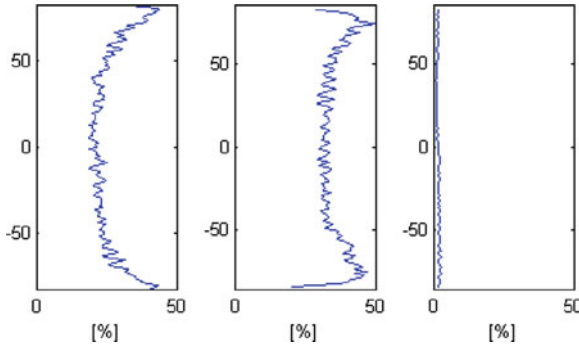
Fig. 11.1 Relative model content averaged over longtitude in the rotated gradients in the LNOF. From *left* to *right* XX, YY, ZZ (Fuchs and Bouman 2011). Vertical axis shows latitude in degrees

11.3 Validation of Gravity Gradients

GOCE gravity gradients can be internally validated by comparing them with GOCE-based gravity field models and vice versa (Bouman and Fuchs 2012). In this paper, however, we perform validation with independent data, in particular satellite altimeter data. We discuss a direct comparison of GOCE gravity gradients and satellite altimetry derived gradients, and combine GOCE with satellite altimeter data.

11.3.1 Direct Comparison of Gravity Gradients and Satellite Altimetry

With satellite radar altimetry the oceanic geoid can be determined with high precision and resolution.[2] Double differentiation of these data along satellite altimeter ground tracks yields along-track gravity gradients that can be used to compute vertical gravity gradients at ground track crossovers. Bouman (2012) discusses the relation between different methods to compute gradients from altimetry. Bouman et al. (2011a) give the exact relation between GOCE and satellite altimetry derived gradients and assessed systematic errors that might occur when using altimeter data.

Although one of the goals of the GOCE mission is to derive the DOT, this does not necessarily mean that in a direct track-wise comparison the DOT signal is visible. For example, the geoid error in the first generation GOCE models is several dm (Gruber et al. 2011), in the same order as the DOT signal. These models were derived combining about 20 million gradients, whereas a track-wise comparison is done using much less data (hundreds—thousands data points), with less averaging. Nonetheless,

---

[2] We here follow the discussion in (Bouman et al. 2011a; Bouman 2012).
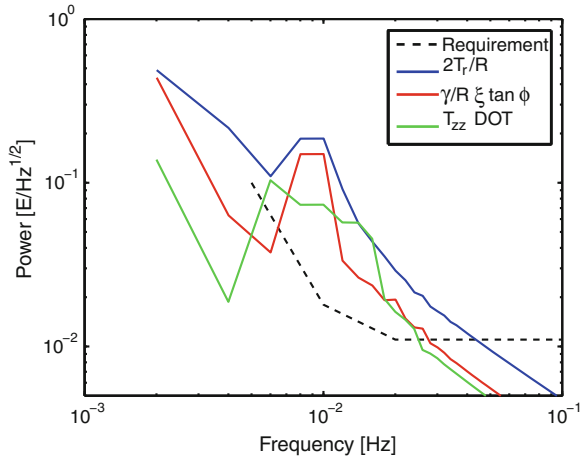
Fig. 11.2 Comparison of systematic differences between GOCE and altimeter gradients (*red and blue lines*), and T_{ZZ} DOT (*green line*) with GOCE gravity gradient trace requirement for the meridian at 45° West in the South Atlantic. All signals were de-trended and the mean has been removed (Bouman 2012)

the DOT signal at GOCE altitude may be above the GOCE requirements, Fig. 11.2. Here T_{ZZ} DOT is the vertical gravity gradient signal due to DOT.

When deriving gravity gradients from satellite altimetry usually the curvature of the Earth and meridian convergence are neglected, which can be expressed as $2T_r/R$ and $\gamma/R\xi\tan\phi$ respectively. Here R is the mean Earth radius T_r is the radial derivative of the disturbing potential, γ is normal gravity, ξ is the north-south deflection of the vertical and ϕ is geocentric latitude. The altimetry derived gradients can therefore not be compared one-to-one with those in a local Cartesian frame. The amplitudes of the two terms are small compared with the total signal, but they may be larger than the satellite altimetry induced stochastic errors and may be above the GOCE requirements, see Fig. 11.2.

11.3.2 Combination of Gravity Gradients and Satellite Altimetry

The GOCE gravity gradients can be combined with satellite altimeter data and other gravity field information in order to obtain global or regional gravity field models. In a global analysis the use of ellipsoidal harmonics may be preferred to fully exploit the high spatial resolution of data given on the ellipsoid. Sebera et al. (2012) discuss numerical stable algorithms for computing these harmonic expansions. Instead of a global approach, however, we use a regional analysis.

The combination of GOCE gradients with satellite altimetry is done by applying the so-called potential method. We use the track-wise approach developed at DGFI to
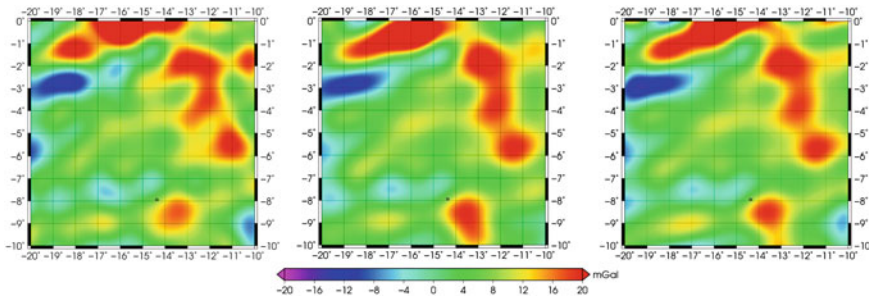
Fig. 11.3 Gravity anomalies modelled using Blackman scaling functions up to level 8 (SH degree 255). Background model is ITG-Grace2010 up to degree 60. GOCE vertical gravity gradients (*left*); ERS-1 GM data (*middle*); Combination GOCE and ERS-1 GM (*right*)

compute the DOT with respect to ITG-Grace03s (Bosch and Savcenko 2010). From multi-mission altimetry the disturbing potential T is derived for a certain region and combined with T_{ZZ} from GOCE. The disturbing potential is expressed in terms of local basis functions of which the scaling coefficients are the unknowns that are to be estimated (Schmidt et al. 2007). Spherical localizing basis functions allow to analyse the gravity field signals at different resolution levels.

We used an area of 10° by 10° in the South Atlantic where we compared GOCE radial gravity gradients with gradients derived from satellite altimeter data, see Fig. 11.3. Gravity anomalies were computed on the WGS84 ellipsoid using GOCE vertical gravity gradients, ERS-1 Geodetic Mission (GM) satellite altimeter data as well as a combination of both data sets. Shown is the gravity field modelling up to level 8 of a multi-resolution decomposition, which roughly corresponds to spherical harmonic (SH) degree 255. The background model is ITG-Grace2010 up to degree 60. The signal amplitudes and spatial structures are quite similar in all three cases. The combination was done using variance component estimation where GOCE receives a weight similar to ERS-1 GM. We also combined both data sets at the much higher level 11, which corresponds to spherical harmonic degrees up to 2047. In this case, the GOCE data receive very little weight, which is to be expected as GOCE is not sensitive to these high degrees.

11.4 Conclusions

The gravity gradients as derived from the GOCE mission are given in the instrument frame, which is only indirectly connected to the Earth. A rotation to the LNOF requires to take the different accuracies of the gradients into account. Replacing the less accurate gradients with model information allows to rotate the tensor, but for the diagonal gradients V_{XX} and V_{YY} the model information can reach up to 50 %, whereas it is only a few percent for V_{ZZ}.

In the direct comparison of GOCE gravity gradients and satellite altimetry derived gradients one has to account for the difference between the along-track altimeter derivatives and the GOCE gradients in a Cartesian frame. Also the DOT signal has to be accounted for as it may be above the GOCE requirements. A validation of GOCE using ERS-1 data shows that both data sets are consistent at levels where GOCE is sensitive. For high spatial resolutions below 40 km wavelength GOCE does not contribute, as expected.

References

Bosch W, Savcenko R (2010) On estimating the dynamic ocean topography. In: Mertikas S (ed) Gravity, geoid and earth observation, IAG symposia. vol 135, Springer, pp 263–269

Bouman J (2007) Alternative method for rotation to TRF. GO-TN-HPF-GS-0193. Issue 1.0

Bouman J (2012) Relation between geoidal undulation, deflection of the vertical and vertical gravity gradient revisited. J Geodesy 86:287–304. doi:10.1007/s00190-011-0520-9

Bouman J, Fuchs M (2012) GOCE gravity gradients versus global gravity field models. Geophys J Int 189:846–850. doi:10.1111/j.1365-246X.2012.05428.x

Bouman J, Bosch W, Sebera J (2011) Assessment of systematic errors in the computation of gravity gradients from satellite altimeter data. Marine Geodesy 34:85–107. doi:10.1080/01490419.2010.518498

Bouman J, Fiorot S, Fuchs M, Gruber T, Schrama E, Tscherning C, Veicherts M, Visser P (2011) GOCE gravitational gradients along the orbit. J Geodesy 85:791–805. doi:10.1007/s00190-011-0464-0

Brieden P, Müller J (2012) Cross-overs assess quality of GOCE gradients. In: This issue. Springer, New York

Fuchs M, Bouman J (2011) Rotation of GOCE gravity gradients to local frames. Geophys J Int 187:743753. doi:10.1111/j.1365-246X.2011.05162.x

Gruber T, Visser P, Ackermann C, Hosse M (2011) Validation of GOCE gravity eld models by means of orbit residuals and geoid comparisons. J Geodesy 85:845–860. doi:10.1007/s00190-011-0486-7

Müller J (2003) GOCE gradients in various reference frames and their accuracies. Adv Geosci 1:33–38

Schmidt M, Fengler M, Mayer-Gürr T, Eicker A, Kusche J, Sánchez L, Han S (2007) Regional gravity modelling in terms of spherical base functions. J Geodesy 81:17–38

Sebera J, Bouman J, Bosch W (2012) On computing ellipsoidal harmonics using Jekeli's renormalization. J Geodesy doi:10.1007/s00190-012-0549-4

Chapter 12
Incorporating Topographic-Isostatic Information into GOCE Gravity Gradient Processing

Thomas Grombein, Kurt Seitz and Bernhard Heck

Abstract Global high-resolution digital terrain models provide precise information on the Earth's topography, which can be used to determine the high- and mid-frequency constituents of the gravity field (topographic-isostatic signals). By using a Remove-Compute-Restore concept these signals can be incorporated into many methods of gravity field modelling. Due to the smoothing of observation signals such a procedure benefits from an improved numerical stability in the calculation process. In this paper the Rock-Water-Ice topographic-isostatic gravity field model is presented that we developed in order to generate topographic-isostatic signals which are suitable to smooth gravity gradients observed by the satellite mission GOCE. In contrast to previous approaches, this model is more sophisticated due to a three-layer decomposition of the topography and a modified Airy-Heiskanen isostatic concept. By using measured GOCE gravity gradients, the degree of smoothing is analyzed, showing a significant reduction of the standard deviation (about 30 %) and the range (about 20–40 %). Furthermore, we validate the performance of the generated topographic-isostatic signals by means of a wavelet analysis.

12.1 Introduction

The high- and mid-frequency components of the Earth's gravity field are mainly influenced by the attraction of the topographic and isostatic masses. By applying a topographic model and an isostatic concept, this signal content can be simulated by means of forward gravity modelling. In classical physical geodesy, topographic-isostatic information was mainly used for mass reductions in order to obtain a mass-free solution domain (e.g. Heiskanen and Moritz, 1967; Forsberg, 1984). More-

T. Grombein (✉) · K. Seitz · B. Heck
Geodetic Institute, Karlsruhe Institute of Technology (KIT), Englerstr. 7, 76128
Karlsruhe, Germany
e-mail: grombein@kit.edu
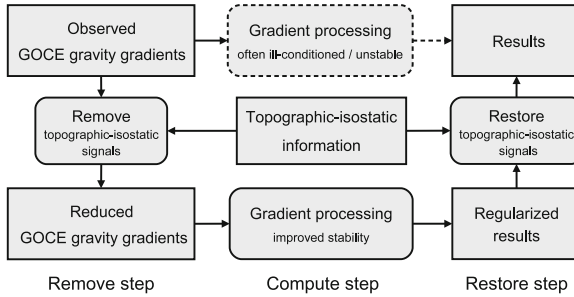
Fig. 12.1 Processing of GOCE gravity gradients by using topographic-isostatic information in a RCR concept

over, topographic-isostatic information can also be incorporated into many modern methods of gravity field modelling, such as Residual Terrain Modelling or the Remove-Compute-Restore technique (Forsberg and Tscherning 1997). In this context, the main purpose is the smoothing of gravity-field-related observations for enhancing the numerical stability, particularly when interpolation and prediction tasks as well as field transformations are carried out. One example is the downward continuation process of airborne or satellite-based gravity field observations.

For the processing of gravity gradients measured by ESA's satellite mission GOCE (Gravity field and steady-state Ocean Circulation Explorer) we propose to use topographic-isostatic information within a Remove-Compute-Restore concept (RCR concept) as demonstrated in Fig. 12.1. In the remove step, topographic-isostatic signals in the observed GOCE gradients are simulated and reduced. Thereby, the high- and mid-frequency components of the gradients are mitigated, and mainly low-frequency constituents remain in the residual signal. In the compute step, the smoothed observation signals can be processed with an improved stability to gain regularized results. In the restore step, finally, consistent topographic-isostatic signals are reconsidered to obtain the results.

Previous investigations based on simulated GOCE gradients (e.g. Wild-Pfeiffer 2008; Janák et al. 2012) have shown that significant smoothing effects in the remove step can be achieved. Furthermore, a closed loop simulation presented in Janák and Wild-Pfeiffer (2010) has verified the benefit of incorporating topographic-isostatic signals into the downward continuation process.

Due to the high sensitivity of gravity gradients a refinement of the commonly used methodology seems to be essential in order to get suitable topographic-isostatic signals (cf. Grombein et al., 2010a). In contrast to conventional modelling approaches that characterizes topographic masses with a constant density value (e.g. $\rho = 2670\,\text{kg/m}^3$), we developed the more sophisticated methodology of the Rock-Water-Ice decomposition of the topography. In Sect. 12.2 this method is presented and the used input data sets are specified. Section 12.3 focuses on numerical investigations that demonstrate the smoothing potential for reduced GOCE gradient measurements. Finally, Sect. 12.4 provides conclusions and final remarks.

12.2 Rock-Water-Ice Methodology

For the calculation of topographic-isostatic signals as required in the remove and restore steps in Fig. 12.1, the topographic and isostatic masses of the Earth have to be quantified. The basic idea of our methodology is a three-layer decomposition of the topography in which the rock, water, and ice masses are modeled individually.

In order to specify the topographic masses, we use the information of the $5' \times 5'$ global topographic data base DTM2006.0 (Pavlis et al. 2007) to construct a vertical three-layer terrain and density model. Each grid element contains a rock (R), water (W), and ice (I) component with different heights of the respective top surfaces (h_R, h_W, h_I). Additionally, we derive layer-specific density values ($\rho_R = 2670 \, \text{kg/m}^3$, $\rho_W = 1000 \, \text{kg/m}^3$, $\rho_I = 920 \, \text{kg/m}^3$) from the specified DTM2006.0 terrain types.

Taking the topographic load into account, the isostatic (compensation) masses can be calculated by applying a mass equality condition. In this context, we adapt the classical Airy-Heiskanen isostatic concept (e.g. Heiskanen and Moritz, 1967, p. 135ff) to the three-layer decomposition of the topography. Furthermore, we improve the concept by incorporating a depth model of the Mohorovičić discontinuity (Moho), which represents the boundary between the Earth's crust and mantle. To this end, we replace the commonly used (anti-)root depths of the Airy-Heiskanen concept by Moho depths of the global CRUST 2.0 model (Bassin et al. 2000). Although this fixes the geometry of the isostatic masses, we satisfy the mass equality condition due to variable density values. Particularly, this means the estimation of location-dependent crust-mantle density contrasts.

Using forward modelling, the gravitational attraction of the topographic-isostatic masses can be determined by a discretization of Newton's integral (e.g. Heiskanen and Moritz, 1967, p. 3). As the used input data sets are specified by geographical coordinates, we use tesseroid bodies (Heck and Seitz 2007; Grombein et al. 2010b; Grombein et al. 2013a) for mass discretization that are arranged on the surface of a GRS80 ellipsoid (Moritz 1980). Initially, we calculate topographic-isostatic effects on a $5' \times 5'$ global grid in the space domain. By applying harmonic analysis (Wittwer et al. 2008), we then utilize these grid values to derive the Rock-Water-Ice topographic-isostatic gravity field model (RWI model) in terms of spherical harmonic coefficients up to degree and order 1800. Figure 12.2 displays the spectral information of the RWI model in terms of degree variances. As can be expected, the influence of the isostatic component is mainly regional and shows a decreasing effect on the combined topographic-isostatic effects with increasing spherical harmonic degree.

With the help of the derived spherical harmonic representation of the RWI model, topographic-isostatic signals can be generated for both the remove and restore steps when applying a RCR concept. For a more detailed description of the RWI model including illustrating figures and the derivation of the used evaluation formulas the reader is referred to our previous publications Grombein et al. (2011, 2013b).
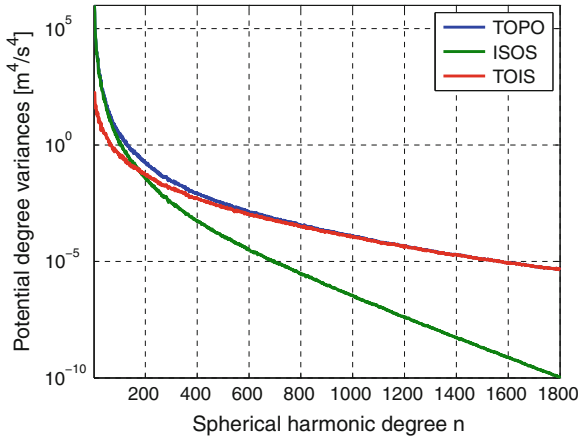
Fig. 12.2 Potential degree variances of the RWI model: Topographic effects (TOPO, *blue curve*); isostatic effects (ISOS, *green curve*); Topographic-isostatic effects (TOIS, *red curve*)

12.3 Numerical Investigations

In numerical investigations we will validate the performance of topographic-isostatic signals obtained from the RWI model. To ensure an improvement of the numerical stability in processing GOCE gravity gradients, the smoothing potential of the topographic-isostatic signals in the remove step is essential.

In Grombein et al. (2013b) we already presented a smoothing potential analysis in which the degree of smoothing was quantified by investigating changes in standard deviation and range. Table 12.1 summarizes the detected improvements within the frequency range of the GOCE measurement bandwidth (5–100 mHz) based on the evaluation of one week of real GOCE measurements (Oct. 27- Nov. 02, 2010).

To have a closer look on the reduced frequency components, we furthermore investigate GOCE time series by means of wavelet analysis. By applying the Morlet wavelet (e.g Torrence and Compo, 1998) we perform a continuous wavelet transform of the gradient signals and constitute wavelet spectrograms. Figure 12.3 visualizes the time series of the V_{zz} gradient signal in the space and frequency domain for the period when the GOCE satellite crossed the Himalaya on Nov. 4, 2010. The wavelet spectrograms in the right panel of Fig. 12.3 represent the time-dependent

Table 12.1 Percentage reductions P in standard deviation and range of measured GOCE gravity gradients by removing topographic-isostatic signals of the RWI model (cf. Grombein et al. 2013b)

(%)	V_{xx}	V_{yy}	V_{zz}	V_{xz}
P_{std}	31.8	27.7	31.5	31.5
P_{range}	43.1	22.0	40.4	43.8
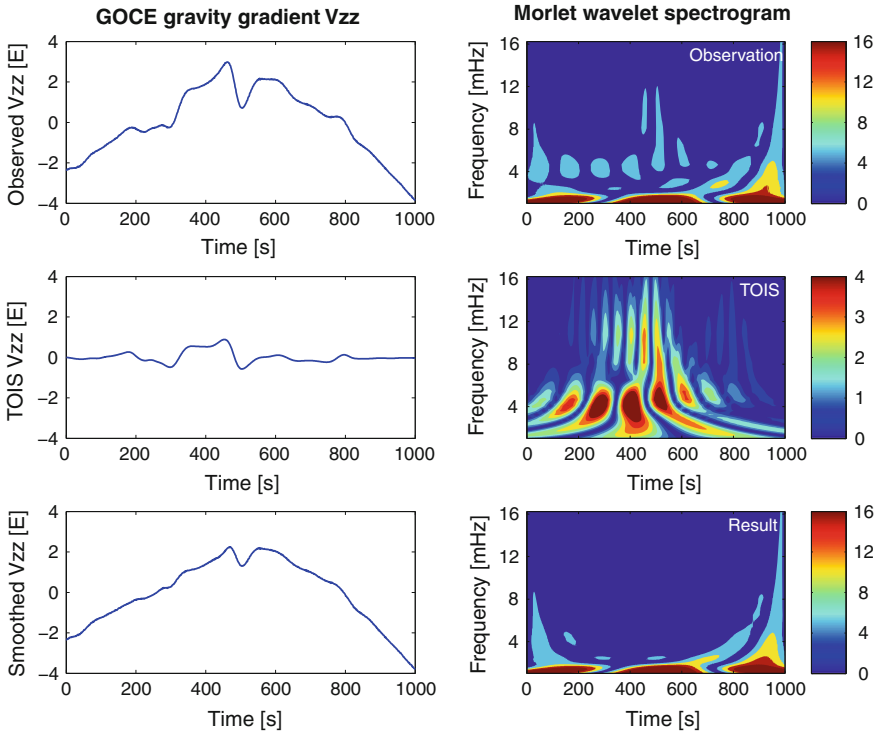
Fig. 12.3 Visualization of the observed gradient component V_{zz} (*top*), the corresponding topographic-isostatic signal derived from the RWI model (*middle*) and the smoothed observation signal after removing the topographic-isostatic signal (*bottom*). The signals are shown in the space domain by time series (*left panel*). In the frequency domain wavelet spectrograms are used, where the colors of the plotted unit-less wavelet coefficients provide information about the amplitudes (*right panel*)

signal structure in the frequency domain, whereby the unit-less wavelet coefficients are plotted color-coded and can be interpreted as amplitudes. Particularly in the middle of the time series, when the central massive of the Himalaya is crossed, it can be realized that most of the high- and mid-frequency signal components are reduced by removing the topographic-isostatic information of the RWI model. Mainly low frequencies and some leakage effects at the edges of the time series remain. This wavelet-based assessment will be presented in detail in an upcoming paper.

12.4 Conclusion

In order to mitigate the numerical instability in the GOCE gravity gradient processing the incorporation of topographic-isostatic information by means of a RCR concept has been proposed. For this issue, we developed the RWI model which is based on a

three-layer Rock-Water-Ice decomposition of the topography with variable density values. Geometry and density information is derived from the global topographic data base DTM2006.0. Additionally, we applied a modified Airy-Heiskanen model, which is improved by incorporating the CRUST 2.0 Moho depths in combination with a variable crust-mantle density contrast. The mass discretization is performed using tesseroid bodies arranged on a GRS80 ellipsoid. By applying the suggested concept to real measured GOCE gravity gradients, we investigated the performance of topographic-isostatic information by means of smoothing potential and wavelet analysis. Both methods confirmed significant smoothing effects on the high- and mid-frequency constituents of the GOCE observations. By removing topographic-isostatic signals the standard deviation could be reduced by about 30 % and the range by about 20–40 %.

Note: As the result of these investigations the RWI topographic-isostatic gravity field model can be downloaded at http://www.gik.kit.edu/rwi_model.php in terms of spherical harmonic coefficients up to degree and order 1800.

References

Bassin C, Laske G, Masters G (2000) The current limits of resolution for surface wave tomography in North America. EOS Trans AGU, 81. F897

Forsberg R (1984) A study of terrain reductions, density anomalies and geophysical inversion methods in gravity field modelling. Rep 355, Department of geodetic science, The Ohio State University, Columbus, USA

Forsberg R, Tscherning C (1997) Topographic effects in gravity field modelling for BVP. In: Sansò F, Rummel R (eds) Geodetic boundary value problems in view of the one centimeter geoid, lecture notes in earth Sciences, vol 65, Springer, pp 239–272. doi:10.1007/BFb0011707

Grombein T, Seitz K, Heck B (2010a) Modelling topographic effects in GOCE gravity gradients. GEOTECHNOLOGIEN Sci Rep 17:84–93. doi:10.2312/GFZ.gt.17.13

Grombein T, Seitz K, Heck B (2010b) Untersuchung zur effizienten Berechnung topographis-cher Effekte auf den Gradiententensor am Fallbeispiel der Satellitengradiometriemission GOCE. KIT Scientific Reports, 7547, KIT Scientific Publishing, Karlsruhe, Germany. doi:10.5445/KSP/1000017531

Grombein T, Seitz K, Heck B (2011) Smoothing GOCE gravity gradients by means of topographic-isostatic reductions. In: Ouwehand L (ed) Proceedings of the 4th International GOCE User Work-shop, ESA Publication SP-696, ESA/ESTEC

Grombein T, Seitz K, Heck B (2013a) Optimized formulas for the gravitational field of a tesseroid. J Geod. Doi:10.1007/s00190-013-0636-1

Grombein T, Seitz K, Heck B (2013b) Topographic-isostatic reduction of GOCE gravity gradients. In: Proceedings of the XXV IUGG, 2011, IAG Symposia, vol 139, Springer, Melbourne, Australia (in print)

Heck B, Seitz K (2007) A comparison of the tesseroid, prism and point-mass approaches for mass reductions in gravity field modelling. J Geod 81:121–136. doi:10.1007/s00190-006-0094-0

Heiskanen WA, Moritz H (1967) Physical geodesy. W. H. Freeman & Co., USA

Janák J, Wild-Pfeiffer F (2010) Comparison of various topographic-isostatic effects in terms of smoothing gradiometric observations. In: Sansò F, Mertikas SPP (eds) IAG symposia, vol 135, Springer, pp 377–381. doi:10.1007/978-3-642-10634-7_50

Janák J, Wild-Pfeiffer F, Heck B (2012) Smoothing the gradiometric observations using different topographic-isostatic models: a regional case study. In: Sneeuw et al. (eds) Proceedings of VII Hotine-Marussi Symposium, Rome, Italy, 2009, IAG Symposia, vol 137, Springer, pp 245–250. doi:10.1007/978-3-642-22078-4_37

Moritz H (1980) Geodetic reference system 1980. Bull Géod 54:395–405. doi:10.1007/BF02521480

Pavlis NK, Factor J, Holmes S (2007) Terrain-related gravimetric quantities computed for the next EGM. In: Kiliçoğlu A, Forsberg R (eds) Proceedings of 1st International Symposium IGFS: Gravity field of the earth, Istanbul, Turkey, 2006. Harita Dergisi, Special Issue 18, pp 318–323

Torrence C, Compo GP (1998) A practical guide to wavelet analysis. Bull Am Meteorol Soc 79(1):61–78. doi:10.1175/1520-0477(1998)079

Wild-Pfeiffer F (2008) A comparison of different mass elements for use in gravity gradiometry. J Geod 82:637–653. doi:10.1007/s00190-008-0219-8

Wittwer T, Klees R, Seitz K, Heck B (2008) Ultra-high degree spherical harmonic analysis and synthesis using extended-range arithmetic. J Geod 82:223–229. doi:10.1007/s00190-007-0172-y

Chapter 13
Global Gravity Field Models from Different GOCE Orbit Products

Akbar Shabanloui, Judith Schall, Annette Eicker and Jürgen Kusche

Abstract In this contribution, the in-house (processed) GOCE products including precise orbit and Earth's gravity field are compared to the official ESA products. The comparison is drawn on orbit product as well as gravity field level. To ensure comparability, gravity field models from both orbits are estimated in an identical fashion, which is particularly true for the stochastical model. We find that the in-house processed orbit is piecewise rather smooth, but contains jumps like discontinuities in the calculated geometrical point-wise positions. This leads to a degradation of the gravity field solution about by a factor of two in terms of degree variances when compared to the solution from the official orbit product.

13.1 Introduction

The gravity gradiometer on-board the Gravity field and steady-state Ocean Circulation Explorer (GOCE, e.g. Drinkwater et al. 2003; Floberghagen et al. 2011) enables measuring detailed gravity field features with high accuracy. Additionally, GOCE is equipped with a Lagrange GNSS receiver for tracking satellite-to-satellite-tracking observations of the high-low configuration (hl-SST). These data are used to determine the precise orbit of the satellite, which is required for geo-locating the gravity gradients. Furthermore, the precise orbit can be utilized to determine and stabilize

A. Shabanloui (✉) · J. Schall · A. Eicker · J. Kusche
Institute of Geodesy and Geoinformation, University of Bonn, Nuß allee 17, 53115
Bonn, Germany
e-mail: shabanloui@geod.uni-bonn.de
J. Schall
e-mail: schall@geod.uni-bonn.de
A. Eicker
e-mail: eicker@geod.uni-bonn.de
J. Kusche
e-mail: kusche@geod.uni-bonn.de

the spherical harmonic coefficients of lower degrees in the series expansion of the gravitational potential.

Precise orbit determination (POD) is performed by the University of Bern in the frame of GOCE High Level Processing Facility (GOCE-HPF) (cf. Bock et al. 2007). These data are officially published by ESA as the precise science orbit (PSO). Complementary, POD results of an in-house developed software are available. Our processing scheme is summarized in the following Sect. 13.2. Geometrical positions of both products are used as pseudo observations for gravity field recovery, which is dealt with in Sect. 13.3. Section 13.4 discusses the results, while Sect. 13.5 gives the conclusions.

13.2 Precise Orbit Determination of GOCE

The determination of precise positions for the instruments on-board the GOCE satellite is based on POD techniques using the tracking data of the GOCE Lagrange GNSS receiver. In this paper, the sequential time differenced approach (see Shabanloui 2008 for further details) has been applied to the GOCE high-low satellite to satellite tracking GPS observations, and the solution has been denoted as geometrical precise orbit determination (GPOD) (refer to Shabanloui 2008). The geometrical POD solution is based on sequential time differenced hl-SST observations, final International GNSS Service (IGS) GPS ephemerides at the interval of 30 s and GPS clocks from Center of Orbit Determination in Europe (CODE) at the interval of 5 s. The final GPS ephemerides and clocks are fixed during the geometrical (point-wise) computation of the GOCE orbit. The orientation of GOCE can be derived from quaternion information which are observed by star tracker camera. In addition, precise Center of Mass (CoM) position of GOCE can be determined based on attitude data (quaternions) and offset between the center of mass and the Center on Mounting Plane (CMP) of the GNSS antenna.

The estimated GPOD of GOCE results are comparable with results of other groups (see Figs. 13.1 and 13.2); but because of different outliers detection and data processing strategies, the GPOD results presented here are more or less different than the results of the other groups. On the one hand, Fig. 13.1 shows differences between in-house calculated geometrical orbits and reduced-dynamic positions (published by ESA as part of the PSO products) of GOCE. On the other hand, Fig. 13.2 shows the 3D root mean squares (rms) of estimated POD of GOCE based on in-house developed POD software and Precise Science Orbit (PSO). In other words, the red curve in Fig. 13.2 shows the 3D rms which are calculated based on the differences between estimated GPOD orbits and ESA's reduced dynamical orbits and the green one in Fig. 13.2 shows the 3D rms which are calculated based on the differences between ESA's kinematical orbits and ESA's reduced dynamical orbits. The averaged 3D rms of estimated orbits for 71 days isin the range of 2.5 cm; the averaged 3D rms of PSO
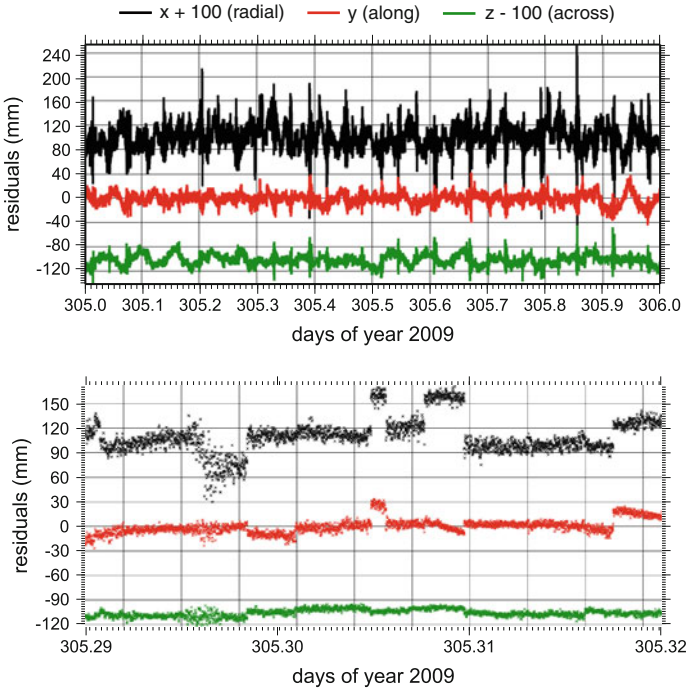
Fig. 13.1 (*Top*) Differences between geometrical and reduced-dynamic positions; (*Bottom*) Jumps like discontinuities which have been caused due to the sequential time difference data processing technique
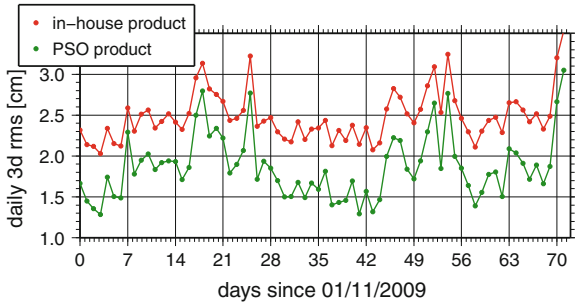
Fig. 13.2 Differences between geometrical and reduced-dynamic positions by means of the daily 3D rms

orbits 1.8 cm. The results show consistency between two orbit products which are estimated with different methods and strategies, but the day to day 'noise' level of the in-house estimated GOCE orbits is higher than the official PSO.

13.3 From GOCE Orbits to the Gravity Field

13.3.1 Theoretical Background

Basically, the satellite movement is related to the gravity field by Newton's equation of motion. Depending on whether this relation is used in its raw form or integrated once or twice, a distinction is made between different approaches for gravity field analysis (see an overview in Ilk et al. 2008). Here we make use of an integral equation approach, which avoids any differentiation of the observed positions (for more details see Mayer-Gürr 2006).

Solving Newton's equation as boundary value problem leads to an integral equation of Fredholm type

$$\mathbf{r}(\tau) = \mathbf{r}_A(1 - \tau) + \mathbf{r}_B \tau + \int_0^1 K(\tau, \tau') \mathbf{f}(\tau', \mathbf{r}, \dot{\mathbf{r}}) d\tau', \tag{13.1}$$

which represents the orbit $\mathbf{r}(\tau)$ at the normalized time τ by the connecting line between the boundary values $\mathbf{r}_A$, $\mathbf{r}_B$ and a correction term integrating the specific forces $\mathbf{f}(\tau', \mathbf{r}, \dot{\mathbf{r}})$ with the kernel term $K(\tau, \tau')$ along the orbital arc. The dependency of force on location is no difficulty since the observed positions provide a sufficiently accurate approximation. The velocity only influences surface forces, which in our case are measured by the gradiometer. Discretization of Eq. 13.1 by numerical integration yields the linear observation equations, which are individually established per orbit arc. The results of the POD serve as (pseudo) observations, the spherical harmonic coefficients, which represents the gravity field, are the primary unknown parameters. The exact boundary positions and an offset per gradiometer axis are further arc wise parameters to be solved for in the Gauss-Markov model.

13.3.2 Model Settings

Gravity field models from both products, the PSO and the in-house orbit, are calculated under the same conditions. The data time span is chosen to be the first calibration period from 1/11/2009 till 11/1/2010, which equals 71 days of GOCE orbit data. The data-sets are synchronized and split up in about 3500 short arcs of 30 min arc length. Next, a reference orbit is reduced, which was integrated from ITG-Grace2010s and its background models as specified in Mayer-Gürr et al. (2010). Additionally, disturbing forces measured by the gradiometer as common mode acceleration were taken into consideration. Representation for the gravity models is a spherical harmonic series expansion up to degree and order 110. No regularization is applied. It is worth pointing out that decorrelation is done using the same stochastical model. This clearly does not lead to the optimal solution in a statistical sense, but enables a comparison purely on the basis of orbit observations.
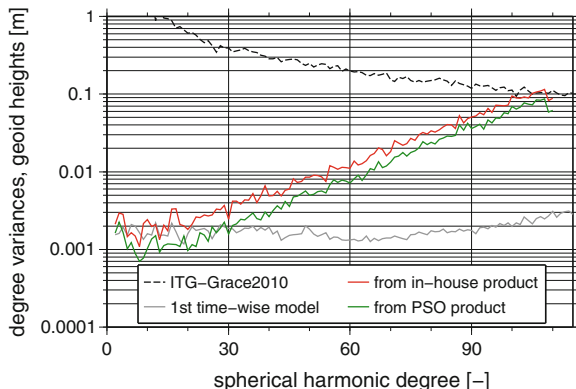
Fig. 13.3 Comparison of GOCE gravity models from different orbit products by means of degree variances excluding low order coefficients. The *dotted line* and the *solid lines* refer to the reference model and difference to the reference model, respectively

13.4 Results

Figure 13.3 shows the gravity recovery results for both orbit products, in-housed processed and ESA PSO, in the frequency domain. In order to keep consistence comparison between different independent gravity models, the first generation time-wise model of GOCE has been added to the Fig. 13.3. The in-house calculated orbit performs worse compared to the official PSO, which is obvious from the up to a factor of two larger differences to the reference models ITG-GRACE 2010s and GO_CONS_GCF_2_TIM_R1 (the first release time-wise of GOCE). This might be explained by the jump like discontinuities, which have already been discussed earlier (see Sect. 13.2). Jumps can be interpreted as high frequency signal, which can not adequately be modeled by a truncated series of spherical harmonics, and leaks therefore into the entire frequency range.

13.5 Conclusion

In this paper, geometrical precise orbits of GOCE based on the sequential time differenced between sequential carrier phase observations are estimated. The results show consistency between in-house estimated POD and official precise orbit (PSO) of GOCE, but the in-house estimated precise orbit performs worse compared to the official PSO. Discontinuities which are caused by the sequential time differenced approach can be interpreted as high frequency signal. These jumps are not adequately be modeled by a truncated series of spherical harmonics to estimate Earth's gravity field, and leaks therefore into the entire frequency range. Due to the discontinuities caused by proposed POD, the recovered Earth's gravity field based on these orbits

differs from the up to a factor of two larger differences to the reference model in terms of degree variances. It should be mentioned that both estimated geometrical GOCE orbits, i.e. in-housed processed and official ESA PSO orbits, are independent of dynamical forces acting on GOCE.

References

Bock H, Jaggi A, Švehla D, Beutler G, Hugentobler U, Visser P (2007) Precise orbit determination for the GOCE satellite using GPS. Adv Space Res 1638–1647

Drinkwater MR, Floberghagen R, Haagmans R, Muzi D, Popescu A (2003) GOCE: ESA's first earth explorer core mission. In: Beutler GB, Drinkwater MR, Rummer R, von Steiger R (eds) Earth gravity field from space—from sensors to earth sciences of space sciences series of ISSIKluwer, vol 18, Academic Publishers, Dordrecht, Netherlands, pp 419–432

Floberghagen R, Fehringer M, Lamarre D, Muzi D, Frommknecht B, Steiger C, Piñeiro J, da Costa A (2011) Mission design, operation and exploitation of the gravity field and steady-state ocean circulation explorer mission. J Geodesy 85:749–758

Ilk KH, Löcher A, Mayer-Gürr T (2008) Do we need new gravity field recovery techniques for the new gravity field satellites? In: VI Hotine-Marussi symposium on theoretical and computational geodesy, vol 132. International Association of Geodesy symposia, Springer

Mayer-Gürr T (2006) Gravitationsfeldbestimmung aus der Analyse kurzer Bahnbögen am Beispiel der Satellitenmissionen CHAMP und GRACE. Ph.D. thesis, Rheinische Friedrich-Wilhelms-Universität Bonn

Mayer-Gürr T, Kurtenbach E, Eicker A (2010) ITG-Grace2010 gravity field model. http://www.igg.uni-bonn.de/apmg/index.php?id=itg-grace2010

Shabanloui A (2008) A new approach for a kinematic-dynamic determination of low satellite orbits based on GNSS observations. Ph.D. thesis, Rheinische Friedrich-Wilhelms-Universität Bonn

Chapter 14
Adjustment of Digital Filters for Decorrelation of GOCE SGG Data

Ina Krasbutter, Jan Martin Brockmann, Boris Kargoll and Wolf-Dieter Schuh

Abstract GOCE satellite gravity gradiometry (SGG) data are strongly autocorrelated within the various tensor components. Consideration of these correlations in the least-squares adjustment for gravity field determination can be carried out by digital decorrelation filters. Due to the complexity of the correlation pattern the used decorrelation filters consist of a cascade of individual filters. In this contribution some of the properties of these filters and their application to GOCE SGG data decorrelation will be presented.

14.1 Introduction

The Tuning Machine, as part of ESA's High-Level Processing Facility (HPF), was designed with the purpose to obtain an independent gravity field solution by GOCE data (cf. Brockmann et al. 2010; Pail et al. 2006; Schuh et al. 2010). The strong autocorrelation of GOCE satellite gravity gradiometry (SGG) data has to be considered within this gravity field determination to reach the ambitious mission goal of 1–2 cm geoid height accuracies at a resolution of at least 100 km. Due to the huge number of observations obtained throughout the GOCE mission (approx. 100 mio. observations per gravity gradient tensor component), the use of the full covariance matrix is not possible; to handle this problem (Schuh 1996) proposed to decorrelate the SGG data by digital filters.

The gradiometer noise has a complex autocorrelation pattern with sharp peaks and a strong increase below the measurement bandwidth (see Fig. 14.1). To take these individual sub-patterns into account, (Siemes 2008) suggested to use filter cascades to achieve a step-wise decorrelation of the SGG data. In this contribution we will

I. Krasbutter (✉) · J. M. Brockmann · B. Kargoll · W.-D. Schuh
Institute of Geodesy and Geoinformation, University of Bonn, Nussallee 17,
53115 Bonn, Germany
e-mail: krasbutter@igg.uni-bonn.de
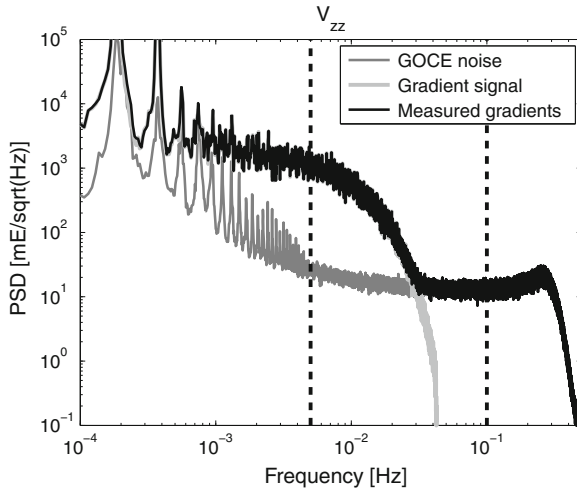
Fig. 14.1 Power spectral density (PSD) of the gradiometer noise (*gray*) for the V_{zz} component, the gradient signal (*light gray*), and the measured gravity gradients (*black*). The gradiometer noise has a complex spectrum with sharp peaks and a strong increase below the measurement bandwidth (frequency range between the *dotted lines*)

present different individual filters (cf. Sect. 14.2), which can be arranged as various filter cascades. In Sect. 14.3 two appropriate decorrelation filter cascades for GOCE SGG data are introduced. This contribution ends with conclusions and an outlook.

14.2 Individual Filters for Decorrelation

In practice, there exists a wide range of filters with distinct properties. For a decorrelation of GOCE SGG data three different types of filters are of special interest: (1) high-pass, (2) notch and (3) whitening filters. These three filters, which we will describe precisely in the next sections, have the common property that they are linear, discrete-time filters and can be expressed by the autoregressive moving-average (ARMA) model equation

$$y_t = \sum_{k=1}^{p} \alpha_k y_{t-k} + \sum_{k=0}^{q} \beta_k u_{t-k}, \qquad (14.1)$$

where u_t is the input data, y_t the output data, α_k, β_k the unknown filter coefficients, and p, q the filter orders.

14.2.1 High-Pass Filter

The general idea of a high-pass filter is to eliminate frequencies up to a specified cutoff frequency from the signal and maintain all the other (higher) frequencies. Many high-pass filters are used, which differ mainly in terms of filter order and width of the transition band. The transition band contains the frequencies, which are neither completely eliminated from the signal nor exactly maintained by filtering. Within the given context, the following three types of filters turned out to be most suitable: the difference filter, best-adapted polynomial filter, and Butterworth filter.

Difference filter: A difference filter determines the first differences between adjacent signal values. Its main advantage is its simplicity (i.e. $\beta_0 = 1$, $\beta_1 = -1$, all other coefficients are zero), its disadvantages are its relatively wide transition band and an amplification of high frequencies.

Polynomial filter: The idea is to fit a polynomial of degree N to $q+1$ equally spaced data points (filter input) and find the midpoint (filter output). The thusly obtained filter is a low-pass filter, which can be transformed easily into a high-pass filter (cf. Hamming 1998; Krasbutter 2009). For instance, a high-pass filter fitted by a straight line through three data points results in: $\beta_0 = -\frac{1}{3}$, $\beta_1 = \frac{2}{3}$, $\beta_2 = -\frac{1}{3}$, all other coefficients are zero. This filter is only slightly more complex than the difference filter, but has the additional advantage of being a symmetric filter, hence its phase shift is zero.

Butterworth filter: Butterworth filters have the advantage that they can be designed by directly specifying the cutoff frequency and the width of the transition band (by specifying the number of poles of the transfer function, with an increasing number of poles resulting in a small width, cf. Oppenheim and Schafer 1999; Siemes 2008). Filter coefficients can be determined via the equations given in Siemes (2008, Sect. 5.4).

14.2.2 Notch Filter

Elimination of one particular frequency from the signal can be realized by a notch filter. The transfer function of such a filter, which is designed by specifying its poles and zeros, is zero for the frequency ω_0, which will be eliminated. The poles are utilized for minimizing the influence of the filter on the other frequencies (cf. Siemes 2008; Krasbutter 2009). The order of this filter is always $p = 2$, $q = 2$ and the filter coefficients are defined by (cf. Widrow et al. 1975):

$$\beta_0 = \beta_2 = 1, \quad \beta_1 = -2\cos(\omega_0), \tag{14.2}$$

$$\alpha_1 = 2(1-\delta)\cos(\omega_0), \quad \alpha_2 = -(1-2\delta), \tag{14.3}$$

where δ is the degree of impact of the filter on the neighboring frequencies of ω_0.

14.2.3 Whitening Filter

In contrast to the filters described in Sect. 14.2.1 and 14.2.2, whitening filters affect and diminish all frequencies to some extent. This filter is used to level the remaining moderate autocorrelations over the entire frequency domain. These filters are determined via a data-adaptive least-squares estimation of the coefficients (cf. Klees et al. 2003; Krasbutter 2009). In its most general form the whitening filter is described by an ARMA filter. In this case the estimation of α_k, β_k is based on a two-step least-squares adjustment. In the first step an MA filter, where $\alpha_k = 0$, for all $k \geq 1$ and typically $q = 1000$, is estimated; in the second step resulting residuals are used to determine the coefficients of a low-order ARMA filter, with typical filter orders $p = q = 50$ (cf. Siemes 2008, Sect. 5.3).

14.3 Filter Cascade for Correlated GOCE SGG Data

As mentioned in Sect. 14.1 (see also Fig. 14.1) the GOCE SGG data displays a strong and complex correlation pattern. To achieve a full decorrelation, this must be completely reversed in the frequency domain. Due to its complexity, a filter cascade consisting of single filters with different characteristics are used. For this purpose, we found the following two filter cascades, comprising some of the filters described in Sect. 14.2, particularly suitable:
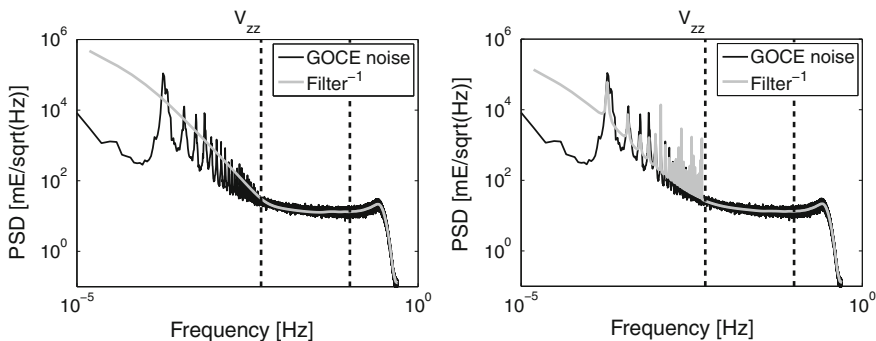
Fig. 14.2 Comparison of the gradiometer noise spectrum (*black*) to the decorrelation filter spectrum (*light gray*, inverse representation). *Left* Filter cascade A, *Right* Filter cascade B

Cascade A: The first cascade consist of two filters: The first one is a difference filter for leveling the very highly correlated and inaccurate low-frequency part of the error spectrum (cf. Fig 14.1) and a whitening filter for the remaining frequencies. The inverse spectrum of this decorrelation filter is shown in Fig. 14.2, its disadvantage is that the sharp peaks of the error spectrum are not taken into account by such a design, its advantage is computational simplicity.

Cascade B: In comparison to cascade A, the sharp peaks are taken into account by a notch filter for each peak (cf. Fig. 14.2). Thus this cascade consists of a difference filter, several notch filters, and a whitening filter. This cascade design results in a more complex decorrelation filter with a high warm-up (i.e. loss of data caused by the fact that the filter produces invalid output values to be discarded as long as the filter does not have a complete set of given input values), which is a drawback especially for short data segments.

In both cascades the difference filter is used as high-pass filter and can also be replaced by a best-adapted polynomial or Butterworth filter. The result, especially the influence on gravity field solution, is in all cases the same as shown in Krasbutter (2009).

14.4 Conclusions and Outlook

Much effort has been put into the design of filter cascade to obtain an adequate decorrelation filter which is used in the gravity field determination. Both cascades described in Sect. 14.3 were applied and compared for decorrelation of GOCE SGG data (in Krasbutter et al. (2010) their different effects on the differences of the estimated coefficients to the ITG-Grace2010s model and on the estimated formal coefficient standard deviations were analyzed). Due to the simplicity and sufficient effectiveness of filter cascade A in the presence of data gaps (which occurred in large numbers in the past), this decorrelation model was applied for computing the three official GOCE gravity field time-wise solutions (cf. Pail et al. 2011). However, we anticipate filter cascade B to have superior performance in the case that future GOCE SGG data will have considerably less data gaps. Whether more sophisticated high-pass filters, such as best-adapted polynomial filters and Butterworth filters, will prove to be more appropriate than the currently used difference filter, will also depend on the future data characteristics.

References

Brockmann JM, Kargoll B, Krasbutter I, Schuh W-D, Wermuth M (2010) GOCE data analysis: from calibrated measurements to the global Earth gravity field. In: Flechtner F, Gruber T, Güntner A, Mandea M, Rothacher M, Schöne T, Wickert J (eds) System Earth via Geodetic-Geophysical space techniques, advanced technologies in Earth sciences. Springer, Berlin, pp 213–229

Hamming RW (1998) Digital Filters, 3rd edn. Dover Publications, Mineola, New York

Klees R, Ditmar P, Broersen P (2003) How to handle colored observations noise in large least-squares problems. J Geod 76(11–12):629–640

Krasbutter I (2009) Dekorrelation und Daten-TÜV der GOCE-Residuen. Diploma thesis, Institute of Geodesy and Geoinformation, University of Bonn, Germany

Krasbutter I, Brockmann JM, Kargoll B, Schuh W-D (2010) Stochastic model refinements for GOCE gradiometry data. Geotechnologien Science Report, No. 17, 70–76

Oppenheim AV, Schafer RW (1999) Zeitdiskrete Signalverarbeitung, 3rd edn. Oldenbourg, Munich, Vienna

Pail R, Metzler B, Lackner B, Preimesberger T, Höck E, Schuh W-D, Alkathib H, Boxhammer C, Siemes C, Wermuth M (2006) GOCE gravity field analysis in the framework of HPF: operational software system and simulation results. In: 3. GOCE user workshop. ESA, SP-627, ISBN 92-9092-938-3, Frascati

Pail R, Bruinsma S, Migliaccio F, Förste C, Goiginger H, Schuh W-D, Höck E, Reguzzoni M, Brockmann JM, Abrikosov O, Veicherts M, Fecher T, Mayrhofer R, Krasbutter I, Sansò F, Tscherning CC (2011) First GOCE gravity field models derived by three different approaches. J Geod 85(11):819–843

Schuh W-D (1996) Tailored numerical solution strategies for the global determination of the Earth's gravity field. vol 81, Mitteilungen der geodätischen Institute der Technischen Universität Graz, TU Graz

Schuh W-D, Brockmann JM, Kargoll B, Krasbutter I (2010) Adaptive optimization of GOCE gravity field modeling. In: Münster G, Wolf D, Kremer M (eds) NIC Symposium 2010, vol 3, IAS Series Jülich, Germany, pp 313–320

Siemes C (2008) Digital filtering algorithms for decorrelation within large least squares problems. PhD thesis, Institute of Geodesy and Geoinformation, University of Bonn. http://hss.ulb.uni-bonn.de/2008/1374/1374.htm

Widrow B, Glover JR, McCool JM, Kaunitz J, Williams CS, Hearn RH, Zeidler JR, Dong E, Goodlin RC (1975) Adaptive noise cancelling: principles and applications. Proc IEEE 63(12):1692–1716

Chapter 15
Stochastic Modeling of GOCE Gravitational Tensor Invariants

Jianqing Cai and Nico Sneeuw

Abstract The aim of the Gravity Field and Steady-State Ocean Circulation Explorer (GOCE) Mission is to provide global and regional models of the Earth's time-averaged gravity field and of the geoid with high spatial resolution and accuracy. The approach based on the rotational invariants of the gravitational tensor constitutes an independent alternative to conventional analysis methods. Due to the colored noise characteristic of individual gradiometer observations, the stochastic model assembly of the rotational invariants is a highly challenging task on its own. In principle, the invariants' variance-covariance (VC) information can be deduced from the gravitational gradients (GG) by error propagation. But the huge number of gradiometer data and the corresponding size of the VC matrix prohibit this approach. The time series of these invariants, however, display similar stochastic characteristics as the gravitational gradients. They can thus be decorrelated by means of numerical filters. A moving-average (MA) filter of order 50 has been estimated and a filter cascade (high-pass and MA filters) has been developed. This filter cascade has been implemented in the decorrelation of the GOCE tensor invariant observation model.

15.1 Introduction

Typically, gradiometer data analysis is performed at the level of individual gravity gradients (GG). This approach embraces a variety of methods commonly classified into space-wise or time-wise methods. Alternatively, gradiometer data analysis can be performed using rotational invariants, which are, in general, non-linear combinations of all GGs. The resulting observation equations are independent from the orientation

J. Cai (✉) · N. Sneeuw
Institute of Geodesy, Universität Stuttgart, Geschwister-Scholl-Straße 24D, 70174
Stuttgart, Germany
e-mail: cai@gis.uni-stuttgart.de

of the gravitational tensor,[1] cf. (Baur et al. 2008; Pedersen and Rasmussen 1990 and Rummel 1986).

Due to the colored noise behavior of gradiometer measurements the stochastic modeling of invariants is of elementary importance. Previous studies on the application of invariants to GOCE data analysis, however, did not take into account stochastic modeling. One possibility to deduce the stochastic model is applying (non-linear) error propagation to the observed GGs. Because of the huge number of gradiometer data, their VC matrix cannot be stored due to memory limitations. For example, the size of this matrix is 1.76 PB just for one month real GOCE SGG observations. According to our actual studies, e.g., (Baur et al. 2010; Cai et al. 2010), it is not possible to simply deduce the invariants' VC information from the originating gravitational gradients by error propagation. However, the time series of the invariants reveal a similar stochastic character as the GGs. Based on, e.g., (Brockmann et al. 2010; Krasbutter et al. 2010 and Schuh et al. 2010), the GOCE invariants can be considered as equidistant time series and therefore be decorrelated by means of numerical filters. In this context, various filters have been tested and applied to approximate the stochastic model of these invariants. A moving-average (MA) filter of order 50 has been estimated and a filter cascade (high-pass and MA filters) has been developed.

In this contribution the stochastic characteristics of GOCE gravitational tensor invariant noise are firstly investigated. Then, a moving-average (MA) filter with order 50 is estimated and the development of a filter cascade (high-pass and MA filters) based on the stochastic characteristics of GOCE invariants are described. These results are summarized in the Sect. 15.4.

15.2 Statistical Study of GOCE Gravitational Invariants

In case of full tensor gradiometry all second-order derivatives of the geopotential $V_{ij}, i, j = 1, 2, 3$ are given. By denoting the tensor coefficient matrix $\mathbf{V} = [V_{ij}]$, the rotational invariants of the symmetrical gravitational tensor are $I_1 = \text{tr} \mathbf{V}$, $I_2 = [(\text{tr} \mathbf{V})^2 - \text{tr} \mathbf{V}^2]/2$ and $I_3 = \det \mathbf{V}$.

Based on the successful experiences of ITG Bonn (Krasbutter et al. 2010; Schuh et al. 2010), the GOCE invariants can be considered as equidistant time series and therefore be decorrelated by means of numerical filters. Figure 15.1 shows measured and computed invariant I_2 for 4 h on 02. Nov. 2009. Both time series are corrected for the mean and GRS80-reduced. Computed invariants are based on the GOCE only gravity field model (GO_CONS_EGM_TIM_1, see Pail et al. 2011), together with the differences as a first estimation for GOCE invariant noise. (The GOCE invariants I_3 show a very similar behaviour, which is therefore not presented here).

In this figure we can see that time series of the invariant I_2 is dominated by a large bias and long-wavelength error. Removing the GRS80 signal from the measured

---

[1] At this location we need a reference to Oli's pioneering work, e.g. the Baur/Grafarend/Sneeuw paper in JoG.
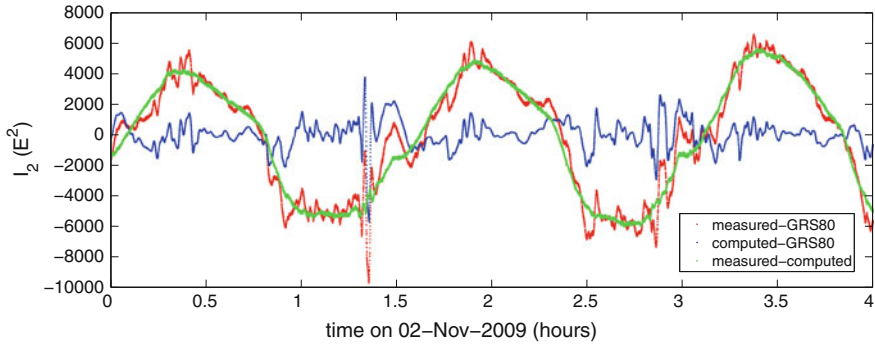
Fig. 15.1 Measured (*red*) and computed (*blue*) invariant I_2 for 4h on 02. Nov. 2009. Both time series are corrected for the mean and GRS80-reduced. Computed invariants are based on the GOCE only gravity field model, together with the differences (*green*) as a first estimation for GOCE invariant noise

and computed invariant I_2 and a mean value from the invariants provides a better impression of the detailed structure of the invariant measurement noise. The mean reduced noise estimation shows now low-frequency oscillations, indicating strong auto-correlations, which imply that the invariant noise is a colored noise process.

As a visual comparison, the measured mean & GRS80 reduced GOCE gradients V_{zz} for the same period on 02. Nov. 2009, together with the differences as a first estimation for GOCE gradients noise are presented in Fig. 15.2. Figures 15.1 and 15.2 demonstrate that both I_2 and V_{zz} suffer from long-wavelength errors (and bias). However, due to the fact that the invariant I_2 is the sum of the six products of two gravity gradients, the variation in amplitude of the invariant I_2 noise time series is obviously greater than the latter.
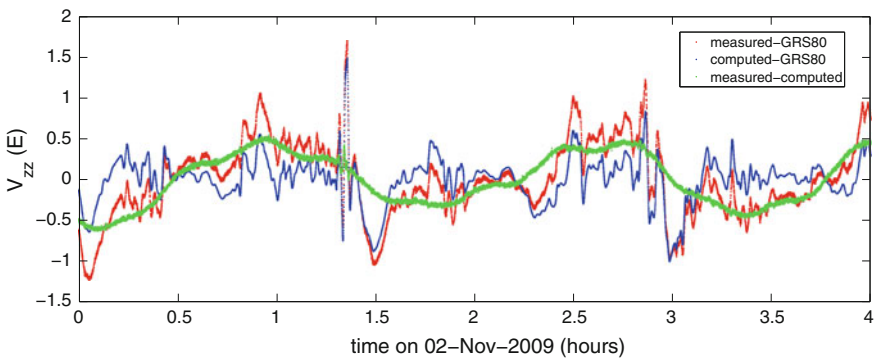
Fig. 15.2 Measured (*red*) and computed (*blue*) GOCE gradients V_{zz} for 4h on 02. Nov. 2009. Both time series are corrected for the mean and GRS80-reduced. Computed gradients are based on the GOCE only gravity field model, together with the differences (*green*) as a first estimation for GOCE gradients noise
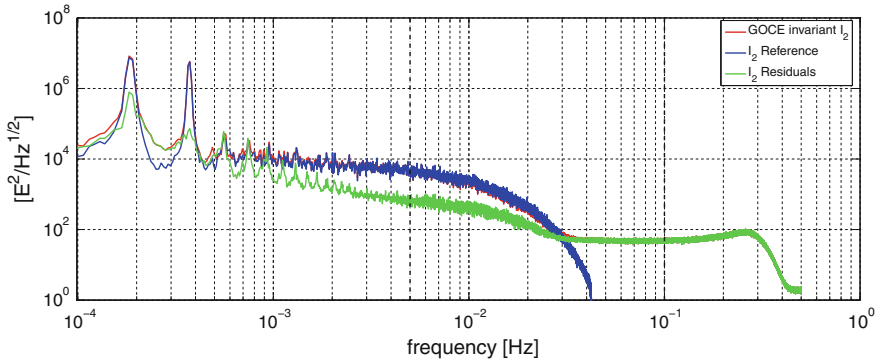
Fig. 15.3 Power spectrum of the GOCE invariant I_2 noise, the GOCE invariant signal and the measured GOCE invariant for Nov. and Dec. 2009

These characteristics of the colored invariant noise process can be more clearly seen in the spectral domain, where the power spectral density (i.e. the Fourier transform of the autocorrelation function) from the invariant noise time series, the GOCE in invariant signal (computed from a gravity field model) and the measurements themselves for the invariant I_2 are plotted in Fig. 15.3. Within the GOCE measurement bandwidth (MBW, between 0.005 and 0.1 Hz), the power spectral density (PSD) is relatively flat, i.e. nearly white; between 0 and 0.005 Hz the spectrum is mainly characterized by an inverse proportional dependence (approx. $1/f$) and a large number of sharp peaks. These characteristics of invariants are also similar to the analytical results of PSDs from GOCE gradients, cf. (Krasbutter et al. 2010; Schuh et al. 2010).

15.3 Modeling the GOCE Invariant Noise

In Baur et al. (2010) and Cai et al. (2010) we have concluded that it is not possible to simply deduce the invariants' VC information from the originating gravitational gradients by error propagation. However, as we have shown in the last section, the time series of the invariants reveal a similar stochastic character (colored noise) as the GGs and therefore can be decorrelated by means of numerical filters that have the inverse spectral characteristics with regard to the estimated noise characteristics, see (Brockmann et al. 2010; Krasbutter et al. 2010; Schuh 1996 and Siemes 2008). With the support from ITG Bonn, a moving-average (MA) filter of order 50 has been estimated and a filter cascade (high-pass and MA filters) has been developed and will be described in detail in the following. The transformed GOCE invariant observation models have white noise and are uncorrelated. Therefore, the least squares adjustment in the gravity field estimation can be performed with the identity matrix as covariance matrix.

15.3.1 Modeling the Long Wavelength Errors

A high-pass filter (differentiation filter) is applied to mod el the noise characteristics for the low frequencies, which down-weights the lower frequencies but keeps all information starting from the MBW. This kind of method is also named as trend elimination by differencing in the analysis of time series (Brockwell and Davis 2002). This filter helps to eliminate the biases and long-wavelength errors in the GOCE invariants. Figure 15.4 presents the noise PSD (in green) and PSD for the inverse high-pass filter (in blue) for GOCE invariant I_2, together with the high pass filter filtered noises (in cyan).

15.3.2 Simple Modeling of the Complete Spectrum

The next step is the application of the ARMA filters to approximate the stochastic model of these invariants. Normally we need to design a filter, whose inverse PSD approximates the PSD of the noise (cf. Fig. 15.3) as good as possible, under the additional condition that it can be described by as few as possible coefficients. In this context, various filters have been tested and applied to approximate the stochastic model of these invariant noises. As presented in Fig. 15.4, a moving-average (MA) filter of order 50 (in red) was designed modeling long wavelength errors as well as the MBW. The relatively smaller order 50 of filter coefficients was used to keep the filtering model simple. The advantages of the MA filter are that it is a simpler filtering method in whitening the colored noises (residuals) and without long warm up time.

Actually this kind of MA filter is also called a nonrecursive filter (Hamming 1989), which is defined by the linear formula
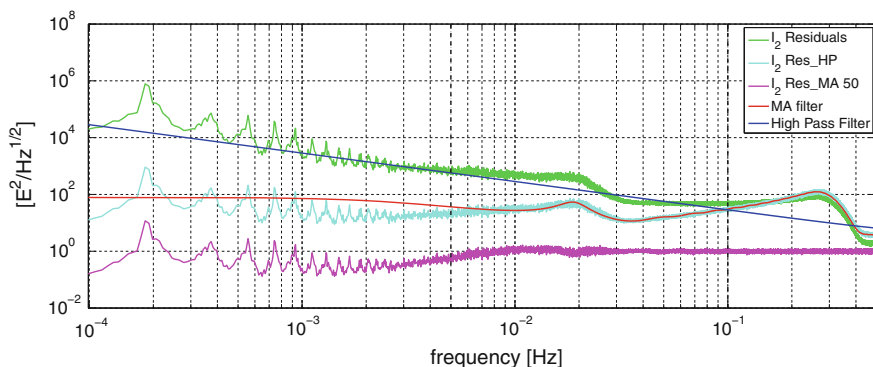
Fig. 15.4 PSDs of GOCE Invariant I_2 residuals (*green*) for Nov. 2009 to Jan. 2010, the inverse high pass filter (*blue*), high pass filter filtered noises (*cyan*), the inverse MA filter (*red*) and MA filter filtered noises (*magenta*) (with the support from ITG Bonn)

$$y_t = \sum_{k=0}^{q} \beta_k u_{t-k},$$

where the coefficients β_k are the constants of the filter, the u_{t-k} the input and y_t the output sequence. The filter coefficients can be estimated using standard analytical numerical procedures (e.g. Oppenheim and Schafer 1999), where the GOCE invariant (colored) noise time series are considered as the autoregressive process.

Analyzing the MA filtered noise (in magenta) in Fig. 15.4, it can be seen that although the n cycles-per-revolution peaks in the spectrum are not modeled individually, the PSD of the filtered noise seems to be linear in the double logarithmic plot.

Combining the features of a differencing filter and the MA filter yields a simple cascade filter model for the entire spectrum. The effects of both cascade components are summarized in Fig. 15.4, which shows the spectral characteristics of this cascade filter. This simple cascade filter represents an apparently overall adequate fit to the invariant noise characteristics, but ignores the sharp peaks in the low-frequency part of the spectrum.

Krasbutter et al. (2010) and Schuh (1996) developed a more complex decorrelation filter with the ARMA filter cascade to take into account the sharp spectral peaks, where the peaks are modeled by means of notch filters, represented by 20 additional individual ARMA(2,2) filters. Their analysis shows that such detailed modeling of the complete spectrum does not lead to a significant improvement of the solution, but it evidently leads to far more realistic accuracy estimates.

The simple cascade filter has been successfully implemented to the GOCE invariant observation model to eliminate the biases and long-wavelength errors of GOCE invariants and decorrelate these invariant observations, which provides one important guarantee in estimating one GOCE invariant-only global gravity field model.

15.4 Summary and Conclusions

According to our studies, it is not possible to simply deduce the invariants' VC information from the originating gravitational gradients by error propagation. However, the time series of the invariants behave stochastically similarly to the GGs. In this contribution, we have investigated the stochastic characteristics of GOCE gravitational tensor invariant noise and developed an appropriate filter cascade (high-pass and MA filters) based on the stochastic characteristics of GOCE invariants, which has been successfully implemented to the decorrelation of the GOCE tensor invariant observation model. These provide a strong basis in deriving a GOCE invariant-only global gravity field model until degree/order 224 based on two months of real GOCE gradient observations, which will be published in another manuscript of the authors.

References

Baur O, Sneeuw N, Grafarend EW (2008) Methodology and use of tensor invariants for satellite gravity recovery. J Geod 82:279–293. doi:10.1007/s00190-007-0178-5

Baur O, Sneeuw N, Cai J, Roth M (2010) GOCE data analysis: realization of the invariants approach in a high performance computing environment. In: Proceedings of the ESA living planet symposium, Bergen, Norway, 28 June-2 July, 2010, ESA SP-686

Brockmann JM, Kargoll B, Krasbutter I, Schuh W-D, Wermuth M (2010) GOCE Data analysis: from calibrated measurements to the global earth gravity field. In: Flechtner F, Gruber T, Guntner A, Mandea M, Rothacher M, Schone T, Wickert J (eds) System earth via geodetic-geophysical space techniques, advanced technologies in earth sciences, Springer, Berlin, pp 213–229

Brockwell PJ, Davis RA (2002) Introduction to time series and forecasting, 2nd edn. Springer, New York

Cai J, Baur O, Sneeuw N (2010) GOCE gravity field determination by means of rotational invariants: first experiences, GEOTECHNOLOGIEN Science Report Nr. 17, Observation of the system earth from space, pp 62–69

Hamming RW (1989) Digital filters, 3ed edn. Prentice Hall, New Jersey

Krasbutter I, Brockmann JM, Kargoll B, Schuh W-D (2010) Stochastic model refinements for GOCE gradiometry data, GEOTECHNOLOGIEN Science Report Nr. 17, Observation of the system earth from space, pp 70–76

Oppenheim AV, Schafer RW (1999) Discrete-time signal processing, Pearson; 2nd edn. Prentice Hall, New Jersey

Pail R, Bruinsma S, Migliaccio F, Förste C, Goiginger H, Schuh W-D, Höck E, Reguzzoni M, Brockmann JM, Abrikosov O, Veicherts M, Fecher T, Mayrhofer R, Krasbutter I, Sansò F, Tscherning CC (2011) First GOCE gravity field models derived by three different approaches. J Geod 85:819–843. doi:10.1007/s100190-011-0467-x

Pedersen LB, Rasmussen TM (1990) The gradient tensor of potential field anomalies: Some implications on data collection and data processing of maps. Geophysics 55(12):1558–1566. doi:10.1190/1.1442807

Rummel R (1986) Satellite gradiometry. In: Sünkel H (ed) Mathematical and numerical techniques in physical geodesy, Lecture notes in earth sciences, 7. Springer, Berlin, pp 317–363. doi:10.1007/BFb0010135

Schuh W-D (1996) Tailored numerical solutions strategies for the global determination of the Earth's gravity field, Mitteilungen der Universität Graz 81

Schuh W-D, Brockmann JM, Kargoll B, Krasbutter I (2010) Refinement of the stochastic model of GOCE scientific data and its effect on the in-site gravity field solution. In: Proceedings of ESA living planet symposium, Bergen, Norway, 28 June - 2 July 2010, ESA SP-686

Siemes C (2008) Digital filtering algorithms for decorrelation within large least squares problems. Ph.D. thesis, Institute of Geodesy and Geoinformation, University of Bonn, Bonn

Chapter 16
Cross-Overs Assess Quality of GOCE Gradients

Phillip Brieden and Jürgen Müller

Abstract We address the important issue of quality assessment of GOCE gravitational gradients. To assess the gradients quality before being used in geophysical research and geodetic applications, a validation method is investigated that compares gradients in satellite track cross-overs (XO). The comparison of two three-dimensional measurements like the GOCE gradient tensors has to be performed in a common coordinate system, which requires tensor rotation. The XO residuals are then analyzed. An anomaly in the V_{yy} component is identified affecting gradients in vicinity of the geographical and magnetic poles that spread to other tensor components (mainly V_{xx} and V_{xz}) in the context of tensor rotation. The analysis of all non-anomaly-affected XO residuals underlines the very good quality of the GOCE gravitational gradients: ΔV_{xx} and ΔV_{yy} have an RMS of only 3.2 mE, the RMS of ΔV_{zz} is only slightly worse with 5.3 mE.

16.1 Introduction

GOCE (Gravity field and steady-state Ocean Circulation Explorer), ESA's first Earth Explorer mission, aims at the determination of the Earth's gravity field by direct observation of acceleration differences in space. Currently, the satellite is in orbit for more than three years and all instruments are working well.

Before GOCE gravitational gradients are used in geophysical research and geodetic applications, their quality assessment is of major relevance. For this purpose, the cross-over (XO) approach is applied here that compares gradients in satellite track XOs. XO analysis for validating gravitational gradients has been studied by our group over the past years (Jarecki 2010; Müller et al. 2010; Brieden and Müller 2013). This paper presents basic processing steps (Sect. 16.2). Its major part will

P. Brieden (✉) · J. Müller
Institut für Erdmessung (IfE), Leibniz Universität Hannover, Schneiderberg 50,
30167 Hannover, Germany
e-mail: brieden@ife.uni-hannover.de

focus on the analysis of XO residuals (Sect. 16.3). In Sect. 16.4, a numerical quality measure is determined, before the summary follows in Sect. 16.5.

16.2 Principle of XO Analysis and Data Pre-Processing

The basis of XO analysis is the assumption of equal measurements in identical points. In the present case, gravity field signal in terms of second order derivatives of the gravitational potential is expected to be identical in satellite track XOs. The actual measurements are differential accelerations measured by the GOCE gradiometer, from which gravitational gradients are derived (e.g. ESA 1999). The 'measurement' which will be compared in XOs are the gravitational gradients (henceforth referred to as measurements). In the case of the GOCE orbit, XOs arise between ascending and descending satellite tracks, respectively.

Due to the fact that a gravitational gradient tensor is a three-dimensional measurement, not only the differences in altitude but also the differences in attitude between the two XO-involved measurements have to be considered. For this reason, the transformation of the gravitational gradient tensor has to be performed, in order to compare the gradients in one coordinate system. The data set that is investigated in Sect. 16.3 shows altitude differences in the XOs up to 6.5 km. The corresponding differences in attitude are dependent on the location of the XO. Because the gradiometer reference frame (GRF) in which the measurements are provided is fixed to the attitude of the satellite and the satellite is oriented almost along its orbit, the largest part of rotation between the two GRFs is the rotation about the almost radially aligned gradiometer z-axis. The corresponding rotation angle can reach magnitudes up to 170° and is strongly dependent on the satellite's geographical position (latitude).

The most important steps of the programmatic implementation of the XO analysis are illustrated in Fig. 16.1:

- Based on measured GOCE data, XO positions and XO points in time are determined in the data set to be analyzed.
- In parallel, a time series of model-derived gravitational gradients (GGs) is computed based on a combined GOCE gravity field model like the GOCO02S (Goiginger et al. 2011).
- The measured and model-derived gradient time series are combined in a filtering procedure. Due to less accurate longer wavelength information in the GOCE GGs, these parts are replaced by highly accurate long-wavelength model information. In addition, the less accurately determined second diagonal elements of the GG tensor V_{xy} and V_{yz} are completely replaced by model information. This is done in order to avoid signal shift between accurate and less accurate tensor components in the course of tensor rotation. Further information can be found, e.g., in Brieden and Müller (2013).
- All data sets are interpolated to the location of the XOs using cubic spline-interpolation.
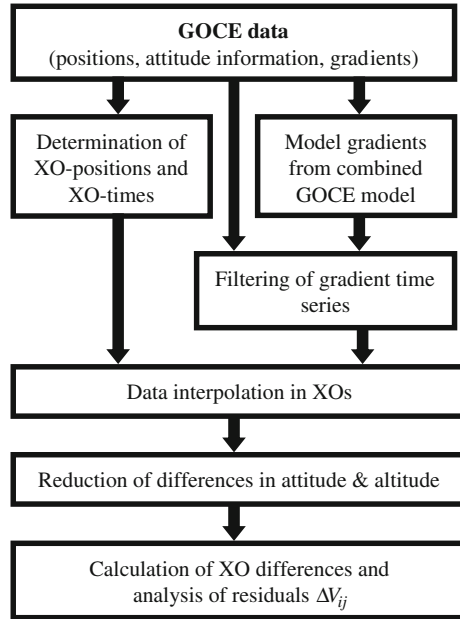
Fig. 16.1 Flowchart showing major steps of XO analysis

- To overcome the differences in attitude, a rotation matrix is used to rotate the GGs from one GRF to the other. The altitude-caused differences are corrected using gradient differences between two model-derived GGs in the corresponding heights and the same orientation.
- Finally, the difference between two GG tensors in one XO is computed:

$$\Delta \mathbf{V}_{ij}^{\text{GRF2}} = \mathbf{V}_{ij}^{\text{GRF2}} - \left(\mathbf{R}_{\text{GRF1} \leftarrow \text{GRF2}} \cdot \mathbf{V}_{ij}^{\text{GRF1}} \cdot \mathbf{R}_{\text{GRF1} \leftarrow \text{GRF2}}^{T} + \Delta \mathbf{V}_{ij}^{\Delta h} \right).$$

The gradient tensor in the GRF of position 1 $\left(\mathbf{V}_{ij}^{\text{GRF1}} \right)$ is rotated using the rotation matrix $\mathbf{R}_{\text{GRF1} \leftarrow \text{GRF2}}$ and height reduced $\left(\Delta \mathbf{V}_{ij}^{\Delta h} \right)$ before being subtracted from the GG tensor in the GRF of position 2 $\left(\mathbf{V}_{ij}^{\text{GRF2}} \right)$, where the final comparison is performed.

- The XO residuals $\Delta \mathbf{V}_{ij}^{\text{GRF2}}$ are further analyzed in Sect. 16.3.

A more detailed description of the necessary calculation steps can be found in Brieden and Müller (2013).

16.3 Analysis of XO Residuals

The current analysis is based on GOCE data in the period from February 11th, 2011 to April 3rd, 2011. The gradients are L1b data; positions as well as attitude information are taken from L2 database. In the data set, about 460.000 XOs can be obtained. This number has already been reduced, as the special-event affected time series segments were removed. Further information on 'special events' and its impact on XO analysis is given in Brieden and Müller (2013).

The following analysis focuses on the residuals $\Delta \mathbf{V}_{ij}^{\mathrm{GRF2}}$ with $ij = \{xx, yy, zz, xz\}$, the components that are determined with high precision (ESA 1999).

Brieden and Müller (2012a) have shown that the XOs' geographical distribution reveals accumulations of higher residuals in certain areas such as south of Australia. It has also been demonstrated that areas around the equator are not influenced by such accumulations of larger differences. Thus, the present study focuses on the areas around the poles.

In Fig. 16.2, the XO residuals of the three main diagonal components in the northern and southern hemisphere (each between 35°–90°) are depicted. The typical polar gap can clearly be seen, which is present because of GOCE's orbit inclination of about 96.5°. Here 1‰ of the largest residuals of each component is eliminated to make the others more clearly visible.

The largest gradient residuals occur in $\Delta \boldsymbol{V}_{yy}$ and are supposed to be caused by solar cross-winds acting on the gradiometer cross-track axis. Since the anomalies increase towards the magnetic poles, the Earth's magnetic field also seems to affect the GOCE gradients. The source of the anomaly is still under investigation. Due to tensor rotation, the $\boldsymbol{V}_{yy}$ anomaly also affects the $\Delta \boldsymbol{V}_{xx}$ component, but the magnitude is smaller than in $\Delta \boldsymbol{V}_{yy}$. This becomes apparent when the residuals ($\Delta \boldsymbol{V}_{xx}$ and $\Delta \boldsymbol{V}_{yy}$) around the South Pole are compared (Fig. 16.2, right). The residuals in $\Delta \boldsymbol{V}_{xx}$ and $\Delta \boldsymbol{V}_{yy}$ show a similar pattern around the poles, within which bands of negative and positive residuals seem to alternate. This is assumed to be caused by an imperfect calibration of the GOCE gradiometer. Residuals in $\Delta \boldsymbol{V}_{zz}$ only show a slight increase towards the poles and their magnitude is significantly smaller compared to $\Delta \boldsymbol{V}_{xx}$ and $\Delta \boldsymbol{V}_{yy}$. The overall noise level of $\Delta \boldsymbol{V}_{zz}$ is increased compared to $\Delta \boldsymbol{V}_{xx}$ and $\Delta \boldsymbol{V}_{yy}$. The cause will be investigated further.

At the beginning of 2012, ESA has finally implemented its new processor version 5.06, where many processing steps have been changed significantly compared to previous versions. First results indicate a significant reduction of the anomalies in $\boldsymbol{V}_{yy}$. Further information on the new processor can be found in, e.g., Siemes (2012).

When interpreting the results, the mixing of model-derived gradients and GOCE measurements during tensor rotation and filtering has to be considered. The impact of this mixing is discussed in Fuchs and Bouman (2011) and will further be investigated with respect to XO analysis in future work.
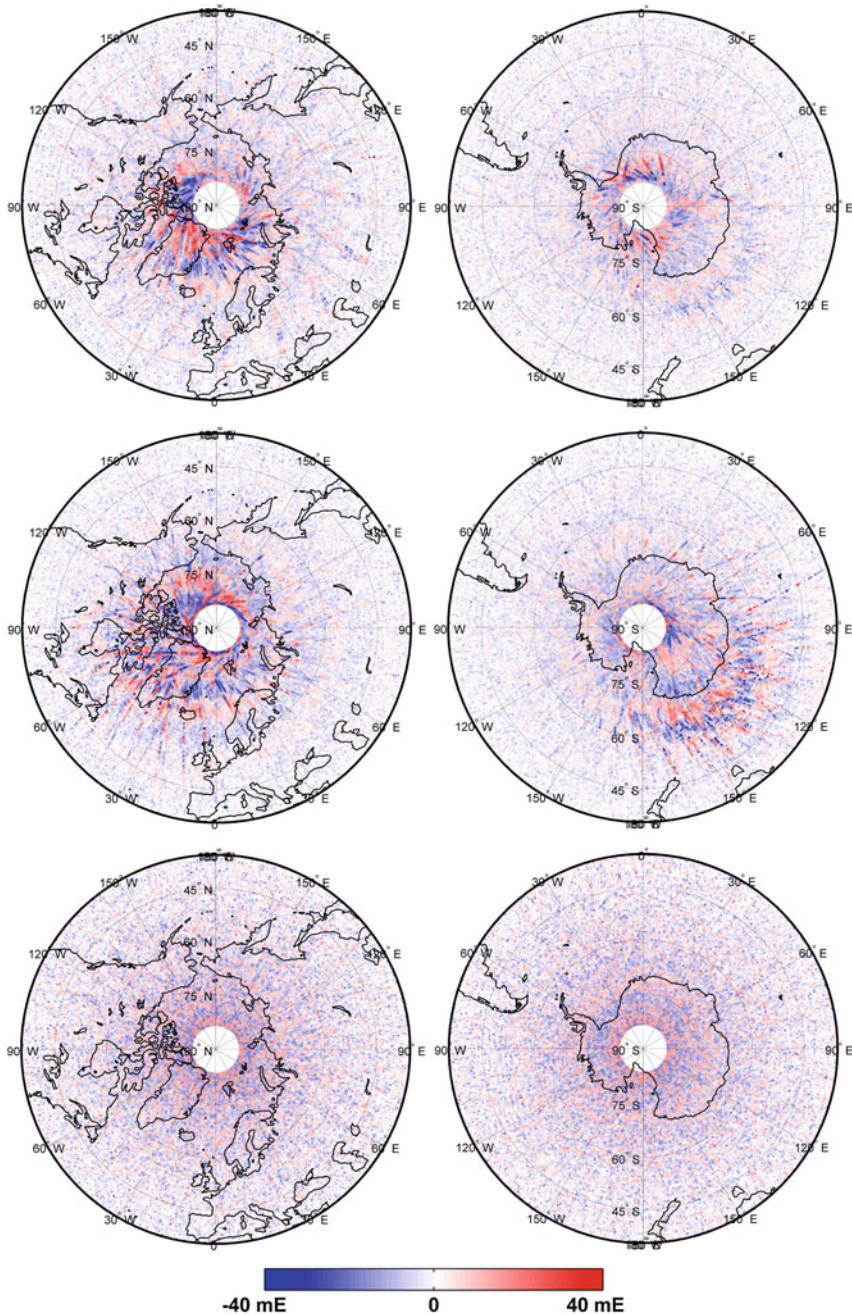
Fig. 16.2 Geographical distribution of XO residuals ΔV_{ij} [mE] in the northern (*left*) and southern (*right*) hemisphere. The residuals of the main diagonal component are presented: ΔV_{xx} (*top*), ΔV_{yy} (*middle*), ΔV_{zz} (*bottom*)

Table 16.1 RMS values [mE] of XO residuals change due to the reduction of the latitudinal zone around the equator

Latitudinal band around the equator	ΔV_{xx}	ΔV_{yy}	ΔV_{zz}	ΔV_{xz}
±90° (all)	4.93	5.48	5.31	6.03
±45°	3.32	3.10	5.32	6.77
±25°	3.25	2.99	5.28	6.72

16.4 Numerical Quality Measures of GOCE Gradients

The XO approach provides residuals of gradient differences in satellite track crossovers, which have already been analyzed in Sect. 16.3. Now, the residuals are used to derive a numerical quality measure for the GOCE gradients.

The investigations in Sect. 16.3 have shown the impact of an anomaly in the V_{yy} component with spread to other components due to tensor rotation. As being evident in Fig. 16.2, anomalies occur down to latitudes of 45°. To determine a representative quality measure, only the XO residuals within a band of ±45° around the equator are considered in the following quality assessment. All anomaly-affected XO residuals are omitted.

Table 16.1 provides the root mean square (RMS) values of XO residuals according to limited latitudinal bands around the equator. The anomaly affected components V_{xx} and V_{yy} show significant improvements in RMS when the band is limited to ±45°. As discussed in Sect. 16.3 already, the RMS of ΔV_{zz} does not change much when reducing the latitudinal band. The RMS of ΔV_{xz} even increases slightly, which is caused by shifted signal from tensor rotation. The anomaly-affected components shift very little signal to V_{xz} in latitudes around 80° and thus the RMS value is low.

16.5 Summary and Conclusions

In the present study, quality assessment of GOCE gravitational gradients is carried out using XO analysis. Two gradients in a XO are compared in a common coordinate system, which necessitates rotation and height reduction of the gradient tensor. The XO residuals ΔV_{xx} and ΔV_{yy} show accumulation of higher residuals towards the geographical and magnetic poles. This is probably due to an anomaly in the V_{yy}-component which spread to ΔV_{xx} in the context of tensor rotation. ΔV_{zz} show a slightly higher noise ratio, but is unaffected with respect to the anomalies. By considering only those XOs that are not in anomaly-influenced areas, the RMS values for ΔV_{xx} and ΔV_{yy} are at the level of 3.2 mE. The RMS of ΔV_{zz} is slightly worse having a magnitude of 5.3 mE. Thus, the high quality of the GOCE gravitational gradient is confirmed.

References

Brieden P, Müller J (2012a) Cross-overs for evaluating GOCE gravitational gradients. Poster at EGU general assembly 2012. http://www.ife.uni-hannover.de/publications.html. Accessed 11 July 2012

Brieden P, Müller J (2013) Validation of GOCE gravitational gradients in satellite track cross-overs. In: Rizos C, Willis P (eds) Earth on the rdge: Science for a sustainable Planet, IAG Symposia Series vol 139, Springer. ISBN: 978-3-642-37221-6

ESA (1999) Reports for mission selection 'the four candidate earth explorer core missions', gravity field and steady-state ocean circulation mission. ESA SP-1233(1). http://esamultimedia.esa.int/docs/goce_sp1233_1.pdf. Accessed 11 July 2012

Fuchs MJ, Bouman J (2011) Rotation of GOCE gravity gradients to local frames. Geophys J Int 187:743–753. doi:10.1111/j.1365-246X.2011.05162.x

Goiginger H, Hoeck E, Rieser D et al (2011) The combined satellite-only global gravity field model GOCO02S. Presented at EGU general assembly 2011, Vienna, Austria

Jarecki F (2010) Spurkreuzungspunktdifferenzen zur Validierung satellitengradiometrischer Messungen. Wissenschaftliche Arbeiten der Fachrichtung Geodäsie und Geoinformatik der Leibniz Universität Hannover, ISSN 0174-1454, Nr. 286, http://www.ife.uni-hannover.de/publications.html

Müller J, Jarecki F, Wolf KI, Brieden P (2010) Quality Evaluation of GOCE Gradients. In: Flechtner F, Gruber Th, Güntner A et al (eds) System earth via geodetic-geophysical space techniques (Advanced Technologies in Earth Sciences), Springer, pp 265–276

Siemes C (2012) GOCE gradiometer calibration and Level 1b data processing. ESA Working Paper EWP-2384. https://earth.esa.int/c/document_library/get_file?folderId=85857&name=DLFE-1312.pdf. Accessed 11 July 2012

Chapter 17
Consistency of GOCE Geoid Information with in-situ Ocean and Atmospheric Data, Tested by Ocean State Estimation

Frank Siegismund, Armin Köhl and Detlef Stammer

Abstract Ocean state estimation is a powerful method to test the consistency of data sets assimilated into an Ocean General Circulation Model (OGCM) among each other and with the initial and boundary conditions of the model. We apply the GOCE-GRACE combined GOCO01s geoid model to reference temporal Mean Sea Surface (MSS) height measured from satellite altimetry to derive the Mean Dynamic Topography (MDT). The consistency of this MDT with ocean and atmospheric data is tested through application of the GECCO (German part of Estimating the Circulation and Climate of the Ocean) model. Three optimizations are performed: One as a reference run applying usual data sets but without assimilation of MDT, and two integrations applying different MSS models in the computation of the MDT. We find improved performance of the state estimation, if MDT is assimilated. The choice of the MSS, however, has no significant impact on the optimization. The MDT is overall consistent with both, the other assimilated ocean data sets as well as the atmospheric forcing.

17.1 Introduction

In oceanography, the deviation of the ocean surface, measured by satellite altimetry, from the geoid is called the Dynamic Topography (DT). Its gradients describe the geostrophic surface circulation and, when combined with density information from hydrographic observations, the ocean's circulation as well as heat and salt transports relevant for climate research.

Highly accurate Sea Surface Height (SSH) data are available from satellite altimetry for the last two decades and have been used widely in studies of DT time

F. Siegismund (✉) · A. Köhl · D. Stammer
Institut für Meereskunde, Centrum für Erdsystemforschung und Nachhaltigkeit,
Universität Hamburg, Bundesstraße 53, 20146 Hamburg, Germany
e-mail: frank.siegismund@zmaw.de

variability. However, to obtain an absolute or temporal mean DT, ocean geoid models are needed to reference the SSH. To significantly improve the current knowledge of the ocean's surface circulation, the geoid models have to be provided with an accuracy of a few centimeters on spatial scales below 1000 km or so.

In a study of Stammer et al. (2007) an early GRACE geoid model was applied to assimilate an MDT in an ocean state estimation experiment. The study implied, that the GRACE geoid model provided a considerably higher accuracy than older geoid models. However, its accuracy was still not sufficient to provide additional information on the ocean dynamics compared to the knowledge obtained from available ocean observations when synthesized with a dynamic ocean model in an ocean state estimation procedure. However, the study detected a potential impact on the ocean synthesis when more accurate geoid models are assimilated in future optimizations.

Through the advent of the GOCE satellite mission, considerable improvements in the determination of the short scales in the geoid height field is expected, with the target of 1–2 cm accuracy at a length scale of 100 km (Johannessen et al. 2003). The accuracy of MDTs using GOCE geoid models has been studied in a number of publications through comparisons to products mainly based on near –surface drifter velocities (Knudsen et al. 2011; Bingham et al. 2011; Siegismund 2013). In contrast, the method we present here carries forward the work of Stammer et al. (2007). We apply ocean state estimation by assimilating the MDT together with other usual ocean data into an OGCM. Rather than validating the MDT through a direct comparison with another data set, this method allows to test the consistency of the MDT with all other assimilated data sets (constraints) as well as the initial and boundary conditions (controls) of the OGCM by using the physical relations between the data sets as described by the OGCM. The data sets are called consistent, if an ocean state can be modeled, where corrections to both, controls and constraints, are comparable to their uncertainty, which has to be provided with the data. A summary of the method is given in Wunsch (1996).

To test the consistency we apply the GECCO model. Here, we are particularly interested in the consistency of the MDT with all other data sets usually assimilated into GECCO and the atmospheric boundary conditions.

17.2 Methodology

17.2.1 Mean Dynamic Topography

The geodetic MDT ζ is computed from

$$\varsigma = h - N, \tag{17.1}$$

with h the MSS from altimetry, and N the geoid height. The computation of ζ has to consider both sources of errors: The omission error in the geoid model, that, if

not treated properly, causes a short scale geoid signal from the MSS remaining in the MDT after applying Eq. 17.1, and the commission error of both, the geoid and the MSS.

The omission error is treated here by adapting the MSS to the resolution of the geoid. This is done by transforming the MSS to spherical harmonic coefficients, cutting off all coefficients beyond the maximum degree and order (d/o) of the geoid, and transforming back to physical space. The commission error is reduced by applying a spatial Gaussian filter to the MDT calculated from Eq. 17.1 (truncated at 3 times the half width filter radius).

We apply the GOCO01s (Pail et al. 2010, max d/o 224) geoid model and the DTU10 (Andersen 2010) and CNES-CLS10 (Schaeffer et al. 2010) MSS models, resulting in two different MDTs, called DTU-GOCO1 and CLS-GOCO1, according to the choice of the MSS. The half width filter radius of the spatial Gaussian kernel is $1.2°$ in both cases.

17.2.2 GECCO

GECCO is based on the Massachusetts Institute of Technology general circulation model (MITgcm; Marshall et al. 1997), which is a numerical implementation of the primitive equations formulated on z-levels on a spherical coordinate system.

The set-up we use for the optimizations here, is basically identical to the 50-yr run (1952–2001) of the GECCO model (Köhl and Stammer 2008). The syntheses use the adjoint method to bring the model into consistency with available hydrographic and satellite data as well as prior estimates of surface fluxes. The estimation of the control parameters was changed from a direct estimation of the fluxes every 10 days to the estimation of daily atmospheric state variables, which include surface air temperature, humidity, precipitation and the 10 m wind. The prior of the atmospheric state derives as in the previous estimate from the National Centers for Environmental Prediction (NCEP).

These control fields are then adjusted by the method to yield model states that are dynamically consistent with the model physics and the assimilated data within given error limits. We refer to Wunsch (1996) for a general introduction of the methodology. As before, the set of assimilated data includes altimeter data, AMSR/E SST, Argo temperature and salinity profiles. The assimilation of MDT consists of a spatial MDT map as constraint of the modeled topography. Since the geoid error is provided as spherical harmonic coefficients, the MDT cost function contribution is evaluated in spectral space.

We discuss here three optimizations for the period 1993–1999. Apart from the assimilation of the MDT, all integrations use the same setup as described above. One optimization assimilates the CLS-GOCO1 MDT, a second applies the DTU-GOCO1 MDT, and a third one is performed without using the MDT as constraint and serves as reference for the other two integrations.

17.3 Results

17.3.1 Consistency with in situ Ocean Data

In all three cases the three optimization process was stopped, when the reduction of the cost function compared to the previous iteration was smaller than 0.2 % and thus almost converged solutions were obtained.

Compared with the reference run both optimizations that included MDT assimilation converged to lower cost functions. Both runs have a similar performance, though the use of the DTU10 MSS resulted in a slightly smaller cost function. The cost function reduction includes all mayor components of the cost function, but is specifically strong for the temporal mean upper hydrography (Fig. 17.1).

The costs for the MDT itself (diagnosed offline for the reference run by comparison with CLS-GOCO and associated a priori errors) experiences the strongest reduction of all constraints when compared to the free model integration performed before starting the optimization (56 % for both, CLS-GOCO and DTU-GOCO optimizations). For comparison, in the reference optimization the reduction is only 19 %.

Accordingly, MDT model-data residuals are strongly reduced in those optimizations that include MDT assimilation. High residuals above 5 cm remain only for the Western Boundary Currents, the Antarctic Circumpolar Current and the tropical North Pacific, part of which might be related to mesoscale activity not resolved by the model (Fig. 17.2, left). Also, significantly lower residuals in Sea Surface Temperature (SST) are achieved, if MDT is assimilated (Fig. 17.2, right). Similarly, model-data residuals for Sea Surface Salinity (SSS) are strongly reduced (not shown), but since
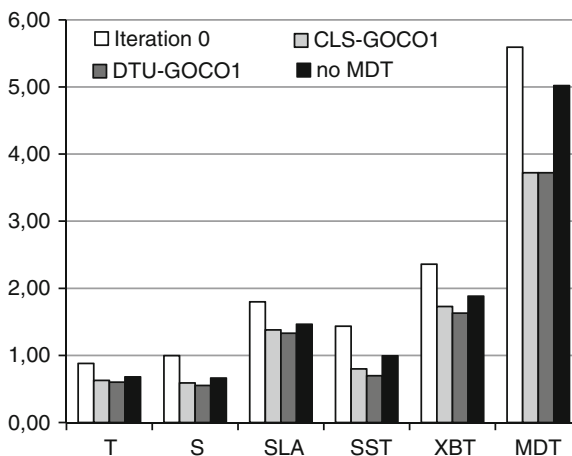
Fig. 17.1 Square root of normalized cost function contributions for the most relevant constraints: Temperature (T) and Salinity (S) climatologies, Sea Level Anomaly (SLA), Sea Surface Temperature (SST), temperature profiles (XBT) and MDT. Normalization is accomplished by dividing by the number of observations
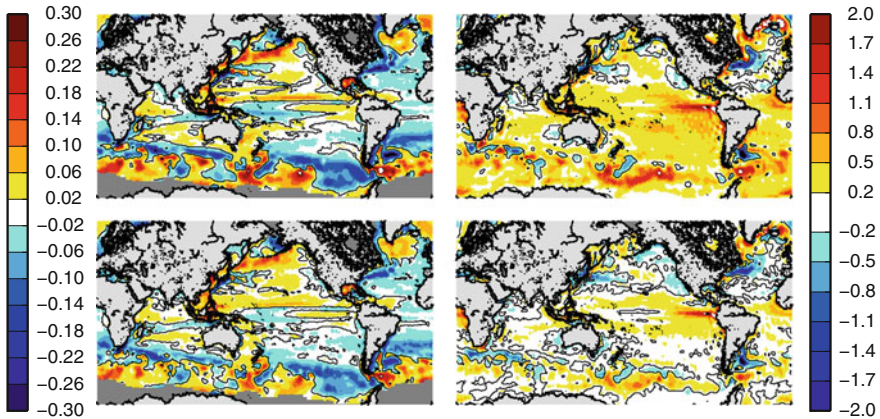
Fig. 17.2 Model-data residuals for (*left*) MDT in [m], and (*right*) Sea Surface Temperature in [K]. (*Top*) reference, (*bottom*) DTU-GOCO1 optimization

observations on SSS are sparse, the absolute contribution to the total cost function is rather weak. Interestingly, the assimilation of MDT also impacts, through nonlinear processes, the modeled temporal variability by bringing modeled sea level variability slightly closer to altimetric Sea Level Anomaly (SLA, see Fig. 17.1).

17.3.2 Consistency with Atmospheric Boundary Conditions

The optimization performed by GECCO iteratively adapts corrections to the boundary and initial conditions (controls) of the OGCM to reduce model-data residuals. These corrections remain below the uncertainties specified for all control parameters in all three optimizations.

Since the optimization process tests the consistency of all included data sets, the corrections applied to the controls should improve their accuracy, given sufficiently low errors of both, the constraints and the OGCM. To test this issue, independent data are needed for comparison.

Large and Yeager (2009) have suggested an independent correction of the NCEP reanalysis data set, the data set we apply to force the OGCM. We have used their corrections for comparisons to ours and found high correlations for zonal wind speed, precipitation (Fig. 17.3) and specific humidity in all three optimizations. The amplitudes of our corrections are smaller than those of Large and Yeager (2009), but increase, if an MDT is assimilated.

We have not found significant correlations for the downward longwave radiation and near surface atmospheric temperature and further investigation is needed here. Overall, the improved correspondence of modeled corrections with the independent suggestions by Large and Yeager (2009), if MDT is assimilated, supports the consistency of the MDT with the atmospheric boundary conditions.
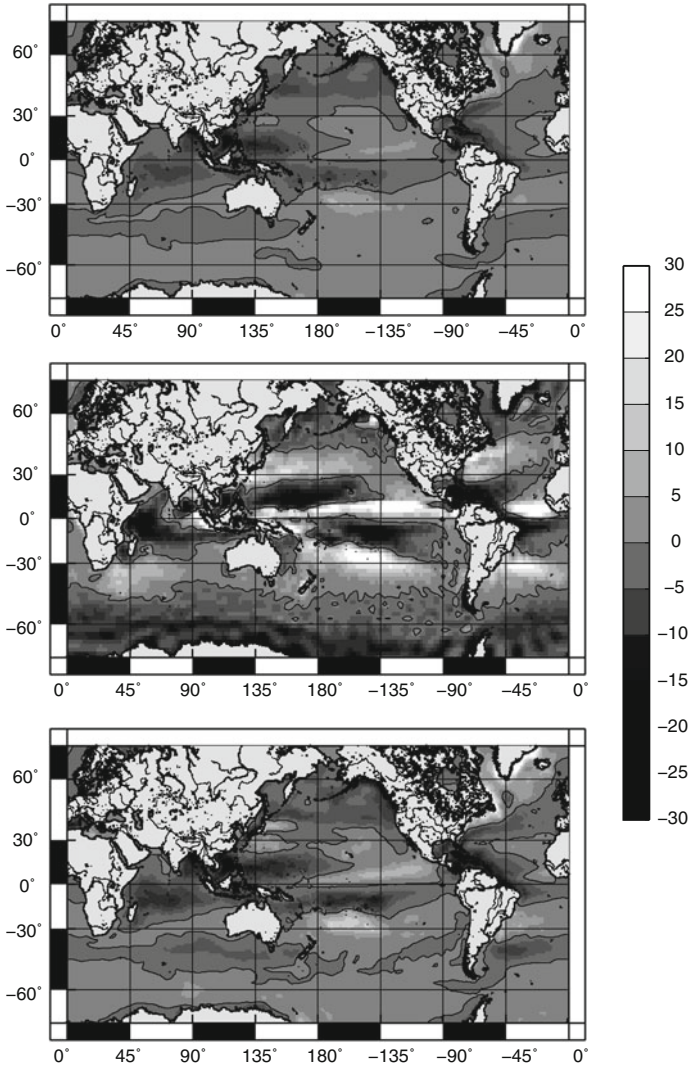
Fig. 17.3 Temporal mean correction for precipitation $[10^{-9}\,\mathrm{m\,s^{-1}}]$ for (*top*) reference and (*bottom*) DTU-GOCO1 optimization, (*center*) correction suggested by Large and Yeager (2009)

17.4 Concluding Remarks

We have investigated the impact of assimilating an MDT referenced to a recent geoid model into an ocean general circulation model. Two MDT models have been investigated, both applying the GOCO01s geoid, but using different MSS models. The focus has been on the consistency of MDT information with other ocean data

assimilated to the ocean model and the atmospheric data applied to force the model and used as controls in the optimization process. As reference, an optimization without MDT assimilation has been performed.

The choice of the MSS model does not play a mayor role for the performance of the optimization. Compared to the reference, the assimilation of both MDTs reduce the costs for all mayor components in the cost function. In particular, the model-data residuals for the MDT and other temporal mean surface and near surface parameters strongly reduce. Comparisons of modeled corrections of control parameters with independent suggestions reveal increased correspondence, if MDT is assimilated. Overall, both MDTs applied in our study are consistent with the assimilated ocean data and the atmospheric forcing data.

References

Andersen OB (2010) The DTU10 Gravity field and Mean sea surface. Second international symposium of the gravity field of the Earth (IGFS2), Fairbanks, Alaska.

Bingham RJ, Knudsen P, Andersen O, Pail R (2011) An initial estimate of the North Atlantic steady-state geostrophic circulation from GOCE. Geophys Res Lett 38:L01606. doi:10.1029/2010GL045633

Johannessen JA, Balmino G, Le Provost C, Rummel R, Sabadini R, Sunkel H, Tscherning CC, Visser P, Woodworth P, Hughes C, LeGrand P, Sneeuw N, Perosanz F, Aguirre-Martinez M, Rebhan H, Drinkwater M (2003) The European gravity field and steady state ocean circulation explorer satellite mission: impact in geophysics. Surv Geophys 24:339–386

Knudsen P, Bingham R, Andersen O, Rio MH (2011) A global mean dynamic topography and ocean circulation estimation using a preliminary GOCE gravity model. J Geod 85:861–879. doi:10.1007/s00190-011-0485-8

Köhl A, Stammer D (2008) Variability of the meridional overturning in the North Atlantic from the 50 years GECCO state estimation. J Phys Oceanogr 38:1913–1930

Large WG, Yeager SG (2009) The global climatology of an interannually varying air-sea flux data set. Clim Dyn 33:341–364

Marshall J, Adcroft A, Hill C, Perelman L, Heisey C (1997) A finite-volume, incompressible Navier Stokes model for studies of the ocean on parallel computers. J Geophys Res 102(C3): 5753–5766

Pail R et al (2010) Combined satellite gravity field model GOCO01S derived from GOCE and GRACE. Geophys Res Lett 37:L20314. doi:10.1029/2010GL044906

Schaeffer P et al (2010) The new CNES CLS 2010 mean sea surface. Oral presentation at OSTST 2010 meeting. http://www.aviso.oceanobs.com/fileadmin/documents/OSTST/2010/oral/19_Tuesday/Schaeffer.pdf

Siegismund F (2013) Assessment of optimally filtered recent geodetic Mean Dynamic Topographies. J Geophys Res 118:1–10. doi:10.1029/2012JC008149

Stammer D, Köhl A, Wunsch C (2007) Impact of accurate geoid fields on estimates of the ocean circulation. J Atmos Ocean Technol 24:1464–1478. doi:10.1175/JTECH2044.1

Wunsch C (1996) The ocean circulation inverse problem. Cambridge University Press, Cambridge, p 458

Chapter 18
Regional Validation and Combination of GOCE Gravity Field Models and Terrestrial Data

Christian Voigt and Heiner Denker

Abstract High-precision terrestrial gravity field data sets in Germany and Europe are utilized to validate recent global gravity field models (GGMs), emphasizing the progress with respect to the latest GOCE GGM releases. The agreement between the release 3 GOCE GGMs and terrestrial data up to degree and order 200 is about 5.5 cm for height anomalies, 1.7 mGal for gravity anomalies, and 0.55" for vertical deflections, respectively, being fully compatible with the relevant error estimates. Furthermore, results from the combination of the GOCE GGMs with terrestrial gravity data in Europe sets are outlined, showing that especially the release 3 GGMs adequately represent the long wavelength gravity field structures, with further improvements expected from the next GGM releases.

18.1 Introduction

The GOCE mission aims at providing gravity anomalies and the geoid with a precision of 1 mGal and 1–2 cm, respectively, both at a resolution of 100 km, corresponding to spherical harmonic degree and order (d/o) 200 (e.g., Pail et al. 2011); this is equivalent to about 0.15" for single vertical deflection components (Voigt and Denker 2013). So far, the GOCE High-level Processing Facility (HPF) generated three releases of global gravity field models (GGMs), which are based on 2, 6, and 12 months of GOCE observations, processed by the direct (DIR), time-wise (TIM), and space-wise (SPW) approach, as outlined in Pail et al. (2011). The maximum d/o of these models ranges from 210 (SPW1) to 250 (TIM3). Furthermore, the GOCE results have been combined with multi-year GRACE, SLR, and CHAMP data, leading to the models GOCO01S, GOCO02S, EIGEN-6S and DIR3 (see Table 18.1). In

C. Voigt (✉) · H. Denker
Institut für Erdmessung (IfE), Leibniz Universität Hannover,
Schneiderberg 50, 30167 Hannover, Germany
e-mail: voigt@ife.uni-hannover.de

Table 18.1 Cumulative (formal) errors for various GGMs up to $n_{\max} = 200$ in terms of geoid (ζ), gravity anomalies (Δg), and vertical deflections (ξ, η)

Model	Data	ζ (cm)	Δg (mGal)	ξ, η (")
TIM1	GOCE (1/6 yr)	11.4	2.9	0.44
TIM2	GOCE (1/2 yr)	7.7	1.9	0.28
TIM3	GOCE (1yr)	5.9	1.5	0.22
GOCO01S	GOCE (1/6 yr), GRACE	11.0	2.6	0.40
GOCO02S	GOCE (1/2 yr), GRACE, CHAMP, SLR	5.9	1.7	0.25
EIGEN-6S	GOCE (1/2 yr), GRACE, SLR	4.9	1.3	0.20
DIR3	GOCE (1yr), GRACE, SLR	3.2	0.8	0.12
EIGEN-6C	GOCE (1/2 yr), GRACE, SLR, terrestrial	2.7	0.7	0.11
EGM2008	GRACE, terrestrial	7.2	1.4	0.21

addition, the satellite data have been combined with terrestrial and altimetry-derived gravity data in EIGEN-6C up to d/o 1420 (Shako et al. 2013).

In order to ensure best quality GOCE products, various internal and external calibration and validation techniques are of vital importance. Within the framework of the REAL GOCE project, one focus is on the external validation of the GOCE GGMs by high-precision terrestrial gravity field data sets in Germany as well as Europe, including terrestrial gravity data, astrogeodetic vertical deflections, GPS/leveling data, and gravimetric quasigeoid models. Regarding Germany, a unique data set of 341 astrogeodetic vertical deflection observations along two 500 km long profiles (precision 0.1"), as well as about 260,000 gravity points (precision about 0.1 –1.0 mGal) and 954 GPS/leveling stations (precision 1–3 cm) exist (for details see Ihde et al. 2010).

In the following, the results from the evaluation of the GOCE GGMs by terrestrial data are described, emphasizing the progress with respect to the recent GOCE GGM releases. Moreover, results from the combination of the GOCE GGMs with terrestrial data sets are outlined.

18.2 Validation of GOCE Gravity Field Models

The above mentioned GOCE based GGMs are evaluated by terrestrial gravity field data sets in conjunction with EGM2008 (d/o 2159), which is complete to d/o 2159 and contains additional coefficients up to degree 2190 (Pavlis et al. 2012); the GGMs are available, e.g., from the International Centre for Global Earth Models (ICGEM; http://icgem.gfz-potsdam.de), where also corresponding references can be found. In this context, the formal error estimates associated with the GGMs are of interest; Table 18.1 shows the cumulative errors (square roots of the sum of corresponding error degree variances) for selected GGMs up to d/o 200, corresponding to the targeted GOCE resolution of 100 km. The formal errors of the GOCE TIM3 GGM are 6 cm for the geoid, 1.5 mGal for gravity anomalies, and 0.22" for vertical deflections,

with improvements from the first to the third release of about 50 %. The formal errors of the combined GGMs are even smaller (especially DIR3 and EIGEN-6C) with the exception of EGM2008, resulting from the employed calibration and combination procedure.

Regarding the comparison between the terrestrial and GGM data, the different spectral characteristics of both data sets must be considered, i.e., the high-frequency signals, which are not included in the GGMs, but represent a significant portion of the entire spectrum, must be taken into account. For this purpose, two approaches are employed. First, regarding gravity and height anomaly grids, the high-frequency components are filtered out by a spectral (low-pass) window (cosine-taper window centered at a certain degree, here $n_{max} = 200$, with a width of 10°), with the window being applied in the space domain. Second, regarding irregularly distributed GPS/leveling and astrogeodetic vertical deflection data, the high frequency signals above a certain degree (here again $n_{max} = 200$) are modeled by EGM2008 up to degree 2190 and order 2159, while beyond this degree detailed topographic information and the residual terrain model (RTM) approach are utilized (see also Gruber et al. 2011); finally, in order to filter out additional unmodeled high-frequency effects, a spatial Gaussian filter with a width of 9 km (corresponding to d/o 2159) is applied (two-step procedure; see Voigt and Denker 2013).

All GGM and terrestrial quantities were referred to GRS80 and the zero-tide system. Table 18.2 shows the statistics of the differences between selected GGMs and the terrestrial data, consisting of 954 GPS/leveling and 341 vertical deflection stations in Germany, as well as gravity anomalies covering the whole of Europe; note that the anomaly comparisons exclude Greenland, Novaya Zemlya, Turkey, and Africa, where the terrestrial data are known to be weak. Furthermore, the results from the comparison of the German GPS/leveling data and the European gravity anomalies with the GOCE models TIM1 and TIM3 up to d/o 200 are depicted in Fig. 18.1. Taking the GOCE time-wise GGMs as one example, significant improvements are obvious from the first to the third release of GGMs, based on a steadily growing amount

Table 18.2 Standard deviations of the differences between various GGMs up to $n_{max} = 200$ and filtered terrestrial data sets in terms of quasigeoid heights (ζ), gravity anomalies (Δg), and vertical deflection components ($\xi \eta$)

Model	ζ (cm)	Δg (mGal)	ξ (")	η (")
TIM1	15.0	3.02	0.83	0.74
TIM2	6.1	1.97	0.57	0.52
TIM3	5.5	1.68	0.57	0.52
GOCO01S	14.2	2.92	0.80	0.72
GOCO02S	6.2	2.15	0.56	0.53
EIGEN-6S	7.7	2.37	0.58	0.53
DIR3	6.0	1.89	0.59	0.53
EIGEN-6C	4.3	1.44	0.55	0.48
EGM2008	2.8	0.90	0.54	0.44
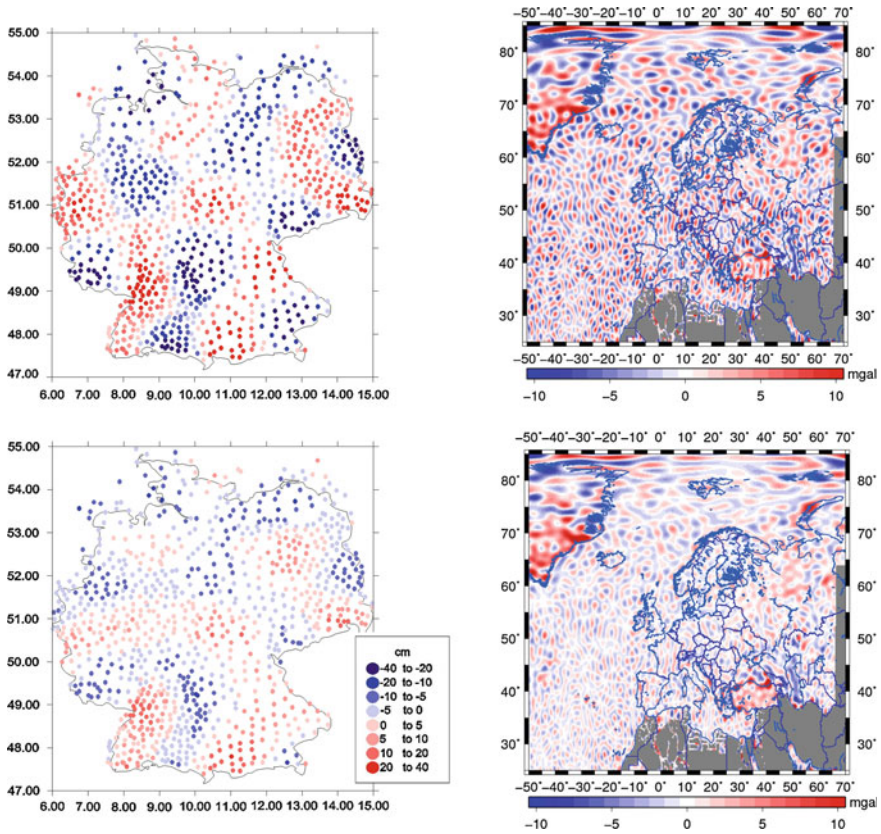
Fig. 18.1 Comparison between the GOCE models TIM1 (*top*) and TIM3 (*bottom*) up to $n_{\max} = 200$ with the filtered GPS/leveling data (*left*) and terrestrial gravity anomalies (*right*)

of GOCE observational data; the standard deviations of the differences between the GPS/leveling, gravity anomaly, and vertical deflection data on the one hand, and the first to third release of the time-wise GOCE GGMs on the other hand, decrease from 15.0 to 5.5 cm, 3.0 to 1.7 mGal, and about 0.80 to 0.55", respectively. The combined satellite models GOCO01S and GOCO02S do not show significant improvements versus the corresponding pure GOCE models TIM1 and TIM2, respectively, as the differences mainly originate from the spectral range recovered from the GOCE data. The improvement of DIR3 over the predecessor model EIGEN-6S is obvious, almost reaching the accuracy level of TIM3. In addition, the GGMs including also altimeter and terrestrial data, such as EIGEN-6C and EGM2008, perform best in the comparisons with all terrestrial data sets, with EGM2008 being clearly superior; however, this is expected to some extent, but also reveals the high quality of the terrestrial gravity anomaly data utilized for the development of these models. Finally, the differences between the different terrestrial data sets and the GOCE GGMs are compatible with

the corresponding formal error estimates, considering that the differences are related to error sources from all involved data sets, to spectral breaks from the augmentation of given GGMs with EGM2008, as well as unmodeled high-frequency effects (see also Voigt and Denker 2013).

18.3 Combination of GOCE and Terrestrial Data

In principle, the satellite gravity field models and the terrestrial gravity field data ideally complement each other, with the satellite data providing accurately the long wavelength gravity field structures, while the terrestrial data sets, with potential weaknesses in the large-scale accuracy and coverage, mainly contribute the short wavelength features. Consequently, also the combination of the GOCE based GGMs with terrestrial gravity and terrain data is of major interest.

For this purpose, the remove-compute-restore (RCR) procedure is employed together with the spectral combination technique and residual terrain model (RTM) reductions, directly corresponding to the European Gravimetric (Quasi) Geoid model EGG2008, which is based on the global model EGM2008 (for further details see Denker 2013). In this context, the spectral weights play an important role, as they allow control of which spherical harmonic degrees are taken from the terrestrial gravity data and which degrees are basically taken over from the global geopotential model. Generally, the spectral weights are determined within the framework of a least-squares adjustment or collocation solution, taking into account the error estimates of the global geopotential model and the terrestrial data, but they may also be defined empirically, e.g., as filter coefficients.

Figure 18.2 (left) shows the spectral weights associated with EGG2008, depending on the error degree variances of a GRACE based geopotential model as well as a 1 mGal correlated noise model for the terrestrial data; in addition, corresponding weights are shown for a CHAMP based model and EGM1996 (used for the computation of EGG1997). However, applying the same procedure to the GOCE GGMs leads to somewhat unrealistic weights, with too much weight given to the terrestrial data, dominating the combination solution (i.e., $w_n > 0.5$) already at degrees 40–75 for the GOCE GGM releases 1–3, respectively, which is due to the poorer precision of the GOCE GGMs at the lower degrees (up to $n \approx 110$), as compared to multi-year GRACE solutions. Therefore, in a first attempt, different weighting schemes (A to E; see Fig. 18.2) were defined empirically based on a cosine taper window.

Table 18.3 shows the results from the comparison of the German GPS/leveling data set with different quasigeoid computations based on the GOCE DIR3 and TIM3 models as well as EGM2008 (used up to $n_{max} = 360$). In addition, the differences between EGG2008 (based on EGM2008) and a corresponding solution based on the TIM3 model with weighting scheme A are depicted in Fig. 18.2 (right). In the GPS/leveling comparisons of the German and other data sets, mostly weighting schemes A and B ($w_n = 0.5$ at degree 120 and 140, respectively) give the best results, where the TIM3 results come close to the corresponding EGM2008 results.
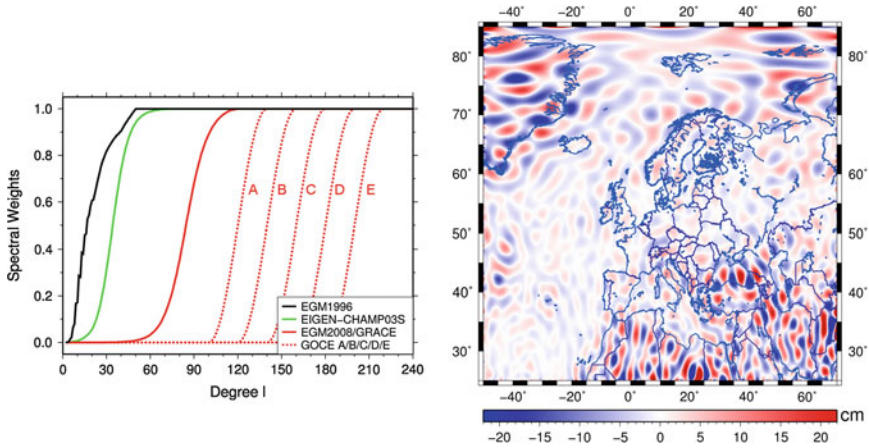
Fig. 18.2 Different weighting schemes for various GGMs (*left*) and differences between the gravimetric quasigeoid model EGG2008 on the basis of EGM2008 and a corresponding solution based on TIM3 and weighting scheme A (*right*)

Table 18.3 Comparison of GPS/leveling data in Germany with EGG2008 on the basis of EGM2008 and corresponding solutions based on the GOCE models DIR3 and TIM3 as well as different weighting schemes. Units are cm

Underlying global geopotential model	RMS	Min	Max
EGM2008	2.7	−6.9	+7.9
DIR3 (A)	3.0	−8.3	+7.9
DIR3 (B)	3.4	−8.6	+9.7
TIM3 (A)	2.8	−7.8	+7.5
TIM3 (B)	3.2	−7.4	+8.6

This indicates that the GOCE mission targets have not yet been fully accomplished, terrestrial gravity data over central Europe (as well as EGM2008) are of high quality, and long wavelength gravity field structures are adequately represented by the latest GOCE GGMs. However, over Greenland, Turkey, and Africa, where the terrestrial gravity data are known to be weak, significant differences show up (see Fig. 18.2), illustrating the impact of GOCE.

18.4 Summary and Conclusions

The validation of the GOCE GGMs by high-precision terrestrial data shows significant improvements from the first to the third release; the agreement between the release 3 GOCE GGMs and terrestrial data up to d/o 200 is about 5.5 cm for height anomalies, 1.7 mGal for gravity anomalies, and 0.55" for vertical deflections, respec-

tively, being fully compatible with the relevant error estimates. Also the combination of GOCE and terrestrial data shows that especially the release 3 GGMs adequately represent the long wavelength gravity field structures, and further improvements can be expected from the next GGM releases.

References

Denker H (2013) Regional gravity field modelling: theory and practical results. In: Xu G (ed) Sciences of geodesy II, Springer, Berlin, pp 185–291

Gruber T, Visser PNAM, Ackermann C, Hosse M (2011) Validation of GOCE gravity field models by means of orbit residuals and geoid comparisons. J Geod 85:845–860

Ihde J, Wilmes H, Müller J, Denker H, Voigt C, Hosse M (2010) Validation of satellite gravity field models by regional terrestrial data sets. In: System earth via geodetic-geophysical space techniques (Advanced Technologies in Earth Sciences), pp 277–296

Pail R, Bruinsma S, Migliaccio F, Förste C, Goiginger H, Schuh WD, Höck E, Reguzzoni M, Brockmann JM, Abrikosov O, Veicherts M, Fecher T, Mayrhofer R, Krasbutter I, Sansò F, Tscherning CC (2011) First GOCE gravity field models derived by three different approaches. J Geod 85:845–860

Pavlis NK, Holmes SA, Kenyon SC, Factor JK (2012) The development and evaluation of the Earth Gravitational Model 2008 (EGM2008). J Geophys Res 117:B04406. doi:10.1029/2011JB008916

Shako R, Förste C, Abrikosov O, Bruinsma S, Marty JC, Lemoine JM, Flechtner F, Neumayer H, Dahle C (2013) EIGEN-6C—a high-resolution global gravity combination model including GOCE data, Chap. 20. In: Observation of the System Earth from Space - CHAMP, GRACE, GOCE and future missions

Voigt C, Denker H (2013) Validation of second-generation GOCE gravity field models by astro-geodetic vertical deflections. IAG Symp. 139 (accepted)

Chapter 19
Height System Unification Based on GOCE Gravity Field Models: Benefits and Challenges

Axel Rülke, Gunter Liebsch, Uwe Schäfer, Uwe Schirmer and Johannes Ihde

Abstract   In addition to the traditional way of realizing height systems based on spirit levelling and local gravity observations methods based on gravity field models and GNSS observations become more important. This contribution validates recent global gravity field models (GGM) with independent GNSS/levelling data in Germany. A European GNSS/levelling data set and a GOCO02S and EGM2008 combined GGM are used to unify the national European height systems. The comparison of the results to the traditional approach results based on the United European Levelling Network (UELN) confirms the high potential of this method although in most cases the satellite only GGMs need to be densified by additional terrestrial observations.

19.1 Introduction

Traditionally, height systems are realized based on spirit levelling in combination with local gravity observations. The global gravity space missions CHAMP, GRACE and GOCE have significantly improved the accuracy of global gravity field models (GGM). Especially the GOCE mission has increased the spatial resolution of the GGMs up to 100 km (half wavelength). In combination with ellipsoidal heights observed by Global Navigation Satellite Systems (GNSS) these models allow an alternative realization of a height system. But the spatial resolution of the satellite based GGMs is limited and need to be improved by terrestrial observations. Especially in widespread countries a gravity field based height reference frame has advantages since nationwide levelling observations are elaborate, expensive and susceptible to systematic error sources.

A. Rülke (✉) · G. Liebsch · U. Schäfer · U. Schirmer · J. Ihde
Bundesamt für Kartographie und Geodäsie, Außenstelle Leipzig, Karl-Rothe-Str. 10-14, 04105 Leipzig, Germany
e-mail: axel.ruelke@bkg.bund.de

In this paper, recent GOCE GGMs are validated with an independent GNSS/levelling data set in Germany. A European GNSS/levelling data set is used to estimate height system offsets between height reference frames in Europe based on GGMs. Finally, the results are compared to the traditional approach based on the United European Levelling Network (UELN).

19.2 Data Sets

The following investigations require two types of data sets, GNSS/levelling data and gravity field models. The German GNSS/levelling data set (D924) consists of 924 points which are evenly distributed with a distance of approx. 30 km. The ellipsoidal heights h are related to the GRS80 ellipsoid, they are specified in the ETRS89/DREF91 reference frame and they are tide-free. The physical heights H are normal heights in the DHHN92 reference frame and refer to the Normaal Amsterdams Peil (NAP) and the mean-tide system.

The European EUVN_DA data set contains more than 1400 points from all over Europe. The ellipsoidal heights are given with respect to GRS80 ellipsoid and are realized in ETRS89 separately by the different countries at epoch 2000.0. Depending on the country the physical heights H are inhomogeneous in terms of its type, its tidal treatment and its geodetic datum (Ihde et al. 2000). Within the UELN the national levelling networks have been combined and homogenized and represent a realization of the European Vertical Reference System (EVRS). Its latest realization is the EVRF2007 (Sacher et al. 2009). This results in normal heights related to NAP and given in the zero-tide system.

Three different approaches have been used to compute GGMs based on GOCE data (Pail et al. 2011): the time-wise approach, the space-wise approach and the direct approach. The time-wise approach is the only approach which abstains from non GOCE a priori information. Therefore, here we concentrate on this approach. Three releases have been published for the time wise approach, based on 3, 6 and 12 months (netto) of observation data, respectively. The GOCO02s GGM is computed as a combination of GRACE, GOCE, CHAMP and satellite laser ranging data (Goiginger et al. 2011). ITG-Grace2010s is the latest model which contains GRACE observations only. It is given up to degree and order (d/o) 180 (Mayer-Gürr et al. 2010). EGM2008 combines satellite data from GRACE, terrestrial gravity data and satellite altimetry to a high resolution model up to d/o 2190 (Pavlis et al. 2012).

For the comparisons and a consistent combination the reference and tidal systems of all data sets need to be homogenized. For this investigation the GRS80 reference system and the zero-tide system have been selected.

19.3 Validation of Global GOCE Gravity Field Models

GNSS/levelling data sets are used to validate GGMs. Figure 19.1 shows the standard deviation of differences between height anomalies synthesized from GGMs and observed by GNSS/levelling at the D924 data set point locations in Germany. The maximum expansion of the spherical harmonic series of the GGMs has been varied between d/o 100 and d/o 250 in steps of d/o 5 (Fig. 19.1, top). For expansions higher than d/o 200 the accuracy is rapidly decreasing which shows the limits of the spatial resolution. In comparison to EGM2008 the GOCE models give slightly better results in the range between d/o 170 and approx. d/o 190. Surprisingly, the time-wise R1 model shows the largest improvements. The limited spatial resolution of the GGMs
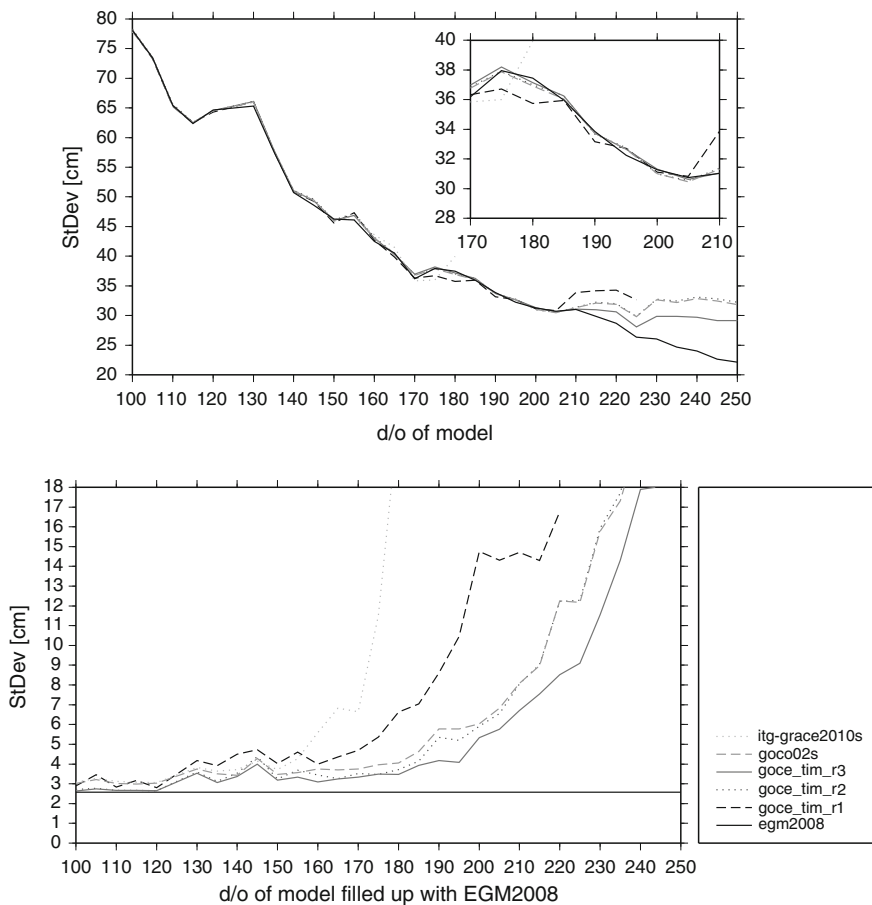
Fig. 19.1 Validation of global gravity field models with 924 observed terrestrial height anomalies in Germany. The spherical harmonic series of the GGM were truncated in steps of d/o 5 starting at d/o 100. *Top* the omission error has not been modelled. *Bottom* the omission error has been modelled by an extension with EGM2008 spherical harmonic coefficients up to d/o 2190

causes an omission error which is approx. 25 cm at d/o 240. For the well-developed areas this is not sufficient for the realization of a height system and thus, the omission error need to be taken into account. Although it is not strictly correct but widely used, the spherical harmonic series of the GGMs have been extended by the corresponding spherical harmonic coefficients of the EGM2008 up to d/o 2190 (Fig. 19.1, bottom). The more recent models based on more observation data and improved analysis methods show clear improvements. The evolution of the time-wise model releases in terms of improved fitting accuracy is clearly visible. While the standard deviation is below 4 cm for the best GOCE models up to d/o 180 it increases considerably at d/o higher than 190.

19.4 Combination of Global and Regional Gravity Field Models by Filtering

A large database of high quality gravimetric observations in Germany and neighbouring countries has been used to compute BKG2011g, a gravimetric geoid for Germany, in a Remove-Compute-Restore approach. In the remove step, the observation data is reduced using the GGM EIGEN-5C up to d/o 360 (Förste et al. 2008). The topography is reduced using the 25 m digital elevation model (DEM) for Germany and a 50 m DEM for the neighbouring countries. In the compute step, a set of point masses is estimated in a least squares adjustment. The point masses are located on a regular grid with a spacing of $2' \times 3'$ (approx. 3.5 km) at a depth of 5 km. In order to get the complete gravity field, the reduced parts are restored in the final step. The accuracy is estimated with 1–2 cm in the lowlands and 3–4 cm in the mountains.

A simple approach to combine existing global and regional gravity field models is based on filtering. A grid of values with a grid size of 5 km by 5 km is synthesized from the global and regional gravity field models, respectively. Assuming a sufficient overlap of the spectral content a low pass filter is applied to the global and a high pass filter to the regional gravity field model. For the combined model both parts are added. Here, a Gaussian filter $G = e^{-2(\pi \sigma f)}$ with $\sigma = b/6$ and filter width b has been used. Different GGMs and the BKG2011g model have been combined varying the filter width b between 100 and 700 km. In order to avoid edge effects, the combined models have been evaluated using 537 points of the D924 GNSS/levelling data set in an area between 7.5°E and 13.5°E and 48.5°N and 53.5°N. The standard deviation of the differences between the model and the GNSS/levelling data set is 2.0 cm for the GOCE time wise R3 based model and a filter width of 420 km. This is a significant improvement compared to the full EGM2008 (2.8 cm) and also to the pure BKG2011g model (2.3 cm). A combination based on the GRACE model ITG-GRACE2010s gives a standard deviation of 2.6 cm with a filter width of 560 km. This shows the improvements from GOCE models in terms of accuracy and spatial resolution. The GOCO02s based combination is slightly worse and results in a standard deviation of 2.5 cm at a filter width of 470 km (Table 19.1). For comparisons, the GOCE time-wise model R3 d/o 190 was extended by the EGM2008 spherical harmonic coefficients

Table 19.1 Standard deviation of differences between height anomalies at bench marks from geoid models and independent GNSS/levelling data

EGM2008	BKG2011g	GOCE TIM R3 d/o 190 + EGM2008	BKG2001g + ITG-GRACE2011s	BKG 2011g + GOCO02s	BKG2011g + GOCE TIM R3
Pure model		SHC combination		Gaussian filter	
2.8 cm	2.3 cm	4.3 cm	4.0 cm/400 km	2.6 cm/400 km	2.1 cm/400 km
			2.6 cm/560 km	2.5 cm/470 km	2.0 cm/420 km

The combinations have been computed by combined spherical harmonic coefficients series (SHC) or by Gaussian filter with filter width of 400 km and an individual optimal filter width

up to d/o 2190. A standard deviation of 4.3 cm clearly indicates the errors of this simple extension of spherical harmonic coefficients from different sources caused by the inconsistency of the method.

19.5   Unification of Height Systems in Europe Based on Gravity Field Models

For the unification of national height systems in Europe height system offsets from GNSS/levelling data $(H - h)$ related to a common geoid model are estimated. The used quasigeoid is a merged model from GOCO02s d/o 200 extended by EGM2008 spherical harmonic coefficients up to d/o 2190. The estimated offsets are displayed in Fig. 19.2. In parentheses the values obtained from the EVRF2007 compared to the national UELN heights are given (Sacher et al. 2009). For comparison purposes, the value for Germany has been set to 39 cm and all other values are given relative to it. The comparison between both methods shows a diverse picture: There is a good agreement between both methods in Eastern Europe, but also in France and Spain. Larger differences up to 10 cm occur in Scandinavia, although the relative differences between the Scandinavian countries fit well. The differences are related to uncertainties within both methods: On the one hand, systematic errors in the European levelling network, especially poor connection lines across national borders (e.g. between Central Europe and Scandinavia) might limit the accuracy of the EVRF2007 values. On the other hand, possible errors in the high frequency part of EGM2008 (e.g. in the Alps) and an imperfect combination of global and regional gravity field models may impact the gravity field based offsets.

19.6   Summary

The recent geodetic gravity field missions CHAMP, GRACE and GOCE have significantly extended the possibilities of the realization of height systems based on gravity field. Especially for large countries, such as the United States, Canada or Australia, or continental height systems, such as the EVRS, time and effort as well
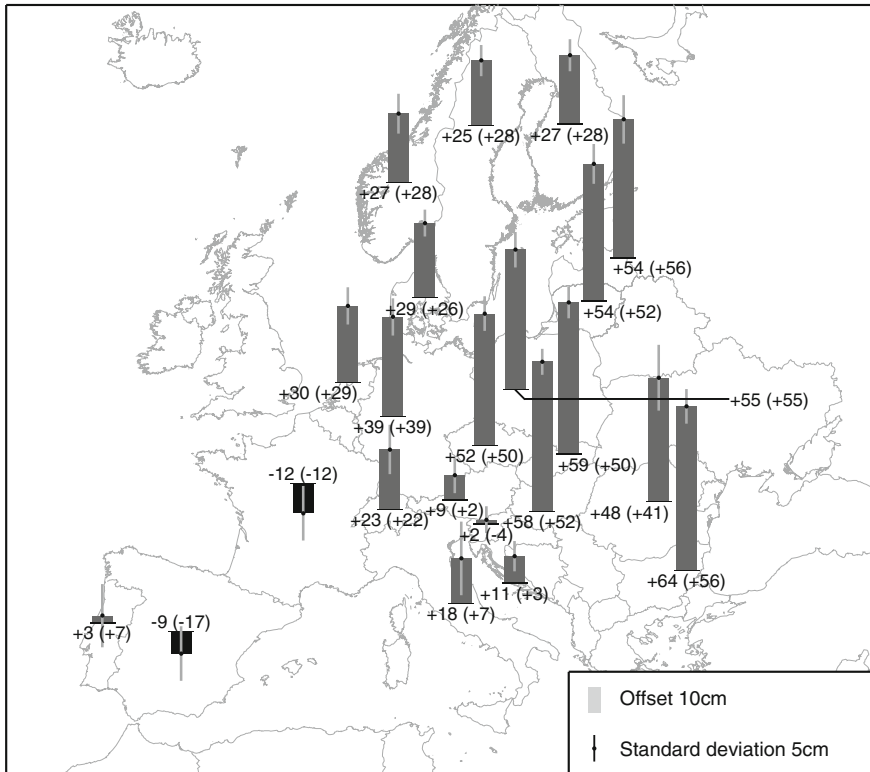
Fig. 19.2 Estimated height offsets [cm] of national height systems in Europe with respect to GOCO02s gravity field model. The offsets obtained from the EVRF2007 analyses are given in parentheses (Sacher et al. 2009). For comparison, the value for Germany was set to 39 cm

as the influence of systematic error sources from levelling observations can be significantly reduced. In the most cases, the satellite gravity field models need further densification by terrestrial observations.

Our comparisons show that GOCE observations have significantly improved the accuracy of global gravity field models between d/o 150 and d/o 190, corresponding to a spatial resolution of approx. 135–105 km. In combination with GNSS observations these models provide an excellent basis for the realization of consistent height systems. In order to improve the limited spatial resolution terrestrial observations are needed. A widely used approach is to merge spherical harmonic coefficient series of different models. It could clearly be shown that in this case the model improvements from GOCE perish due to the inconsistency of the method. A more consistent method is a real combination of gravity field models. Based on the existing gravimetric model of Germany BKG2011g and the GOCE time wise R3 model a combination using Gaussian filters is introduced. Although it is a very simple approach, the resulting model shows a good performance in comparison to observed GNSS/levelling data

in Germany. The computed standard deviation of 2.0 cm is better than EGM2008 and also better than the pure BKG2011g model. The independency of these models allows the investigation of systematic error sources in GNSS/levelling data for the first time.

A combined model consisting of GOCO02s and EGM2008 and national observed GNSS/levelling heights are used to estimate height system offsets for European national height systems. This method is independent of the main drawbacks of levelling networks: the unpropitious error propagation and the limited number of connection lines between national levelling networks. There is a good agreement between these estimated offsets and the height system offsets computed within the EVRF2007 for many countries relative to Germany. Nevertheless, differences between both methods up to 10 cm occur.

References

Förste C, Flechtner F, Schmidt R, Stubenvoll R, Rothacher M, Kusche J, Neumayer K-H, Biancale R, Lemoine J-M, Barthelmes F, Bruinsma J, Koenig R, Meyer U (2008) EIGEN-GL05C—A new global combined high-resolution GRACE-based gravity field model of the GFZ-GRGS cooperation. Geophys Res Abs 10, EGU2008-A-06944

Goiginger H, Hoeck E, Rieser D, Mayer-Guerr T, Maier A, Krauss S, Pail R, Fecher T, Gruber T, Brockmann J, Krasbutter I, Schuh W-D, Jaeggi A, Prange L, Hausleitner WOBO, Kusche J (2011) The combined satellite-only global gravity field model GOCO02S. Geophys Res Abs 13, EGU2011-A-10571

Ihde J, Ádám J, Gurtner W, Harsson BG, Sacher M, Schlüter W, Wöppelman G (2000) The EUVN height solution—report of the EUVN working group. In: Proceedings of the EUREF2000 symposium, Tromsø, Norway, 22–24 June. Veröffentlichungen der Bayerischen Kommission für die Internationale Erdmessung der BAW 61:132–145

Mayer-Gürr T, Kurtenbach E, Eicker A (2010) ITG-Grace2010. http://www.igg.uni-bonn.de/apmg/index.php?id=itg-grace2010

Pail R, Bruinsma S, Migliaccio F, Förste C, Goiginger H, Schuh W-D, Höck E, Reguzzoni M, Brockmann J, Abrikosov O, Veicherts M, Fecher T, Mayrhofer R, Krasbutter I, Sansó F, Tscherning C (2011) First GOCE gravity field models derived by three different approaches. J Geod 85:819–843. doi:10.1007/s00190-011-0467-x

Pavlis NK, Holmes SA, Kenyon SC, Factor JK (2012) The development and evaluation of the earth gravitational model 2008 (EGM2008). J Geophys Res 117(B4):B04406. doi:10.1029/2011JB008916

Sacher M, Ihde J, Liebsch G, Mäkinen J (2009) EVRF2007 as realization of the European Vertical Reference System. Bollettino di Geodesia e Scienze Affini 68(1):35–50

Chapter 20
EIGEN-6C: A High-Resolution Global Gravity Combination Model Including GOCE Data

Richard Shako, Christoph Förste, Oleh Abrikosov, Sean Bruinsma, Jean-Charles Marty, Jean-Michel Lemoine, Frank Flechtner, Hans Neumayer and Christoph Dahle

Abstract GOCE satellite gradiometry data were combined with data from the satellite missions GRACE and LAGEOS and with surface gravity data. The resulting high-resolution model, EIGEN-6C, reproduces mean seasonal variations and drifts to spherical harmonic degree and order (d/o) 50 whereas the mean spherical harmonic coefficients are estimated to d/o 1420. The model is based on satellite data up to d/o 240, and determined with surface data only above degree 160. The new GOCE data allowed the combination with surface data at a much higher degree (160) than was formerly done (70 or less), thereby avoiding the propagation of errors in the surface data over South America and the Himalayas in particular into the model.

20.1 Introduction

High-resolution global gravity field models play a fundamental role in geodesy and Earth sciences, ranging from practical purposes like precise orbit determination to scientific applications like investigations of the density structure of the Earth's interior. Such gravity field models are constructed by combining satellite and surface gravity data (e.g. Förste et al. 2008a; Pavlis et al. 2012). Each data type is sensitive to a specific spectral range of the gravity field, i.e. it contains usable signal in a certain bandwidth. The inclusion of the GOCE mission data allows a homogeneous satellite-based mapping of the gravity field to approximately degree and order

R. Shako · C. Förste (✉) · O. Abrikosov · F. Flechtner · H. Neumayer · C. Dahle
GFZ German Research Centre for Geosciences, Dept 1 "Geodesy and Remote Sensing",
Telegrafenberg A17, 14473 Potsdam, Germany
e-mail: foer@gfz-potsdam.de

S. Bruinsma · J.-C. Marty · J.-M. Lemoine
Groupe de Recherche de Géodésie Spatiale (GRGS), 18 Avenue Edouard Belin, 31401
Toulouse, France
e-mail: sean.bruinsma@cnes.fr

(d/o) 200, corresponding to a model resolution of 100 km half-wavelength (e.g. Pail et al. 2011). The shorter wavelengths must be inferred from surface gravity data. Here we report on the combined model EIGEN-6C (EIGEN = European Improved Gravity model of the Earth by New techniques) which is the first combined global gravity field model using GOCE data. This model is complete to degree and order 1420 (corresponding to a model resolution of 14 km half-wavelength) and was jointly elaborated by GFZ Potsdam and CNES/GRGS Toulouse. This paper gives a short overview on the composition and main characteristics of this model.

20.2 Used Data and Combination Strategy

The global combined gravity field model EIGEN-6C was constructed using the following satellite and terrestrial data:

(a) LAGEOS-1/2 Satellite Laser Ranging data and GRACE GPS Satellite-to-Satellite Tracking and K-band range-rate data from January 2003 to June 2009 (6.5 years). The LAGEOS and GRACE data processing was performed within the GRGS RL02 GRACE processing (Bruinsma et al. 2010b). The LAGEOS/GRACE normal equations contain 5 time variable parameters for each spherical harmonic coefficient up to d/o 50:

$$\bar{C}_{nm}(t) = \bar{C}_{nm}^0 \; + \; \dot{\bar{C}}_{nm} \; \Delta t + \bar{C}_{nm}^A \; \sin \; \frac{2\pi}{T_A}\Delta t \; + \; \bar{S}_{nm}^A \; \cos \; \frac{2\pi}{T_A}\Delta t$$
$$+ \; \bar{C}_{nm}^{2A} \; \sin \; \frac{2\pi}{T_{2A}}\Delta t \; + \; \bar{S}_{nm}^{2A} \; \cos \; \frac{2\pi}{T_{2A}}\Delta t$$
$$\text{with} \quad \Delta t \; = \; t \; - \; t_{2005.0} \tag{20.1}$$

These coefficients correspond to the mean (superscript 0), drift (dot), sine and cosine annual terms (A = annual) and sine and cosine semi-annual (2A = semi-annual) terms, respectively. A gravity field model including these time variable parameters represents the mean temporal variations of the Earth's gravity field very well, as can be gleaned from Fig. 5 in Bruinsma et al. (2010b). Taking the mean temporal variations in the gravity field into account leads to more accurate orbits in Precise Orbit Determination (POD).

(b) GOCE satellite gravity gradient (SGG) data: 6.7 months of SGG data from the time span November 2009 to June 2010. We computed individual normal equations of maximum d/o 240 for each component (T_{xx}, T_{yy} and T_{zz}) by means of the GOCE direct approach (Pail et al. 2011). During the generation of the observation equations we applied a 100–8 s band-pass filter for all three SGG components, which means the SGG signal is filtered-out below degree ∼ 50.

(c) We took the DTU10 global gravity anomaly data set (Andersen et al. 2009; Andersen 2010) as surface gravity observations. This was obtained from altimetry over the oceans and EGM2008 over land. From this gravity anomaly data set
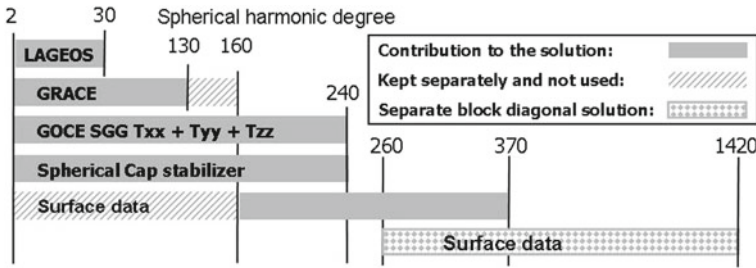
Fig. 20.1 Combination scheme of EIGEN-6C

we computed a full normal equation of maximum d/o 370 for combination with the satellite data and an additional block diagonal solution up to d/o 1420.

The combination of the satellite and surface data has been done by accumulating the normal equations of the individual satellite-based contributions and the DTU10 surface data. The normal matrix accumulation was performed according to the combination scheme as shown in Fig. 20.1, where the GRACE-based contribution between degrees 130 and 160 and the surface part up to degree 160 was kept separate during the accumulation. This means that only the green parts of the normal equations in Fig. 20.1 contribute to the final solution from the full normal equation up to d/o 370. In principle, this band-limited combination method is an enhancement of the degree-dependent normal equation combination technique used for EGM96 (Lemoine et al. 1998), where the spherical harmonic coefficients up to degree/order 5 were adjusted separately for the surface gravity. To avoid any imbalance in the satellite data due to the GOCE polar gap, the GOCE-SGG normal equation was stabilized by the Spherical Cap Regularization (Metzler Band and Pail 2005) using an internal GFZ combined gravity field model called EIGEN-52C in the polar gaps. EIGEN-52C was computed with the same LAGEOS/GRACE and DTU10 data as used for EIGEN-6C. Lastly, the coefficients obtained from the solution of the accumulated normal equation were supplemented by those of the block diagonal surface solution to obtain the final model up to d/o 1420. In this context Fig. 20.1 shows an overlapping of the full and the block-diagonal normal equations between degrees 260 and 370. This symbolizes that the spherical harmonic coefficients of EIGEN-6C in this degree range are arithmetic mean values of the coefficients obtained from the full and the block diagonal normal equations. This kind of overlapping has been made to get a smooth transition between the full and block diagonal contributions.

From the EIGEN-6C satellite contribution a satellite-only model was computed too, This model called EIGEN-6S is complete up to d/o 240.
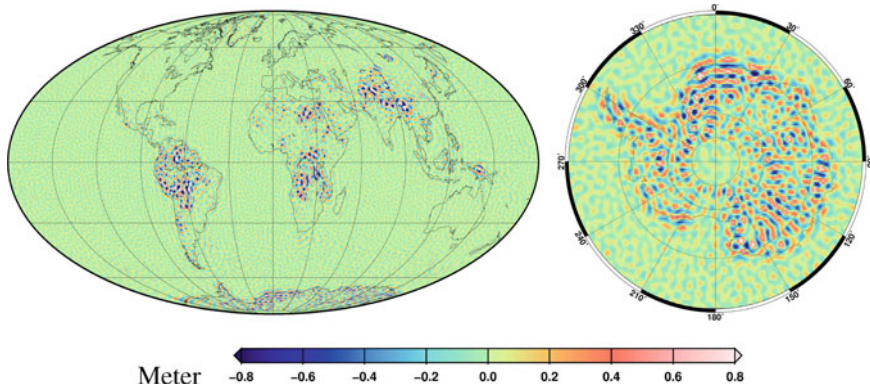
Fig. 20.2 Geoid height differences between EIGEN-6C and EGM2008 up to d/o 1400 in a global view (*left*) and for Antarctica (*right*)

20.3 Main Characteristics and Evaluation of EIGEN-6C

In Fig. 20.2 geoid height differences between EIGEN-6C and EGM2008 up to d/o 1400 are shown in a global view and for Antarctica. In some regions of the globe, he difference patterns indicate impressively where the global gravity field.

Modelling is enhanced by the novel GOCE data (e.g. in South America, the Himalayas, Central Africa or Antarctica). Furthermore, the GOCE polar gap can be clearly seen in Antarctica.

Figure 20.3 shows the spectral behaviour of EIGEN-6C in comparison to EGM2008, EIGEN-6S, GIF48 (Ries et al. 2011) and the satellite-only model GOCO02S (Pail et al. 2010; Goiginger 2011). The "bump" in the green curve between degrees 100 and 200 indicates the new information from GOCE compared to EGM2008 and GIF48, which are based on GRACE plus terrestrial data only. GIF48 shows a shorter bump in the difference to EGM2008, which is probably caused by the larger amount of included GRACE data with respect to EGM2008. The comparison with EIGEN-6S and GOCO02S indicates the onset of the terrestrial data at degree 160 according to the combination scheme in Fig. 20.1.

An independent comparison with external data can be made using geoid heights determined point-wise by GPS positioning and leveling ("GPS/Leveling"). Table 20.1 shows the results for EIGEN-6C in comparison to several other recent gravity field models using GPS/leveling points of the USA (Milbert 1998), Canada (M. Véronneau, Natural Resources Canada, personal communication 2003), Germany (Ihde et al. 2002), Europe (Ihde, personal communication, 2008) and Australia (G. Johnston, Geoscience Australia and W. Featherstone, Curtin University of Technology, personal communication 2007). For this comparison, height anomalies were calculated from the spherical harmonic coefficient data sets and reduced to geoid heights (c.f. Rapp 1997). The topographic correction was done using the DTM2006.0 model, which is available in spherical harmonic coefficients (Pavlis et al. 2007). The coeffi-
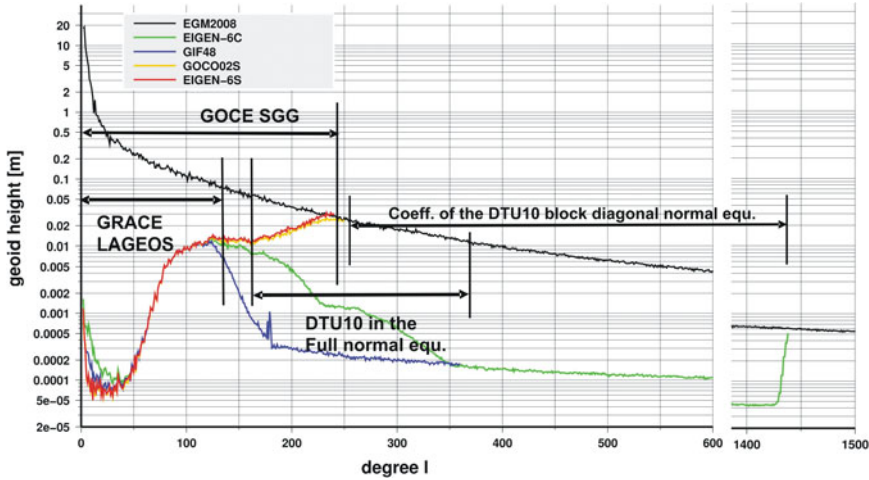
Fig. 20.3 Difference degree amplitudes in terms of geoid height for EIGEN-6C, GIF48, GOCO02S and EIGEN-6S with respect to EGM2008. The signal degree amplitudes of EGM2008 (*black*) are given for comparison

Table 20.1 GPS/Leveling fit: Root mean square (cm) about mean of GPS-Levelling minus model-derived geoid heights (number of points in brackets), for maximum d/o 360

GPS/Leveling data set	GGM03C	EIGEN-GL04C	EIGEN-5C	EIGEN-51C	EIGEN-6C	EGM2008
Europe (1234)	33.3	33.6	30.2	28.8	27.5	26.9
Germany (675)	18.8	17.8	15.2	14.8	15.4	14.2
Canada (1930)	27.8	25.3	25.1	24.4	22.9	22.9
USA (6169)	34.5	33.9	33.9	33.3	31.6	31.8
Australia (201)	25.8	24.4	24.3	23.3	23.6	23.6

cients were used only to d/o 360 in this comparison. Except for Germany, EIGEN-6C fits better in comparison to EIGEN-GL04C (Förste et al. 2008a), EIGEN-5C (Förste et al. 2008b), EIGEN-51C (Bruinsma et al. 2010a) and GGM03C (Tapley et al. 2007). This indicates that EIGEN-6C is of almost the same performance as EGM2008 for the short wavelengths.

One measure of a gravity field model's long-to-medium wavelength accuracy is satellite orbit fits. For our evaluation of EIGEN-6C we computed GOCE dynamic orbits using several recent gravity field models (See Table 20.2). As observations we used kinematic orbit positions from the SST_PSO_2 GOCE Level-2 end user product. We chose 60 arcs (arc length = 1.25 days) from 1st November through 31st December 2009 and carried out the orbit computations for three different maximum d/o (c.f. Table 20.2). The following empirical accelerations were estimated in addition to the state vector at epoch:

Table 20.2 GOCE orbit fit residuals (cm) after a dynamic orbit computation based on kinematic orbit positions as derived from for 60 arcs of 1.25 day arc length

Gravity field model/maximum d/o	120×120	150×150	180×180
EGM2008	**4.0**	**2.9**	**2.8**
GGM03C	**3.6**	**2.4**	**2.3**
EIGEN-5C	**3.4**	**2.3**	**2.2**
EIGEN-51C	**3.2**	**2.0**	**1.8**
ITG-GRACE2010S (Mayer-Gürr et al. 2010)	**3.3**	**1.8**	**1.7**
GO_CONS_GCF_2_DIR	**3.9**	**2.6**	**2.4**
GOCO02S	**3.3**	**1.8**	**1.6**
EIGEN-6C (at epoch 01.12.2009)	**3.2**	**1.6**	**1.5**

- Two cross track, radial and along track biases per orbit revolution, and
- One cross track and one radial accelerometer scale factor per arc. The along track scale factor was fixed to 1.0 since this component is kept drag-free.

Each number in Table 20.2 is the mean of the 60 root mean square values of the individual orbit fit residuals. The results in this table can be summarized as follows:

- The maximum d/o 180×180 gives the best results for all tested models. This means GOCE orbits are sensitive at least up to this d/o.
- ITG-GRACE2010S gives better results than the GOCE-only model GO_CONS_ GCF_2_DIR. This means GOCE-only models are not as good as GRACE models for GOCE orbit computation.
- The best GOCE orbit fit results are obtained with combined GRACE and GOCE models (both GOCO2S and EIGEN-6C), but EIGEN-6C shows slightly better results which is obviously due to its time variable parameters.

20.4 Summary

EIGEN-6C is the first high resolution global combined gravity field model including GOCE data. Our GPS/Leveling comparisons indicate that this model has almost the same performance as EGM2008 in the short wavelengths. In our GOCE orbit adjustment computations EIGEN-6C fits best in comparison to other recent gravity field models.

EIGEN-6C and its associated satellite-only model EIGEN-6S are available for download at http://icgem.gfz-potsdam.de/ICGEM.

References

Andersen OB, Knudsen P, Berry P (2009) DNSC08 mean sea surface and mean dynamic topography models. J Geophys Res 114(c11001):12. doi:10.1029/2008JC005179

Andersen OB (2010) The DTU10 Gravity field and Mean sea surface (2010), Second international symposium of the gravity field of the Earth (IGFS2). Fairbanks, Alaska

Bruinsma SL, Marty JC, Balmino G, Biancale R, Förste C, Abrikosov O, Neumayer H (2010a) GOCE Gravity Field Recovery by Means of the Direct Numerical Method, presented at the ESA living planet symposium, 27th June–2nd July 2010, Bergen, Norway. See also: earth.esa.int/GOCE

Bruinsma SL, Lemoine JM, Biancale R, Vales N (2010b) CNES/GRGS 10-day gravity field models (release 2) and their evaluation. Adv Space Res 45:587–601. doi:10.1016/j.asr.2009.10.012

Förste C, Schmidt R, Stubenvoll R, Flechtner F, Meyer U, König R, Neumayer H, Biancale R, Lemoine JM, Bruinsma S, Loyer S, Barthelmes F, Esselborn S (2008a) The GeoForschungsZentrum Potsdam/Groupe de Recherche de Gèodésie Spatiale satellite-only and combined gravity field models: EIGEN-GL04S1 and EIGEN-GL04C. J Geodesy 82:331–346. doi:10.1007/s00190-007-0183-8

Förste C, Flechtner F, Schmidt R, Stubenvoll R, Rothacher M, Kusche J, Neumayer H, Biancale R, Lemoine J-M, Barthelmes F, Bruinsma S, Koenig R and Meyer U (2008b) EIGEN-GL05C—A new global combined high-resolution GRACE-based gravity field model of the GFZ-GRGS cooperation. Geophys Res Abstr 10:EGU2008-A-03426

Goiginger H, Hoeck E, Rieser D et al (2011) The combined satellite-only global gravity field model GOCO02S. Geophys Res Abstr 13: EGU2011-10571

Ihde J, Adam J, Gurtner W, Harsson BG, Sacher M, Schlüter W, Wöppelmann G (2002) The height solution of the European Vertical Reference Network (EUVN). Mitteilungen des BKG, Bd. 25, EUREF Publication No. 11/I, Frankfurt a. M., pp 53–79

Mayer-Gürr T, Kurtenbach E, Eicker A (2010) ITG-Grace2010 gravity field model. http://www.igg.uni-bonn.de/apmg/index.php?id=itg-grace2010

Lemoine FG, Kenyon SC, Factor JK et al (1998) The development of the joint NASA GSFC and the National Imagery and Mapping Agency (NIMA) geopotential model EGM96. NASA Technical Paper NASA/TP-1998-206861, Goddard Space Flight Center, Greenbelt

Metzler B, Pail R (2005) GOCE data processing: The spherical cap regularization approach. Stud Geophys Geod 49:441–462. doi:10.1007/s11200-005-0021-5

Milbert DG (1998) Documentation for the GPS Benchmark Data Set of 23-July-1998. IGeS Int Geoid Ser Bull 8:29–42

Pail R, Goiginger H, Schuh W-D, Höck E, Brockmann JM, Fecher T, Gruber T, Mayer-Gürr T, Kusche J, Jäggi A, Rieser D (2010) Combined satellite gravity field model GOCO01S derived from GOCE and GRACE. Geophys Res Lett 37:L20314. doi:10.1029/2010GL044906

Pail R, Bruinsma S, Migliaccio F, Förste C et al (2011) First GOCE gravity field models derived by three different approaches. J Geodesy 85(11):819–843. doi:10.1007/s00190-011-0467-x

Pavlis NK, Factor JK, Holmes SA (2007) Terrain-related gravimetric quantities computed for the next EGM. In: Proceedings of the 1st international symposium of the international gravity field service "Gravity field of the Earth" (Istanbul 2006), Harita Dergisi, year 73, special issue 18, pp 318–323, General Command of Mapping, Ankara/Turkey, ISSN 1300–5790

Pavlis NK, Holmes SA, Kenyon SC, Factor JK (2012) The development and evaluation of the earth gravitational model 2008 (EGM2008). J Geophys Res 117:B04406. doi:10.1029/2011JB008916

Rapp RH (1997) Use of potential coefficient models for geoid undulation determinations using a spherical harmonic representation of the height anomaly/geoid undulation difference. J Geod 71:282–289

Ries JC, Bettadpur S, Poole S, Richter T (2011) Mean background gravity fields for GRACE processing, GRACE science team meeting, Austin, TX, 8–10 August 2011

Tapley B, Ries J, Bettadpur S, Chambers D, Cheng M, Condi F, Poole S (2007) The GGM03 mean earth gravity model from GRACE. Eos Trans AGU 88(52), Fall Meet. Suppl., Abstract G42A–03

Part III
Future Missions

Chapter 21
Future Gravity Field Satellite Missions

Tilo Reubelt, Nico Sneeuw, Siavash Iran Pour, Marc Hirth, Walter Fichter, Jürgen Müller, Phillip Brieden, Frank Flechtner, Jean- Claude Raimondo, Jürgen Kusche, Basem Elsaka, Thomas Gruber, Roland Pail, Michael Murböck, Bernhard Doll, Rolf Sand, Xinxing Wang, Volker Klein, Matthias Lezius, Karsten Danzmann, Gerhard Heinzel, Benjamin Sheard, Ernst Rasel, Michael Gilowski, Christian Schubert, Wolfgang Schäfer, Andreas Rathke, Hansjörg Dittus and Ivanka Pelivan

---

T. Reubelt (✉) · N. Sneeuw · S. Iran Pour
Institute of Geodesy, University of Stuttgart, Geschwister-Scholl-Straße 24D,
70174 Stuttgart, Germany
e-mail: reubelt@gis.uni-stuttgart.de

M. Hirth · W. Fichter
Institute of Flight Mechanics and Control, University of Stuttgart, Pfaffenwaldring 7a,
70569 Stuttgart, Germany

J.Müller · P. Brieden
Institute of Geodesy, Leibniz Universität Hannover, Schneiderberg 50, 30167 Hannover, Germany

F. Flechtner · J. C. Raimondo
German Research Centre for Geosciences, Helmholtz Centre Potsdam, Telegrafenberg,
14473 Potsdam, Germany

J. Kusche · B. Elsaka
Institute of Geodesy and Geoinformation, Rheinische Friedrich-Wilhelms-Universität Bonn,
Nussallee 1, 53115 Bonn, Germany

T. Gruber · M. Murböck
Institute for Astronomical and Physical Geodesy, Technical University of Munich, Arcisstraße 21,
80333 Munich, Germany

R. Pail
Institut für Astronomische und Physikalische Geodäsie, Technische Universität München,
80290 München, Germany

B. Doll · X. Wang · R. Sand
SpaceTech GmbH, Seelbachstraße 21, 88090 Immenstaad, Germany

V. Klein
Kayser-Threde GmbH, Wolfratshauser Straße 48, 81379 Munich, Germany

M. Lezius
Menlo Systems GmbH, Am Klopferspitz 19, 82152 Martinsried, Germany

K. Danzmann · B. Sheard · G. Heinzel
Albert-Einstein-Institut, Max Planck Institut für Gravitationsphysik, Callinstraße 38,
30167 Hannover, Germany

21.1 Introduction

21.1.1 Historical Background

The project "*Future Gravity Field Satellite Missions*" (FGM) was a logical consequence of two previous phases in Theme 2 "*Observation of the System Earth from Space*" in the BMBF/DFG (Federal Ministry of Education and Research/German Research Foundation) Research and Development Programme GEOTECHNOLOGIEN. In these two phases several projects related to the space gravimetry missions CHAMP (Challenging Minisatellite Payload, Reigber et al. 2002), GRACE (Gravity Recovery and Climate Experiment, Tapley et al. 2004) and GOCE (Gravity field and steady-state Ocean Circulation Explorer, ESA 1999) were funded, dealing with high-performance data processing, sensor analysis, improvement of algorithms, system calibration, validation and related technological issues. During these years an enormous pool of expertise was built up. The GEOTECHNOLOGIEN programme, in short, enabled science groups in Germany to play a prominent role in the international spaceborne gravimetric community.

The second phase of Theme 2 ended in August 2008, giving rise to the risk of dissipation of the aforementioned expertise. At the same time, due to technical reasons, the launch of GOCE was delayed until September 2008. Moreover, NASA (National Aeronautics and Space Administration) approved a GRACE mission extension for several more years. The critical situation arose that the investments made within two phases of Theme 2 would dissipate before the scientific benefits could be harvested.

The GEOTECHNOLOGIEN Bureau had acknowledged this dilemma and reacted by soliciting for three projects in the area of spaceborne gravimetry as a follow-up to Theme 2:

1. Consistent reprocessing of CHAMP-GRACE products
2. Analysis of real GOCE data
3. Future mission concepts

The first two projects clearly addressed the dilemma sketched above. The third one was needed to ensure and enhance the strong scientific and technological German lead. To that end the German key players from academic and industry communities

E. Rasel · C. Schubert · M. Gilowski
Institute for Quantum Optics, Leibniz Universität Hannover, Welfengarten 1,
30167 Hannover, Germany

W. Schäfer
TimeTech GmbH, Curiestraße 2, 70563 Stuttgart, Germany

A. Rathke
EADS Astrium GmbH, Claude-Dornier-Straße, 88090 Immenstaad, Germany

H. Dittus · I. Pelivan
Institute of Space Systems, National Aeronautics and Space Research Centre,
Robert-Hooke-Straße 7, 28359 Bremen, Germany
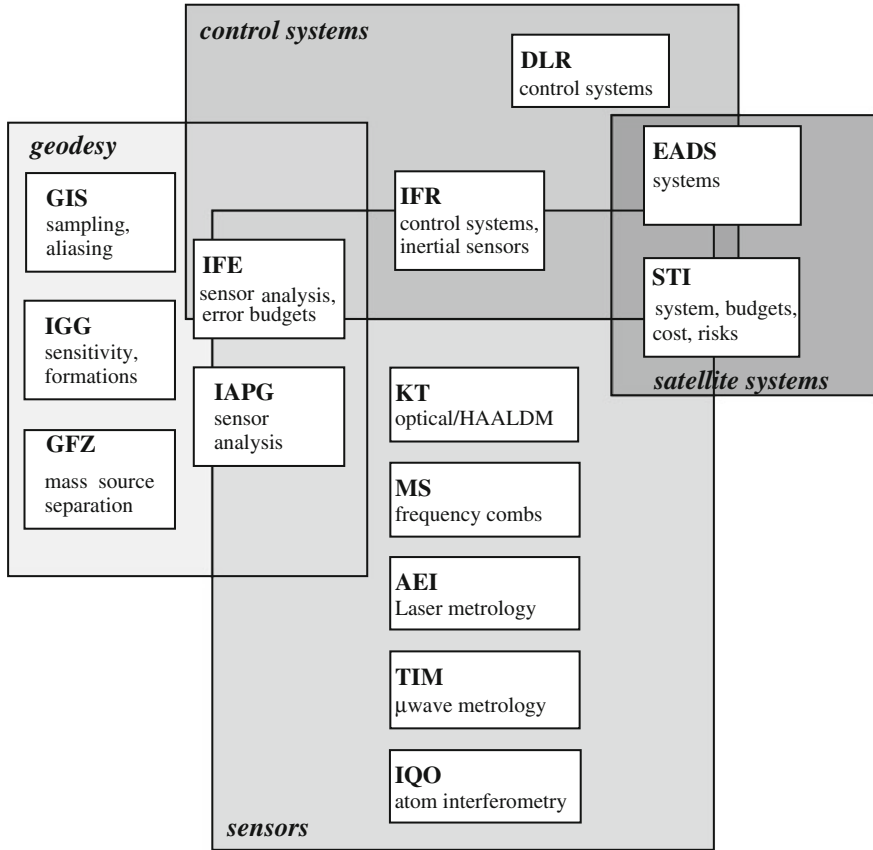
Fig. 21.1 Composition of the project team and project goals; the project partners are: Institute for Geodesy, University of Stuttgart (GIS), Institute of Geodesy and Geoinformation, Rheinische Friedrich-Wilhelms-Universität Bonn (IGG), German Research Centre for Geosciences, Helmholtz Centre Potsdam (GFZ), Institute of Geodesy, Leibniz Universität Hannover (IFE), Institute for Astronomical and Physical Geodesy, Technical University of Munich (IAPG), Institute of Flight Mechanics and Control, University of Stuttgart (IFR), Institute of Space Systems, National Aeronautics and Space Research Centre (DLR), Kayser-Threde GmbH, Munich (KT), Menlo Systems GmbH, Martinsried (MS), Albert-Einstein-Institut, Hannover (AEI), TimeTech GmbH, Stuttgart (TIM), Institute for Quantum Optics, Leibniz Universität Hannover (IQO), Astrium GmbH, Immenstaad (EADS), SpaceTech GmbH, Immenstaad (STI)

(Fig. 21.1) had put forward a project proposal which aimed at developing technological concepts for the next generation of gravity field satellite missions.

The current contribution reports on the main findings of this project. It details the methodology behind the simulation and analysis tools used in the project, assesses the available metrology for future gravity missions and, moreover, highlights the mission selection process from an initially broad pool of potential mission scenarios to a small selection of thoroughly designed missions.

21.1.2 Objectives

The overarching goal of this project is to come to a roadmap for future gravimetric satellites in the post-GRACE and post-GOCE era. Most focus will be on the mid-term future. That is to say, the project aims to arrive at a description of feasible mission scenarios that may in due time serve as a response to a call-for-missions from space agencies. To put it more directly: 3 year after project kick-off we would be able to propose a gravimetric satellite mission to, e.g., the European Space Agency (ESA).

The word feasible in the previous paragraph denotes that the proposed mission scenarios will not only be able to meet the geoscientific requirements, which will be corroborated through extensive closed-loop simulations, but will also be realistic from the perspective of technological readiness and from the perspective of system engineering and cost efficiency. For that reason the project team was composed of experts with diverse backgrounds from geodesy, from metrology groups and from system engineering.

Drawing on experience from GRACE data analysis (e.g. Schrama et al. 2007) the scientific challenges were already identified at the outset of the project. Any future mission should focus on both higher precision and higher resolution in space and time. Relative to the current generation of missions, the FGM project set itself the ambitious goal to design future missions with a higher spatial resolution (below 100 km), a higher time resolution (e.g. weekly or better), an improved sensitivity (e.g. 100 times better than GRACE), and a longer mission duration (e.g. 10 years and longer).

This goal mandates (1) the reduction of the current level of aliasing of high frequency phenomena, in particular tides, into the gravity time series, (2) the elimination of systematic distortions, caused by the peculiar non-isotropic sensitivity of a single pair low-low SST, and (3) the improvement of the separability of the observed geophysical signals. The latter challenge is to be met by improved geophysical background modeling.

Tackling the challenges of aliasing and the systematic distortions, on the other hand, are at the core of this project. Improved sensor accuracy alone, e.g. by replacing a GRACE-type radio link by laser-based metrology, does not necessarily lead to an improved gravity field recovery if the problem of aliasing is not addressed. A delicate mixture of improved sensor technology, design of relative orbits, constellations of missions and control system needs to be balanced to design optimal missions (Sect. 21.1.3). This task is only feasible with the appropriate analysis and simulation tools, which are described in the methodology Sect. 21.2.

Potential sensor technology, mostly laser based, is detailed in Sect. 21.3 after mission requirements and technical constraints are clarified. Moreover, Sect. 21.3 elucidates the selection process from a vast quantity of initial mission scenarios towards the 2 final scenarios. The analysis of the final scenarios is then concluded in Sect. 21.4. Moreover, the final scenarios are reviewed from a system engineering viewpoint, leading to alternative mission options.

21.1.3 Technical Challenges and Constraints

Within the FGM study different scenarios have been investigated which should offer improved spatial and temporal resolution of the Earth's geopotential. These scenarios can be understood as advanced variants of the well proven GRACE mission as they are based on the same basic measurement principles, i.e. determination of the individual non-gravitational accelerations on each spacecraft (S/C) and measurement of inter-satellite distance variations.

Despite this general degree of compliance, the added geodetic value does not come for free but with numerous technical challenges brought up by the specific differences compared to the GRACE mission. All issues described throughout this section have been traded within the study and possible solutions have been elaborated. A general issue during this process is the nature of a satellite gravity mission itself. While 'standard' missions (e.g. telecommunication) have a clear separation between payload and satellite bus/sensors, there is complex interaction between different subsystems, payload sensors, satellite and its environment (Fig. 21.2). Changing one parameter in one field has an impact on many fields and intensive iteration is required to get to a final solution.

The major technical challenges that were faced are related to the orbit and formation selection of the satellite tandem and the employment of a different satellite-to-satellite tracking (SST) technology and will be briefly presented below.

Orbit-Induced Issues

While the GRACE orbit height is about 450 km, the FGM scenarios consider altitudes in the range of 300–350 km but for a comparable baseline mission lifetime of at least five years. The lower orbits lead to stronger gravity signals but induce significantly larger atmospheric drag disturbances acting on the S/C bodies.

The first consequence is an increased need of propellant mass in case of cold-gas thrusters or power in case of electrical propulsion. This has a direct impact on the satellite design in terms of tank accommodation/solar panel sizing and might become crucial concerning the feasibility in terms of overall system mass and volume with

respect to the launcher capabilities and system cost.[1] Although no explicit constraint (e.g. orbit height limit) arises from this fact, it implies intensive design iteration with respect to above mentioned key factors (see also Sect. 21.4).

Another issue is related to the measurement of the non-gravitational accelerations. State-of-the-art electrostatic sensors such as the SuperSTAR (Space Three-axis Accelerometer for Research mission) accelerometer or the GRADIO accelerometer flown on GRACE and GOCE have a maximum DC range in the order of some $\mu m/s^2$ (Touboul 2001; Marque et al. 2008) while disturbance accelerations of at least the same order of magnitude are expected due to larger S/C cross-sections for above mentioned reasons. Thus, apart from the purpose of maintaining the orbit height, continuous drag-compensation has to be applied using thrusters with sufficiently high resolution to keep the acceleration sensors in their operational range ($\approx 6\,\mu m/s^2$ for GRADIO). Other accelerometer related issues are further discussed in Sect. 21.3.3.

SST Measurement Issues

Another part of the proposed improvement of the gravity recovery is based on the use of shorter wavelength of the onboard SST metrology, i.e. a transition from the
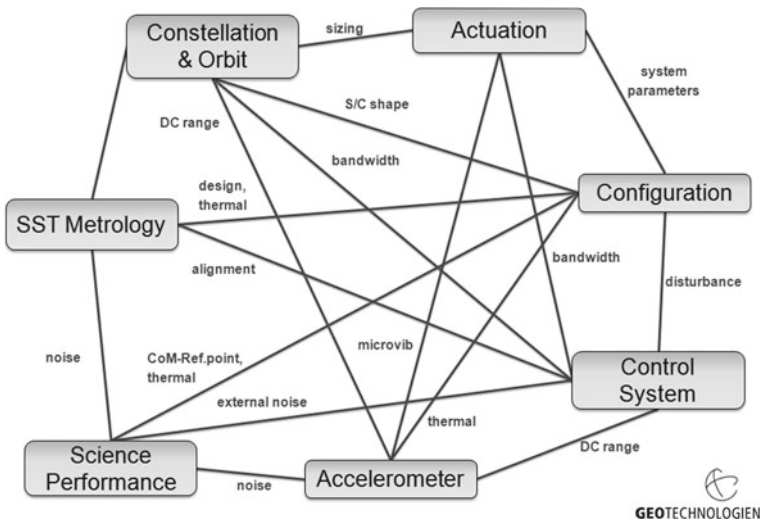
Fig. 21.2 Complex interaction between different 'subsystems'

---

[1] Note that even though the FGM orbits are still far from the air-drag environment of the feasible GOCE orbit (∼270 km altitude), GOCE is designed for a baseline lifetime of 18 month only which would be incompliant with the envisaged mission requirements, i.e. insufficient for the purpose of long-term monitoring of the gravity field for at least five years.

microwave region to the infrared. The benefit is expected to be a better resolution of the distance variation measurement of at least one order of magnitude.

However, the first technical challenge in this case comes with the laser technology itself as none of the proposed concepts (see Sect. 21.3.2) has been flown up to now, thus technological readiness is directly an issue.

Second, the divergence angle for the optical signals is much smaller than for Ka/K band systems (e.g. on GRACE), the need of a precise alignment (roughly 100 μrad) of transmitter and receiver axes requires an accurate pointing performance of the satellite attitude control system and a special treatment for the initial laser-link acquisition. This already implies the selection of an active transponder system for the considered FGM scenarios with an additional laser device installed on the 2nd satellite which is phase-locked to the incoming beam. The alternative solution—a retro reflector system—was discarded (although generally advantageous in terms of system complexity) for reasons of available power and required aperture size. Finally, there are more topics concerning the distance metrology which are closely related to the satellite formation issues discussed in the next section.

Formation Issues

Both GRACE and GOCE missions have a constant nominal orientation of the satellites with respect to the orbit plane which simplifies an optimized design of the spacecraft with respect to external disturbances.

In contrast, the FGM gravity recovery improvement partially relies on dedicated formation flights of the satellite tandem ('pendulum', 'cartwheel' and 'helix', see Sect. 21.3.4). These formations imply a large continuous periodic line-of-sight variation with respect to the orbit plane which cannot be covered by a 'static' SST metrology device due to the restricted detector field of view. Generally two principles are possible to maintain the SST link: steering the beam or the spacecraft only. A trade-off resulted in the decision to follow the latter principle as the former is considered to be afflicted with too many severe drawbacks concerning the complexity and feasibility of the metrology. Accurate and low-noise actuators for optical elements (e.g. piezo) are available for small ranges (mrad) only but not for the required range of tenth of degrees. Furthermore, the accommodation of the metrology itself poses a problem as a 'free-view' along the line-of-sight has to be guaranteed 'through' the surrounding spacecraft structure. Finally a pivoting telescope leads to significant mass movement and complex pathlength variations, both undesired from a data processing point of view for the science measurement.

The decision to favor S/C pointing to maintain the SST-link also has its drawback and brings up a set of constraints. Large deviations from a dedicated reference attitude impede the S/C design in terms of finding drag-optimized bus geometry, avoidance of attitude sensor and SST-metrology blinding, power generation or ground-link availability. For that reasons a 'soft' limit for the permitted pitch and yaw angle of ±30° (with respect to a typical nadir-pointing attitude) was established which

further restricts the selection of feasible formations together with the Doppler-shift constraint described below.

Apart from a variation of the line of sight direction, the FGM scenarios also imply a significant variation of the relative distance between the satellites over one orbit, thus a Doppler shift in the measurements that has to be properly accounted for in the metrology (readout) design. Derived from limitations of the laser technology with the highest technological readiness level (continuous wave heterodyne detection, see Sect. 21.3.2.1) a relative velocity constraint of about ± 10 m/s was defined.[2] Higher photodetector bandwidths (factor of 1.5-2 expected for the near future, possibly at the cost of increased power consumption or degraded noise performance), explicitly taking into account the time-varying Doppler shift or using a different metrology principle (see e.g. Sect. 21.3.2.2) could principally allow larger relative velocities but technological readiness remains an issue.

21.2 Methodology, Analysis Challenges and Tools

A series of methodologies and tools were developed in order to investigate possible future mission design options and to deal with their analysis challenges. From a geodetic point of view, the quick-look and full-scale Simulation Tools are very important instruments for selecting, designing and evaluating future mission scenarios. These tools are described in Sects. 21.2.1 and 21.2.2. A very important link between system/metrology design and geodesy is played by the sensor and system noise characteristics. On the one hand they describe the quality of the sensor and system output and on the other hand they are a serious restriction for the gravity field quality. Within this project, the sensor noise is described in terms of power spectral densities which have to be transformed into noise time series for application in full-scale simulations. These aspects are treated in Sect. 21.2.3. The process of estimation and validation of the sensor performance is described in Sect. 21.2.4. Especially the laser metrology and devices for inertial sensing (i.e. accelerometry) are considered. Finally, Sect. 21.2.5 deals with the tools and strategy for sensor and system simulation. The attitude and orbit control system, mission analysis and S/C design are outlined.

---

[2] The one way Doppler shift is given by $\Delta f = v/\lambda$ where v is satellites' relative velocity and λ the laser wavelength. Current photodetector/phasemeter prototypes have a bandwidth of 20 MHz with (Footnote 2 continued)

beatnote frequencies around 1–20 MHz (e.g. Bykov et al. 2009). In an offset-locked transponder configuration the beatnote frequency at the main S/C is twice the one-way Doppler shift plus the offset introduced by the transponder. If $\Delta f = 9.5$ MHz an offset of 1 MHz implies a 20 MHz beatnote, if $\Delta f = -9.5$ MHz an offset of 20 MHz gives a beatnote frequency of 1 MHz at the main S/C. For (a typical) $\lambda = 1064$ nm the tolerable relative velocity then results to ± 10 m/s.

21.2.1 Quick-Look Tools

Identifying suitable satellite missions for gravity recovery requires a huge number of satellite orbits and gravity recovery simulations. A variety of satellite orbit parameters such as inclination, repeat orbit and altitude, the inter-satellite distance, the formation type and orientation and the measurement noise level contribute to the search space of optimal future gravity missions. In order to avoid time-consuming full-scale gravity recovery simulations, two quick-look tools (QLT) have been developed as fast simulation software for sensitivity and time-variable gravity recovery analysis from ll-SST (low-low satellite-to-satellite tracking) missions. The QLT for sensitivity analysis (Sneeuw 2000) employs a semi-analytic error propagation to investigate the influence of the orbital parameters and measurement error PSD (Power Spectral Density) on the gravity field estimates, while the gravity recovery tool is based on the formulation of the equation for range-accelerations for the gravity recovery of certain time intervals.

Assuming a circular orbit with constant inclination ($r = r_0$, $I = I_0$) allows to perform an order-wise efficient block-diagonal error propagation with even and odd degree separation from the observational and stochastic model to gravity field errors (Sneeuw 2000). Then, a gravitational signal $f(t)$ along the satellite orbit can be represented by the lumped coefficients as

$$f(r, u, I, \Lambda) = \sum_m \sum_k A_{mk}^f(r, I) e^{i\psi_{mk}} \tag{21.1}$$

$$A_{mk}^f(r, I) = \sum_l \underbrace{\frac{GM}{R} \left(\frac{R}{r}\right)^{l+1} \bar{F}_{lmk}(I) \, K_{lm}}_{H_{lmk}^f(r,I)}$$

where K_{lm} are the complex spherical harmonic (SH) coefficients, $\bar{F}_{lmk}(I)$ is the inclination function, and the composite angular variable ψ_{mk} is $\psi_{mk} = ku + m\Lambda$. As the transfer coefficients $H_{lmk}^f(r, I)$ and the lumped coefficients $A_{mk}^f(r, I)$ are constant for a nominal orbit, the normal equation becomes order-wise block-diagonal. For a ll-SST-mission with inline formation, the transfer coefficient $H_{lmk}^f(r, I)$ reads as

$$H_{lmk}^{\rho} \approx 2 \sin(\eta \beta_{mk}) H_{lmk}^{\Delta x}, \text{ with } \sin \eta = 0.5 \frac{\rho_0}{r} \text{ and } \beta_{mk} = \frac{\dot{\psi}_{mk}}{n}$$

Utilizing block-wise variance-covariance propagation, the SH accuracy can be estimated by (where $\mathbf{Q}_y$ is the variance-covariance matrix of the observations):

$$\mathbf{Q}_{\hat{x}} = \left(A^T \mathbf{Q}_y^{-1} A\right)^{-1} \tag{21.2}$$

The semi-analytical QLT can be employed for the investigation of the effect of orbital parameters and measurement noise on the gravity products, illustrated as formal errors in terms of degree-RMS (root mean square), spherical harmonic triangle plots, spatial covariance functions and geoid errors per latitude (Sneeuw 2000). However, derivation of constant transfer coefficients for other formations than the GRACE-like (inline) formation has not been achieved yet. For these advanced formations, a pseudo-QLT is employed which is based on the equation for range accelerations:

$$\ddot{\rho} - \frac{1}{\rho}\left((\Delta\dot{\mathbf{X}}_{12})^2 - \dot{\rho}^2\right) = \mathbf{e}_{12}\left(\nabla V\left(\mathbf{X}_2\right) - \nabla V\left(\mathbf{X}_1\right)\right) \qquad (21.3)$$

The right side of this equation contributes to the design matrix, where the positions of the satellites at time epoch t, i.e. $\mathbf{X}_1(t)$ and $\mathbf{X}_2(t)$, are calculated by (i) assuming the center of both satellites to move along the nominal repeat orbit and (ii) generating the relative movement of the two satellites by the homogeneous solution of the Hill equations (Sharifi et al. 2007):

$$\begin{aligned}
x(t) &= -2A\sin(nt + \alpha) - \tfrac{3}{2}nz_{\text{off}} + x_{\text{off}} \\
y(t) &= B\cos(nt + \beta) \\
z(t) &= A\cos(nt + \alpha) + z_{\text{off}}
\end{aligned} \qquad (21.4)$$

where

$$A = \frac{1}{n}\sqrt{\dot{z}_0^2 + (2\dot{x}_0 + 3nz_0)^2}, \quad B = \frac{1}{n}\sqrt{\dot{y}_0^2 + (ny_0)^2},$$

$$\tan\alpha = \frac{\dot{z}_0}{2\dot{x}_0 + 3nz_0}, \quad \tan\beta = \frac{\dot{y}_0}{ny_0}$$

and

$$x_{\text{off}} = x_0 - \frac{2}{n}\dot{z}_0 - \frac{2}{n}\dot{z}_0, \, z_{\text{off}} = \frac{2}{n}(\dot{x}_0 + 2nz_0)$$

For the formations of this study, the following initial values have to be employed (supposed that the start point of each mission is over the equator):

- inline: $x_0 = \rho$, with ρ the along-track distance of two satellites,
- pendulum: $x_0 = \rho_x$, $y_0 = \rho_y$, with ρ_x the along-track distance and ρ_y the maximum cross-track distance between the satellites,
- cartwheel: $z_0 = \rho_r$, $\dot{x}_0 = -2n\rho_r$, with $\rho_x = 2\rho_r$ the maximum along-track and ρ_r the maximum radial distance,
- LISA-type (from: *Laser Interferometer Space Antenna*): $y_0 = -\sqrt{3}\frac{\rho}{2}$, $z_0 = \frac{\rho}{2}$, $\dot{x}_0 = -n\rho$, with the constant satellite distance ρ,
- trailing Cartwheel: $x_0 = \rho_{\text{x-offset}}$, $z_0 = \rho_r$, $\dot{x}_0 = -2\rho_r$, which is a Cartwheel formation with a shift $\rho_{\text{x-offset}}$ in along-track direction,
- helix: $x_0 = \rho_{\text{x-offset}}$, $y_0 = -\sqrt{3}\frac{\rho}{2}$, $z_0 = \frac{\rho}{2}$, $\dot{x}_0 = -n\rho$, which is a trailing LISA-type formation with a shift $\rho_{\text{x-offset}}$ in along-track direction.

Finally, by means of error propagation within a closed loop simulation a sensitivity analysis for the different formations can be performed by this approach. However, in its present state, the pseudo-QLT is only able to deal with white noise.

For the (reduced-scale) gravity recovery, the gradient of the time-variable potential of the Earth at the positions of the satellites is calculated by the provided time-variable gravity field models (AOHIS and ocean tides, see Sect. 21.2.2) at those epochs. The calculated values for the right side of the Eq. (21.3) are then set to the left side as the observables at those epochs, and the spherical harmonics coefficients for selected time intervals are estimated by means of least squares adjustment. Although the assumption of keeping the satellites in a perfect nominal orbit is not realistic, the tool provides a quick comparison of gravity recoveries of different formations, which can be studied later by more precise and realistic full-scale tools. Here, an evaluation of the QLT for reduced-scale gravity recovery is made with the ll-SST acceleration approach applied to orbits from real orbit integration where the observations ρ, $\dot{\rho}$, $\ddot{\rho}$ can be rather generated directly from the orbit. However, despite the fundamental differences between both methods, they provide the same results to a large extent (Iran Pour et al. 2013).

21.2.2 Full-Scale Simulation (Methodology)

The GFZ gravity field recovery simulations were carried out using the GFZ Earth Parameter and Orbit System (EPOS) software constituted by a collection of tools around the core module OC (Orbit Computation). EPOS-OC is based on a batch least squares estimator, and is able to process many observation types like Global Positioning System (GPS), Satellite-to-Satellite (SST) K-band, Satellite Laser Ranging (SLR), Doppler Orbitography and Radiopositioning Integrated by Satellite (DORIS) or altimetry.

The simulation done for an arc length of 32 days creates 32 one-day data batches including GPS code/phase measurements, surface forces time series (zeros for the drag-free missions) as well as the SST range-rate data. The mean Keplerian elements are transformed first in osculating elements for orbit integration.

The forward simulation is achieved in two steps. In a first step both satellites are sequentially integrated over the complete 32 days period with dedicated models for the surface force accelerations (if not drag-free). The orbit integrator not only yields the 32 days long orbit files but also "measured" surface forces computed from the non-gravitational forces models (accelerometer data) as well as the star camera data which are also used by the IGG group in Bonn. From the orbit files, initial elements are created for midnight on every day and the simulated acceleration data are chopped into pieces of one day length. In a second step, those initial states and acceleration data are fed into 32 individual jobs of one-day length that simulate GPS and SST range-rate data. For the surface forces acceleration the models are switched off and replaced by the one-day accelerometer data batches created in the first step.

The backward simulation (recovery) is also achieved in two steps. First the background models used for the forward simulation are replaced by the background models used for de-aliasing in order to take into account realistic model errors. Then colored noise (see Sects. 21.2.3 and 21.3.4.2) is added to the noise-free observations. Further on, the one-day data batches of simulated GPS/SST data are fed into 32 adjustment jobs where arc-specific parameters, like accelerometer calibration factors, empirical SST parameters, daily initial satellite positions and velocities as well as GPS phase ambiguities are recovered while the gravity field coefficients are kept fixed. At this point it has to be mentioned that in the presence of accelerometer noise the number of accelerometer parameters has to be dense enough to allow a good recovery of the gravity field. In these simulations we estimated an accelerometer bias parameter every 35 min to try to reach some kind of similarity with the simulations made in parallel at IGG Bonn where shorter (35 min) arcs were used. When convergence has been achieved, an additional run is started with the gravity field coefficients added to the list of solve-for parameters and the design equation files are created. In the second step, day-wise normal equations for every observation type are computed from the design equations. Those normal equations are added up to the whole 32 days, the resulting equation is then solved and yields the adjusted gravity field.

The IGG full-scale numerical simulations have been performed using the Gravity Recovery Object Oriented Programming System (GROOPS) software which has been developed by the Astronomical, Physical and Mathematical Geodesy group at IGG of Bonn University. The simulation process is based on the solution of the Newton-Euler's equation of motion, formulated as a boundary value problem, in the form of a Fredholm type integral equation for setting up the observation equations (Mayer-Gürr 2006).

First, all observations including the satellite orbits, accelerometer, inter-satellite range-rate and attitude data files provided by the GFZ group have been split into short arcs of 35 min. The observation equations for each short arc are set up as a linearized Gauss-Markov model, where the design matrices for each short arc are obtained as partial derivatives of the range-rate measurements (and kinematic orbits) with respect to the unknown parameters (corrections to input gravity field parameters and arc-related parameters as e.g. boundary values, biases, …). After accumulation of the normal equations for each arc the optimal solution is obtained by means of least squares adjustment where the inversion of the normal matrices is performed by Cholesky decomposition. The variance factor σ^2 of each arc can be estimated by means of variance-component estimation (Kusche 2002).

Models Used for the Simulation:

- static gravity field model: EIGEN-GL04C (Foerste et al. 2008)
- time variable gravity field model: Atmosphere, Ocean, Hydrology, Ice, Solid Earth: AOHIS (Gruber et al. 2011)
- ocean tides model: EOT08a (Savcenko and Bosch 2008), only the 8 main constituents Q1,O1,P1,K1,N2,M2,S2,K2

- planetary ephemerides: DE405 (Standish 1998), only Sun and Moon
- permanent tide: C20 from EIGEN-GL04C
- air-drag density model: MSIS86 (Hedin 1987)
- solar radiation pressure including umbra and penumbra
- Earth albedo and Earth infra-red radiation according to Knocke et al. (1988)

Further Assumptions:

- no relativity
- no precession, nutation and polar motion
- simple expression for Greenwich sidereal time:

$$\theta_{gr} = 2\pi(0.779057273264 + 1.00273781191354448(MJD(UTC) - 51544.5))$$

- no Earth tides and pole/ocean pole tides

Models Substituted for the Recovery Process:

- static gravity field model: EGM96 (Lemoine et al. 1998)
- time variable gravity field model: 90 % of AOHIS
- ocean tides model: GOT4.7 (Ray 2008), only the 8 main constituents Q1,O1,P1, K1,N2,M2,S2,K2

Background model restoring: The differences between the simulated gravity model (static background model EIGEN-GL04C (="A") + 100 % AOHIS (="B")) and the adjusted mean gravity model over 32 days (="C") have to be corrected by the mean AOHIS (="D") over 32 days in the following way $(A - B) - (C + D) = (A - C) + (B - D)$ where $A - C$ is the difference between the background and adjusted mean models and $B - D$ the difference between the corresponding time variable fields (10 % AOHIS).

21.2.3 Analysis at PSD Level in Terms of Range Rates

Gravity field determination is based on measurements from different types of sensors: mainly SST instruments and accelerometers. Both sensor types provide a major contribution to gravity field determination and affect the results in different frequency bands: long-wavelength gravity field signals are currently limited by SST noise, whereas short-wave signal components are limited by accelerometer noise. Due to the strong frequency dependence of sensor measurements, comparative analyses are performed in the frequency domain—in terms of PSD.
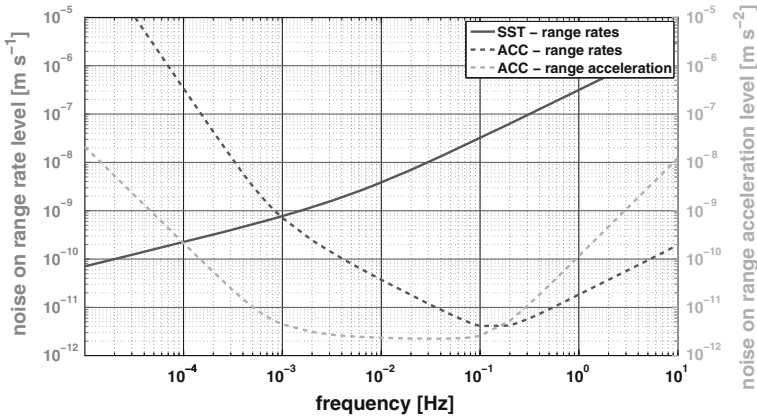
Fig. 21.3 PSD of SST and accelerometer sensor performances in terms of range rates (*left axis*) and accelerometer noise in terms of range accelerations (*right axis*) are illustrated. The conversion-related tilting is obvious. The PSDs are attributed to the (conservative) pendulum simulation (see Sect. 21.3.4.2)

21.2.3.1 Analyses at the Level of Range Rates

The ll-SST measurements are carried out in terms of ranges or range rates while accelerometers provide disturbing accelerations. To permit a comparison and joint processing, both measurement types have to be transformed into the same level. Within the FGM project, the selected baseline of gravity observations is range rates. The conversion of ranges (S_x) to range rates ($S_{\dot\rho,x}$) is obtained by differentiation, i.e. a multiplication with frequency (f) in the frequency domain:

$$\sqrt{S_{\dot\rho,x}} = \sqrt{S_x} \cdot 2\pi f. \tag{21.5}$$

The conversion of accelerations (S_a) to range rates ($S_{\dot\rho,a}$) is obtained by integration, i.e. a division by frequency (f) in the frequency domain:

$$\sqrt{S_{\dot\rho,a}} = \sqrt{S_a} \cdot \frac{1}{2\pi f}. \tag{21.6}$$

By considering the noise performance of a sensor in the frequency domain, differentiation and integration lead to 'tilting' of the PSD curves: differentiation implies a counter-clockwise tilt, integration leads to a clockwise tilt (see Fig. 21.3).

21.2.3.2 Power Spectral Density Estimation

Both the analyses of (simulated) measurements and the assessment of the results are performed in the frequency domain. Due to the frequency dependency of sen-

sor performances, the conversion of measured or simulated time series from the time domain to the frequency domain is a key issue. For this transformation, various computational procedures are available, which might produce different density spectra. The FGM group decided to apply the periodogram-based Welch's overlapped segment averaging (WOSA) method (Welch 1967). The reason is the simplicity of implementation and the fact that it is implemented and tested in a *MATLAB* toolbox, the LTPDA,[3] used by various members of the FGM group.

LTPDA is based on object-oriented programming. In its core the MATLAB function 'pwelch' is used for PSD estimation, which corresponds to the WOSA method. The basic formula and important calculation steps are:

$$
\hat{S}_X^{(WOSA)}\left(f_j\right) = \frac{\Delta t}{K} \sum_{k=0}^{K-1} \left| \sum_{t=0}^{Ns-1} x_{t+t_k} w_n \, e^{-i2\pi t j/Ns} \right|^2, \quad j = 0, \, 1, \, \ldots, \, \frac{Ns}{2}
$$

(21.7)

- The input time series $X(t) = [x_0,\ldots,x_{N-1}]$ is segmented into K overlapping segments each of length Ns. Starting indices of kth segment is t_k.
- A specified window $w = [w_0,\ldots,w_{Ns-1}]$ is applied to each segment in the time domain in order to reduce edge effects and to prevent spectral leakage. The loss of signal information from the windowing is counteracted by means of overlapping segments.
- A periodogram is computed for each windowed segment, which is the squared magnitude of a Discrete Fourier Transform (DFT) of the time series. As the Fast Fourier Transform (FFT) algorithm of MATLAB is used, the segment length is selected to a power of two or it is increased to the next higher power of two using zero-padding.
- The K modified periodograms are averaged to form the spectrum estimate.
- The resulting spectrum estimate is scaled to the PSD.

A detailed representation of the relations can be found, e.g., in Percival (2006); notes to the implementation are included in the *MATLAB* documentation for 'pwelch' and the LTPDA toolbox.

The WOSA method produces output that is equidistantly spaced on the frequency axis. Very often, however, a logarithmic frequency axis is more suitable. Logarithmic power spectral density (LPSD) has been developed for this case. It aims to compute the spectral density at frequencies that are equidistant on a logarithmic frequency axis. Otherwise, it shares the properties of the WOSA method. Time-domain window functions, overlap, etc. can be applied correspondingly. The difference is most obvious at the highest frequencies, where WOSA produces many results at very closely spaced frequencies, which are rather noisy due to limited averaging, while LPSD uses optimized averaging at each frequency and thus reduces the variance of

---

[3] LISA Technology Package Data Analysis (LTPDA) is a MATLAB toolbox being implemented in the framework of the LISA gravitational wave detection mission. Further information as well as the toolbox itself—downloadable for free—is available via www.lisa.aei-hannover.de/ltpda.

the result. Further information about the LPSD algorithm implemented in LTPDA toolbox can be found in Troebs and Heinzel (2006).

21.2.3.3 Generating Noise Time Series from PSD

Often, the reverse way to compute time series from given PSDs is of great interest. Within the FGM project this method is used to compute colored noise time series from given sensor performance PSDs that are added to error-free simulated sensor time series. The resulting sum is used as input for full-scale simulations (see Sect. 21.3.4.2). The noise time series are generated with the *MATLAB* function 'noisegen1D' of the LTPDA toolbox. The basic processing steps are:

- The square root of the PSD is fitted in the frequency domain in terms of discrete transfer functions using partial fraction expansion.
- Each element of the partial fraction expansion can be seen as an Infinite Impulse Response (IIR) filter and the complete expansion is a parallel filterbank.
- The filters are applied to a white noise time series.
- The filtering results in an arbitrary time series whose spectral behavior is 'identical' to the input PSD.

A description of the 'noisegen1D' function and further references are available in the LTPDA user manual on the LTPDA website. Within the FGM project, all analysis techniques presented here have been summarized in technical notes.

21.2.4 Sensor Performance Breakdown and Budget

The quality of the gravity field determination is mainly dependent on the performance of the SST and non-gravitational acceleration determination. Thus special focus has been set on the understanding and modeling of the performance contributors of the respective sensors, i.e. accelerometers and laser metrology. As the inputs to QLTs and full-scale simulations rely on PSDs, the whole modeling is based on spectral density as far as possible.

21.2.4.1 Laser Metrology

Concerning the intrinsic noise models for the laser metrology, expert knowledge was directly available due to the industry partners in the project team. As different technologies were investigated (see Sect. 21.3.2, different performance predictions have been worked out starting from low level contributors. Exemplary the following effects were accounted for and models on spectral density level were derived:

- Noise dependence on the (round-trip) distance between the two satellites

- Frequency noise
- Doppler-shifts due to relative velocity between satellites
- Pump and cavity noise
- Photo-detector noise and read-out noise
- Wave-front errors

Apart from these internal noise sources, external sources such as couplings of the S/C pointing stability into the optical pathlength measurement exist. While parts of this contribution—the purely geometrical coupling of S/C pointing noise with the lever arm from the gravitational reference point, traditionally the S/C center of mass (CoM), to the effective phase center of the laser metrology—are principally easy to model, the exact determination of this lever arm requires first a detailed layout of the optical bench and telescope, second a detailed design of the satellite structure and payload accommodation which was out of scope of the study for the different metrology designs. To account for this noise source (and similar effects such as pathlength changes due to non-nominal incident beam orientation on the individual optical elements on the bench), additional white noise of reasonable magnitude was introduced in the budget.

21.2.4.2 Inertial Sensor

Concerning the internal noise of state-of-the-art electrostatic accelerometers (e.g. the Office National d'Etudes et de Recherche Aérospatiales (ONERA) sensors used on GRACE and GOCE there is a general information gap, except for specific noise spectra published by ONERA (Marque et al. 2008; Christophe et al. 2010) or provided by ONERA in the context of the e.motion (Panet et al. 2012) proposal.

QLT results using the latter information revealed a dominating contribution of the acceleration noise at lower frequencies compared to the distance metrology. To get an insight into the nature and sensitivity to different important parameters of the contributors, a detailed lower-level parametric model was derived based on the spare information (e.g. Christophe et al. 2010, or Willemenot and Touboul 1999) and the experience of project partners gained in the context of the LISA Pathfinder project. The model accounts for the following internal noise sources:

- Parasitic acceleration noise on the sensor test mass (TM), such as contact potential differences on the electrodes, gold wire damping and thermal stability effects such as radiometer effect and radiation pressure
- Measurement noise (from analog-to-digital converters (ADC))
- Detection noise (from capacitive sensing noise on voltage level and ADC)
- Actuation noise (from amplifiers and digital-to-analog converters)

The closed-loop behavior of the sensor was modeled by simplified single-input single-output (SISO) control loops for the TM position. Tuning of the parameters within reasonable ranges resulted in a good agreement with the results from ONERA, i.e. in the typical 'bathtub' shape with a noise level of 1-2 pm/s^2.

Apart from sensor intrinsic effects, external sources are important for the total acceleration performance. The real acceleration **a** at the TM CoM is given by:

$$\mathbf{a} = \left(\mathbf{U} - \dot{\tilde{\boldsymbol{\omega}}} - \tilde{\boldsymbol{\omega}}^2\right) \mathbf{r_A} - \mathbf{a_{ng}} + \mathbf{b}. \tag{21.8}$$

a_{ng} represents the desired quantity to be measured, the non-gravitational accelerations acting on the S/C. Furthermore, there are direct forces on the TM (the constant ('DC') part **b** of the parasitic accelerations described above), couplings of gravity gradient (**U**) and rotational dynamics of the S/C (**ω**—terms, where '∼' represents a cross-product matrix) with the offset **r_A** from the S/C CoM.

Equation (21.8) is also used to set up a DC acceleration budget which delivers insight into the question to what extent drag compensation is needed and how accurate the sensor has to be placed with respect to the S/C CoM to ensure operation in the accelerometer measurement range. For an inline formation, the terms in brackets coupling with the CoM offset are basically constant, while for the FGM scenarios the terms vary significantly over an orbit in case the S/C is pointed to maintain the SST link. Special focus has been put on this issue for both DC and noise performance (see Sect. 21.3.3).

The relevant quantity for the gravity recovery is the measured acceleration **a_m** along the SST reference direction. It can be expressed using the following relation with respect to the real acceleration **a** on one sensor TM from Eq. (21.8):

$$\mathbf{a_m} = \mathbf{\Phi}\left(\mathbf{K_s}\,\mathbf{K_{CC}}\,\mathbf{a} + \mathbf{n_a}\right). \tag{21.9}$$

n_a represents the sensor intrinsic noise, the matrices **K_s** and **K_{ss}** represent scale factor errors due to knowledge of the voltage-force conversion and cross-coupling errors due to non-orthogonality of the sensor axes respectively. **Φ** accounts for the attitude of the sensor axes with respect to the line of sight. To assess the impact of different external noise sources individually in the budget, Eq. (21.9) was broken down using a first order approximation for the possible fluctuations (preceded by 'δ' in the following for all axes $i = x,y,z$):

$$\delta\mathbf{a_m} = \sqrt{\left(\frac{\partial\mathbf{a_m}}{\partial\Phi_i}\delta\Phi_i\right)^2 + \left(\frac{\partial\mathbf{a_m}}{\partial K_{s,i}}\delta K_{s,i}\right)^2 + \left(\frac{\partial\mathbf{a_m}}{\partial\dot{\omega}_i}\delta\dot{\omega}_i\right)^2 + \left(\frac{\partial\mathbf{a_m}}{\partial\omega_i}\delta\omega_i\right)^2 + \left(\frac{\partial\mathbf{a_m}}{\partial r_{A,i}}\delta r_{A,i}\right)^2 + (\mathbf{\Phi}n_A)_i^2}$$
$$\tag{21.10}$$

Equation (21.10) consists of numerous contributions of the form 'amplitude x noise' which are assumed to be mutually uncorrelated for the break-down. Fluctuations of the scale factors ($\delta K_{s,i}$) were empirically approximated and the stability of the CoM offset ($\delta r_{A,i}$) was approximated using the thermal stability of ZERODUR® (assuming mounting of accelerometer and laser metrology on a common optical bench). Fluctuations related to S/C rotation ($\delta\omega_{,i}$ and its derivative) and pointing ($\delta\Phi_{,i}$) were derived from a simplified SISO closed-loop model of the attitude control system. Inputs to this model are again spectral models of the thruster and attitude readout noise. The latter is based on the accurate two-axis readout from the laser

metrology itself using differential wave front sensing (e.g. Heinzel et al. 2004) and the expected performance of a state-of-the-art star tracker for the third axis. Thruster torque noise is modeled using an average device number and lever arm together with performance predictions for the force noise of suitable thrusters (coldgas thrusters (Matticari et al. 2011) and electrical propulsion (Di Cara et al. 2011)). An additional benefit of this closed-loop model in the budget is that it allows a quick trade of controller parameters (bandwidth, margins) with respect to the science performance.

The amplitudes in Eq. (21.10) can be interpreted in multiple ways. For an inline formation only DC amplitudes (maximum drag, nominal CoM offset, maximum pointing offset, nominal gravity gradient, etc.) have to be taken into account. However, advanced formations lead to a necessary extension of the model (in case the S/C is used to maintain the SST link) as the 'amplitude' terms are not only composed of constants but also contain periodic terms at once/twice the orbital frequency which modulate the related noise $\delta x_{,i}$ and lead to a special kind of non-stationary random process called cyclo-stationary.

In order to link this noise to the common PSD of a stationary random process the non-stationary process needs to be 'stationarized', thus resembling the original process in average, while losing information about the underlying process. If each of the periodic components in $\partial \boldsymbol{a_{m,i}}/\partial x_i \cdot \delta x_{,i}$ in Eq. (21.10) is approximated as $A_{p,i} \cdot \sin{(2\pi f_{p,i}t)} \cdot \delta x_{,i}$ with amplitude $A_{p,i}$ and $f_{p,i}$ the modulation frequency (multiple of the orbit frequency), then the resulting noise spectrum $\delta x_{p,i}$ can be expressed as function of the original stationary spectrum $\delta x_{,i}$ (Bendat and Piersol 2000):

$$\delta x_{p,i}(f) = \frac{A_{p,i}}{2}\sqrt{\delta x_i(f + f_{p,i}) + \delta x_i(f - f_{p,i})} \qquad (21.11)$$

The whole break-down and budget described in this section is realized in *Mathematica* as it allows symbolic computations and together with the parametric model approach a quick adaption of models and parameter trade-offs. Furthermore time series or DC and harmonic amplitudes (e.g. external disturbances from simulations, see next section) can easily be imported and extracted.

Further results of the performance budget for both DC and noise together with their consequences are briefly discussed in Sect. 21.3.3.

21.2.5 Sensor and System Simulation

Parallel to the analytical description of system/sensor performances different simulations have been set up which will be briefly described in this section.

21.2.5.1 AOCS Simulation

For the design and test of the basic Attitude and Orbit Control System (AOCS) algorithms, a simulator was established in a *Matlab/Simulink* environment. Most of the implemented models and algorithms are based on s-functions in C. The simulation environment takes into account the fully coupled 6-degree of freedom dynamics of two individual rigid-body satellites. States and auxiliary outputs can be represented in various coordinate frames.

The Earth gravity field is represented by the EGM96 model (Lemoine et al. 1998) up to degree and order 30, the Earth magnetic field is derived from coefficients of the International Geomagnetic Reference Field (IGRF) up to degree and order 9 (Finlay et al. 2010) and is extrapolated to the simulation epoch of the FGM scenarios. The solar model accounts for the actual sun position and shadowing by the Earth using a conical shadow model (Montenbruck and Gill 2001). The atmosphere model is based on a Harris-Priester density model (Montenbruck and Gill 2001) with data sets for various solar activities (represented by F10.7 values) and includes variations due to the diurnal density bulge.

Both forces and torques due to solar pressure and air drag require a model of the satellite geometry. The simulator allows the inclusion of a simplified geometry using a set of plane surfaces defined by their normal vector, surface areas, position of the centers of area in the body frame and surface specific properties such as drag, diffuse and specular reflectivity coefficients. While the assumption of an average drag coefficient (21.2) is used for all surfaces, the reflectivity coefficients have been derived from available data (Bettadpur 2007). Forces and torques are then determined dependent on the angle between velocity or sun direction and the surface normal. Although no shadowing between mutual faces can be considered, this approach is sufficient for AOCS simulation purposes and to extract the main characteristics and magnitudes of the important environmental disturbances.

Concerning the actuators, an arbitrary number of thrusters with individual orientation can be realized. The current model allows definition of maximum and minimum thrust levels and additional noise. The noise models are equivalent to the ones used for the analytical performance analysis described in Sect. 21.2.4.

In addition the simulator includes models for the main sensors, namely star trackers, accelerometer and laser metrology. The star tracker model allows the definition of multiple star tracker heads with arbitrary orientation, field-of-view limitation and noise levels for the boresight and cross-axes. The laser metrology model is based on geometry only, i.e. the measurement model is related to the distance variation between two body-fixed phase centers only. In addition, the angular measurement (differential wave front sensing, see e.g. Heinzel et al. 2004) is modeled as well and can be defined via noise model and field of view constraints. Finally, an accelerometer model is included which is based on Eq. (21.8), concerning both noise and required inputs.

The colored noise time series required for the sensor and actuator models are realized by feeding white noise of unity power through a transfer function with magnitudes fitted to the ones of the desired noise spectrum (see Sect. 21.2.3).

With this simulator, basic control algorithms (based on Proportional-Integral-Derivate (PID) and quaternion feedback control) were successfully tested for both the 'science mode' (i.e. maintaining the SST-link via S/C pointing only) and the 'acquisition mode' (i.e. initial establishment of the SST-link before relative attitude information is available from the laser metrology itself).

Apart from AOCS simulation, the simulator was used throughout the study to:

- support the S/C design and optimization by providing time series and maxima of forces and torques for different geometries and solar activity levels
- deliver DC and periodic amplitudes for performance budgeting
- determination of applicable torques via magnetic torquers for thruster support and propellant saving

The main limitation of the simulator is that it cannot be used to qualify the science performance, i.e. serve as input for full-scale simulators as e.g. the gravity field resolution is not sufficient, the required distance measurement accuracy (apart from level of detail) in nm range cannot be provided and as it is not suitable for long time series that are required (e.g. 30d cycles).

21.2.5.2 Mission Analysis and Spacecraft Design

S/C analyses and design have been performed with the STI in-house developed tool SPADES (Spacecraft Performance Analysis with Dynamic Environment Simulation). This tool has been used for power analysis based on irradiation input, solar generator configuration, shunt and battery simulation. For each scenario the power generation in dependence of STO angles has been estimated.

The space environment (gravity, atmosphere, solar radiation, Earth's magnetic field) has been simulated based on models which are in accordance to ESA standards. The JGM3 model (Tapley et al. 1996), the Jacchia Bowman 2006 model (Bowman et al. 2008) and IGRF model (Finlay et al. 2010) have been used for gravity field, atmosphere and magnetic field, respectively. Solar radiation has been simulated based on solar power and surface properties. The tool also allows specification of sensor and actuator models (e.g. thrusters, reaction wheels, magnetic torquers, gyroscopes, star trackers) with different levels of detail. It has been used for dimensioning of the thrusters, estimation of the propellant/power demand for drag compensation and determination of blinding conditions for the star tracker assembly for the selected scenarios. The S/C design plots have been generated using the $PTC^{®}Pro/E$ - $Creo$ $Parametric$ software.

21.3 Analysis and Selection of Mission Scenarios

The selection and analysis of possible missions was a main task within the Future Gravity Missions project. Besides the choice of suited orbit and formation parameters

also the selection of tailored metrology equipment and system design play a dominant role in FGM design. Establishing mission selection, it has to be considered that even a strong correlation between mission parameters is apparent, which makes the enormous search space more complex.

For instance, the current constraint of heterodyne lasers on the maximum range-rate restricts the amount of possible formations and formation parameters, and issues as air-drag put limits on lowering orbit heights and increasing pendulum amplitudes or aim at sun-synchronous orbits. In order to deal with the huge non-linear and correlated search space strategies have to be applied to find possible candidates for FGM. In this section, the mission selection is outlined.

In Sect. 21.3.1 basic mission requirements on the gravity field accuracy and sensor noise are derived from geophysical phenomena to be detected. In Sect. 21.3.2 different metrologies for establishing ll-SST links are presented and evaluated with respect to accuracy and technological readiness levels. A special focus was put in Sect. 21.3.3 on the disturbing acceleration measurement, especially concerning drag compensation and issues of inertial sensor positioning. Finally the selection and analysis of basic and final mission scenarios is described in Sect. 21.3.4.

21.3.1 Basic Mission Requirements

The science objectives (Sect. 21.1.2) form the basis for deriving mission and sensor requirements. The four fields of primary focus for a FGM are continental water and ice, ocean and solid-Earth. Signals representing very important processes to be observed in these domains are listed in Table 21.1. The numbers in the table represent approximate signal magnitudes in terms of geoid heights. The nominal mission profile required to observe such kind of signals has a duration (life time)

Table 21.1 Fields of prioritization with their spatial and temporal resolution and approximate signal magnitudes

	Description	Spatial resolution	Temporal resolution	Signal magnitude in geoid heights
1	Melting of ice sheets (with separation of GIA)	100–1000 km	Seasonal – secular	0.01–1 mm/year (secular)
2	Non-steric component of sea-level variations at seasonal and shorter time scales	Global to basin level	Interannual – Secular	0.1 mm/year (Secular)
3	Ground water (soil moisture and snow) at larger spatial scales	10–200 km	Seasonal – secular	0.05–1 cm (seasonal)
4	Post-seismic deformation	10–200 km	Sub-seasonal	1 mm (sub-seasonal)

Table 21.2 Requirements in terms of maximum CGE for monthly solutions (the number in the gray boxes correspond to the first column of Table 21.1)

	Resolution	10000 km	1000 km	200 km	100 km	10 km
	SH degree	2	20	100	200	2000
	10 mm			3		
CGE	1 mm	2			4	
	0.1 mm		1			

The shaded areas on the right mark the restriction to more realistic values in case of a monthly satellite gravity field

Table 21.3 Requirements in terms of CGE for monthly gravity field retrieval

SH degree	150	200	250
CGE (mm)	0.1	1	10

of 11 years in order to observe long term trends and to cover one solar cycle and a repeat cycle of about one month in order to identify mass variations in these domains. In addition, polar satellite orbits are assumed in order to cover the polar caps allowing the observation of important mass changes due to ice sheet dynamics. Table 21.2 translates Table 21.1 into maximum cumulative geoid error (CGE) for monthly retrievals in terms of spherical harmonic (SH) expansions. Use was made of the rule-of-thumb that the resolution (or half-wavelength) of a signal is equal to the circumference of the Earth (40.000 km) divided by two times the SH degree. The next step is a restriction of obtained values to more realistic requirements for the CGE obtained by a FGM. Therefore the three boxes (1, 3 and 4) are reduced to lower SH degrees (shaded areas). On a monthly basis it is far beyond observation capabilities from space to achieve a 0.1 mm geoid up to SH degree 200 or a 1 cm geoid up to SH degree 2000. This yields CGE values as shown in Table 21.3 which are the result of a trade-off between maximum scientific and societal return and technological feasibility. The CGE complete to spherical harmonic degree and order 150, 200 and 250 should be below 0.1, 1 and 10 mm, respectively, for the ideal FGM (Anselmi et al. 2011).

Table 21.4 Required noise levels for the combination of ll-SST and acceleration sensor noise (ACC) for a monthly gravity field retrieval with a baseline of 75 km

Altitude (km)	SST (nm/$\sqrt{}$ Hz)	ACC (pm/s^2/$\sqrt{}$ Hz)	CGE (mm)		
			150	200	250
300	8.0	7.0	0.09	0.62	4.31
350	3.0	2.0	0.09	0.86	9.09
400	0.5	0.4	0.05	0.64	9.32
450	0.1	0.1	0.02	0.49	10.15

So-called gravity field quick-look tools based on the semi-analytical approach (Sneeuw 2000, Sect. 21.2.1) are used to derive sensor precision requirements. As a baseline, ll-SST range rate observations are taken as measurements but the impact of Satellite Gravity Gradiometry (SGG) observations can be assessed as well. Initial results revealed that the largest improvements for time variable global gravity field recovery can be achieved by enhanced ll-SST observing systems. For the subsequent simulations realistic shapes of PSDs of sensor errors are used. For the distance measurement sensor the square-root PSD in $[m/\sqrt{Hz}]$ is assumed to have a white noise behavior above $f = 10$ mHz and a $1/f$-part below 10 mHz. The square-root PSD of the accelerometer sensor in $[m/s^2/\sqrt{Hz}]$ is assumed to have a flat behavior between 1 and 100 mHz, a $1/f^2$-part below 1 mHz and a f^2-part above 100 mHz. The distance between the two S/C is chosen to be 75 km. The required noise levels (in the measurement band) for a complement of ll-SST and acceleration sensors and a range of satellite altitudes are displayed in Table 21.4. The CGE for different maximum SH degrees and orders is included in the most right columns. It is obvious that required sensor precisions increase rapidly with increasing altitude: the required ll-SST sensor noise for the measurement bandwidth is e.g. 8 (3) $nm/\sqrt{Hz}$ for altitudes of 300 (350) km respectively. Associated levels for the accelerometer noise are 7 (2) $pm/s^2/\sqrt{Hz}$.

It has to be noted that the derived sensor requirements by the QLTs are optimistic, since only instrumental noise is propagated and no processing errors are taken into account. It is assumed that the derived sensor requirements in the different mission scenarios assure that the low-low SST measurements are sensitive to the most important science objectives. Of course, this is necessary to derive global gravity fields including these signals. Processing errors with a strong influence of temporal aliasing add another important error source. These aspects are analyzed in the numerical full-scale simulations.

21.3.2 Laser Metrology and Atom Interferometry

GRACE has demonstrated that the principle of distance measurement between two formation flying S/C is a powerful tool for long term investigation of the Earth's time-variable gravity field. These activities are currently based on state-of-the-art microwave technology (K-/ K_a-band), which is also the basic technology for the upcoming GRACE Follow-On mission (GFO). Within the frame of this study it was shown that optical systems—operating at much shorter wavelength—have the potential for significantly improved accuracy and precision of future metrology systems in geodesy research. Four optical principles have been identified that appear well suited for future high precision space borne applications. The following passages summarize the basics of these metrology techniques; highlighting their main features and explaining their operational principles by means of illustrations.

21.3.2.1 Continuous Wave (CW) Laser Interferometry

Laser interferometry is a promising technique both for measuring variations in inter-satellite distance, as well as for position sensing of free-flying test masses. In the case of Satellite-to-Satellite Interferometry (SSI), laser interferometry is expected to be superior to the presently used microwave ranging due to its potentially much lower noise (1–100 nm/$\sqrt{\text{Hz}}$ as opposed to 1–2 μm/$\sqrt{\text{Hz}}$ in GRACE). Moreover, the technique of Differential Wavefront Sensing (DWS) allows a very precise sensing of the relative alignment of each satellite with respect to the optical axis towards the other satellite. The quantity to be measured is the distance variation between the two S/C centers of mass, or rather between the two test mass reference points in the usual case of a test-mass serving as accelerometer/drag-free sensor to compensate for non-gravitational forces. The most straightforward geometry would be to use in both directions a single optical path along the connecting line. For the Laser Ranging Interferometer (LRI) of the GFO, this is impossible due to existing equipment in that path. Therefore an alternative geometry, the so-called "racetrack", was devised (Fig. 21.4), which makes use of a partial triple mirror, the vertex of which can be placed in the accelerometer CoM.

The main noise sources in an SSI laser system are laser frequency noise and pointing jitter. With presently available and space-compatible techniques for laser frequency stabilization (optical cavities), the resulting noise is a few 10 nm/$\sqrt{\text{Hz}}$. The effect of pointing jitter is more complicated and involves several coupling mechanisms. Most of them turn out to be the product of a static alignment imperfection, like an offset of the optical axis from the relevant rotation point or CoM, with typical magnitudes of order 50–200 μm, and the pointing jitter of the S/C in pitch and yaw, ranging typically between 100–1000 μrad/$\sqrt{\text{Hz}}$.

The US-German GFO mission, to be launched in 2017, will contain the experimental LRI as technology demonstrator (Sheard et al. 2012) which will be the first inter-S/C laser ranging system. Its aims for demonstration of the techniques listed above and improvement of the GFO mission data itself.

21.3.2.2 Optical Comb Heterodyne Interferometry

Within the study the application of Optical Frequency Combs (OFC) to precise long distance ranging has been investigated. OFCs are precision lasers that provide up to 10^5 narrow bandwidth laser lines (<1 Hz) which are equally spaced and referenced to a Radio Frequency (RF) standard (Udem et al. 2002). This can be used to advance precision interferometry, nowadays reaching an accuracy of <1 nm (Schuldt et al. 2009). In addition, OFCs are femtosecond lasers capable of time-of-flight (TOF) ranging with an accuracy of <10 μm (Cui et al. 2009). However, both techniques suffer from a limited duty cycle, limiting ranging at high relative velocities and accelerations typical for dynamic formation flights. A technique that would overcome such limits has been suggested recently: Dual-comb heterodyning (Coddington et al. 2009). It provides a duty cycle of several kHz, at large relative velocities up to 3 km/s, reaching a precision of <10 nm. For formation flight ranging it is suggested
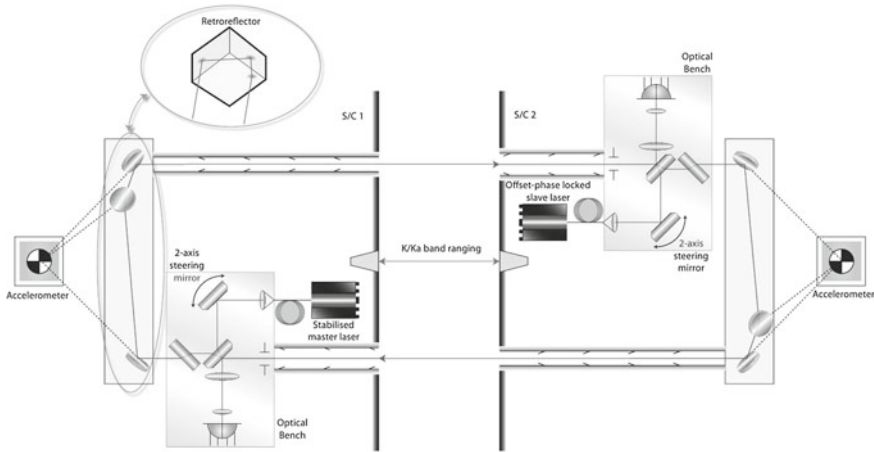
Fig. 21.4 Schematic of the laser ranging interferometer for GFO (Sheard et al. 2012)

to combine dual comb heterodyning with additional Doppler shift detection, TOF measurement and angular speed detection. A simplified scheme of such a system is depicted in Fig. 21.5.

The expected range noise PSD based on a linear combination of noise from comb, interferometer, detector and data processing has been simulated. For the comb noise PSD, an upper limit given by -115 dBc rad^2/Hz/f for $f < 500$ kHz and -137 dBc rad^2/Hz is assumed (Haboucha et al. 2011). This PSD simulation suggests that the overall accuracy of dual comb heterodyning should be better than 10 nm, which supports highly dynamic inter-satellite ranging for formation flights.

21.3.2.3 Femtosecond Laser Based Heterodyne Interferometry

High precision measurement using Femtosecond Laser Systems (FLS) is capable to measure distances in vacuum up to 500 km with an accuracy and resolution better than 1 µm. Using the frequency spectrum of the pulses, extreme high measurement rates are possible. Kayser-Threde GmbH is currently working on an extreme stable FLS with an all-in-fiber setup as can be seen in Fig. 21.6.

During nominal operation the FLS is emitting a continuous train of pulses (width $<10^{-13}$ s; tunable pulse repetition time (T) appr. 10 ns). These pulses are split up into a precisely known internal reference path and towards a remote target (S/C) with unknown distance. The return pulses which come back from the target are superimposed with the pulses from the reference path (Ye 2004).

In the frequency domain the FLS output is the repetition frequency ($1/T$) of the FLS. The beat frequencies of the two different pulse trains are $1/(T - dT_1)$ and $1/(T - dT_2)$. The advantage of using beat frequencies is the possibility of frequency locking this heterodyne signal to a reference frequency. The simplest way is to change
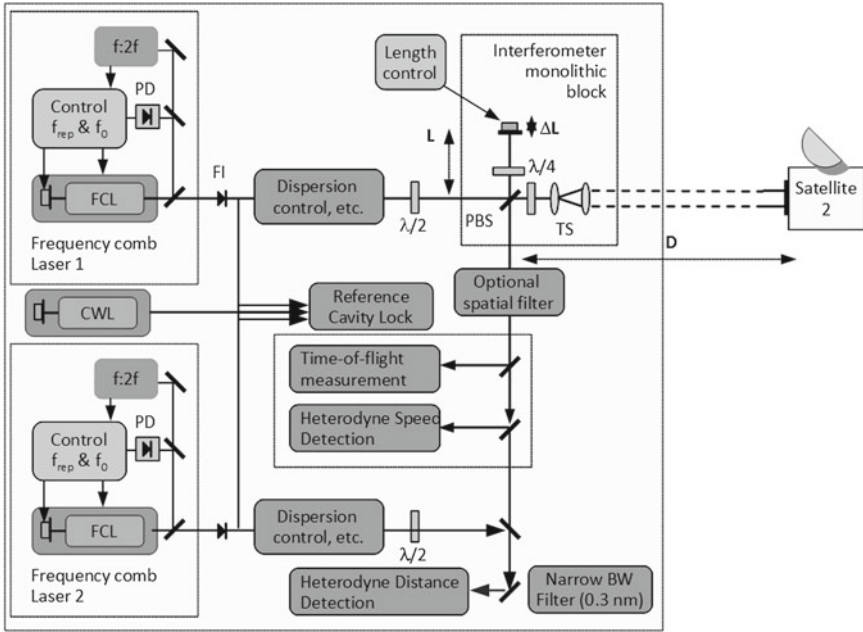
Fig. 21.5 Dual comb based high precision distance metrology (*FCL* frequency comb laser, *CWL* continuous wave laser, *PD* photodiode, *PBS* polarizing beam splitter, *TS* telescope)

T as long that $dT_1 \rightarrow T$ and $dT_2 \rightarrow 0$. Thus the heterodyne frequency is exactly the repetition rate ($1/T$) of the FLS.

Absolute distance measurements are possible by varying the repetition rate. After locking the beat frequency to the repetition rate, the measurement rate is about 1000 Hz. The frequency lock is an electrical mixer using the different frequency inputs of the repetition rate and the heterodyne signal.

21.3.2.4 Atom Interferometry

Initially used in atomic clocks, which nowadays define the second, atom interferometers have developed into a powerful tool for measurements of inertial forces with absolute accuracy. The coherent interaction between light and matter allows for forming interferometers, where atoms act as microscopic test masses. The sensitivities of these devices have been shown to be as good as $2 \cdot 10^{-8}$ m/s^2/$\sqrt{\text{Hz}}$ for local gravity measurements (Peters et al. 1999) and $8 \cdot 10^{-8}$ rad/s/$\sqrt{\text{Hz}}$ for rotation rates (Stockton et al. 2011).

Compared to light interferometers atomic Sagnac interferometers have an intrinsic large sensitivity for rotations, which allows for performing rotation measurements with smaller areas enclosed by the interferometer. Common to all atomic devices is the gain in sensitivity by extending the time of free fall of the matter waves and
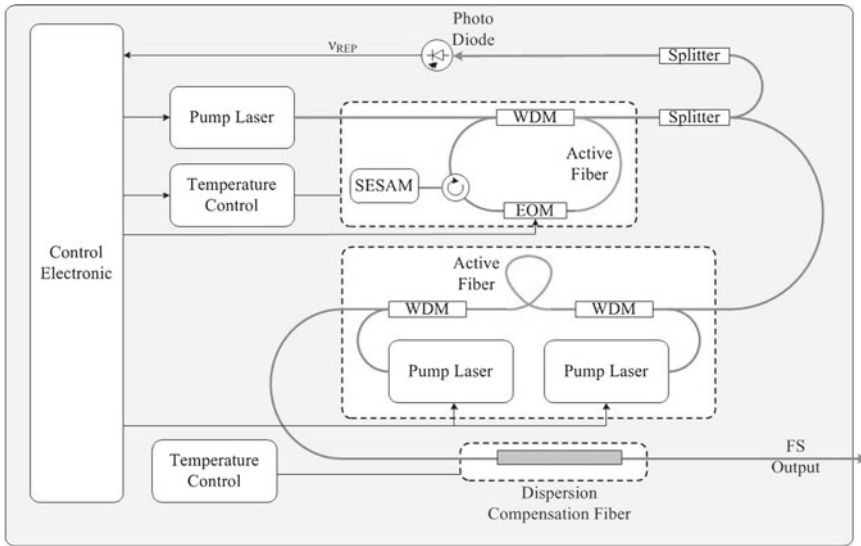
Fig. 21.6 Functional block diagram for the femtosecond laser based heterodyne interferometer (*WDM* wavelength division multiplexing, *EOM* electro-optical modulator, *SESAM* semiconductor saturable absorber mirror)

the reduction of systematic errors by using cold atoms. Atom interferometers have already demonstrated their robustness in campaigns at parabolic flights (Geiger et al. 2011) and prototyping activities in the drop tower at Bremen (van Zoest et al. 2010), where atomic sensors are developed for high precision tests of the Einstein equivalence principle in the extended free fall.

At the Institute of Quantum Optics in Hanover these devices are an important focus of research. Among other activities, the institute develops (i) Sagnac interferometers with laser-cooled atoms (Tackmann et al. 2012), which spans surfaces before only accessible with beams of fast atoms, (ii) a dual gravimeter for testing the Einstein principle of equivalence, which also serves for local gravimetric measurements, and (iii) robust sensors based on atom chips.

21.3.2.5 Summary

The above introduced systems are demonstrating that new optical metrology technologies emerge which are optimized by breadboard activities and further qualification processes for future use in space systems. These developments will result in a significant increase in precision and accuracy for application in geo research. The decision, whether CW laser systems, pulsed laser systems or a combination of both is to be used will be determined by corresponding mission requirements. In any case,
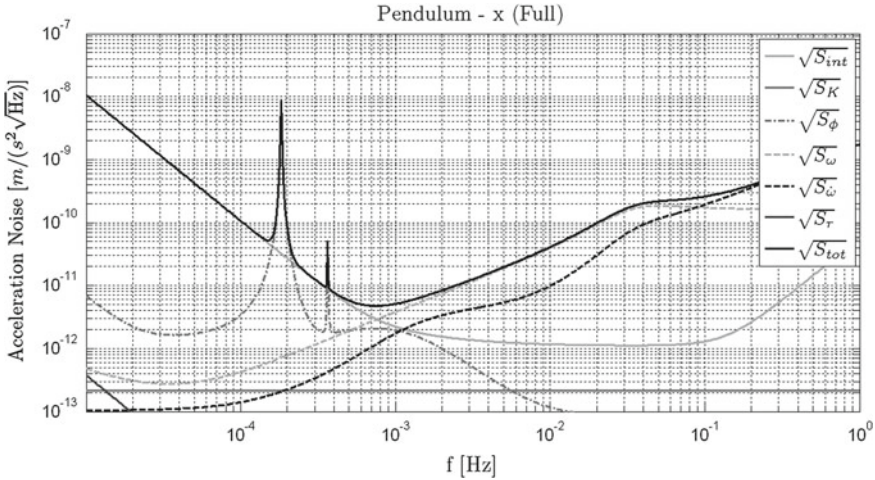
Fig. 21.7 Total acceleration measurement noise along SST-reference direction (x) for $r_A = 1\,\mathrm{cm}$ and 0.05 Hz attitude control bandwidth including cyclo-stationary components. Individual contributions correspond to the terms in Eq. (21.10)

the versatility of these metrology techniques enables new possibilities to realize even complex research missions.

21.3.3 Inertial Sensor Positioning and Gravitational Reference Point

As pointed out in Sect. 21.2.4 a special focus was put on the acceleration measurement performance due to the low orbits (DC range) and the periodic motion (noise couplings) of the FGM scenarios. Recalling Eq. (21.8), additional apparent accelerations are measured whenever an offset between S/C CoM and the test mass is present. Concerning the DC range of the accelerometers, even large offsets ($>10\,\mathrm{cm}$) do not contribute significantly and the need for drag compensation is caused by the dominating external disturbance acceleration. From a DC point of view, the location of the sensor is consequently uncritical (compare also GOCE where the individual sensors are located 0.25 m from the S/C CoM (Marque et al. 2008)). However, concerning the noise budget—evaluated using the performance models described in Sect. 21.2.4— even the coupling of comparably small offsets ($<1\,\mathrm{cm}$) with angular acceleration and angular velocity noise (dashed contributors in Fig. 21.7 exemplary for the conservative pendulum scenario) leads to dominating contributions over large parts of the measurement bandwidth.

At its upper end (around 20 mHz) the noise reaches up to about $100\,\mathrm{pm/(s^2\sqrt{Hz})}$ which is two magnitudes above the internal sensor noise level and results in a sig-

nificant degradation of the science performance.[4] Trades concerning the attitude controllers have been carried out to decrease these couplings but the impact can only be mitigated to some extent (e.g. due to limitations in the available controller bandwidth).

An exact determination of the S/C CoM is difficult as it is varying over the mission lifetime. For GRACE this issue is handled using dedicated calibration procedures and adapting the S/C CoM with a mass-trim system to align it with the accelerometer CoM. Apart from additional system complexity and cost, a further drawback of this principle is a repeated interruption of the science measurements. Based on the experience gained in other projects, a different approach came up during the study: The selection of the S/C CoM as reference for the measurement as inherited from GRACE is typical, but it is not unique. The 'requirements' on the gravitational reference point can be summarized as follows:

- the non-gravitational accelerations must be known or measureable
- the SST metrology measurement must be properly linked to it
- its equations of motion have to be affected by the S/C dynamics
- the inertial position must be known (for 'geolocation' of the measurement)

These statements also hold if the CoM of the accelerometer TM is chosen as reference point but with dedicated advantages compared to the 'traditional' approach.

Concerning the non-gravitational accelerations, Eq. (21.8) is still valid as the whole system is physically unchanged, i.e. the apparent accelerations coupling with the S/C CoM offset are still present. However, their interpretation is different. While being a measurement error that has to be corrected for when using the S/C CoM as reference, they now turn directly into desired accelerations to be measured (i.e. these accelerations are only present due to the electrostatic suspension of the test mass to the sensor housing/satellite, thus disturbing the purely gravitational 'free-fall' of the test mass). The consequences for the performance budget are significant, as the aforementioned dominating contributions are basically nulled, leaving a noise floor at the level of the sensor intrinsic noise over a wide frequency range.

Another advantage is the mapping of the distance measurement of the SST metrology. Under the reasonable assumption that laser metrology and accelerometer are mounted on a common optical bench, the relative distance between accelerometer test mass CoM and metrology phase center both are well known and highly stable. Again there is no extra effort with the alternative approach, as the metrology phase center is generally different from the S/C CoM and the distance would have to be referred to a different point anyway. The third 'requirement' that the equations of motion of the reference point have to be affected by the S/C dynamics rises from the fact that the SST distance variation is affected by forces and torques acting on the S/C only. Thus, for a proper combination of the two main measurements this also

---

[4] Note that the peaks at once and twice the orbital frequency in the coupling with pointing noise (dash-dotted line) exceed the internal noise level by far as well and originate from cyclo-stationary noise. However, this contribution is hardly affected by the CoM offset and according to QLT analysis the noise power does not significantly degrade the science performance.

has to hold for the accelerometer test mass CoM. In fact, it is realized by its electrostatic suspension to the sensor housing, except for the direct 'bias' forces acting on the test mass which are not 'seen' from the laser metrology and accounted for in the SST measurement.[5] However, this systematic error is also present in the traditional approach using the S/C CoM as measurement, as it cannot be individually be determined (i.e. separated from the external acceleration on the S/C) and as the accelerations under consideration are very small (in the order of some pm/s^2). Finally, concerning determination of the reference points' inertial position for 'geolocation' and orbit determination, there is no major difference when using the accelerometer CoM as reference, one could even expect a slight improvement due to better relative position knowledge with respect to the navigation sensors.

The idea of selecting a gravitational reference point different to the S/C CoM is not generally new and has been applied or considered in several missions and studies. During the Hyper study analyses were carried out concerning the selection of an arbitrary 'drag-free-point' within the S/C body (Szerdahelyi et al. 2003). The LISA Pathfinder mission (Bortoluzzi et al. 2005) realizes a drag-free motion of two 'out-of-CoM' free-flying test masses in selected degrees of freedom.

Parallel to the FGM study development, we discovered that for the BepiColombo mission a similar principle is realized (Iafolla et al. 2011) which is based on considerations described in Milani and Gronchi (2010) pointing out that writing the equations of motion for the accelerometer are simpler than the ones for the S/C CoM, and they do no longer depend on the position of the latter. However the approach is new to a SST type gravity mission with dedicated advantages even compared to the one for BepiColombo. While there 3 one-axis spring accelerometers are used, a mapping to an artificial common reference point is a required compromise. Thus—although a good knowledge of its position exists—it is still necessary to correct for dynamic coupling terms (thus angular rate and accelerations have to be measured sufficiently accurate) which is not required with a single three-axis sensor as foreseen for the SST mission. In addition, BepiColombo is one single satellite whose orbit is observed via radiometric tracking. Thus also accurate knowledge of the inertial orientation is of great importance for proper 'orientation' of the measurements in the post-processing. In the SST case—for the relevant projection on the line-of-sight—accurate relative attitude is necessary which can be provided with high quality from the differential wave front sensing signals (full 3-axis inertial orientation is still available from state-of-the-art star trackers).

Actually, the selection of the proposed alternative reference points seems a very promising approach in combination with the 'virtual corner cube principle' foreseen for the laser metrology on GRACE Follow-on (Sect. 21.3.2.1 or Sheard et al. 2012)

---

[5] At first glance the contributions of the apparent accelerations (i.e. the angular velocities and accelerations coupling with the CoM offset) may seem uncovered by the SST distance metrology. However, the metrology phase center is subject to the same extent to the S/C rotation (in terms of pointing with its respective lever arm to the S/C CoM), i.e. the contribution is implicitly covered. For this reason treating metrology and accelerometer budgets as fully uncorrelated leads to conservative results as there is in fact a certain degree of correlation.

although this approach originated from a necessary compromise due to limited available space (the laser metrology is experimental, no main payload). It basically allows placing the effective phase center of the metrology at an arbitrary location. If this location is chosen to be the accelerometer test mass CoM, theoretically no further correction or mapping of the main measurements is necessary.

A possible limitation of this approach is the possible effort of the integration in the existing post-processing algorithms for the gravity field recovery as they currently all rely on the traditional approach and an assessment of this issue in the context of further studies is proposed.

21.3.4 From Initial to Final Selected Scenarios

The selection and geodetic validation of possible mission scenarios is a central task in the FGM design. However, the search space for mission design consists of an enormous amount of parameters, which can be dealt only with effective tools and strategies for its reduction, as e.g. QLTs and genetic algorithms. In Sect. 21.3.4.1 the strategy for mission selection is outlined and 8 scenarios (6 basic + 2 extended) for further evaluation are suggested. These scenarios are analyzed by two independent full-scale simulation tools in Sect. 21.3.4.2. Finally, the results from the full-scale simulations are validated from science viewpoint concerning geophysical signals of interest such as hydrology, ice and solid Earth in Sect. 21.3.4.3. Based on these evaluations two final scenarios for further consideration and investigation of the technological satellite system and metrology design are selected.

21.3.4.1 Strategy of Mission Selection

The development of an advanced future gravity field mission for time variable gravity field recovery is a difficult task. Numerous options exist to improve the performance, accuracy and sensitivity compared to GRACE. Besides technological progress in satellite system and metrology a variety of geodetic parameters exist which can be tuned in order to improve the mission. These geodetic parameters include the orbit height, the satellite distance, the inclination, the repeat mode, the sensor type, the formation and a possible multi-satellite/formation mission. Especially the last two options—advanced formations and multi-formation missions—are regarded as the key instruments to improve the main weaknesses of GRACE, which are (i) North-South striations caused by anisotropy of the measurements and (ii) aliasing due to temporal undersampling of time-variable signals. By means of advanced formations, which are able to detect signals different from the along-track-direction a higher isotropy and sensitivity is reached and striations might be reduced or avoided. Aliasing might be reduced by multi-formation missions, which improve the temporal/spatial sampling.

In the context of finding optimal scenarios, a variety of studies were published in the last years. For instance, Sharifi et al. (2007) compared the performance of

various formation types. Wiese et al. (2009) investigated the performance of 2 and 4 satellite inline and cartwheel missions. In two ESA funded studies the capability of single inline formations and multi inline-formation missions with identical and different inclinations (Bender-design (Bender et al. 2008)) was studied (van Dam et al. 2008; Visser et al. 2010; Reubelt et al. 2010) as well as the performance and technical realization of different formations and two satellite pairs in Bender design (Anselmi et al. 2011). The arrangement of a second, inclined satellite pair in a Bender design was the objective of a publication by Wiese et al. (2011), where a Monte-Carlo method was applied to deal with the enormous search space. A similar study based on genetic algorithms, also allowing a pendulum formation for the inclined pair, was performed in Ellmer (2011). Besides these investigations other publications exists (e.g. Elsaka and Kusche 2010; Iran Pour et al. 2013) where the concepts of alternative formations and two-satellite pair missions are picked up. As a common result, all these studies show that a significant increase in accuracy and sensitivity is expected by alternative formations and two-satellite pair missions in Bender-design.

Based on these results, a pendulum, cartwheel and LISA-like helix formation have been selected as basic mission scenarios as well as a two-inline-formation mission in a Bender design. For the latter, the inclination I for the second pair was chosen as $I = 63°$ (Anselmi et al. 2011; Bender et al. 2008) although (Wiese et al. 2011) suggest an inclination between $70°$ and 75. The suggestion from Ellmer (2011), where the second pair should be established as a pendulum ($\rho_x = 225$ km, $\rho_y = 75$ km) on an inclined orbit ($I = 58°$), was discarded due to the technical complexity. As a reference for the evaluation of these basic missions, two scenarios similar to the current GRACE mission (orbit height $h \approx 460$ km, SST range $\rho \approx 220$ km) and the recently approved GFO (a moderate pendulum on $h = 420$ km with $\rho_x = 220$ km and $\rho_y = 25$ km) were added to the basic missions.

The task is then to select optimal orbit (orbit height h, inclination I, repeat mode β/α (β revolutions in α days)) and formation parameters (satellite distance ρ (or ρ_x), in case of a pendulum additionally the maximum cross-track distance ρ_y, and for the helix the along-track offset $\rho_{x-\text{offset}}$, see Sect. 21.2.1). Ideally, in order to identify suitable parameters, a vast amount of time-consuming full-scale gravity retrievals have to be performed in order to take all effects, especially the severe aliasing, into account. To reduce the search space dramatically, QLTs (Sect. 21.2.1) are of great benefit (Reubelt et al. 2011). While the QLT for sensitivity analysis are powerful to identify the sensitivity of orbit/formation parameters, the aliasing analysis QLT (reduced-scale tool) is additionally very helpful in identifying suited repeat modes.

At first the SST distance ρ and the orbit height h are investigated by the semi-analytic QLT (Sneeuw 2000) for an inline formation on a polar orbit assuming a noise scenario of a future laser and accelerometer/drag-free system (Anselmi et al. 2011; Sheard et al. 2012). As depicted in Fig. 21.8, the best geodetic sensitivity is reached for a large SST distance and a low orbit height. However, a low orbit height is problematic due to a higher air drag limiting the mission lifetime and a large satellite distance faces problems with the laser technology (pointing issues, signal strength, noise). Thus, an orbit height of $h = 350$ km and a satellite distance of $\rho = 100$ km seem to be a good compromise between geodetic sensitivity and technological feasibility. Furthermore

Fig. 21.8 shows that the increase of accuracy is quite low for SST-distances larger than 100 km, where the impact of the distance dependent laser noise becomes more important.

A series of investigations show that the ground track coverage and choice of repeat mode can have an influence on the quality of retrievals. For instance Visser et al. (2010) obtain better results for a (79/5) repeat orbit compared to a (125/8) repeat cycle for short time solutions (5-8 days), and Wiese et al. (2011) concluded that 13 day repeat orbits are an optimal choice for Bender-type constellations. Wagner et al. (2006) showed that large unobserved gaps caused by short repeat cycles degrade GRACE-solutions seriously. A similar observation was made in Iran Pour et al. (2013) in future mission studies. Here, it was suggested to choose longer repeat modes (e.g. 32 days) to guarantee a dense spatial sampling in monthly solutions. Simultaneously, a homogeneous ground track gap evolution should be selected and large unobserved gaps in the ground track evolution should be avoided. In order to select optimal repeat cycles, the gap evolution graph (Anselmi et al. 2011, Iran-Pour et al. 2013) and the aliasing analysis QLT are helpful. Figure 21.9 shows gap evolution graphs for two repeat orbits. While the (503/32) repeat cycle shows a homogeneous gap evolution with a mild subcycle and pseudo-subcycles of 7 and 4 days, respectively, the drifting (511/32) orbit shows large unobserved gaps over the whole time evolution. In Iran Pour et al. (2013) a variety of repeat patterns is analyzed with the aliasing analysis QLT. As a result, a homogeneous gap evolution is not only important for a full repeat cycle recovery, but also for the estimation of short time interval solutions (3–6 days). The (503/32) repeat orbit, originally suggested by Anselmi et al. (2011) thus is a good choice and fulfills the assumptions on the orbit height with $h \approx 335$ approximately.

Concerning the inclination a near polar orbit ($I = 89.5°$) is chosen to avoid larger polar gaps for the benefit of ice studies. For the inclination selection of the second pair in a Bender-type mission, the semi-analytic QLT can be applied. Figure 21.10 shows the corresponding geoid errors for 5° steps in the interval [45°, 90°]. As a
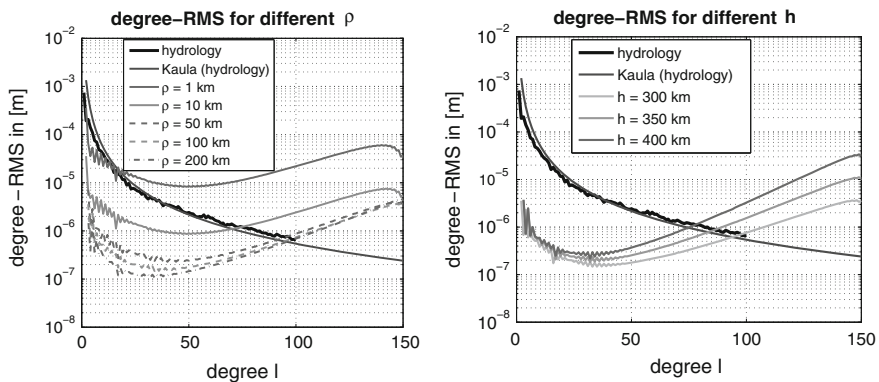

Fig. 21.8 Impact of different SST distance and orbit height on the accuracy of the gravity field recovery

result, $I \approx 65°$ is a good choice, which proves the assumptions made in Bender et al. (2008) and Anselmi et al. (2011).

The application of QLT for sensitivity analysis is also very helpful for the selection of suited formations and formation parameters. Although the (average) SST-distance was already selected as $\rho_{avg} = 100$ km, for some of the formations additional parameters have to be determined, as e.g. the maximum cross-track distance for the pendulum, and the along-track offset for the helix. Figure 21.11 displays the relative movement of the advanced formation designs in the Hill-system. Obviously, these formations contain additional measurement components compared to the inline formation. As visible, the pendulum adds cross-track information over equatorial regions while the cartwheel is sensitive for radial information. The LISA-formation is a combination of both and thus gathers both cross-track and radial information. In general, the feasibility of the LISA-formation is regarded as problematic due to the rotating yaw-/pitch-angle. Thus a LISA-like formation with an along-track shift—the helix—is introduced, which unfortunately contains again a dominant along-track component. It is expected that the advanced formations will lead to a higher isotropy and thus an improved sensitivity.

Figure 21.12 (left side) shows the performance in terms of geoid errors for pendulums with different opening angles. Based on this result, an optimal choice would be $\alpha \approx 40°-60°$, but even angles $\alpha > 20°$ show a strong improvement compared to the inline-formation. Figure 21.13 displays the formal errors and spatial correlation functions for different opening angles. It can be seen, that a larger opening angle leads to a higher homogeneity of the formal errors (i.e. improvement of higher orders such that the errors of coefficients of one degree are more similar) and to a larger isotropy of the spatial correlation.

Finally, Fig. 21.12 (right side) shows a comparison in terms of degree-RMS for the mentioned formation types with an average SST distance $\rho_{avg} = 100$ km. All advanced formations show an improvement of up to one order of magnitude compared
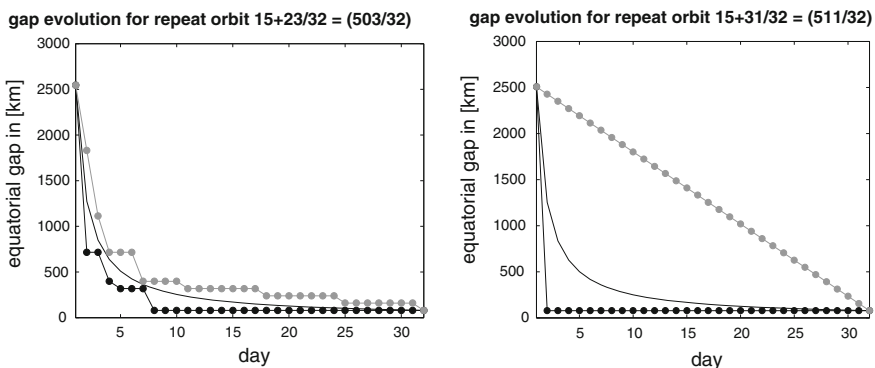
Fig. 21.9 Gap evolution (maximum gap: *grey circles*; minimum: *black circles*; average: *black line*) for two different repeat orbits

Fig. 21.10 Geoid errors for different inclinations of the second pair in a Bender-type mission, estimated with the semi-analytic QLT; noise PSD level $= 10^{-10}\,\mathrm{m/s^2}/\sqrt{\mathrm{Hz}}$
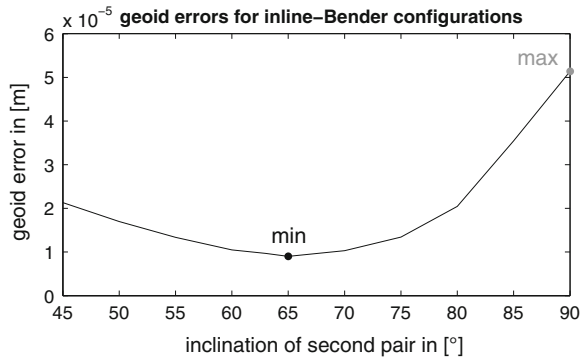

to the inline formation, and an improvement in the homogeneity and isotropy (not shown here). The pendulum shows the best performance, the performance of the helix is reduced by a factor of ≈ 2 compared to the LISA formation.

However, from technological side of view, the implementation of these advanced formations is quite complex and critical. Among other problems, especially two mission constraints (see Sect. 21.1.3) were considered:

(1) the maximum range-rate should be kept within ± 10 m/s.
(2) the line-of-sight angle between the two satellites should be kept within $\pm 30°$ in yaw-/pitch-direction.

The fulfillment of the first constraint enables the application of heterodyne lasers for the SST-link (Sheard et al. 2012), which are already in an advanced technological readiness-level (TRL, see Sect. 21.3.2). The second constraint is important to keep the energy-consumption in a moderate state and thus enable suited mission lifetimes. However if the range-rates and yaw-/pitch-angles of the advanced formations are analyzed (Reubelt et al. 2011), the advanced formations of Fig. 21.11 exceed these constraints by far. By tuning the formation parameters it is possible to design pendulums fulfilling these constraints, and by considering additional inertial orientation criteria, also cartwheels can be kept within the constraints. However, the constraints should not be considered as a fundamental restriction for all formations due to possible future developments. For instance, the frequency-comb technology (Sect. 21.3.2.2) shows restrictions only in the km/s-level. However, the TRL for ll-SST application is quite low and a comparable performance to pure heterodyne lasers is not proved so far. In detail, the following selections are made:
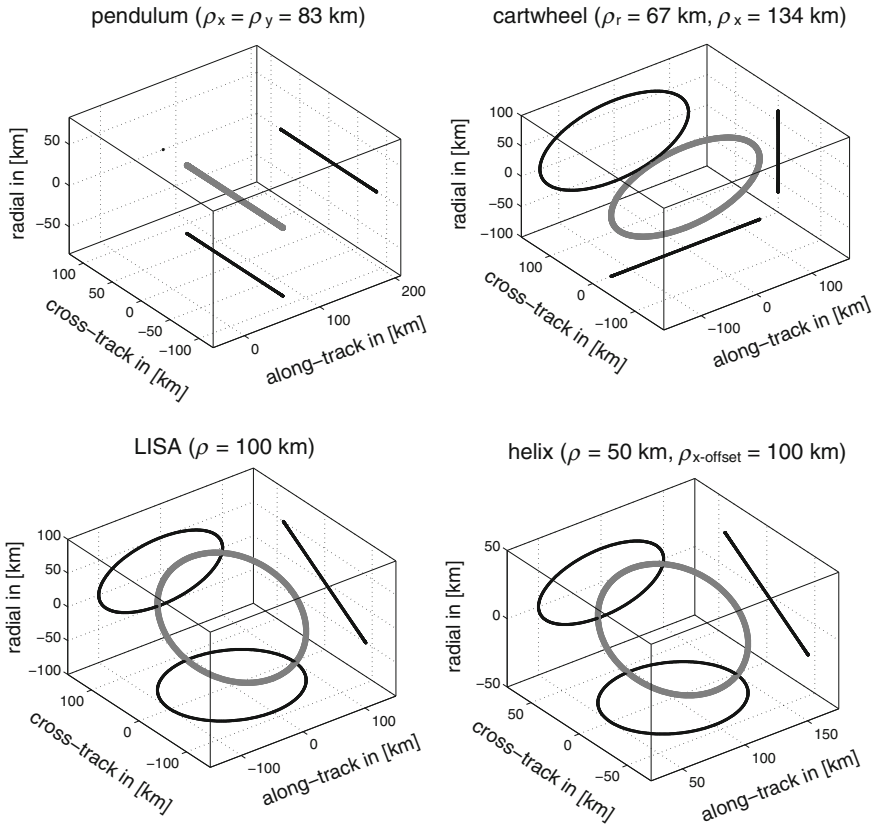
Fig. 21.11 Relative movement of advanced formations in the Hill system, assuming an average inter-satellite distance of $\rho_{avg} = 100$ km

(i) Pendulum

The above pendulum features maximum range-rates of ± 40 m/s and yaw-angles of $45°$, respectively (Reubelt et al. 2011). Both values can be controlled by reducing the cross-track component and/or the average satellite distance. Two options are considered to meet the range-rate limits: (i) applying a maximum yaw angle of $30°$ and downscaling the average range to <100 km or (ii) selecting a maximum yaw angle $<30°$ such that an average range of 100 km can be maintained. Here the more promising case (ii) with the larger satellite-distance is chosen due to the strong dependence of the sensitivity on the satellite distance (Fig. 21.8) resulting in the formation parameters $\rho_x = 96$ km, $\rho_y = 43$ km and $\alpha = 24°$. Obviously such a pendulum leads to less isotropy (Fig. 21.13), but still provides an improvement of half an order of magnitude compared to an inline-formation (Reubelt et al. 2011). For completeness it is mentioned that such a pendulum shows the highest sensitivity
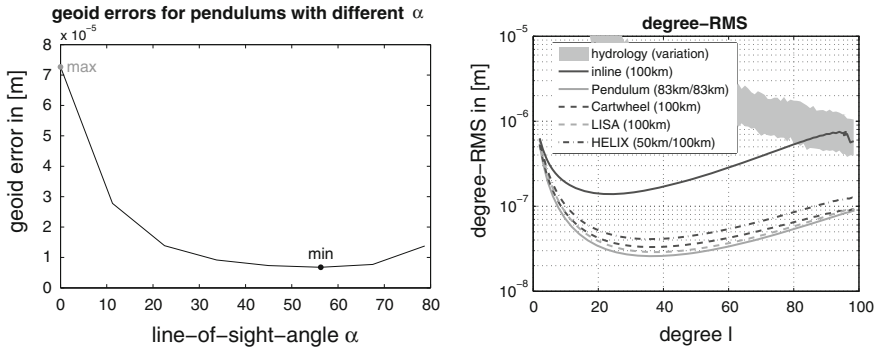
Fig. 21.12 *Left* geoid errors for pendulums with different maximum opening angle α; *right* degree-RMS for various formations with an average SST distance $\rho_{avg} = 100$ km; noise PSD level $= 10^{-10}\,\mathrm{m/s^2}/\sqrt{\mathrm{Hz}}$
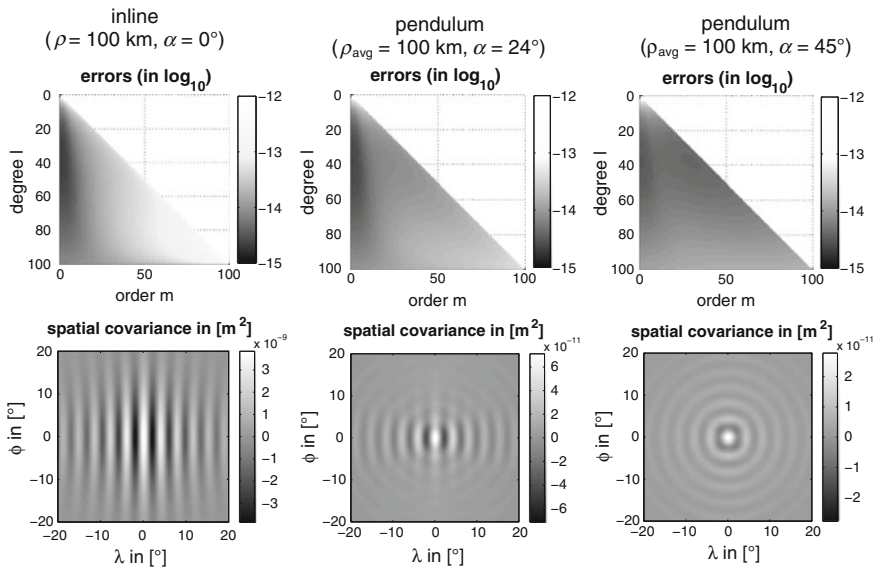
Fig. 21.13 Formal errors and spatial covariance functions (at the equator) for pendulums with different opening angles α; $\rho_{avg} = 100$ km; noise PSD $= 10^{-10}\,\mathrm{m/s^2}/\sqrt{\mathrm{Hz}}$

of all formations strictly adapted to the constraints (Reubelt et al. 2011) and seems the most preferable option from technological point of view.

(ii) Cartwheel

The cartwheel exhibits maximum range rates of ±75 m/s and pitch-angles $360°$ per Earth revolution (Reubelt et al. 2011). Obviously, the pitch-angle can only be kept within the limits if it is regarded within the space-fixed system, where it stays within $\pm20°$. However only cylindrical or spherical satellites with a similar drag

coefficient in every possible air-drag direction seem to be an option with serious technical problems still remaining (e.g. power, sensor blinding or ground link). The constraint for the maximum range-rate can be met, if the SST-distance is downscaled significantly to approximately 15 km. However, due to the considerably decreased sensitivity for short baselines (see Fig. 21.8) such a cartwheel performs worse than an inline-formation with $\rho = 100$ km (Reubelt et al. 2011) and thus is no option. Assuming future technology developments (e.g. frequency-comb systems) a cartwheel with a larger baseline of $\rho_{avg} = 75$ km is chosen.

(iii) LISA and helix

The LISA-formation seems to be perfect regarding the range-rate since it has almost no dynamical range. However, the yaw- or pitch-angles cannot be kept within the limits, neither in the Hill-system nor in the space-fixed system. Furthermore, due to the perigee-drift of about 4° for a near polar orbit (caused by the Earth's flattening), the circular motion will deform to an elliptic motion for certain periods, which will lead to large range-rates similar as for the cartwheel. Thus this formation was discarded. However, by shifting the second satellite of a LISA formation in along-track direction it is possible to keep the yaw-/pitch-angles inside the constraints, but on the cost of sensitivity. Furthermore, the range-rate constraints are fulfilled only for a very short SST-distance ($\approx$15 km) or if the maximum cross-track/radial components are reduced considerably which leads to a severe loss of sensitivity (Reubelt et al. 2011). Thus, under the same technological assumptions as for the cartwheel, a helix with an along-track offset of 100 km and a circular LISA motion of 50 km (corresponding to $\rho_{avg} \approx 106$ km and maximum range-rates of about $\pm$ 60 m/s) is chosen.

The orbit and formation parameters of the six selected basic missions are displayed in Table 21.5. As ll-SST metrology the standard K-band link is assumed for GRACE, a heterodyne laser for GFO, pendulum and inline-Bender and frequency-combs or advanced lasers for cartwheel and helix. For the simulations the noise level of the heterodyne laser and frequency combs was assumed to be equal and the noise time series were generated using an average satellite distance of 100 km. The advanced missions assume drag-free/-compensation technology and thus higher accuracy compared to GRACE Super-STAR accelerometer measurements.

The performance of the six basic missions was evaluated by QLT simulations in Fig. 21.14 (sensitivity and aliasing tool) and finally by full-scale simulations in Sect. 21.3.4.2, taking all error sources into account. All three kinds of analysis indicate a similar relative behavior of the six basic missions, although clear differences show up on the absolute level. Concerning the QLT results in Fig. 21.14, a significant increase in the absolute error level for the laser-missions can be observed from the results of the aliasing analysis tool compared to those of the sensitivity analysis tool (especially for degrees below 50). This shows that the aliasing error is above the laser noise. In contrast, the error curves for GRACE as reference (using K-band ranging and Super-STAR sensors) are similar for both QLT which indicates that the K-band measurement noise is the dominant error source in this case. Thus an improvement of the error level of about two orders of magnitude by laser/drag-free systems, as suggested by sensitivity analysis, seems not feasible with the current knowledge

Table 21.5 Basic missions and their parameters (unmentioned parameters are zero)

| Scenario	Orbit parameters	Formation parameters	Mean Kepler elements (absolute, differential)
GRACE (as reference)	$h \approx 460$ km non-repeat $I = 89°$	$\rho = 220$ km	$\Delta a = \Delta e = \Delta i = \Delta \omega = \Delta \Omega = 0,$ $\Delta M = 1.8453°$
GRACE-Follow-On	$h \approx 420$ km $\beta/\alpha = 478/31$ $I = 89°$	$\rho_x = 220$ km $\rho_y = 25$ km $(\rho_{avg} = 221$ km$)$	$\Delta a = \Delta e = \Delta i = \Delta \omega = 0,$ $\Delta \Omega = 0.2248°, \Delta M = 1.8453°$
Pendulum (conservative)	$h \approx 335$ km $\beta/\alpha = 503/32$ $I = 89.5°$	$\rho_x = 96$ km $\rho_y = 43$ km $(\rho_{avg} = 100$ km$)$	$\Delta a = \Delta e = \Delta i = \Delta \omega = 0,$ $\Delta \Omega = 0.3670°, \Delta M = 0.8194°$
Cartwheel	$h \approx 335$ km $\beta/\alpha = 503/32$ $I = 89.5°$	$\rho_{avg} = 75$ km	$\Delta a = \Delta e = \Delta i = \Delta \Omega = 0,$ $\Delta \omega = \Delta M = 180°$ $e_1 = 3.72\text{e-}3$
Helix	$h \approx 335$ km $\beta/\alpha = 503/32$ $I = 89.5°$	$\rho_{LISA} = 50$ km $\rho_{x-offset} = 100$ km $(\rho_{avg} = 100$ km$)$	$\Delta a = \Delta e = \Delta i = 0, \Delta \Omega = 0.3696,$ $\Delta \omega = -180.8535°, \Delta M = 180°$ $e_1 = 1.862\text{e-}3, \omega_1 = 0.4268°$
Inline-Bender	$h \approx 335$ km/352 km $\beta/\alpha = (503/32)/(481/31)$ $I = 89.5°/63°$	$\rho = 100$ km	$\Delta a = \Delta e = \Delta i = \Delta \omega = \Delta \Omega = 0,$ $\Delta M = 0.8993°$

of background models and is restricted to approximately one order of magnitude. A comparison between the aliasing analysis QLT and full-scale simulations (internal document) shows that the QLT is too optimistic (up to half an order of magnitude for high degrees), but shows similar characteristics.

Finally, full-Scale Simulation analysis (Sects. 21.3.4.2 and 21.3.4.3) shows that the results can be classified in three quality groups: (i) *lower quality group* with GRACE and GFO, where the latter shows an improvement up to one order of magnitude for the higher degrees, (ii) *medium quality group* with the advanced formations in lower orbit of conservative pendulum, cartwheel and helix, showing an improvement of up to one order of magnitude compared to GFO and (iii) the *high quality group* consisting of the inline-Bender mission, showing a further improvement of a factor 2-3 over the whole spectrum, even for the degrees below 40.

Based on these results, it was decided to select the *conservative pendulum* as final scenario no. 1 of Sect. 21.4. The reason is that already a similar performance as for the cartwheel and helix was reached, while the constraints for range-rate and maximum yaw-/pitch angle are still fulfilled. By increasing the pendulum angle, which contradicts the constraints in a similar way as the cartwheel and helix, a further improvement in accuracy seems possible, outperforming these two formations. The promising inline-Bender mission was discarded for the Final Scenarios, since it is always an option due to its high TRL (two inline-formations, laser link). In contrast, it is of interest to concentrate investigations on advanced formations due to two reasons: (i) possible reductions of costs of an advanced pendulum with similar performance
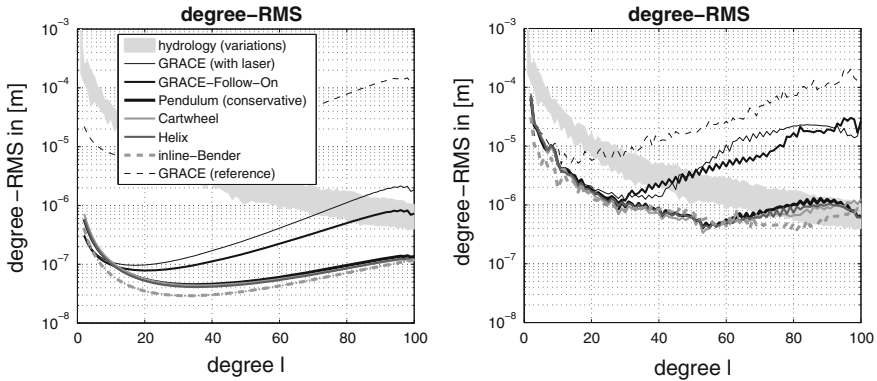
Fig. 21.14 Quick-look analysis of the six basic missions including a GRACE-like scenario using a laser-link. *Left side* sensitivity analysis tool; *right side* aliasing analysis tool
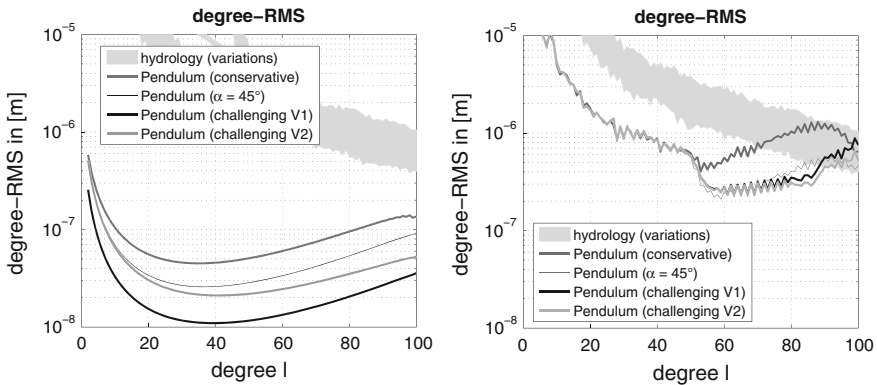
Fig. 21.15 Performance analysis of various pendulums by means of QLTs. *Left side* sensitivity analysis tool; *right side* aliasing analysis tool

compared to the costs caused by the 4 satellites of the inline-Bender mission and (ii) a further gain in accuracy by replacement of one of the inline-formations within a Bender design by a pendulum.

Based on these considerations a *challenging pendulum* with larger pendulum angle of $\alpha = 45°$ and a lower orbit height $h \approx 300$ km was selected as final mission no. 2.

The performance of different options for challenging pendulums is investigated by QLTs in Fig. 21.15. As visible from the sensitivity analysis on the left side, an increase of the pendulum angle to $\alpha = 45°$ (Pendulum, $\alpha = 45°$) leads to an improvement of a factor 2–3. If the orbit height is reduced additionally to $h \approx 300$ km (Pendulum (challenging V2)), a further increase for higher degrees seems possible. Increasing also the average SST distance to $\rho_{avg} = 200$ km (Pendulum (challenging V1)) an additional improvement of a factor 2-3 shows up. However, taking also aliasing into account (Fig. 21.15, right side), the extension of the pendulum angle has the most

impact, while the influence of the lower orbit height and the larger SST distance seems quite low. The two challenging pendulum versions V1 and V2 were in addition analyzed by full-scale simulations in Sect. 21.3.4.2. There, the impact of the larger SST distance proves also to be low, thus the challenging pendulum V2 was selected as 2nd Final Scenario. This challenging pendulum shows an improvement compared to the conservative pendulum of about a factor 3 and a similar accuracy as the inline-Bender mission (better for degrees >40, slightly worse below). The orbit/formation parameters of the challenging pendulum (V2) are $h \approx 298\,\text{km}$ ($\beta/\alpha = 507/32$), $I = 89.5°$, $\rho_\text{x} = \rho_\text{y} = 83\,\text{km}$ ($\rho_\text{avg} = 100\,\text{km}$), $\Delta a = \Delta e = \Delta i = \Delta \omega = 0$, $\Delta \Omega = 0.3670°$, $\Delta M = 0.8194°$.

21.3.4.2 Full-Scale Numerical Simulations of Future Gravity Missions

In the following, we provide the gravity field results from full-scale simulations of the mission scenarios defined in the previous section. Accordingly, many tasks corresponding to the optimization of the gravity field determination from future satellite missions have been defined (Elsaka and Kusche 2010; Elsaka et al. 2012). In order to simulate the reality as close as possible colored noise time series from the PSDs of the involved sensors are computed and added to the simulated error free measurements from GFZ. The final full-scale results have been implemented using both the IGG-GROOPS and GFZ-EPOS software systems. Both full-scale results sets are analyzed in the spectral and spatial domain of the gravity field (up to maximum SH degree $L = 120$).

Generating colored noise from sensor PSD
The noise time-series for SST and ACC measurements were generated according to Sect. 21.2.3. Under the simplified assumption that only direct factors like thermal effects affect the sensor performance frequency-dependent noise characteristics are modeled for SST and ACC measurements. Interactions between satellite instruments as well as orbit or attitude dependent factors are not considered. Further details regarding the sensor modeling and the assumptions can be found in Sects. 21.2.4 and 21.2.5 and are recorded in an internal technical note of the project.

In the simulation scenarios the following sensor performances were taken as a basis: For SST measurements the LRI (see Sect. 21.3.2.1) was used. Its performance is modeled in terms of PSD with the distance-dependent factor, i.e. the average distance between two satellites:

$$\sqrt{\text{PSD}_\text{SST}} = \sqrt{\left(50 \cdot 10^{-9}\right)^2 + \frac{100}{f}\left(355 \cdot 10^{-12} \cdot \frac{\rho_\text{avg}}{100\ \text{km}}\right)^2} \cdot 2\pi f \cdot \text{SF} \quad (21.12)$$

Equation (21.12) contains the additional 'safety factor' SF which is set to 2 for the current analysis. The accelerometer noise model is derived from a GRADIO sensor (see Sect. 21.2.4). The full-scale simulations assume three-axis accelerometers of this

type with same high sensitivity on all axes. The underlying SST/accelerometer noise PSDs are represented by the conservative pendulum example in Fig. 21.3. A detailed description of the assumptions on both sensor performances was documented in an internal technical note.

On the basis of sensor PSDs arbitrary time series are generated according to the methods described in Sect. 21.2.3. To get an impression on the magnitude of the generated noise time series an extract is illustrated in Fig. 21.16: The high-frequency SST noise is clearly visible which has a range of about $\pm 2 \cdot 10^{-8}$ m/s. Moreover the much longer wavelength components of the accelerometer noise with a range of up to $\pm 8 \cdot 10^{-10}$ m/s^2 can be identified.

Full-scale gravity field solutions

The results from full-scale gravity field recovery are visualized in terms of error degree-variances in Fig. 21.17, as SH coefficient errors in the triangle plots of Fig. 21.18 and as spatial geoid error maps in Fig. 21.19. The errors are obtained from the difference between output (gravity recovery results) and input (EIGEN-GL04C).

As expected there is a very good agreement between both solution sets from IGG-GROOPS and GFZ-EPOS. Figure 21.17 shows that the gravity solutions of FGM scenarios perform approximately one to two orders of magnitude better than the GRACE reference solution, especially at the short wavelength range. The reason is the contribution of cross-track and radial measurement components of the investigated FGM scenarios in addition to the pure along-track components of a GRACE-like inline-formation which leads to significant improvements in terms of noise levels and a more isotropic distribution of the errors. This is already obvious in Fig. 21.18 which shows the error of each SH coefficient.

Both challenging Pendulum configurations V1 and V2 provide strongest improvements, however, their mission concepts are in demand for further investigations due to the higher relative velocities between the satellites (approx. 80 m/s and 40 m/s for V1 and V2, respectively). Similar improvements have been found for the In-line Bender configuration, which shows a slightly better performance for the
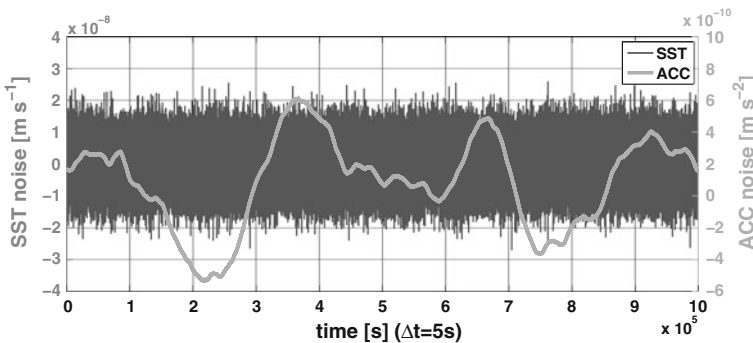
Fig. 21.16 Extract from the generated noise time series of SST and one accelerometer axis by the example of the (conservative) pendulum configuration
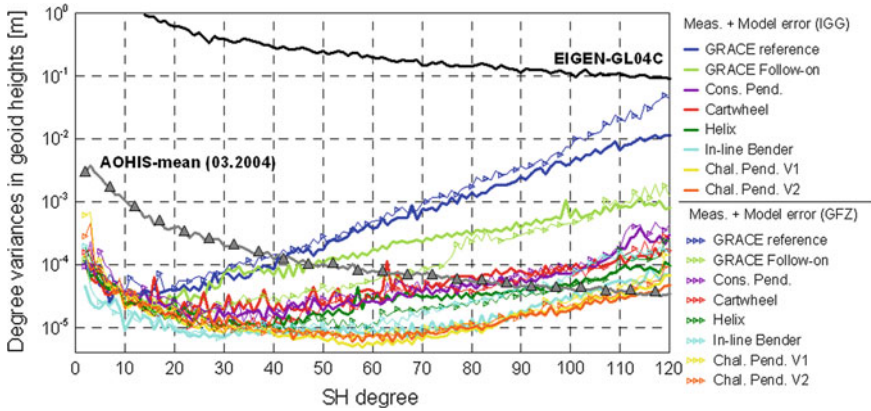
Fig. 21.17 Degree-variances of the six basic missions and two challenging pendulums estimated from IGG-GROOPS (*solid lines*) and GFZ-EPOS (*solid lines* with *triangles*)

longer wavelengths (SH degrees $l < 35$) and slightly worse results for the higher degrees $l > 35$ compared to the challenging pendulums (Fig. 21.17). The isotropy of the error distribution of various FGM solutions can be seen in Fig. 21.19 compared to the GRACE solution which displays strong striping pattern. The In-line Bender configuration shows the most isotropic error distribution of the geoid errors and the best gravity field among the six basic mission scenarios and a comparable behaviour to the challenging pendulums.

The GRACE formation is confirmed to be sub-optimal in terms of gravity field recovery. From the results, the aliasing effects are so far the main problem that will be faced by a future mission, especially for the GRACE Follow-on configuration.

21.3.4.3 Evaluation of Scenarios from Science Viewpoint

To determine the observable geophysical signals of each scenario, a signal-to-noise ratio (SNR) is computed in the SH domain (max. SH degree 120) for each simulated mission described in Sect. 21.3.4.2 and for each subsystem of the underlying geophysical mass transport models Atmosphere (A), Ocean (O), Hydrology (H), Ice (I) and Solid Earth (S) (Gruber et al. 2011). It turns out that the FGM scenarios can be put into three quality groups. The best group showing similar maximum spatial resolutions for AOHIS includes the double pair Bender mission and the two challenging pendulum scenarios V1 and V2.

Signals for the SNR are the monthly mean signals of the five geophysical data sets (AOHIS), noise data comprises the two independently estimated sets (IGG and GFZ) of SH coefficient errors. The results are SNRs in the SH domain from which spatial resolutions are derived. These resolutions are computed by dividing the Earth's circumference by two times the maximum SH degree at which the SNR exceeds 1.
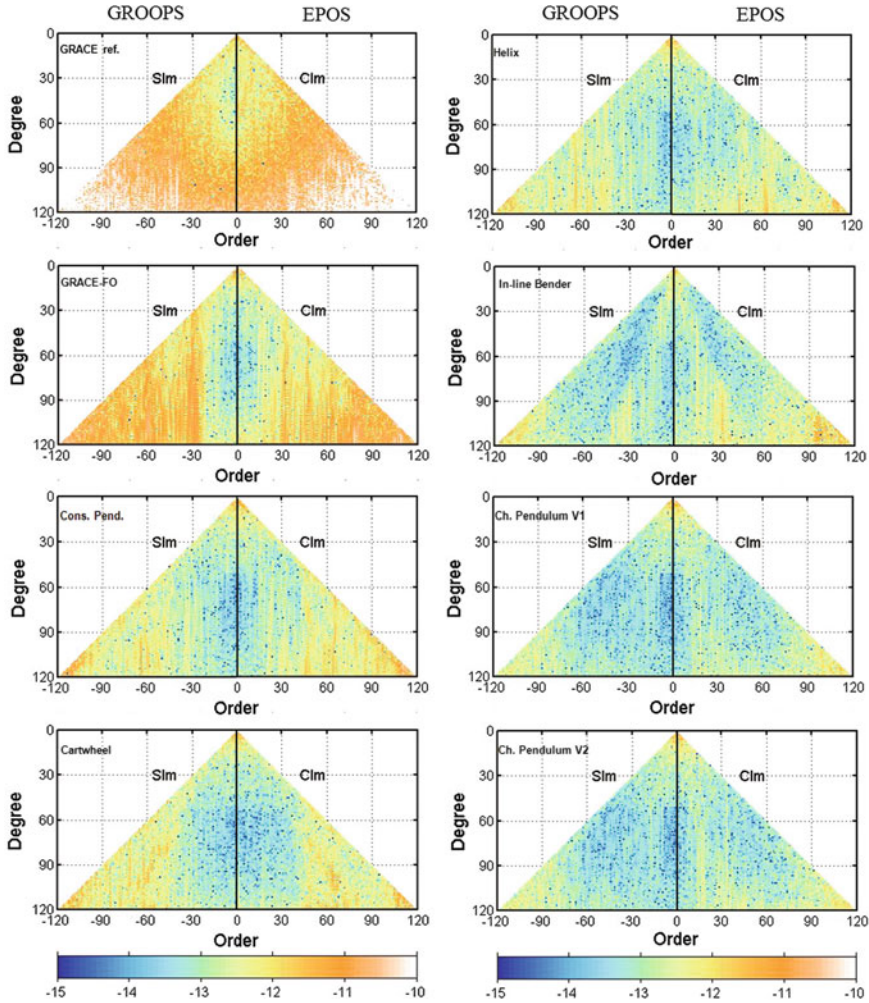
Fig. 21.18 Triangle plots of SH coefficient obtained from full-scale retrievals of the FGM scenarios. The *left half* of each triangle (s_{lm} errors) are from IGG-GROOPS and the *right half* (c_{lm} errors) are from GFZ-EPOS. Note that one half of a triangle plot is already representative for the error due to the similarity of s_{lm} and c_{lm} errors

On the other hand the average SNR up to the maximum SH degree where SNR > 1 provides a significance level of the observability of the different geophysical signals.

The missions with the lowest errors for most of the SH degrees are the two challenging pendulum versions (V1 and V2). Their errors remain below the mean AOHIS signal until SH degree 110. Figure 21.20a, b shows SH degree geoid errors compared with the five mean signals of AOHIS for the challenging pendulum V1 scenario. In (c) and (d) simple divisions of the mean signals by the errors as a SH
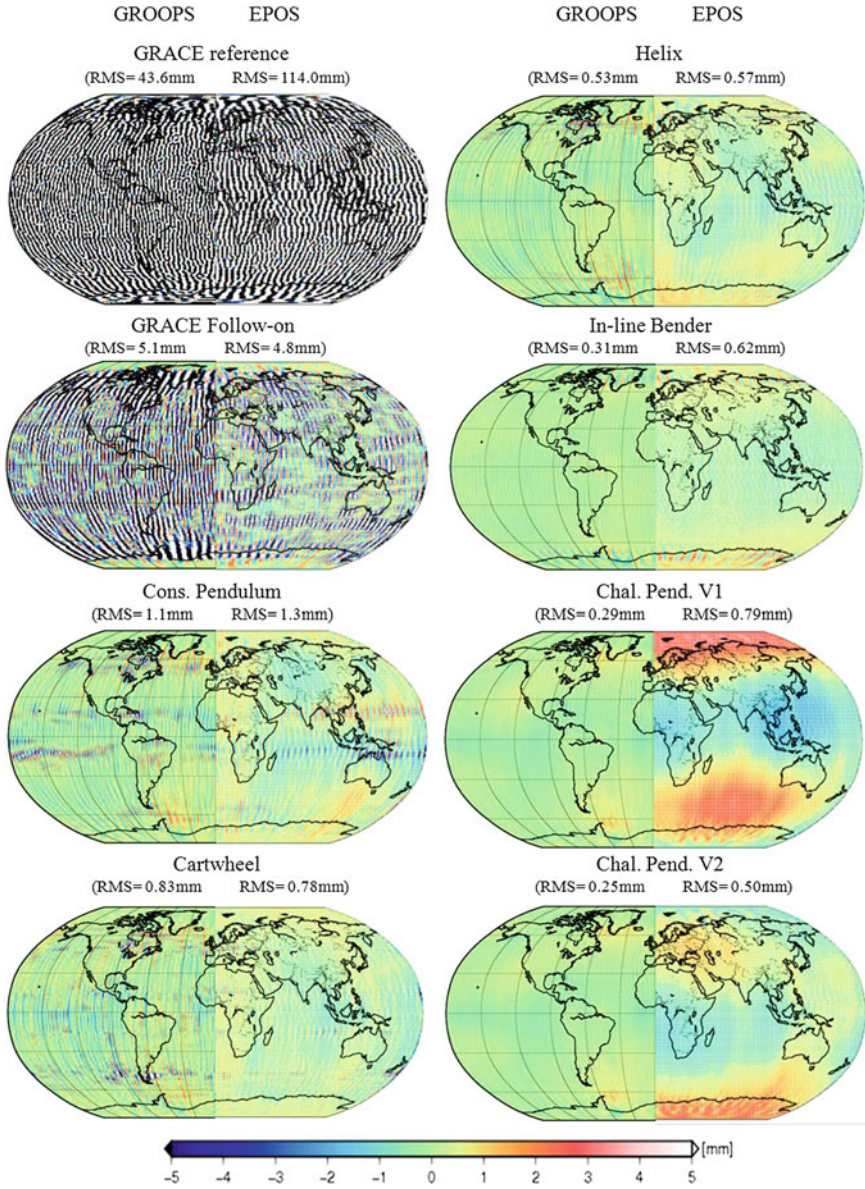
Fig. 21.19 Geoid height errors (in mm) of the gravity recoveries from the FGM scenarios. The *left half* of the world maps shows results obtained from IGG-GROOPS and the *right half* shows results from GFZ-EPOS

SNR are shown (only the SNR for the IGG results as for this scenario the SH degree errors of the two groups are consistent).
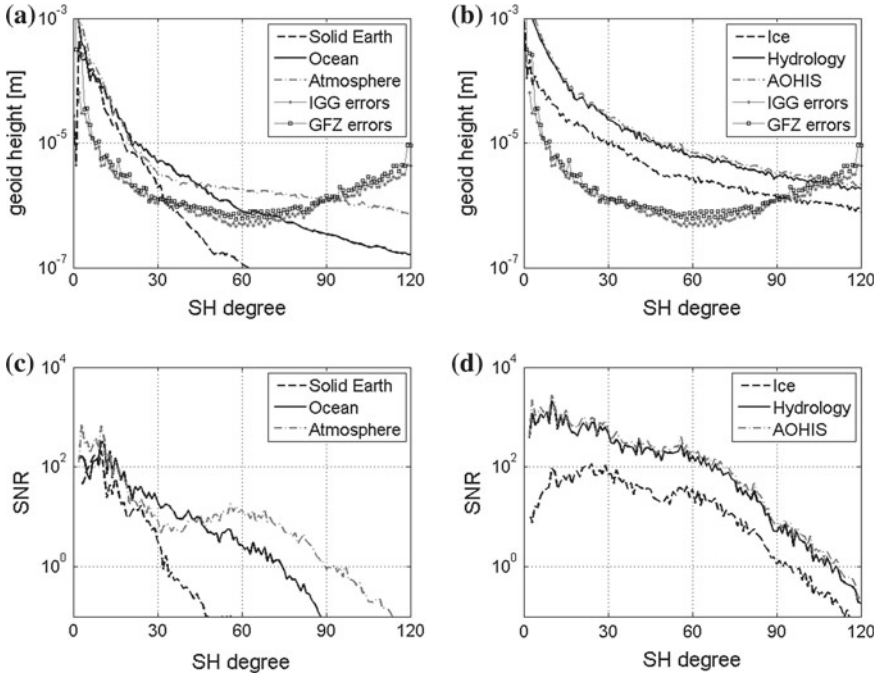
Fig. 21.20 SH degree errors of IGG and GFZ in geoid heights for the Challenging pendulum V1 compared to the mean signal of S, O and A (**a**) and I, H and AOHIS (**b**); SNR per SH degree for S, O and A (**c**) and I, H and AOHIS (**d**)

It is assumed that each AOHIS signal contribution can be observed when SNR > 1 (Fig. 21.20c, d), the corresponding maximum SH degree l defines the maximum resolution $r = 2\pi R_E/(2l)$ (where R_E is the Earth's radius). Another important parameter is the average SNR up to the maximum SH resolution. It is derived from the area between the curves in Fig. 21.20c, d and SNR = 1 divided by the maximum SH resolution. The average SNR gives a relative redundancy and tells how significant the different AOHIS signals can be observed up to the maximum resolution. The maximum spatial resolution in kilometer together with the dimensionless average SNR in brackets is shown for each scenario separately for IGG and GFZ in the Tables 21.6 (for S, O and A) and 21.7 (for I, H and the sum of all five parts AOHIS).

Table 21.8 shows the mean values of IGG and GFZ for all scenarios and signal parts. The scenarios are sorted by the mean maximum spatial resolution of all five AOHIS sources (the scenario with the best spatial resolution is in the bottom row). The best scenarios are the double-pair Bender mission and the two challenging Pendulum missions (V1 and V2). They are expected to observe mass variations from Hydrology, Ice and Atmosphere down to 200 km spatial resolution, whereas the conservative Pendulum, Cartwheel and Helix reach values around 300 km for these signals. The two GRACE missions show the worst resolutions (the spatial

Table 21.6 Maximum spatial resolutions with the mean SNR in brackets for all FGM scenarios and the S, O and A signal separately for IGG and GFZ

[km]([-])	S		O		A	
	IGG	GFZ	IGG	GFZ	IGG	GFZ
GRACE	870 (14)	1000 (13)	741 (19)	833 (17)	800 (29)	952 (34)
GFO	769 (13)	714 (15)	690 (20)	488 (13)	769 (33)	625 (24)
Pend (cons.)	667 (13)	714 (9)	426 (13)	444 (10)	400 (9)	435 (8)
Cartwheel	690 (15)	606 (15)	444 (12)	444 (23)	435 (10)	351 (10)
Helix	606 (14)	606 (16)	426 (20)	351 (14)	345 (10)	282 (9)
Bender	571 (38)	606 (38)	290 (18)	351 (25)	225 (14)	274 (15)
Ch. Pend. V2	645 (16)	606 (13)	274 (9)	286 (10)	206 (8)	206 (8)
Ch. Pend. V1	606 (19)	606 (11)	270 (13)	286 (9)	206 (11)	225 (9)

The different gray shadings from 0 % for white to 40 % mark different steps of spatial resolutions r ($r < 200$: 0 %, $200 \leq r < 300$: 10 %, $300 \leq r < 500$: 20 %, $500 \leq r < 700$: 30 %, $r \geq 700$: 50 %)

Table 21.7 Maximum spatial resolutions [km] with the mean SNR in brackets for all FGM scenarios and the I, H and AOHIS signal separately for IGG and GFZ

[km] ([-])	I		H		AOHIS	
	IGG	GFZ	IGG	GFZ	IGG	GFZ
GRACE	571 (8)	690 (7)	488 (50)	488 (29)	476 (58)	488 (37)
GFO	645 (12)	444 (12)	417 (35)	308 (38)	417 (45)	303 (45)
Pend (cons.)	313 (9)	323 (7)	247 (37)	247 (25)	230 (36)	241 (30)
Cartwheel	357 (10)	323 (14)	267 (34)	238 (40)	267 (44)	230 (45)
Helix	313 (14)	253 (12)	217 (35)	211 (50)	211 (40)	204 (57)
Bender	220 (23)	253 (21)	196 (104)	217 (86)	189 (112)	213 (100)
Ch. Pend. V2	204 (13)	215 (15)	179 (58)	185 (61)	177 (73)	182 (74)
Ch. Pend. V1	211 (20)	220 (14)	180 (77)	185 (55)	179 (96)	185 (71)

resolutions of GRACE-FO for each signal are significantly better than the one of GRACE). Mass variations in the oceans show similar resolutions, but for solid-Earth signals it is quite different. This signal mainly is caused by the post glacial rebound and its mean signal magnitude decreases much stronger with increasing SH degree. This leads to maximum resolutions for the solid-Earth part for GRACE of 935 km and for all other scenarios from 600 km down to 700 km.

21.4 Final Scenarios

In Sect. 21.3 a set of basic scenarios was evaluated by means of full-scale simulations and comparison to geophysical models. Based on this analysis two 'final missions'

Table 21.8 Maximum spatial resolutions [km] with the mean SNR in brackets for all FGM scenarios and the I, H and AOHIS signal, mean values between IGG and GFZ

[km] ([-])	S	O	A	I	H	AOHIS
GRACE	935 (14)	787 (18)	876 (31)	631 (7)	488 (40)	482 (48)
GFO	742 (14)	589 (17)	697 (28)	545 (12)	362 (36)	360 (45)
Pend (cons.)	690 (11)	435 (11)	417 (9)	318 (8)	247 (31)	235 (33)
Cartwheel	648 (15)	444 (17)	393 (10)	340 (12)	252 (37)	248 (44)
Helix	606 (15)	388 (17)	313 (10)	283 (13)	214 (42)	207 (49)
Bender	589 (38)	320 (22)	249 (14)	236 (22)	207 (95)	201 (106)
Ch. Pend. V2	626 (14)	280 (9)	206 (8)	210 (14)	182 (60)	179 (73)
Ch. Pend. V1	606 (15)	278 (11)	215 (10)	215 (17)	183 (66)	182 (83)

have been further investigated concerning system and metrology design: a 'conservative' pendulum with a moderate pendulum angle $\alpha = 24°$ and orbit height $h = 335$ km and a 'challenging' pendulum ($\alpha = 45°$ and $h = 298$ km), both flying on near polar orbits ($I = 89.5°$). Further details on orbit and formation parameters together with evaluation of the geodetic performance are provided in Sects. 21.3.4.1–21.3.4.3. It has to be mentioned that the term 'conservative' is misleading as the 'conservative' pendulum already faces numerous technical challenges, discussed below relative to state-of-the-art GRACE-type design. Section 21.4.1 describes the system design approach for the conservative pendulum and defines an alternative fallback scenario on a sun-synchronous orbit in order to reduce costs. The design approach for the challenging pendulum is presented in Sect. 21.4.2. In order to increase the mission lifetime up to a reasonable level (≥ 5 years) another fallback scenario makes use of an increased orbit height. Finally, the influence of the fallback scenarios on the expected gravity field quality is investigated in Sect. 21.4.3 by means of the QLTs.

21.4.1 System Design Approach for the Conservative Pendulum

Based on the primary mission parameters several design and technology concepts have been developed. The S/C configuration in Fig. 21.21 is called "modified-GRACE". It is based on previous design iterations and optimized for drag compensation performance.

The main equipment accommodation is shown in Fig. 21.22, where the four large circles indicate the cylindrical tanks of the foreseen cold gas propulsion system. The dot in the center represents the laser path, the plate and squares indicate the main equipment panel and the instrument boxes, respectively.

Alternatively a disc-shape S/C called "modified-disc" was designed. In order to maintain the relative balance/center of gravity, i.e. keeping the negative effects of fuel sloshing and consumptions relatively low, the shape of the S/C has been optimized as
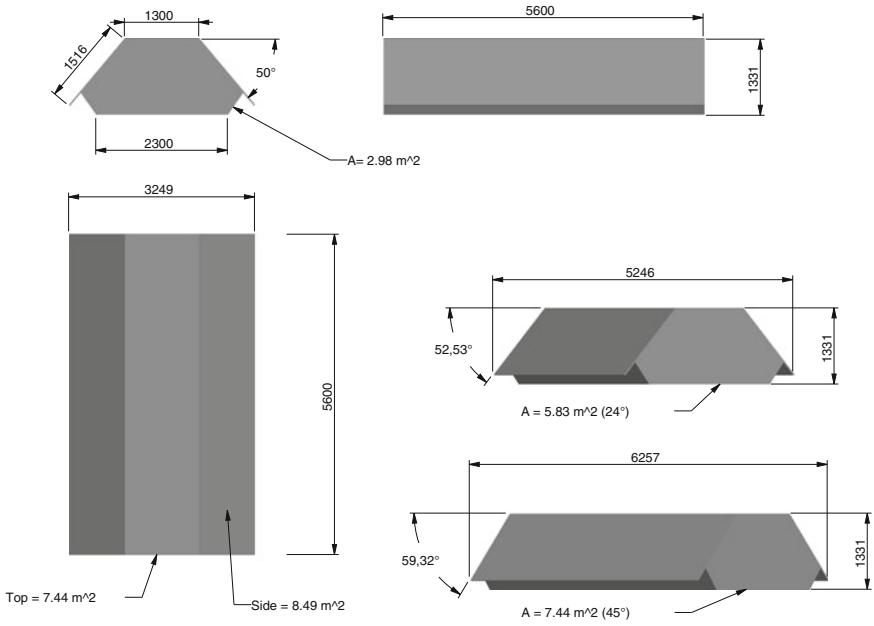
Fig. 21.21 Dimensions of the modified-GRACE configuration [mm and m^2]
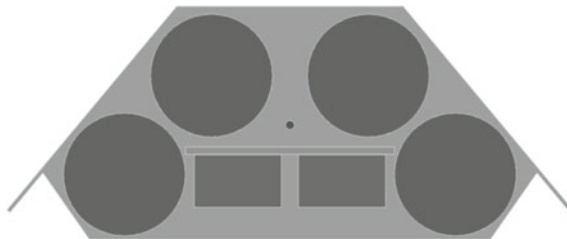

Fig. 21.22 Accommodation of tanks for modified-GRACE configuration

seen in Fig. 21.23. Three cylindrical tanks have been accommodated in the corners of the main S/C structure. This configuration features large deployable solar panels in order to generate enough power for the electric propulsion system.

Table 21.9 Power generation for 335 km orbit height

| Power at 335 km (W)/STO angle (°)	0	15	30	45	60	75	90
Modified-GRACE	1068	1075	1093	1173	1277	1648	1667
Modified-Disc/ Roll-flip angle	1285	1247	1115	894	936/ 10°	908/ 15°	1314/ 20°
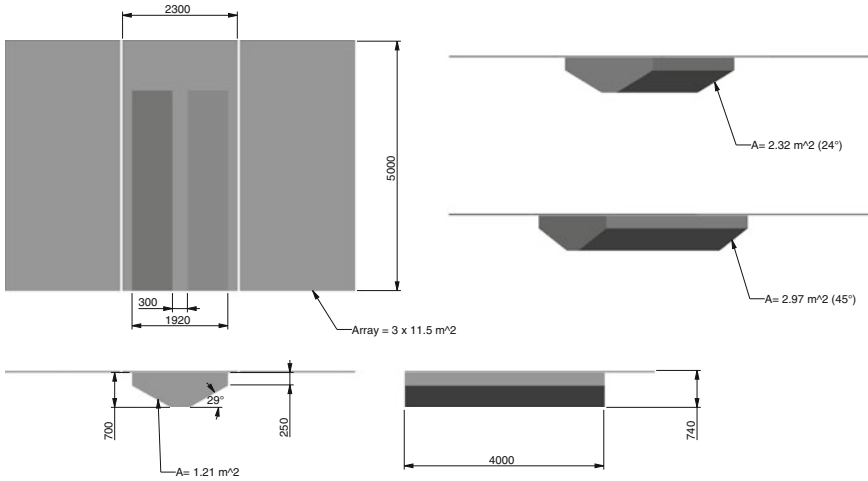
Fig. 21.23 Dimensions of the modified-disc configuration [mm and m^2]

Table 21.9 shows the power generation for both configurations. For the modified-disc configuration a roll-flip manoeuvre may be necessary in order to generate sufficient power for high sun-to-orbit (STO) angles. It should be noted that the roll-flip manoeuvre may introduce new challenges for the overall system (e.g. need for more efficient drag compensation). Alternative solutions are either planning a "hibernation time" where the satellite provides no (or only degraded) measurements or considering a noon orbit with fixed local time, where both the power demand and scientific requirements can be fulfilled. However the gravity recovery performance can be compromised due to the fixed local time and polar gaps.

Based on a planned 5-year mission life, the propellant and power demand has been estimated between 2020 and 2030 using predictions of atmospheric parameters (Schatten et al. 1996). The analysis suggests a launch in the year 2026 to benefit from low solar activity (i.e. 10.7 cm solar radio flux from ≈85 to 140). The results of the mission analysis have been summarized in Table 21.10.

Figure 21.24 shows the external disturbance acceleration and force magnitudes for the feasible scenarios (naming according to Table 21.10.) exemplary over one orbit for the worst case solar activity (thus air density) within the suggested mission lifetime.

The disturbances are fully dominated by the atmospheric drag while solar radiation pressure is negligible. For all 'baseline' scenarios the worst case acceleration remains below 3 µm/s^2 and thus within the DC range of the accelerometer (e.g. 6 µm/s^2 for the GRADIO sensor, Marque et al. 2008) and no drag compensation would be required for that purpose. Only scenario 2 exceeds this limit (up to 8 µm/s^2) due to the additional annual roll angle variation in superposition with the pendulum motion and active drag compensation would be necessary for periods with large roll angles.
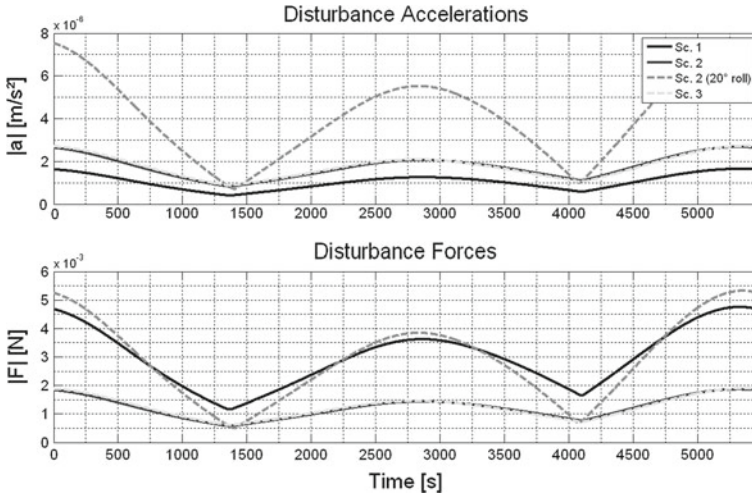
Fig. 21.24 Disturbance acceleration at CoM (*top*) and disturbance forces on the S/C (*bottom*) for conservative pendulum scenarios (over one orbit)

However, due to uncertainties in the solar activity prediction model and the air density in general, drag-compensation will be foreseen in terms of AOCS algorithms and actuation for all above-mentioned scenarios.

The propulsion system for the modified-GRACE configuration features 8 clusters and each cluster consists of 4 individual thrusters. The central thruster is oriented perpendicular to the panel and the remaining ones are separated by 120° from each other with an elevation angle of 30° to the panel.

The propulsion system for the modified-disc configuration consists of 6 clusters (identical to those of the modified-GRACE configuration). Both thruster accommo-

Table 21.10 Summary of feasible mission scenarios (conservative pendulum)

Scenario no.	1	2	3
Configuration	Modified- GRACE	Modified- disc*	Modified-disc
Orbit parameters	$h = 335$ km, $I = 89.5°$, $\alpha = 24°$		Same, but $I = 96.8°$ **
Propulsion system	Cold gas	Electric propulsion	
Mission life [years]	5	5	5
Launcher	Falcon 9 ***	Dnepr	Dnepr
Recommended launch date	2026	2026	2026

* With roll-flip manoeuvre or possible hibernation periods
** With fixed local time (e.g. noon orbit) and polar gaps
*** Relatively high launch cost but provides much larger launch mass/volume. Total mission cost may be similar, since electric propulsion/power is much more expensive than large cold gas tanks and the corresponding S/C structures

dations (symmetric front and back panel) can be seen in Fig. 21.25. The thruster configurations are compatible for both cold gas and electric propulsion.

Complementary to the thrusters, internally redundant on-board magnetic torquers are used to compensate the disturbance torques (see top of Fig. 21.26) acting on the S/C.

As magnetic torques can only be realized perpendicular to the Earth's magnetic field, torquer actuation alone is not sufficient but helps to reduce the residual torques to be realized by the thrusters to about 35–70 % depending on the scenario (see center and bottom of Fig. 21.26 exemplary for scenario 2 with the additional roll-flip).

It is assumed that the remaining disturbing torques can be compensated simultaneously with the force compensation. This means that the disturbance torques can be compensated by slightly varying the thrust level of the thrusters of different lever arms, such that the torque compensation does not require extra power/propellant.

For all scenarios, one single 3-axis accelerometer (GRADIO-type or similar further development) is foreseen which is placed close to the nominal S/C CoM. Small (around 1 cm) initial displacements or their variation over the mission time is considered uncritical for the reasons mentioned in Sect. 21.3.3. With maximum relative velocities between the satellites of about 10 m/s, a continuous wave heterodyne laser metrology is the baseline using the virtual corner cube principle that allows a placement of the effective phase center at the test mass CoM location (see Sect. 21.3.2).

Additionally the AOCS relies on GPS devices for orbit control (and for determination of the SST reference frame) and a set of 4 star tracker camera heads used for attitude control. Sensor blinding analyses have been carried out for this setup and confirmed full availability over each orbit.

A functional control system design has been developed to handle the variety of different scenarios, however further performance optimization and tailoring for the final selection will be necessary. The final SST-tracking via satellite rotation is realized by the sensor data fusion of the absolute inertial star tracker information (around roll-axis, i.e. line of sight) and accurate relative attitude information directly from the laser metrology via DWS.
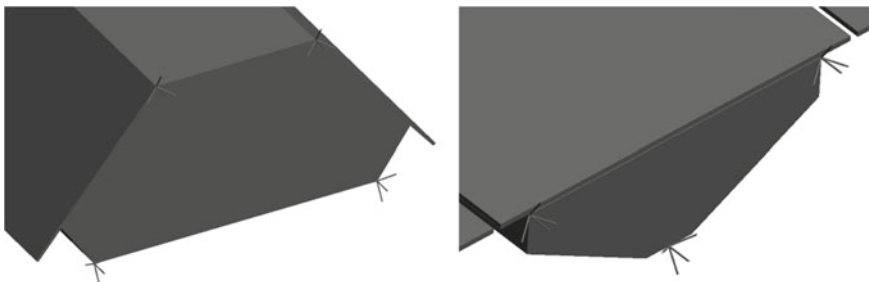
Fig. 21.25 Thruster accommodation for modified-GRACE (*left*) /-disc configuration (*right*)
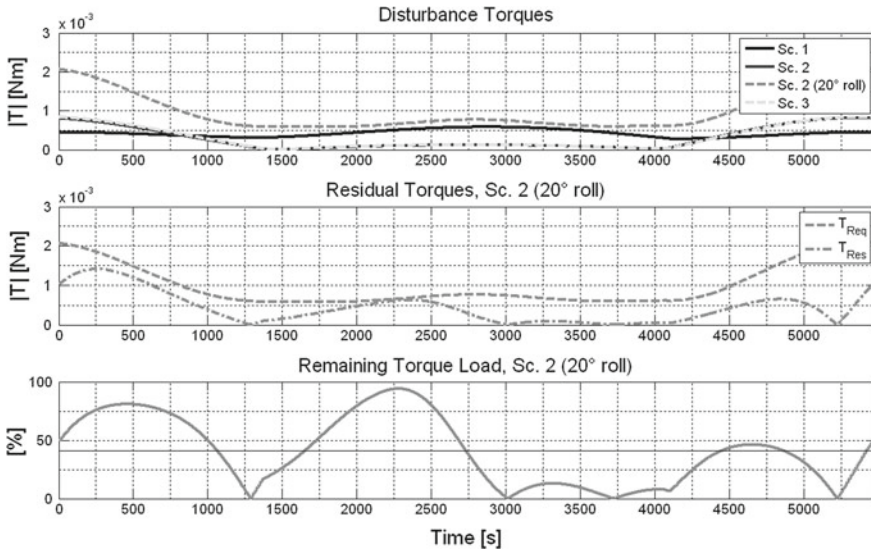
Fig. 21.26 Conservative pendulum: disturbance torques acting on the S/C (*top*), exemplary absolute residual torque load after magnetic compensation (*center*) and relative compensation capability (*bottom*)

21.4.2 System Design Approach for the Challenging Pendulum

Both satellite configurations and thruster accommodation for the challenging pendulum and the conservative pendulum scenarios are identical and again a start window in 2026 is recommended due to the low solar activity.

The modified-GRACE configuration would require about 2550 kg of cold gas to support the mission for 5 years which implies a total tank and propellant weight of about 4080 kg, which already exceeds the maximum launch mass of 4000 kg per satellite of the Falcon 9 launcher. Fulfilling the Falcon 9 mass limitations reduces the mission life to about 2.5 years only. Electric propulsion is no alternative for this configuration since the power demand cannot be ensured with the available solar array area.

The situation is even worse for the modified-disc configuration. To ensure enough power for the propulsion system over the whole mission life, the satellites have to perform larger roll-flip manoeuvres even at lower STO angles. This requires more detailed analysis which is out of scope of the current project phase, classifying the modified-disc configuration as not feasible at this stage.

Orbit height plays an important role for air drag and the corresponding propellant/power demand for compensation of the disturbing forces. Table 21.11 lists the air drag in proportion to a 335/298 km orbit derived from a Harris-Priester model (Montenbruck and Gill 2001). It highlights the considerable reduction of the air

drag for comparably small changes in altitude which could significantly ease the propellant/power demand and thus offer more options for the system design.

As a fallback option, a higher orbit of 355 km has been simulated for the modified-GRACE configuration which exploits above-mentioned flexibility for the system design, such as:

- A flexible start date between 2020 and 2026 is possible without compromising the mission lifetime.
- A longer mission life may be possible (e.g. start in 2026) since propellant should no longer be the dominant mission life constraint.
- A smaller S/C design may be possible, which allows choosing a less expensive launcher.

Therefore, a trade-off study between the advantages of a higher altitude for the system design and the degradation in gravity recovery performance is recommended. The results of the analysis for the challenging pendulum have been summarized in Table 21.12.

In addition, time domain simulations have been carried out as for the conservative pendulum scenarios. Figures 21.27 and 21.28 show time series of the external disturbances and feasible magnetic torque compensation exemplary over one orbit at maximum solar activity within the suggested mission lifetime.

For the low orbit of scenario 1 the disturbance acceleration is close to the level where drag compensation would be required to keep the accelerometer in its operational range while the scenario 2 is uncritical from this point of view. For the reasons already mentioned in the previous section the possibility of drag-compensation will be realized anyhow.

Concerning main payload sensors and AOCS design, the challenging pendulum scenarios significantly differ only with respect to the laser metrology. As the large pendulum angle of 45° implies large relative velocities between the satellites (≈ 40 m/s) continuous wave heterodyne detection is likely to be no longer feasible (detector bandwidth versus Doppler shifts).

Alternatively, optical frequency comb technology is a promising candidate here as it is basically not limited by relative velocity constraints (at least not in the considered range) and still allows the possibility to retrieve relative attitude information directly from the instrument.

Table 21.11 Estimated drag ratio with respect to 335 km and 298 km

Orbit height (km)	300	335	355	375	395	425
Drag ratio to 335 km (conservative pendulum)	2.3	1	0.64	0.42	0.28	0.15
Drag ratio to 298 km (challenging pendulum)	0.95	0.42	0.27	0.17	0.12	0.065

**Table 21.12** Summary of feasible mission scenarios (challenging pendulum)

No.	configuration	Orbit parameters	Propulsion	Mission life (years)	Launcher	Launch date (recomm.)
1	Modified-GRACE	$h = 298$ km $I = 89.5°$ $\alpha = 45°$	Cold gas	≈ 2.5	Falcon 9	2026
2	Modified-GRACE	Same, but 355 km	Cold gas	$> = 5^*$	Falcon 9	2020–2026

* Other lifetime constraints (e.g. battery, electronics) need to be examined carefully

21.4.3 Geodetic Comparison of Goal and Fallback Scenarios

Based on the results of Sects. 21.3.4.2 and 21.3.4.3 two final scenarios have been
suggested for further investigation: (i) a conservative pendulum on an orbit height h
≈ 335 km with a pendulum angle of $\alpha = 24°$ and (ii) a challenging pendulum on a
lower orbit height $h \approx 298$ km with a larger pendulum angle of $\alpha = 45°$, assuming
progress in laser technology and orbit control systems.

Within this section, the system design for these two pendulums was investigated.
It was found out that the realization of these final scenarios have a serious impact
on satellite design and costs, and fallback scenarios have been designed in order to
reduce costs, especially for the conservative pendulum, or enable a longer mission
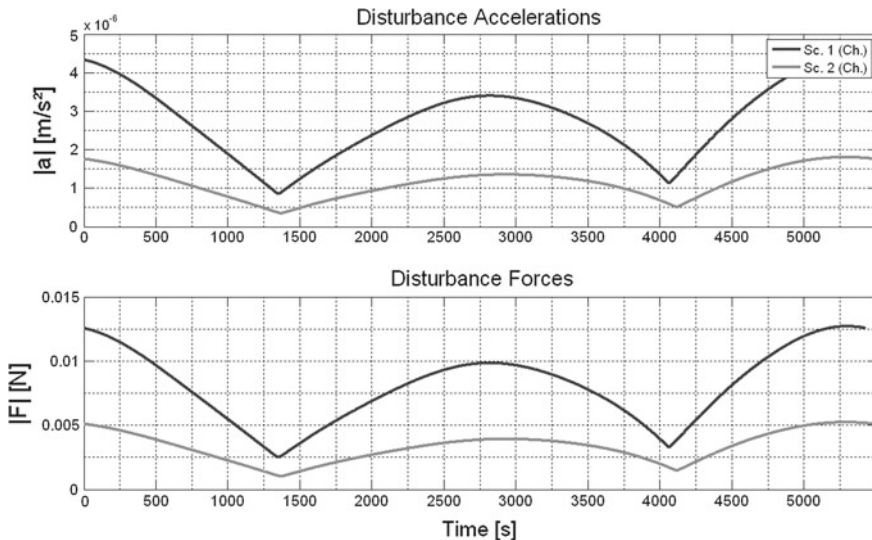
Fig. 21.27 Challenging pendulum: disturbance acceleration at CoM (*top*) and disturbance forces
on the S/C for (*bottom*) over one orbit
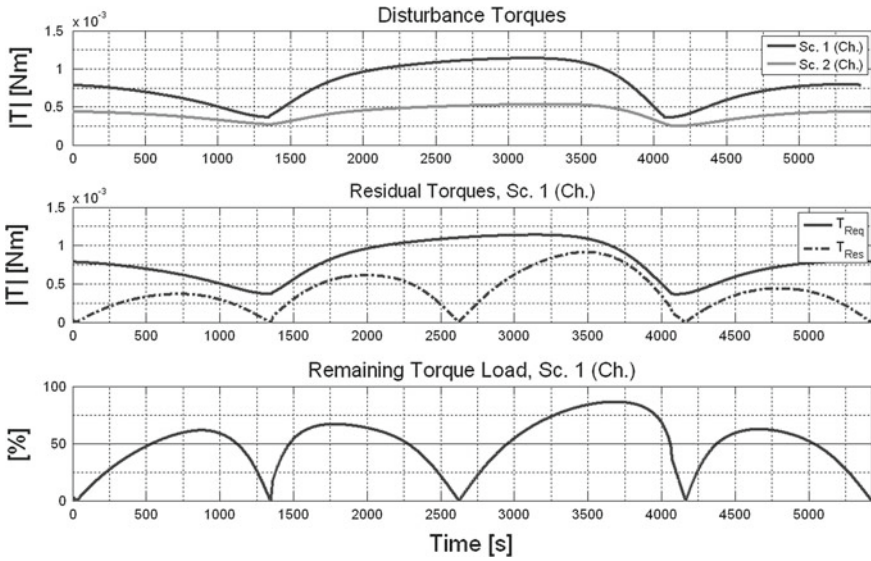
Fig. 21.28 Challenging pendulum: disturbance torques acting on the S/C (*top*), absolute residual torque load after magnetic compensation (*middle*) and relative compensation capability (*bottom*)

lifetime in case of the challenging pendulum. The geodetic impact of the fallback-scenarios is investigated by the aliasing-analysis QLT, described in Sect. 21.2.1.
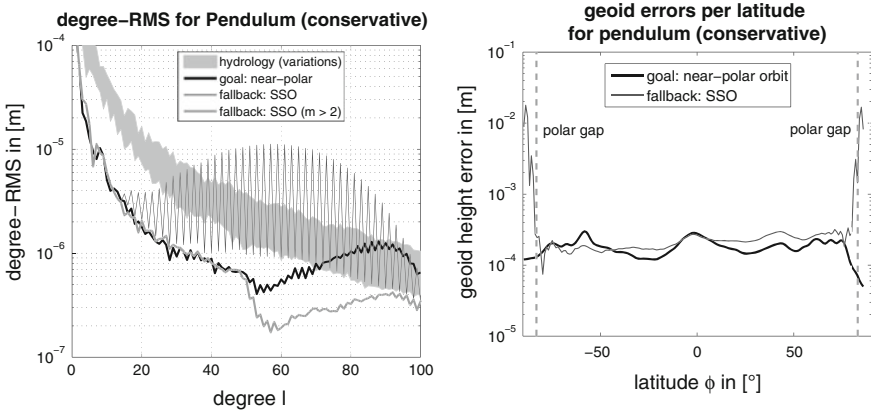
Fig. 21.29 Geodetic performance of goal/fallback scenarios (conservative pendulum)

21.4.3.1 Conservative Pendulum

The system design for the conservative pendulum based on a modified-GRACE configuration makes use of cold-gas propulsion and a Falcon-9 launcher. In order to reduce the launcher costs, the modified-disc configuration with electric propulsion was designed as a fallback option, which can be carried by a cheaper Dnepr-launcher. However, in order to enable electric propulsion by solar panels without raising the air-drag, only a sun-synchronous (SSO) orbit with noon-orientation is possible, and the cost may grow again due to the more expensive electric propulsion system. The geodetic performance of the two options goal (near polar orbit) versus fallback (sun-synchronous orbit, $I = 96.8°$) is displayed in Fig. 21.29. As well known, the polar gap generated by a SSO has a serious influence on the geoid errors for these areas and on the zonal and near-zonal spherical harmonic (SH) coefficients of low orders (van Gelderen and Koop 1997). As soon as their influence is discarded in the degree-RMS representation (here: orders $m < 3$ are removed for degrees $l > 25$), a similar or even better performance is obtained compared to the near-polar orbit. Possible explanations for the improved performance visible for degrees $l > 50$ is, that (i) over equatorial regions the angle between line-of sight and North-direction is increased by the polar gap to approximately $45° + 7° \approx 52°$, if the leader-satellite of the pendulum is on the left side for ascending arcs and (ii) a denser and more homogeneous sampling (intersection angle between descending and ascending nodes grows) around the polar gaps is achieved. Concerning the geoid errors per latitude, the negative effect of the polar gaps is mainly restricted to the polar gaps, but leakage-out of the polar gaps may still affect regions outside polar gaps. Since the most important regions for ice mass loss studies, as Greenland and Antarctic shelves, are outside the polar gaps, SSO might be an option. But further, more detailed studies are necessary in order to guarantee that no negative effect is induced in these important study regions.

21.4.3.2 Challenging Pendulum

Investigations of the system design show, that the only option to establish the challenging pendulum is a modified GRACE-shaped satellite with a cold-gas propulsion system. However, due to the enormous drag to be compensated in the low orbit, only a lifetime of about 2.5 years is estimated, which is too short for the investigation of time-variable processes. Thus a fallback option on a higher orbit of $h \approx 355$ km was studied, which should enable a 5 years mission lifetime.

The geodetic performance of the goal and fallback option for the challenging pendulum is displayed in Fig. 21.30. As visible, the increased orbit height induces a loss of sensitivity for the higher degrees. Especially for degrees $l > 50$ a reduction of accuracy up to half an order of magnitude appears. Compared to Fig. 21.29, this means, that the performance of the challenging pendulum fallback scenario is similar to the conservative pendulum goal scenario. Thus, a lower orbit height than $h = 355$ km should be aimed for the challenging pendulum fallback design to obtain an apparent improvement compared to the conservative pendulum.

21.5 Results and Outlook

21.5.1 Lessons Learnt

The project management followed an integrative way approach to achieve the project objectives. The project team was composed accordingly, consisting of science groups from geodesy (both university based and research institutes) and technology oriented groups from sensor technology, control and system engineering (both academic and from industry). At the downside the diverse communities bring with them different "languages", terminology and conventions, which inevitably decelerates the activities at project start. However, throughout the project lifetime, the need for such a broad constellation proved itself indispensable. Particularly the question as to how (geodetic) science requirements and mission performance requirements interact could be resolved. Thus, the first lesson learnt is formulated here as a recommendation: it is mandatory that science and technology communities participate in similar projects in the future. This recommendation is probably even more valid in the future than now. A secondary recommendation in this context is that these communities then undertake to learn to speak each other's language.

Pendulum formations may serve to illustrate the above recommendation. From geodetic gravity recovery simulations, the superiority of such pendulum design relative to a GRACE-type mission was known from literature and corroborated by the simulation approach in the FGM project. However, in the course of the project the high degree of complexity of a pendulum design soon became clear: large relative velocities would violate the Doppler shift constraints of the laser metrology and deal-
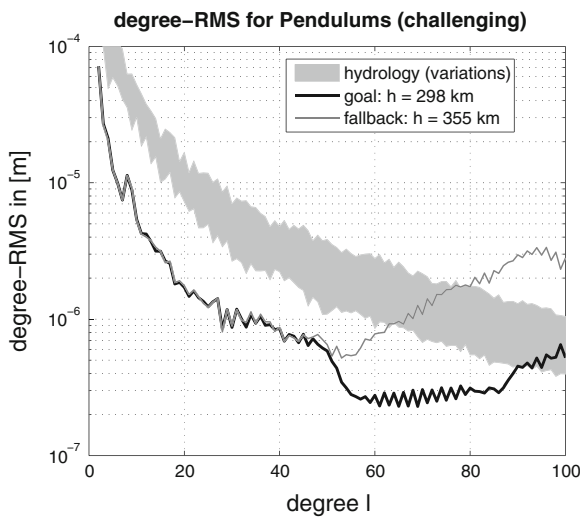

Fig. 21.30 Geodetic performance of goal/fallback scenarios (challenging pendulum)

ing with the time-variable baseline orientation would be a challenge either through an active beam-steering mirror assembly or by active satellite attitude control. Identification of this complexity early on in the project allowed the team to focus on more realistic mission scenarios.

Collaborative configurations of more than one pair have shown to be a highly effective tool for dealiasing. It was demonstrated within FGM that two satellite pairs in a well-coordinated orbital configuration, e.g. with one polar pair and one inclined pair (so-called Bender configurations), outperform the combined result of two unco-ordinated satellite pairs. Besides the improved temporal sampling and improved ground-track geometry, such a configuration leads to a near-isotropic error behaviour, with strongly reduced striping effects. This improvement already takes place when both pairs fly en echelon in GRACE style, thus eliminating the need for the complexities of pendulum motion.

At a more technological level, the project has taught us the benefits of having the accelerometer test mass center serve as reference point as opposed to the conventional satellite's center of mass. Not only does this choice support the performance budget, it also may lead to manufacturing benefits and, hence reduce cost. The laser metrology and accelerometer are supposed to be mounted on a common optical bench, such that the relative distance between accelerometer test mass center and metrology phase center are both well-known and highly stable.

Concerning the geodetic simulations, mainly two aspects can be pointed out. First, the quick-look tools for sensitivity analysis are very helpful for efficient pre-selection of mission parameters. Although they are not able to capture aliasing effects, which are the most dominant error source for most of the investigated scenarios, they are able to assess the relative error distribution among the different missions options. The quick-look-tools for reduced scale gravity recovery are an efficient tool for the investigation of aliasing errors and for simplified full-scale-gravity recovery. The comparison with full-scale gravity recovery shows that similar error structures are obtained, even though a bit too optimistic.

Second, full-scale simulations yielded that the parameters for gravity recovery, e.g. arc-lengths and time-intervals for estimation of accelerometer biases and empirical accelerations, have to be selected carefully in the individual software packages. By taking over the parameter settings from GRACE gravity recovery without adaption, unsatisfying results have been obtained. The results from both full-scale software packages applied in this study show that similar results can received by proper parameter selection, although slight and systematic differences between the solutions from both systems are apparent. For control of the results a redundancy of software packages is desirable, as the project showed.

21.5.2 Roadmap

Recall that the FGM project was set up to come to a roadmap towards future gravity missions and to prepare the German community for future calls for proposals

from space agencies. As it happened, ESA had issued a call for proposals for the next Earth Explorer Opportunity missions (EE-8) in October 2009, i.e. soon after project start. Despite being partially unprepared, several German key players from the FGM project teamed up with European colleagues to prepare a proposal for a future gravity field satellite mission under the name "*Earth System Mass Transport Mission—e.motion*". From the German side the e.motion effort was led by Dr. Thomas Gruber, TU (Technical University) Munich. Despite a positive review, the proposal was ultimately rejected for not fitting within the EE8-budget.

April 2012 the German National Aeronautics and Space Research Centre (DLR) had issued a call for proposals for innovative mission concepts for geoscientific monitoring. This time the FGM expertise could be invoked. Several groups from the FGM team were able to put forward a pre-proposal for a future gravity mission. The pre-proposal, which aims to work out a concrete mission concept for the long-term monitoring of mass variations in the Earth system, draws strongly on the FGM project results. Although the first reactions are positive, at the time of writing no decision has been taken yet.

In view of science achievements and the current performance of GRACE the geoscience community early on supported the idea of a GRACE follow-on mission based on the present configuration, with emphasis on the uninterrupted continuation of time series of global gravity changes. This goal was pursued throughout the FGM project lifetime within the triangle of GRACE stakeholders: CSR (Center for Space Research, University of Texas, Austin), JPL (Jet Propulsion Laboratories) and GFZ. From the German side the GRACE Follow-On initiative was led by Flechtner. During fall 2011 the GRACE-FO mission obtained the go-ahead from US and German side. Launch is planned for fall 2017. Further participants from the FGM project are STI for system analysis and support and AEI for the laser distance metrology, which is to fly as demonstrator package. Although GRACE-FO is nominally designed as a GRACE mission copy, the idea of pendulum motion, prominently featuring in the FGM project, is taken up as optional orbital motion.

The idea of collaborative multi-agency configurations, in which individual agencies launch their own satellite pair, should be pursued at scientific level and be resolved at political level. This matter deserves more attention. Given the budgets involved, it would be both a scientific and an economical loss if such coordination efforts (between agencies) do not happen. There is a certain degree of urgency to this matter, as well. Dual pair configurations, e.g. the so-called Bender constellations, might be realized within the lifetime of GRACE-FO (roughly 2017–2027). Such constellations were investigated in the FGM project, but require more detailed scrutiny in terms of orbit inclination, repeat modes, space-time sampling, technological readiness, and so on. Exactly the scientific assessment of dual pair constellations/configurations was the topic of a recent invitation to tender by ESA, fall 2012. Again, at the time of writing no decision has been taken yet.

Although a wide variety of mission options has been investigated indeed, the FGM project nevertheless followed by and large the GRACE paradigm. Despite different sensor technology (laser) and more advanced relative motion (pendulum, helix), the basic mission design remained that of a low-low SST mission. Future research should

attempt to think outside the box, as the expression goes. Initial innovative ideas have been generated within FGM in terms of laser-based gradiometry or in terms of a laser system on a master satellite that tracks more than one co-orbiting slave satellites. Within the wider community further ideas have been floated, e.g high-low laser-SST between a few geostationary satellites to a Low Earth Orbiter (LEO) orbiter, or measurement of potential differences through high-precision clocks. Moreover, instead of pursuing high-tech solutions, one strategy could be to develop a swarm of low-tech and, hence, cheap satellites, of which absolute and/or relative motion is tracked, e.g. by GPS or KBR (K-band-ranging).

The FGM project has clearly revealed the need for technology development. One of the most stringent mission design constraints for a heterodyne laser SST concept was the maximum relative intersatellite velocity of about 10 m/s, due to Doppler shift. Such a limit gravely restricts the options for satellite formations like pendulum or cartwheel-type motion. Tentative solutions with frequency combs were presented that would relax the relative velocity constraint by orders of magnitude. In general, new optical metrology technologies are emerging which are being optimized by breadboard activities and further qualification processes for future use in space systems.

Atom interferometry has been assessed within FGM as a future inertial sensing metrology for spaceborne gravimetry. Such techniques carry enormous potential for purposes of accelerometry, attitude sensing or gradiometry in terms of miniaturization and cost minimization. The technological readiness of such quantum sensors, although an active field of research, requires a longer development span, though. The spaceborne gravimetry community must keep a keen eye on such developments for planning missions in the longer future.

Most of the technological challenges for the design of a future gravity mission have been cleared in the course of the FGM project. Further details will be clarified by the aforementioned studies at DLR, ESA and other agencies. The key test will be the laser metrology flying as demonstrator package on GRACE-FO. Under the assumption that the geoscience communities convince their respective governments and space agencies of the need for continued monitoring of time variable gravity, it appears realistic that a mission, as described in this report, can be launch in the timeframe around 2025.

References

Anselmi A, Visser PNAM, van Dam T, Sneeuw N, Gruber T, Altès B, Christophe B, Cossu F, Ditmar PG, Murböck M, Parisch M, Renard M, Reubelt T, Sechi G, Texieira da Encarnacao JG (2011) Assessment of a Next Generation Gravity Mission to monitor the variations of Earth's gravity field, ESA-contract No. 22643/09/NL/AF, Executive summary, Thales Alenia Space report SD-RP-AI-0721, 2011.

Bendat JS, Piersol AG (2000) Random data analysis and measurement procedures, 3rd edn. Wiley, NewYork

Bender PL, Wiese DN, Nerem RS (2008) A possible dual-GRACE mission with 90 degree and 63 degree inclination orbits. ESA (ed) Proceedings of the third international symposium on formation flying, missions and technologies, 23–25 April 2008. ESA/ESTEC, Noordwijk, pp 1–6

Bettadpur S (2007) GRACE 327–720, Gravity recovery and climate experiment, product specification document. Rev. 4.5, CSR-GR-03-02, ftp://podaac.jpl.nasa.gov/allData/grace/docs/ProdSpecDoc_v4.5.pdf, last accessed 24 September 2012.

Bortoluzzi D, Hoyle CD, Hueller M, Vitale S, Heinzel G, Danzmann K, Lobo A, Anza S, Navau C, Chen DX, Sanchez A, Araujo H, Wass P, Grimani C (2005) Science requirements and top-level architecture definition for the Lisa Technology Package (LTP) on Board LISA Pathfinder (SMART-2). LTPA-UTN-ScRD-Iss003-Rev1, Project Documentation, available on ESA website, http://www.rssd.esa.int/SP/LISAPATHFINDER/docs/Top_level_documents/LPF_ScRD.pdf, last accessed on 24 September 2012

Bowman BR, Tobiska WK, Marcos FA, Valladares C (2008) The JB2006 empirical thermospheric density model. J Atmos Sol Terr Phys 70(5):774–793. doi:10.1016/j.jastp.2007.10.002

Bykov I, Delgado JJE, Garcia AF, Marin AFG, Heinzel G, Danzmann K (2009) LISA phasemeter development: Advanced prototyping. J Phys Conf Ser 154:012017. doi:10.1088/1742/154/1/012017

Christophe B, Marque J-P, Foulon B (2010) Accelerometers for the ESA GOCE Mission: one year of in-orbit results. Presentation at EGU 2010, Vienna, available on the ESA GOCE website, http://earth.esa.int/pub/ESA_DOC/GOCE/AccelerometersfortheESAGOCEMission-oneyearofin-orbitresults.pdf, Last accessed 24 September 2012

Coddington I, Swann WC, Nenadovic L (2009) Newbury NR (2009) Rapid and precise absolute distance measurements at long range. Nat Photonics 3:351–356

Cui M, Zeitouny M, Bhattacharya N, van den Berg S, Urbach H, Braat J (2009) High-accuracy long-distance measurements in air with a frequency comb laser. Opt Lett 34:1982–1984

Di Cara D, Massotti L, Cesare S, Musso F, Castorina G, Feili D, Lotz B (2011) Performance verification of the NRIT-2.5 thruster on the Nanobalance facility, IEPC-2011-013. In: Presented at the 32nd international electric propulsion conference, Wiesbaden.

van Dam T, Visser P, Sneeuw N, Losch M, Gruber T, Bamber J, Bierkens M, King M, Smit M (2008) Monitoring and modelling individual sources of mass distribution and transport in the earth system by means of satellites ESA-contract 20403, Final Report.

Ellmer M (2011) Optimization of the orbit parameters of future gravity missions using genetic algorithms, MSc thesis, Geodetic Institute, University of Stuttgart, http://elib.uni-stuttgart.de/opus/volltexte/2012/7122/pdf/Ellmer.pdf

Elsaka B, Kusche J (2010) Optimized gravity field determination from future satellite missions. In: Münch U, Dransch W (eds) Observation of the System Earth from Space, GEOTECHNOLOGIEN Science Report No. 17, Status Seminar, 4 (October 2010) Rheinische Friedrich Wilhelms Universität Bonn. Koordinierungsbüro GEOTECHNOLOGIEN, Potsdam

Elsaka B, Kusche J, Ilk KH (2012) Recovery of the Earth's gravity field from formation-flying satellites: temporal aliasing issues. Adv Space Res, http://dx.doi.org/10.1016/j.asr.2012.07.016

ESA (1999) The four candidate earth explorer core missions–gravity field and steady-state ocean circulation mission. ESA SP-1233.

Finlay CC, Maus S, Beggan CD, Bondar TN, Chambodut A, Chernova TA, Chulliat A, Golovkov VP, Hamilton B, Hamoudi H, Holme R, Hulot G, Kuang W, Langlais B, Lesur V, Lowes FJ, Lühr H, Macmillan S, Mandea M, McLean S, Manoj C, Menvielle M, Michaelis I, Olsen N, Rauberg J, Rother M, Sabaka TJ, Tangborn A, Tøffner-Clausen L, Thébault E, Thomson AWP, Wardinski I, Wei Z, Zvereva TI (2010) International Geomagnetic Reference Field: the eleventh generation. Geophys J Int 183(3):1216–1230. doi:10.1111/j.1365-246X.2010.04804.x

Foerste C, Schmidt R, Stubenvoll R, Flechtner F, Meyer U, Koenig R, Neumayer H, Biancale R, Lemoine JM, Bruinsma S, Loyer S, Barthelmes F, Esselborn S (2008) The GeoForschungsZentrum Potsdam/Groupe de Recherche de Geodesie Spatiale satellite-only and combined gravity field models: EIGEN-GL04S1 and EIGEN-GL04C. J Geod 82(6):331–346. doi:10.1007/s00190-007-0183-8

Geiger R, Ménoret V, Stern G, Zahzam N, Cheinet P, Battelier B, Villing A, Moron F, Lours M, Bidel Y, Bresson A, Landragin A, Bouyer P (2011) Detecting inertial effects with airborne matter-wave interferometry. Nat Comm 2(2011):474. doi:10.1038/ncomms1479

van Gelderen M, Koop R (1997) The use of degree variances in satellite gradiometry. J Geod 71:337–343

Gruber T, Bamber JL, Bierkens MFP, Dobslaw H, Murböck M, Thomas M, van Beek LPH, van Dam T, Vermeersen LLA, Visser PNAM (2011) Simulation of the time-variable gravity field by means of coupled geophysical models. Earth Syst Sci Data 3:19–35. doi:10.5194/essd-3-19-2011

Haboucha A, Zhang W, Li T, Lours M, Luiten AN, Coq L, Santarelli G (2011) Optical-fiber pulse rate multiplier for ultralow phase-noise signal generation. Opt Lett 36:3654–3656

Hedin A (1987) MSIS-86 thermospheric model. JGR 92(A5):4649–4662. doi:10.1029/JA092iA05p04649.

Heinzel G, Wand V, García A, Jennrich O, Braxmaier C, Robertson D, Middleton K, Hoyland D, Rüdiger A, Schilling R, Johann U, Danzmann K (2004) The LTP interferometer and phasemeter. Class Quantum Gravity 21:S581–S587

Iafolla V, Fiorenza E, Lefevre C, Nozolli S, Peron R, Reale A, Santoli F (2011) The ISA accelerometer for BepiColombo mission. Mem SA It Suppl 16:22

Iran Pour S, Reubelt T, Sneeuw N (2013) Quality assessment of sub-Nyquist recovery from future gravity satellite missions. Adv Space Res. doi:http://dx.doi.org/10.1016/j.asr

Knocke PC, Ries JC, Tapley BD (1988) Earth radiation pressure effects on satellites. Proceedings of the AIAA/AAS astrodynamics specialist conference, Washington, In, pp 577–586

Kusche J (2002) A Monte-Carlo technique for weight estimation in satellite geodesy. J Geod 76(11):641–652

Lemoine FG, Kenyon SC, Factor JK, Trimmer RG, Pavlis NK, Cox CM, Klosko SM, Luthcke SB, Torrence MH, Wang YM, Williamson RG, Pavlis EC, Rapp RH and Olson TR (1998) The Development of the Joint NASA GSFC and the National Imagery and Mappping Agency (NIMA) Geopotential Model EGM96. NASA/TP-1998-206861, July, 1998.

Marque JP, Christophe B, Liorzou F, Bodovillé G, Foulon B, Guérard J, Lebat V (2008) The ultra sensitive accelerometers of the ESA GOCE mission. In: 59th international astronautical congress, IAC-08-B1.3.7.

Matticari G, Materassi M, Noci G, Fallerini L, Siciliano P (2011) Use of a "wide dynamic range" electronic flow regulator to increase the flexibility and versatility of electric and cold gas small propulsion systems. In: IEPC-2011-096. Presented at the 32nd international electric propulsion conference, Wiesbaden.

Mayer-Gürr T (2006) Gravitationsfeldbestimmung aus der Analyse kurzer Bahnbögen am Beispiel der Satellitenmissionen CHAMP und GRACE. Dissertation, Schriftenreihe des Instituts für Geodäsie und Geoinformation der Rheinischen Friedrich-Wilhelms Universität Bonn, ISSN 1864–1113, Nr. 8, Bonn 2008.

Milani A, Gronchi G (2010) Theory of orbit determination. Cambridge University Press, Cambridge

Montenbruck O, Gill E (2001) Satellite orbits: models, methods, applications. 1st edition, corr. 2nd printing, Springer, Berlin.

Montenbruck O, Gill E (2001) Satellite orbits: models, methods, applications. 1st edn, corr. 2nd printing, Springer, Berlin.

Panet I, Flury J, Biancale R, Gruber T, Johannessen J, van den Broeke MR, van Dam T, Gegout P, Hughes C, Ramillien G, Sasgen I, Seoane L, Thomas M (2012) Earth system mass transport mission (e.motion): a concept for future earth gravity field measurements from space. Surveys in Geophysics, vol 2012, Springer. doi:10.1007/s10712-012-9209-8.

Percival DB (2006) Spectral analysis of clock noise: a primer. Metrologia 43:S299. doi:10.1088/0026-1394/43/4/S18

Peters A, Chung KY, Chu S (1999) Measurement of gravitational acceleration by dropping atoms. Nature 400(1999):849–852. doi:10.1038/23655

Ray R (2008) GOT4.7 (private communication). Extension of Ray R (1999) A global ocean tide model from Topex/Poseidon altimetry GOT99.2. NASA Tech Memo 209478, Sept. 1999.

Reigber C, Lühr H, Schwintzer P (2002) CHAMP mission status. Adv Space Res 30:129–134

Reubelt T, Sneeuw N, Iran-Pour S (2011) Quick-look gravity field analysis of formation scenarios selection. In: Münch U, Dransch W (eds) Observation of the system earth from space, GEOTECHNOLOGIEN Science Report No. 17, Status Seminar, 4 (October 2010) Rheinische Friedrich Wilhelms Universität Bonn. Koordinierungsbüro GEOTECHNOLOGIEN, Potsdam

Reubelt T, Sneeuw N, Sharifi MA (2010) Future mission design options for spatio-temporal geopotential recovery. In: Mertikas SP (ed) Gravity, geoid and earth observation. IAG Commission 2: Gravity Field, Chania, Crete, Greece, pp 23–27 June 2008. International association of geodesy symposia, vol 135, Springer.

Savcenko R, Bosch W (2008) EOT08a–empirical ocean tide model from multi-mission satellite altimetry. Report No. 81, Deutsches Geodätisches Forschungsinstitut (DGFI), München.

Schatten K, Myers DJ, Sofia S (1996) Solar activity forecast for solar cycle 23. Geophys Res Lett 23(6):605–608

Schrama EJO, Wouters B, Lavallee DD (2007) Signal and noise in Gravity Recovery and Climate Experiment (GRACE) observed surface mass observations. J Geo-phys Res 112:(B08407). doi:10.1029/2006JB004882.

Schuldt T, Gohlke M, Weise D, Johann U, Peters A, Braxmaier C (2009) Picometer and nanoradian optical heterodyne interferometry for translation and tilt metrology of the LISA gravitational reference sensor. Class Quantum Gravity 26:085008

Sharifi M, Sneeuw N, Keller W (2007) Gravity recovery capability of four generic satellite formations, In: Kilicoglu A, Forsberg R (eds) Gravity field of the earth, general command of mapping, ISSN 1300–5790. Spec Issue 18:211–216

Sheard BS, Heinzel G, Danzmann K, Shaddock DA, Klipstein WM, Folkner WM (2012) Intersatellite laser ranging instrument for the GRACE follow-on mission. J Geod 29: doi:10.1007/s00190-012-0566-3

Sneeuw N (2000) A semi-analytical approach to gravity field analysis from satellite observations, DGK, Reihe C, Heft 527, Verlag der Bayerischen Akademie der Wissenschaften, ISBN (Print) 3-7696-9566-6, ISSN 0065-5325, 2000.

Standish EM (1998) JPL Planetary and Lunar Ephemerides, "DE405/LE405". IOM 312.F-98-048, August 26 1998.

Stockton JK, Takase K, Kasevich MA (2011) Absolute geodetic rotation measurement using atom interferometry. Phys Rev Lett 107(2011):133001. doi:10.1103/PhysRevLett.107.133001

Szerdahelyi L, Fichter W, Schleicher A, Johann U (2003) HYPER Secondary AOCS Performance. HYP-2-01 v4.1, Technical Note, available on ESA website http://sci2.esa.int/hyper/docs/HYP-2-01-v41.pdf, last accessed 24 September 2012

Tackmann G, Berg P, Schubert C, Abend S, Gilowski M, Ertmer W, Rasel EM (2012) Self-alignment of a compact large-area atomic Sagnac interferometer. New J Phys 14(2012):015002. doi:10.1088/1367-2630/14/1/015002

Tapley BD, Bettadpur S, Ries JC, Thompson PF, Watkins MM (2004) GRACE measurements of mass variability in the Earth system. Science 305:503–505. http://dx.doi.org/10.1126/science.1099192

Tapley BD, Watkins MM, Riess JC et al (1996) The joint gravity model 3. JGR 101:28029–28049

Touboul B (2001) Space accelerometers: present status. Lecture notes in physics, vol. 562/2001, pp 273–291, Springer. doi:10.1007/3-540-40988-2_13.

Troebs M, Heinzel G (2006) Improved spectrum estimation from digitized time series on a logarithmic frequency axis. Measurement 39:120–129. doi:10.1016/j.measurement.2005.10.010, seealsotheCorrigendumatdoi:10.1016/j.measurement.2008.04.004

Udem T, Holzwarth R, Hänsch TW (2002) Optical Frequency Metrology. Nature 416:233

Visser PNAM, Sneeuw N, Reubelt T, Losch M, van Dam T (2010) Spaceborne gravimetric satellite constellations and ocean tides: aliasing effects. Geophys J Int 181:789–805

Wagner C, McAdoo D, Klokočník J, Kostelecký J (2006) Degradation of geopotential recovery from short repeat-cycle orbits: application to GRACE monthly fields. J Geod 80(2):94–103

Welch PD (1967) The use of fast fourier transform for the estimation of power spectra: a method based on time averaging over short, modified periodograms. IEEE Trans Audio Electroacoust 15(2):7073

Wiese DN, Folkner WM, Nerem RS (2009) Alternative mission architectures for a gravity recovery satellite mission. J Geod 83:569–581. doi:10.1007/s00190-008-0274-1

Wiese DN, Nerem RS, Lemoine FG (2011) Design considerations for a dedicated gravity recovery satellite mission consisting of two pairs of satellites. J Geod 86:81–98. doi:10.1007/s00190-011-0493-8

Willemenot E, Touboul B (1999) On-ground investigations of space accelerometers noise with an electrostatic torsion pendulum. Rev Sci Instrum 71:302. doi:10.1063/1.1150197

Ye J (2004) Absolut measurement of a long, arbitrary distance to less than an optical fringe. Opt Lett 29(10):1153–1155

van Zoest T, Gaaloul N, Singh Y, Ahlers H, Herr W, Seidel ST, Ertmer W, Rasel E, Eckart M, Kajari E, Arnold S, Nandi G, Schleich WP, Walser R, Vogel A, Sengstock K, Bongs K, Lewoczko-Adamczyk W, Schiemangk M, Schuldt T, Peters A, Könemann T, Müntinga H, Lämmerzahl C, Dittus H, Steinmetz T, Hänsch TW, Reichel J (2010) Bose-Einstein condensation in microgravity. Science 328:1540–1543. doi:10.1126/science.1189164